Wisconsin Highway Research Program

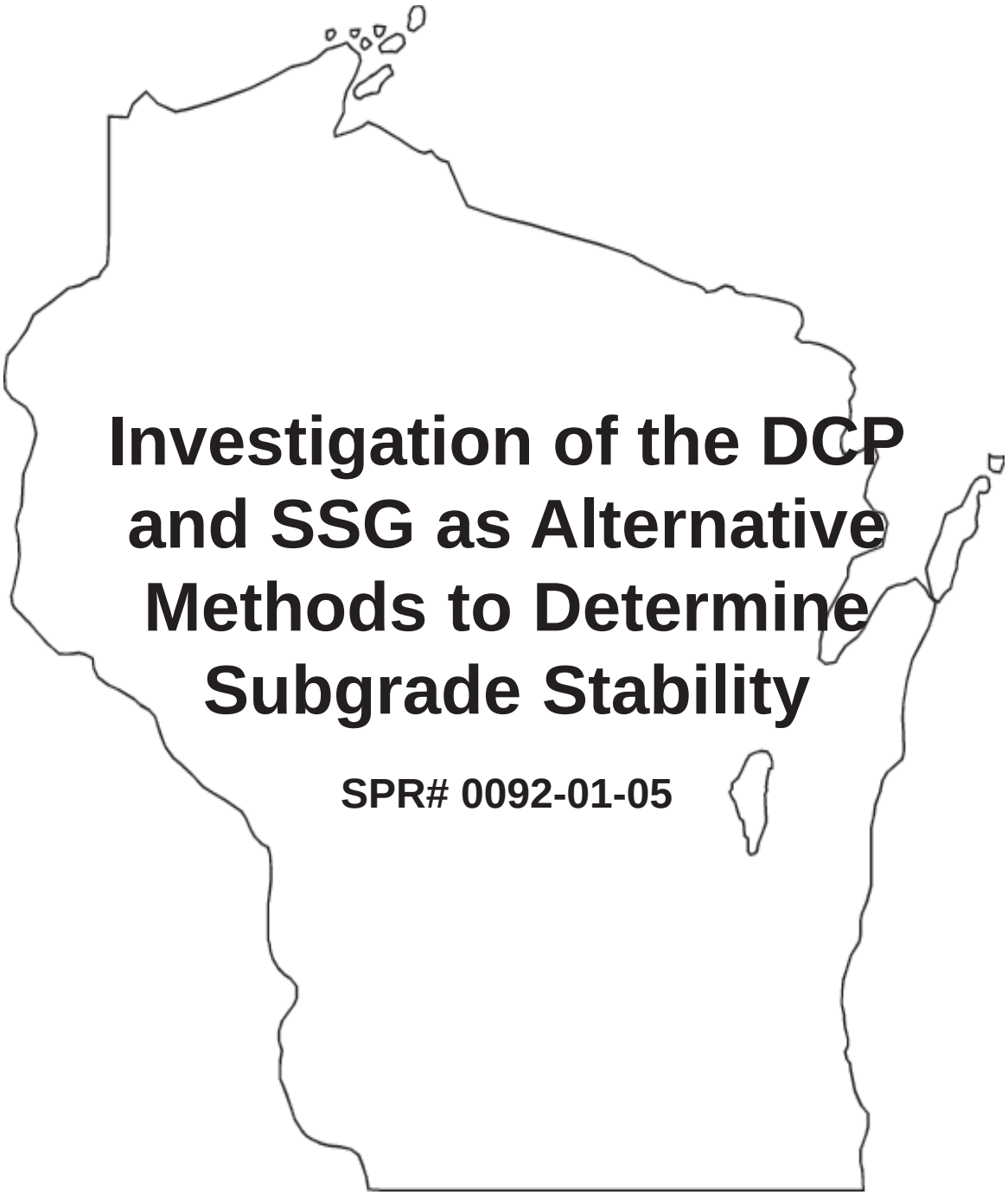

Investigation of the DCP and SSG as Alternative Methods to Determine Subgrade Stability

SPR# 0092-01-05

Tuncer B. Edil and Craig H. Benson
Department of Civil and Environmental Engineering
University of Wisconsin-Madison

September 2005

WHRP 05-14

ACKNOWLEDGEMENT

Financial support for the study described in this paper was provided by the Wisconsin Department of Transportation. Additionally, Mr. A. Sawangsuriya received financial support through a scholarship from the Royal Thai Government. The contents of this report are those of the authors and do not reflect the opinions or policies of WisDOT. Messrs., David A. Staab and M. Fredrickson assisted with the laboratory and field tests. Dr. P. Bosscher provided valuable suggestions for data analysis. Finally, we also acknowledge the cooperation of Mr. Robert Arndorfer and other WisDOT personnel for their cooperation in arranging access to the sites.

DISCLAIMER

This research was funded through the Wisconsin Highway Research Program by the Wisconsin Department of Transportation and the Federal Highway Administration under Project # 0092-01-05. The contents of this report reflect the views of the authors who are responsible for the facts and accuracy of the data resented herein. The contents do no necessarily reflect the official views of the Wisconsin Department of Transportation or the Federal Highway Administration at the time of publication.

This document is disseminated under the sponsorship of the Department of Transportation in the interest of information exchange. The United State Government assumes no liability for its contents or use thereof. This report does not constitute a standard, specification or regulation.

The United States Government does not endorse products or manufacturers. Trade and manufacturers' names appear in this report only because they are considered essential to the object of the document.

Technical Report Documentation Page

1. Report No. 0092-01-05	2. Government Accession No	3. Recipient's Catalog No
4. Title and Subtitle *Investigation of the DCP and the SSG as Alternative Methods to Determine Subgrade Stability*		5. Report Date 6. Performing Organization Code
7. Authors Tuncer B. Edil and Auckpath Sawangsuriya		8. Performing Organization Report No.
9. Performing Organization Name and Address Department of Civil and Environmental Engineering University of Wisconsin-Madison 1415 Engineering Drive Madison, WI 53706		10. Work Unit No. (TRAIS) 11. Contract or Grant No.
12. Sponsoring Agency Name and Address Wisconsin Department of Transportation 4802 Sheboygan Avenue *Madison, WI 73707-7965*		13. Type of Report and Period Covered 14. Sponsoring Agency Code
15. Supplementary Notes		

16. Abstract

The use of the soil stiffness gauge (SSG) and dynamic cone penetrometer (DCP) for earthwork property evaluation is investigated in this study. SSG and DCP survey data of natural earthen materials, industrial by-products, chemically stabilized soils, and other materials from thirteen construction sites around the state of Wisconsin are presented along with their correlation with each other as well as with density and moisture content obtained from traditional tests. Weighted average of DCP penetration index (DPI) over depth of measurement is employed to obtain a representative strength index of the material. This approach provided better correlations than the arithmetic average. The dependency of SSG stiffness and DPI strength index on dry unit weight and water content followed, in general, a pattern consistent with those in other research on stiffness and strength. A simple linear semi logarithmic relationship is observed between SSG stiffness and DPI. DPI weighted average over a DCP penetration depth of 152 mm yields the highest coefficient of determination and also yields a statistically significant relationship between the SSG stiffness and DPI for all materials except fly ash-stabilized soils. This depth is consistent with the significant depth of measurement for the SSG as shown in a previous study. The SSG and DCP provide a convenient means of assessing stiffness and strength of earthen construction materials in the field.

17. Key Words soil stiffness, DCP penetration index, dry unit weight, water content, soil stiffness gauge, dynamic cone penetrometer, nuclear density test	18. Distribution Statement No restriction. This document is available to the public through the National Technical Information Service 5285 Port Royal Road Springfield VA 22161

19. Security Classif.(of this report) Unclassified	19. Security Classif. (of this page) Unclassified	20. No. of Pages	21. Price

Form DOT F 1700.7 (8-72) Reproduction of completed page authorized

EXECUTIVE SUMMARY

SSG and DCP survey data of natural earthen materials, industrial by-products, chemically stabilized soils, and other materials from thirteen construction sites around the state of Wisconsin are presented along with their correlation with each other as well as with density and moisture content obtained from traditional tests. The data display considerable dispersion characteristic of the conditions and sampling sizes typical during construction. SSG provides in-place near-surface soil stiffness averaged over a zone, whereas DCP provides individual points of an index of in situ shear strength expressed as DCP penetration index (DPI) as a function of depth. Therefore, each fundamentally relates to a different material property and is presented in a spatially different manner. To deal with the latter issue, weighted average of DPI over depth of measurement is employed to obtain a representative strength index of the material. This approach provided better correlations than the arithmetic average.

The dependency of SSG stiffness and DPI strength index on dry unit weight and water content is obscured by large dispersion of the data although individual material appears to follow a pattern consistent with those expected from other research on stiffness and strength. However, it is also clear that dry unit weight or water content alone does not control stiffness or strength. It is also noted that the standard error associated with DPI is considerably larger than that of the SSG stiffness, reflective of the nature of the two tests.

A simple linear semi logarithmic relationship is observed between SSG stiffness and DPI. DPI weighted average over a DCP penetration depth of 152 mm yields the highest coefficient of determination and also yields a statistically significant relationship between the SSG stiffness and DPI for most materials. This depth is consistent with the significant depth of measurement for the SSG as shown in previous studies. The relationship is indicative of the fact that although there is not always a one-to-one relationship, stiffness and strength are related in a general sense.

A comparison of moduli obtained from different laboratory tests (seismic, bender elements, resonant column, resilient modulus, SSG, and triaxial compression) indicates that the moduli obtained from these tests follow the conventional modulus degradation-strain amplitude curve. The estimated range of shear strain amplitude for the SSG

suggests that the SSG modulus should be higher than that given by the device and closer to that from seismic tests. It is not clear if the modulus reported by the SSG device has been reduced by a factor. Both the operating stress level and shear strain amplitude of different tests are important parameters that should be considered in comparing moduli obtained from different tests. If resilient modulus is considered to be the modulus representative of the field traffic loading conditions, the SSG would provide an unconservatively higher modulus (about 25% to 50%) than the resilient modulus for granular soils. A reduction factor (experimentally obtained or estimated from the modulus degradation-strain amplitude curve) can be used to adjust the small-strain modulus (e.g., SSG) to obtain the large-strain resilient modulus.

The study indicates that either or both devices show good potential for future use in the pavement and subgrade property evaluation during construction phase. The in situ stiffness and strength properties of various materials can be rapidly and directly monitored in companion with the conventional compaction control tests (e.g., nuclear density or laboratory moisture content samples) during earthwork construction. Stiffness and strength are material properties that are needed in different phases of highway design, i.e., for long-term pavement performance and during-construction working platform support and stability, respectively. The experience with recycled and reclaimed materials as well as chemically stabilized soils is limited compared to natural earthen materials in terms of moisture-density relationships and the related mechanical behavior. Direct monitoring of stiffness and strength of these new materials using these two devices also appears to be as effective as in natural earthen materials.

Use of the convenient SSG and DCP in conjunction with conventional moisture-density measurements enhances quality control during earthwork construction by achieving more uniform structural property and aids developing a design modulus. SSG stiffness normalized by the deviation of compaction moisture content from the optimum moisture content and the DPI normalized by the deviation of compaction moisture content from the optimum moisture content are remarkably constant around a value equal to -2.4 and -8.4, respectively for compacted natural earthen materials. In addition, there is potential for using SSG alone with an independent moisture measurement for both density and stiffness control with further evaluation.

TABLE OF CONTENTS

LIST OF FIGURES

LIST OF TABLES

CHAPTER ONE
INTRODUCTION

1.1 Problem Statement

An accurate determination of subgrade stability is important during construction to ensure that economical and long lasting subgrades and pavement structures are obtained. WisDOT has used various methods to determine the stability of subgrades during construction, including proof rolling, moisture-density tests, visual inspection, and observation of construction equipment. All of these methods have drawbacks. Some are very subjective and may even result in a misleading degree of stability.

Several agencies have recently proposed and used two new methods to monitor pavement performance. These separate methods involve the use of two devices: the soil stiffness gauge (SSG) and the dynamic cone penetrometer (DCP). The SSG, which directly measures stiffness, and the DCP, which provides an index of strength, offer a means of more directly monitor stiffness and strength of surficial materials. SSG stiffness and DCP penetrometer index (DPI), in turn, have been correlated to properties used in design such as resilient modulus (Sawangsuriya et al. 2003) and California bearing ratio (CBR) (Livneh 1989), respectively. To date, there has been only limited research on the use of these devices for WisDOT projects. In additional to these devices, there may be other methods that accurately determine subgrade stability.

1.2 Research Objectives

The main objective of this research is to analyze the data collected and to assess the soil stiffness gauge (SSG) and dynamic cone penetrometer (DCP) for earthwork property evaluation. Additionally, the degree of correlation between the data generated by each tool is explored. For this purpose, measurements were made at thirteen construction sites around the state of Wisconsin. Recommendations with respect to the methods of measurement, use, and interpretation of these two methods are made. This research was not designed to generate correlations under controlled conditions but to look at the quality of data generated under ordinary field conditions.

The field data are analyzed to examine if a reasonable correlation between SSG stiffness and DCP penetrometer index (DPI) can be established. The correlation between the mechanical properties (i.e., stiffness and strength) and the index properties of soils (i.e., density and moisture content) obtained from traditional tests are also explored. In addition, the appropriate effective depth zone for statistically significant empirical correlations between the two methods is established for various types of materials including industrial by-products.

CHAPTER TWO
BACKGROUND

2.1 Background and Understanding of the Problem

Subgrade and base materials are important elements of a pavement structure. Their quality impacts construction costs, construction productivity, and the long-term performance of highways. A cross-section of a highway pavement system employing an asphalt surface layer (a "flexible" pavement design) is shown in Fig. 2.1. The pavement system consists of four layers (from bottom to top): subgrade, subbase, base, and the surface layer. Subgrade is the natural soil existing at the bottom of the pavement. Subbase is an optional layer that is used to distribute and reduce loads on the subgrade and to provide a filter between the subgrade and the base. Adding a less costly subbase layer can reduce the required thickness of the base layer. Base is a freely draining layer constructed with coarse materials (i.e., crushed stone or gravel) that provides the primary foundation for the overlying surface layer made of asphaltic concrete. The cost of the layers increases from bottom to top, with the base and surface layers being particularly costly. Consequently, improvements that can reduce the thickness of the layers, particularly the base and asphalt, are desirable.

The quality of subgrade and base materials can be improved by compaction and stabilization during construction. Subgrade is the natural soil over which the pavement structure is placed and may or may not be suitable for direct highway construction over it. Existing subgrades that are suitable for highway construction are compacted to optimize their load bearing capacity and stiffness. The quality of subgrade is monitored during compaction to ensure that uniform and optimum subgrade improvement has been achieved. However, nearly 60% of the State has "poor soils" for highway construction. WisDOT is encouraging use of select materials in areas of poor soils for alternative cost-effective approaches towards solving the soft subgrade problem. Means to reduce construction problems and costs associated with soft subgrades are currently being researched and reviewed by WisDOT. If select materials and methods are used in subgrade preparation because a subgrade is poor for highway construction, the quality of compaction of these materials also needs to be monitored during construction.

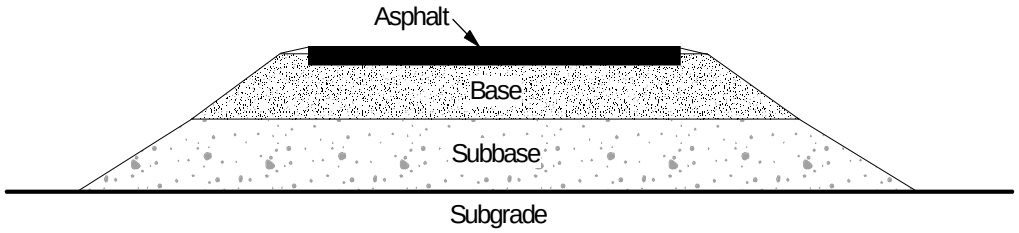

Fig. 2.1. Cross-section of highway pavement system.

Given the importance of soil stiffness and strength in earthwork evaluation, there has been a concerted effort in recent years to develop methods to measure stiffness and strength during construction. Direct monitoring of stiffness and strength is consistent with the movement of pavement design from empirical to mechanistic-empirical pavement design procedures (Pidwerbesky 1997, Fleming et al. 1998, Pinard 1998, van Niekerk et al. 1998, Siekmeier et al. 1999). Traditionally, quality control monitoring has been achieved through moisture-density tests, visual inspection, observation of construction equipment, and proof rolling. All of these methods provide a qualitative assessment of the subgrade quality, and do not provide a direct assessment of stiffness or strength. These methods, in general, do not ensure that a minimum stiffness or strength is achieved because different soils prepared at the same compaction density have different stiffness and strength unless stiffness and strength are related to moisture-density in a two-step process (Holtz and Kovacs 1981). An exception is the proof rolling method that WisDOT is currently developing as a quantitative tool. Direct monitoring of stiffness and strength would facilitate quantitative evaluation of alternative construction practices and materials, such as recycled and reclaimed materials that result in cost savings and environmental benefits (Fleming et al. 1998). For instance, the use of recycled and reclaimed materials both as working platform over poor subgrades and as a subbase in pavement structure is being explored by the transportation community. Evaluation of these new materials on the basis of index property measurements such as moisture-density or past subjective experience based on natural soil behavior is severely limited. A number of in situ devices are currently available to assess stiffness and strength of the pavement materials and are summarized in Table 2.1, which provides the test principle, advantages and disadvantages. Authors had access to three of these devices (FWD, DCP, and SSG). FWD is an established procedure and it is not further researched, however, interpretation of FWD modulus is reported elsewhere (Tanyu et al. 2003) and it is not included in this report. This study, however, involved two devices, namely the soil stiffness gauge (SSG) and the dynamic cone penetrometer (DCP) and their correlation with each other. Detailed description of each device is given in the following sections.

Table 2.1. Summary of Methods/Devices for Investigating Subgrade Stability and Modulus

Test Method	Standard	Test Principle	Advantage	Disadvantage	References
Soil Stiffness Gauge (SSG)	ASTM D 6758	Stiffness is obtained internally by imparting a small dynamic force electronically generated inside the device through a ring-shaped foot and measuring the resulting displacement time history over a range of frequencies.	-Simple operation -Direct measure of stiffness parameter -Rapid assessment -Portable -Nondestructive	-Near-surface monitoring (i.e., less than 0.3 m) -Small-strain levels -Layered materials may influence the measurement	Fiedler et al. (1998, 2000), Humboldt (1999b), Lenke et al. (2001, 2003), Sawangsuriya et al. (2002, 2003, 2004)
Dynamic Cone Penetrometer (DCP)	ASTM D 6951	Penetration resistance (i.e., index of strength) expressed as DCP penetration index is determined as the slope of the relationship between depth of penetration and number of blows at a given linear depth segment.	-Simple operation -Economic -Rugged -Portable	-Indirect property test -Invasive -Vertical confinement (due to rigid pavement structure or upper granular/cohesive layers) and rod friction (due to collapse of the granular material during penetration) may affect the measurement	Scala (1956), Van Vuuren (1969), Kleyn (1975), Kleyn et al. (1982), Chua (1988), Livneh (1987), Webster et al. (1992), Livneh et al. (1995), Konrad and Lachance (2001)
Light Drop Weight (LDW)[1]	German standard testing procedure[2]	Stiffness is determined based on an applied light impulse load, which generates by dropping a mass onto a circular plate, and the center deflection of the plate measured using either the attached velocity sensor or accelerometer.	-Rapid assessment -Portable -Nondestructive	-Operation experience required -Time consuming for interpretation of data -Small-strain levels	Newcomb and Birgissson (1999), Siekmeier et al. (1999), Fleming et al. (2000), Livneh and Goldberg (2001), Müller (2003), Hoffmann et al. (2004)

Falling Weight Deflectrometer (FWD)	None	Stiffness of layered materials is backcalculated based on the dynamic force generated by means of a hydraulic actuator and the resulting surface deflections measured by a linear array of geophones spaced at equal intervals starting from the center of the load.	-Rapid assessment -Nondestructive -Strain levels associated with actual loading (trafficking) conditions	-Expensive -Operation experience required -Time consuming for interpretation of data (i.e., backcalculation of elastic parameters of layered materials) -Non-portable - Inversion of data for properties may involve ambiguities	Claessen et al. (1976), Hoffman and Thompson (1981), Smith and Lytton (1984), Lytton (1989), Chen et al. (1999), Siekmeier et al. (1999), Newcomb and Birgissson (1999), Tanyu et al. (2003)
Spectral Analysis of Surface Wave (SASW)	None	Stiffness of subsurface profiles is determined by utilizing the dispersion characteristics of surface (Rayleigh) waves (i.e., measurements of surface wave velocity at various wavelengths or frequencies).	-Layer boundaries and thicknesses can be resolved or identified -Nondestructive -Portable	-Small-strain level -Test experience required -Time consuming for testing and interpretation of data (i.e., inverse problem)	Nazarian and Stokoe (1987), Sanchez-Salinero et al. (1987), Rix and Stokoe (1989), Nazarian et al. (1994), Wright et al. (1994), Newcomb and Birgissson (1999), Mayne et al. (2001)

[1] Also known as Light Falling Weight Deflectrometer (LFWD), Portable Falling Weight Deflectrometer (PFWD), or Dynamic Load Plate, [2] widely used in European countries

2.2 Soil Stiffness Gauge (SSG)

Soil stiffness gauge (SSG) (Fig. 2.2), which is currently marketed as the Humboldt GeoGauge™, is a recently developed instrument for directly measuring in situ stiffness of soils. The SSG was conceived and developed partially by funding from FHWA in partnership with several private firms (Fiedler et al. 2000). The SSG is a 28 cm in diameter and 25.4 cm in height portable cylinder with a 114-mm-outer diameter and 88-mm-inner diameter ring-shaped foot extending from the bottom of the device. It weighs approximately 10 kg. The SSG measures near-surface stiffness by imparting small dynamic force to the soil though a ring-shaped foot at 25 steady state frequencies between 100 and 196 Hz. Based upon the force and displacement-time history, the stiffness is calculated internally as the average force per unit displacement over the measured frequencies and reported. In a previous investigation, the acceleration and corresponding displacement were measured (Sawangsuriya et al. 2003). Given knowledge of the soil properties, the force produced during the SSG measurement is determined to be 10 to 17 N (Sawangsuriya et al. 2003). A measurement takes only about 1.5 minutes. Due to the small stress and strain levels, the stiffness measurement using the SSG is closed to that required for the calculation of strain and displacement around a range of geotechnical engineering applications, including pavement, bedding, and foundation (Fiedler et al. 2000).

To evaluate the SSG measurement characteristics, Sawangsuriya et al. (2002) studied the zone of measurement influence and the effects of layered materials on the SSG measurement in granular materials. The SSG measurements were conducted in a test box. Their results indicated that the radius of measurement influence extends to 300 mm. According to Sawangsuriya et al. (2004), results obtained experimentally were also in good agreement with those obtained from the numerical studies using a finite element analysis. Therefore, caution should be taken when the SSG measurement is to be used in a 152-mm diameter Proctor mold due to the significant boundary effects caused by the small volume of soil and the dynamic nature of the SSG measurement (Lenke et al. 2003, Sawangsuriya et al. 2004). For two-layer materials with different stiffness, the SSG starts to register the stiffness of an upper-layer material of 125 mm or thicker. The effect of the lower layer may continue to be present even at an upper-layer material thickness of 275

Fig. 2.2. Soil Stiffness Gauge (SSG) or GeoGauge™.

mm, depending on the relative stiffness (or contrast) of the layered materials (Sawangsuriya et al. 2002, 2004).

Soil stiffness (or modulus) is known to change as a function of strain amplitude and stress state; consequently any modulus must be defined and understood in terms of these factors. A comparison of moduli of granular soils obtained from the SSG with moduli obtained from other tests on the basis of comparable stress levels indicates that the SSG measures moduli in the very small strain amplitude range (i.e., $2.7x10^{-4}$ to $4.3x10^{-4}$%, which is less than 10^{-3}%). The SSG induced strain amplitudes are lower than the strain amplitudes induced in the resilient modulus test, but are larger than the strain amplitude of the seismic test (Sawangsuriya et al. 2003). The study also indicated the importance of the fact that the SSG induces a relatively small strain amplitude under a low confining pressure in interpreting the SSG's utility for design purposes. If resilient modulus is considered to be the modulus representative of the field traffic loading conditions, the SSG would provide an unconservatively higher modulus (about 25% to 50%) than the resilient modulus for granular soils (Sawangsuriya et al. 2003).

2.3 Dynamic Cone Penetrometer (DCP)

Scala (1956) developed the Scala penetrometer for assessing in situ California bearing ratio (CBR) of cohesive soils. In the last decade, the Scala penetrometer has evolved into the dynamic cone penetrometer (DCP) test for determining in situ CBR and elastic modulus. The DCP is now being used extensively in South Africa, the United Kingdom, the United States, Australia, and other countries because it is simple, rugged, economical, and able to provide a rapid in situ index of strength and more indirectly modulus of subgrade as well as pavement structures.

The DCP is used for measuring the material resistance to penetration in terms of millimeters per blow while the cone of the device is being driven into the pavement structure or subgrade. The typical DCP consists of an 8-kg hammer that drops over a height of 575 mm, which yields a theoretical driving energy of 45 J or 14.3 J/cm^2, and drives a 60^o 20 mm base diameter cone tip vertically into the pavement structure or subgrade (Fig. 2.3). The steel rod to which the cone is attached has a smaller diameter than the cone (16 mm) to reduce skin friction. The number of blows during operation is

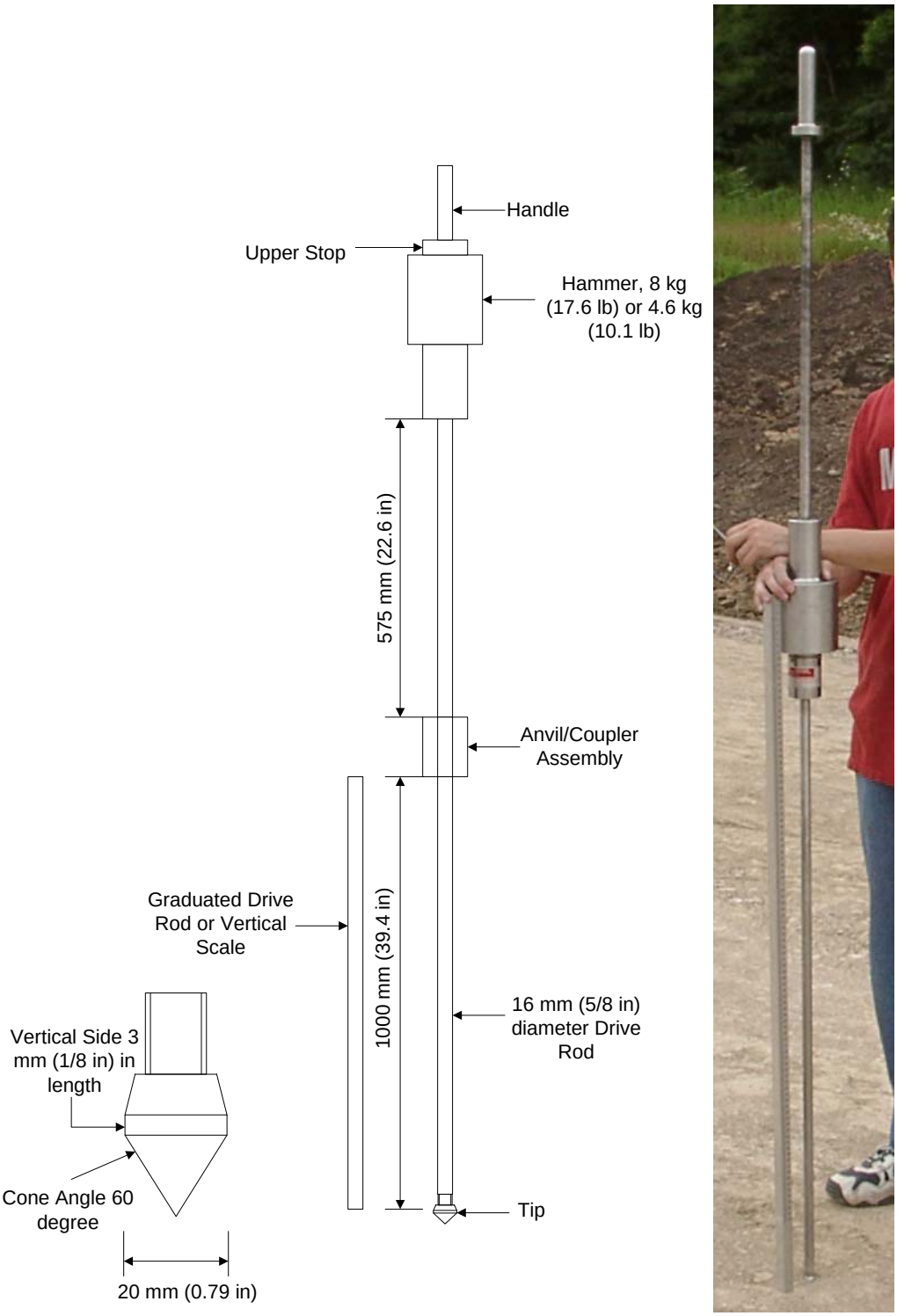

Fig. 2.3. Dynamic Cone Penetrometer (DCP).

recorded with depth of penetration. The slope of the relationship between number of blows and depth of penetration (in millimeters per blow) at a given linear depth segment is recorded as the DCP penetration index (DPI). In addition to soil profiling (i.e., the thickness and nature of each layer in a given pavement), DCP data are correlated with various pavement design parameters, i.e., CBR, shear strength, elastic modulus, and back-calculated elastic modulus from the FWD (Kleyn et al. 1982, Chua 1988, Newcomb et al. 1996, Syed and Scullion 1998, Saarenkento et al. 1998). The DCP has been available longer than the SSG and has been used as a convenient field tool; however, it is not a direct property test but an index test based on dynamic impact loading.

2.4 SSG and DCP Correlations to Other Methods

The measured soil stiffness from the SSG can be used to calculate the elastic modulus of the materials at near surface. For a rigid ring-shaped foot resting on a linear-elastic, homogeneous, and isotropic infinite half-space, the stiffness (K_{SSG}) is related to Young's modulus (modulus of elasticity) of soil (E_{SSG}) (Egorov 1965):

$$K_{SSG} = \frac{E_{SSG} R}{(1-\nu^2)\omega(n)} \tag{2.1}$$

where ν is Poisson's ratio of the materials, R is the outside radius of the ring (57.15 mm), and $\omega(n)$ is a constant that is a function of the ratio of inside diameter and the outside diameter of the ring. Table 2.2 summarizes the values of Poisson's ratio for various materials (Huang 1993). Note that E_{SSG} and K_{SSG} are in MPa and MN/m, respectively. For the ring geometry of the SSG, the constant $\omega(n)$ is equal to 0.565 and hence Eq. (2.1) is expressed as:

$$K_{SSG} = \frac{1.77 E_{SSG} R}{(1-\nu^2)} \tag{2.2}$$

The Young's modulus (E_{SSG}) and shear modulus (G_{SSG}) are related through $E_{SSG} = 2G_{SSG}(1+\nu)$, which results in the following:

$$K_{SSG} = \frac{3.54 G_{SSG} R}{(1-\nu)} \tag{2.3}$$

Because of the very small strain amplitudes induced by the SSG, an elastic response of the soils is assumed, and the use of Eq. (2.2) and Eq. (2.3) is justified.

Table 2.2. Values of Poisson's Ratio for Various Materials (Huang 1993)

Material	Range	Typical
Hot mix asphalt	0.30-0.40	0.35
Portland cement concrete	0.15-0.20	0.15
Untreated granular materials	0.30-0.40	0.35
Cement-treated granular materials	0.10-0.20	0.15
Cement-treated fine-grained soils	0.15-0.35	0.25
Lime-stabilized materials	0.10-0.25	0.20
Lime-fly ash mixtures	0.10-0.15	0.15
Loose sand or silty sand	0.20-0.40	0.30
Dense sand	0.30-0.45	0.35
Fine-grained soils	0.30-0.50	0.40
Saturated soft clays	0.40-0.50	0.45

2.4.1 Correlation between SSG Stiffness and Back-Calculated Resilient Modulus from FWD Test

Back-calculated resilient moduli of subgrade and bases from the falling weight deflectrometer (FWD) test have been used extensively in pavement design, construction, and maintenance. Wu et al. (1998) found that the relationship between the SSG stiffness (K_{SSG}) and the back-calculated modulus from the FWD (E_{FWD}) can be presented in the following form:

$$E_{FWD} = 22.96e^{0.12K_{SSG}} \quad R^2 = 0.66 \tag{2.4}$$

Note that K_{SSG} and E_{FWD} are expressed in MN/m and MPa, respectively. Wu et al. (1998) also noted that the difference between these methods can be ascribed to the in situ variability of the material properties. As E_{FWD} is obtained through inversion based on all seven deflection measurements, which cover a distance of about 2 meters, E_{FWD} of pavement layers is therefore a weighted average value over 2 meters. On the other hand, the SSG measures only the near-surface soil stiffness right underneath its ring foot with the measurement influence of less than 0.3 meters. Moreover, on the basis of the test results, they concluded that the SSG is much more sensitive when the materials are soft and the FWD becomes more sensitive as the materials are stiffer. In the other studies, Chen et al. (1999a) suggested that a general linear relationship between K_{SSG} and E_{FWD} is discernable as the following:

$$E_{FWD} = 37.65K_{SSG} - 261.96 \quad R^2 = 0.82 \tag{2.5}$$

Again, K_{SSG} and E_{FWD} are expressed in MN/m and MPa, respectively. A previous study by Chen et al. (1999a) also indicated that the base moduli from the SSG are smaller than those from the FWD. In addition, they reported that the discrepancies between E_{FWD} and K_{SSG} might be explained by the inaccuracies associated with E_{FWD} and the fact that the SSG may lose accuracy when measuring stiffness greater than 23 MN/m. Additional research is however required to determine a more confident relationship between E_{FWD} and K_{SSG}.

2.4.2 Correlation between SSG Stiffness and Modulus from Seismic Tests

Wu et al. (1998) provided the correlation between SSG stiffness and modulus from seismic tests including dirt-seismic pavement analyzer (D-SPA) and spectral

analysis of surface wave (SASW) for soft- to medium-stiff subgrades to very stiff bases. They indicate that the elastic modulus obtained from the SSG is about three times smaller than that obtained from seismic tests. A linear relationship is obtained between the SSG stiffness (K_{SSG}) and the seismic modulus (E_{SEIS}):

$$E_{SEIS} = 47.53K_{SSG} + 79.05 \quad R^2 = 0.62 \tag{2.6}$$

Note that K_{SSG} and E_{SEIS} are expressed in MN/m and MPa, respectively. The discrepancy between these two tests is explained by the difference in the stress-strain levels used as well as the uncertainty of the effective depth of the SSG, which varies with stiffness, density, and types of materials being tested (Wu et al. 1998).

Chen et al. (1999a) also conducted a similar study and indicated that the relationship between K_{SSG} and E_{SEIS} from D-SPA and SASW for soft- to medium-stiff subgrades to very stiff bases can be expressed as follows:

$$E_{seismic} = 55.42K_{SSG} - 162.94 \quad R^2 = 0.81 \tag{2.7}$$

Again, the units of K_{SSG} and $E_{seismic}$ are in MN/m and MPa, respectively. The relationship between K_{SSG} and E_{SEIS} is found to be obvious and convincing. The operation of the SSG is very simple and feasible for the purpose of quality control; however, it yields a stiffness value at near surface. The seismic tests can generate a stiffness-depth profile, but its operation is more complicated (Chen et al. 1999a).

2.4.3 Correlation between DCP Penetration Index and CBR

To assess the structural properties of the pavement materials, the DCP penetration index (DPI) values are usually correlated with the California bearing ratio (CBR) of the pavement materials. Extensive research has been conducted to develop an empirical relationship between the DCP penetration index (DPI) values and the California bearing ratio (CBR) for a wide range of pavement and subgrade materials. This includes research by Kleyn (1975), Harison (1987), Livneh (1987), McElvaney and Djatnika (1991), Webster et al. (1992), Livneh and Livneh (1994), and Livneh et al. (1995). Based on their researches, many of the relationships between DPI and CBR can be quantitatively presented in the following form:

$$\log(\text{CBR}) = \alpha + \beta \log(\text{DPI}) \tag{2.8}$$

where α and β are coefficients ranging from 2.44 to 2.56 and -1.07 to -1.16, respectively, which are valid for a wide range of pavement and subgrade materials. Note also that CBR is in percent and DPI is in millimeters per blow (mm/blow). For a wide range of granular and cohesive materials, the US Army Corps of Engineers use the coefficients α and β of 2.46 and -1.12, which have been also adopted by several agencies and researchers (Webster et al. 1992, Livneh et al. 1995, Siekmeier et al. 1999, Chen et al. 2001) and are in general agreement between the various sources of information. Livneh et al. (1995) also show that there exists a universal correlation between DPI and CBR for a wide range of pavement and subgrade materials, testing conditions, and technologies. In addition, the relationship between DPI and CBR is independent of water content and dry unit weight because water content and dry unit weight influence DPI and CBR equally.

2.4.4 Correlation between CBR (also DPI) and Modulus from Other Tests

Empirical correlations between elastic modulus (E) and CBR (also DPI) have been proposed by a number of researchers. A well-known UK Transportation Research Laboratory (TRL) equation developed between elastic modulus (E) and CBR of the subgrade soil has been given by Powell et al (1984). This equation has been established primarily from the comprehensive data relating modulus measured by wave propagation to in situ CBR tests on both remolded and undisturbed subgrade soils (Jones 1958). After taken into account the effects of the very low strain levels generated in the wave propagation technique and other information obtained from repeated load triaxial test conducted at realistic stress levels and in situ measurements of transient stress and strain in experimental pavements, the modulus from the seismic test was adjusted and the corresponding equation is expressed as follows (Powell et al. 1984):

$$E_{SEIS-MOD} = 17.6 \times CBR^{0.64} \tag{2.9}$$

Note that, for the sake of clarity, the modulus used in Eq. (2.9) is denoted as the modulus from the seismic test after adjustment to realistic stress and strain levels for the pavement ($E_{SEIS-MOD}$). $E_{SEIS-MOD}$ and CBR units are in MPa and percent, respectively.

Another well-known relationship, which is widely used in North America, is the one proposed by Heukelom and Foster (1960). It has been adopted by the American

Association of State Highway and Transportation Officials (AASHTO) in the Guide for Design of Pavement Structures (AASHTO 1993).

$$E_{RM} = 10 \times CBR \tag{2.10}$$

where E_{RM} is the modulus from the resilient modulus test, in MPa.

In addition to these two well-known relationships, Chen et al. (1999b) suggested the relationship between back-calculated moduli from the FWD (E_{FWD}) and DPI:

$$E_{FWD} = 338 \times DPI^{-0.39} \tag{2.11}$$

where E_{FWD} and DPI are in units of MPa and millimeters per blow (mm/blow), respectively.

Konrad and Lachance (2001) presented a relationship between DPI using a 51-mm diameter cone and elastic modulus of unbound aggregates, gravelly, and sandy soils back-calculated from plate load tests (E_{PLT}) by the following equation:

$$\log(E_{PLT}) = -0.884 \log(DPI) + 2.906 \tag{2.12}$$

where DPI is the DCP penetration index in millimeters per blow (mm/blow) using a 51-mm diameter cone and a 63.5-kg hammer dropping 760 mm and E_{PLT} is expressed in MPa.

Livneh and Goldberg (2001) carried out comparative German light drop weight (LDW) and DCP tests. The relationship between the modulus measured by the LDW (E_{LDW}) and the in situ CBR values obtained from the DCP is expressed as follows for clayey and sandy soils, respectively.

$$E_{LDW} = 600 \times \ln \frac{300}{300 - 6.019 \times CBR^{(1/1.41)}} \tag{2.13}$$

$$E_{LDW} = 600 \times \ln \frac{300}{300 - 4.035 \times CBR^{(1/1.41)}} \tag{2.14}$$

where E_{LDW} and CBR are in units of MPa and percent, respectively.

CHAPTER THREE
MATERIALS AND TESTING PROGRAM

3.1 Materials Classification and Properties

3.1.1 Natural Earthen Materials

Samples were collected either along the centerline or near the shoulder of the roadway from thirteen construction sites (twelve highway construction sites and one sludge lagoon cap construction) to determine index properties, soil classification, and compaction characteristics. Table 3.1 summarizes the natural earthen materials encountered and their properties together with their classification. Compaction curves corresponding to standard compaction effort described in ASTM D698 were developed, except for breaker run. Note that breaker run is the excavated and crushed rock including cobbles (75-350 mm in diameter) with a soil fraction. It was retrieved from the cuts in parts of the project route. Its soil fraction consisted of approximately 30% gravel, 65% sand, and 5% fines.

Table 3.1. Properties of Natural Earthen Materials and their Classification

(a) Fine-Grained Soils

Site	Soil Name	Specific Gravity	Liquid Limit	Plasticity Index	Classification		W_N (%)	W_{OPT} (%)	$\gamma_{d\ max}$ (kN/m^3)
					USCS	AASHTO			
STH 60 (Test Section)	Joy Silt Loam	2.70	39	15	CL-ML	A-6(16)	25.0	19.0	16.5
Scenic Edge Development	Plano Silt Loam	2.71	44	20	CL	A-7-6(20)	27.0	20.0	16.2
Gils Way Development	Plano Silt Loam	2.71	46	20	CL	A-7-6(20)	23.4	19.5	16.3
STH 26	Lean Clay with Sand	2.64	32	11	CL	A-6(7)	20.7	13.5	19.2
STH 100	Lean Clay with Sand	2.74	29	14	CL	A-6(9)	14.2	14.4	18.2
STH 44	Silty, Clayey Sand	2.70	23	7	SC-SM	A-4(0)	9.8	11.7	19.8

(b) Granular Soils

Site	Soil Name	Specific Gravity	D_{10} (mm)	D_{60} (mm)	C_u	% Fines	Classification		W_{OPT} (%)	$\gamma_{d\ max}$ (kN/m^3)
							USCS	AASHTO		
USH 12	Clayey Sand[1]	2.69	NA	0.2	NA	34.45	SC	A-2-4(0)	10.0	18.9
STH 131	Poorly Graded Sand with Silt	2.62	0.09	0.35	3.9	6.54	SP-SM	A-3(0)	8.0	18.0
STH 58	Clayey Sand[2]	2.62	NA	0.25	NA	25.50	SC	A-2-4(0)	8.5	19.8
STH 154	Poorly Graded Sand with Silt	2.63	0.07	0.4	5.7	11.46	SP-SM	A-3(0)	9.0	18.7
USH 2	Poorly Graded Sand with Silt	2.68	0.07	0.4	5.3	11.11	SP-SM	A-3(0)	7.5	18.8
STH 60 (Test Section)	Breaker Run	NM	0.25	29.0	116	3.12	GW	A-1-a(0)	None	NM
CTH E	Poorly Graded Sand	2.65	0.17	0.5	2.9	3.10	SP	A-3(0)	12.6	17.6

Note: NM = not measured, [1] LL=24, PI=7, [2] LL=24, PI=8

3.1.2 Processed Construction Materials

The properties of the processed construction materials (i.e., other than the natural earthen materials) along with their classification are summarized in Table 3.2. These materials are subdivided into three main categories: (a) industrial by-products, (b) chemically stabilized soils, and (c) a cap material. The by-products consisted of bottom ash, foundry slag, and foundry sand. Bottom ash and foundry slag are well-graded coarse-grained sand-like materials, and thus are insensitive to moisture content during compaction. Foundry sand is primarily a mixture of fine sand and sodium bentonite (~10% by weight) that also contains small percentages of other additives. The foundry sand is sensitive to water content when compacted, and exhibits a conventional compaction curve.

Chemical stabilization involved a mixture of natural soil and either fly ash or lime. The fly ash-stabilized soil at STH 60 test section and Scenic Edge development sites was prepared by mixing Class C fly ash from Unit 2 of Alliant Energy's Columbia Power Station in Portage, Wisconsin with subgrade soil at its natural water content (wetter than the optimum water content). Analysis from a series of mix designs evaluated in the laboratory indicated that the subgrade soil stabilized using a fly ash content of 10% for the STH 60 test section site and 12% for the Scenic Edge development site (on the basis of dry weight) provided sufficient strength and hence was adopted for field construction. The lime-stabilized soil at Gils Way development in Cross Plains, Wisconsin was prepared by mixing 5% of lime with subgrade soil at its natural water content (wetter than the optimum water content).

The cap material is a mixture of wood chips and soil (approximately 50:50 mixture by volume). The soil component is classified as SW and A-1-b(0) according to the Unified Soil Classification System (USCS) and American Association of State Highway and Transportation Officials (AASHTO) classification system, respectively.

Table 3.2. Properties of Processed Construction Materials (Industrial By-Products, Chemically Stabilized Soils, and Cap Material) and their Classification

(a) Industrial By-Products

Site	Soil Name	Specific Gravity	D_{10} (mm)	D_{60} (mm)	C_u	% Fines	Classification		W_{OPT} (%)	$\gamma_{d\ max}$ (kN/m^3)
							USCS	AASHTO		
STH 60 (Test Section)	Bottom Ash[1]	2.65	0.06	1.9	31.7	13.23	SW	A-1-b(0)	None	15.1
	Foundry Sand[2]	2.55	0.0002	0.23	1150	28.92	SC	A-2-7(2)	16.0	16.1
	Foundry Slag[1]	2.29	0.13	2.0	15.4	5.27	SW	A-1-b(0)	None	10

[1] Non-plasticity, [2] LL=44 and PI=25

(b) Chemically Stabilized Soils

Site	Soil Name	Chemical Stabilized Content (%)	Stabilized Soil (No Delay)		Stabilized Soil (2-hr Delay)		Soil Component	
			W_{OPT} (%)	$\gamma_{d\ max}$ (kN/m^3)	W_{OPT} (%)	$\gamma_{d\ max}$ (kN/m^3)	W_{OPT} (%)	$\gamma_{d\ max}$ (kN/m^3)
STH 60 (Test Section)	Fly Ash-Stabilized Soils	10	20	16.6	21.0	16.1	19.0	16.5
Scenic Edge Development	Fly Ash-Stabilized Soils	12	21.0	16.2	21.0	15.6	20.0	16.2
Gils Way Development	Lime-Stabilized Soils	5	NM	NM	NM	NM	19.5	16.3

Note: NM = not measured

(c) Cap Material

Site	Soil Name	Wet Unit Weight (kN/m^3)	Dry Unit Weight (kN/m^3)	Water Content (%)
MMSD Project	Wood Chip-Soil Mixture	6.3-10.5	4-6.8	20-25

3.2 Field Testing Program

3.2.1 Location and Description of Test Sites

STH 60 test section is located approximately 40 km north of the city of Madison, WI and consists of a 1.4 km segment of the highway between Lodi and Prairie du Sac. This project consisted of a field demonstration of alternative soft subgrade reinforcement methods. The test sections include subgrades constructed with foundry and coal combustion by-products, geosynthetic reinforcement, and fly ash stabilization. Detailed descriptions of each test section are given in Edil et al. (2002). The SSG, DCP, and nuclear density gauge (NDG) tests were conducted in each test section.

Scenic Edge development project is a 0.7 km city street constructed as a residential subdivision in Cross Plains, WI by stabilizing the soft subgrade in place with fly ash. The fly ash was mixed into the moist subgrade to form a stiff substance as subbase layer material. This subbase layer material has a thickness of approximately 30 cm. The subgrade soil was tested using the SSG and DCP. The fly ash-stabilized subgrade layer was tested using the SSG, DCP, and NDG.

Gils Way development project, which uses a soil-lime mixture, is also located in Cross Plains, WI. The construction section was approximately 400 m long. An approximately 400-mm thick soil-lime mixture layer was generated by mixing lime into the subgrade. Because of the time constraint, only the SSG was performed before the liming process, i.e., on the untreated subgrade. The SSG and DCP were performed after the liming process, i.e., on the lime-stabilized subgrade layer.

Eight highway construction sites that involved use of only natural earthen materials were from different soil regions of Wisconsin. The sites consist of STH 26, STH 100, STH 44, USH 12, STH 131, STH 58, STH 154, and USH 2. Table 3.3 provides a list of the project characteristics of these sites. The SSG, DCP, and NDG were performed on the exposed subgrade soils that were either compacted (six sites) or had not been re-compacted (two sites).

An experimental installation of large diameter (1.2 m) high density polyethelene (HDPE) culvert pipe project is located in Northwestern Wisconsin on CTH E between STH 48 and CTH W (northeast part of the county). This project has been conducted by

Table 3.3. Project Characteristics of Highway Construction Sites

Project Designation	Location	Type of Project	Project/Test Section Length	State of Compaction
STH 26	Rosendale	Reconstruction	152 m	Not re-compacted
STH 100	Milwaukee	New construction	305 m	Compacted
STH 44	Ripon	Reconstruction	150 m	Not re-compacted
USH 12	Middleton-Sauk City	Reconstruction	27.2 km	Compacted
STH 131	Rockton-Ontario	Reconstruction	5.8 km	Compacted
STH 58	Ithaca-Cazenovia	Reconstruction	5.8 km	Compacted
STH 154	STH 58-East County Line	Reconstruction	5.8 km	Compacted
USH 2	Iron River	Reconstruction	9.6 km	Compacted

Note: Types of subgrade soils are listed in Table 3.1.

WisDOT in order to investigate the cost of the materials, installation, life cycle costs, construction, and performance issues as compared with standard metal and concrete pipes. After removal of the existing pipe, the bed was prepared with a 0.45 m lift of sand and compacted prior to the placement of the first pipe sections. Five lifts of sand were then backfilled and compacted in 0.3-m increments and three more lifts of sand of approximately 0.45 m were placed and compacted up to the roadway level. The SSG, DCP, and NDG were used to evaluate the soil properties of each lift.

The construction of the cap over a lagoon filled with wastewater treatment sludge was located at the Madison Metropolitan Sewerage District (MMSD). The cap was constructed using a wood chip-soil mixture, which provided a lightweight working platform. The description of the sludge lagoons capping project is given in Edil and Aydilek (2001). The SSG and the sand cone density tests were respectively used to evaluate the stiffness and unit weight of the cap at the site.

3.2.2 In Situ Measurements and Testing Procedures

A Humboldt SSG manufactured by Humboldt Mfg. Co. was used to measure the in-situ stiffness properties of the pavement materials in this study. The SSG stiffness measurements were made in accordance with ASTM D6758. The SSG assesses near-surface stiffness with a maximum depth of approximately 300 to 380 mm. Sawangsuriya et al. (2002) and Sawangsuriya et al. (2003) reported that the depth of measurement significance ranges from 125 to 178 mm, where the higher stress-strain conditions occur within the measurement zone (i.e., 125 to 300 mm) and this is also beyond a blind zone that exists at less than 125 mm in SSG measurements. These findings were based on granular soils, but similar conditions can also be expected in fine-grained (cohesive) soils.

A DCP manufactured by Kessler Soils Engineering Products, Inc. was used to measure the in-situ strength index properties of the pavement materials in this study. DCP penetration index (DPI), in millimeters per blow, which can be used to estimate the shear strength characteristics of soils, was calculated in accordance with ASTM D6951. The DCP is typically used to assess the material properties to a depth of 1m below the ground surface. The size of the cone tip relative to the average grain size of the material

that is penetrated is found to influence the penetration resistance (Konrad and Lachance 2001). This is because of the number of grains that come into contact with the face of the cone and the failure surface. Therefore, the DCP cannot be used in very coarse-grained materials containing a large percentage of aggregates greater than 50 mm, or in highly stabilized or cemented materials.

The nuclear density gauge (NDG) was used to measure in-place dry unit weight and moisture content of the soil. NDG measurements were made in accordance with ASTM D2922. In this study, two probe depths: 203 mm or 305 mm were used. The soil samples were also taken from the field where the tests were performed and were brought to the laboratory for moisture content determination in accordance with ASTM D2216.

The sand cone density test (ASTM D1556) was used to measure in-place unit weight of the cap material constructed using a wood chip-soil mixture at the sludge lagoon test site, MMSD project. The soil samples were also collected from this site for moisture content determination.

At all test sites, the SSG measurements were made prior to the other companion tests. The NDG or sand cone test was performed at the exact location of the SSG measurement. The DCP was performed at approximately 0.30 m from the NDG measurement location. The soil samples were collected after all tests were completed. Table 3.4 provides a summary of the field testing program.

Table 3.4. Summary of the Field Testing Program

Site	Location	County	In Situ Measurement
STH 60 Test Section	Lodi-Prairie du Sac	Columbia	S, D, N[1]
Scenic Edge Development	Cross Plains	Dane	S, D, N[1]
Gils Way Development	Cross Plains	Dane	S, D[2]
STH 26	Rosendale	Fond du Lac	S, D, N
STH 100	Milwaukee	Milwaukee	S, D, N
STH 44	Ripon	Fond du Lac	S, D, N
USH 12	Middleton-Sauk City	Dane	S, D, N
STH 131	Rockton-Ontario	Vernon	S, D, N
STH 58	Ithaca-Cazenovia	Richland	S, D, N
STH 154	STH 58-East County Line	Richland	S, D, N
USH 2	Iron River	Bayfield	S, D, N
CTH E	STH 48-CTH W	Polk	S, D, N
MMSD Project	Madison	Dane	S, SC

Note: S = Soil Stiffness Gauge (SSG); D = Dynamic Cone Penetrometer (DCP); N = Nuclear Density Gauge; SC = Sand Cone
[1] Nuclear density gauge was not performed on subgrades, [2] DCP was not performed on subgrades.

CHAPTER FOUR
EVALUATION OF STIFFNESS AND STRENGTH PARAMETERS

4.1 Analysis of the DCP data

As DCP testing is basically a measure of penetration resistance, expressed as DCP penetration index (DPI), the analysis of the DCP data must be interpreted, following a standardized procedure, to generate a representative value of penetration per blow for the material being tested. This representative value can be obtained by averaging the DPI across the entire penetration depth at each test location. Two methods of calculating the representative DPI value for a given penetration depth of interest are considered: (i) arithmetic average and (ii) weighted average. The arithmetic average can be obtained as follows:

$$DPI_{avg} = \frac{\sum_{i}^{N} (DPI)_i}{N} \tag{4.1}$$

where N is the total number of DPI recorded in a given penetration depth of interest. The weighted average technique uses the following formula:

$$DPI_{wt\,avg} = \frac{1}{H} \sum_{i}^{N} \left[(DPI)_i \cdot (z)_i \right] \tag{4.2}$$

where z is the penetration distance per blow set and H is the overall penetration depth of interest. These two methods are graphically presented in Fig. 4.1 for a lean clay with sand (STH 100 in Table 3.1a). Allbright (2002) reported that the weighted average method yielded a narrower standard deviation for the representative DPI value and provided better correlations with other field tests than the arithmetic average method based on available field data. In this study, the weighted average method is employed to calculate the representative DPI value.

The influence of layers below and above the cone tip must also be considered in the analysis of the DCP data. As cone penetration is associated with the development of a failure surface, the penetration resistance is influenced by the presence of a layer if the cone tip is located within a few cone diameters of the interface of two highly contrasting layers. Little effect on penetration resistance is noticed as the cone tip approaches the interface if both layers have similar properties. The extent of the zone of influence

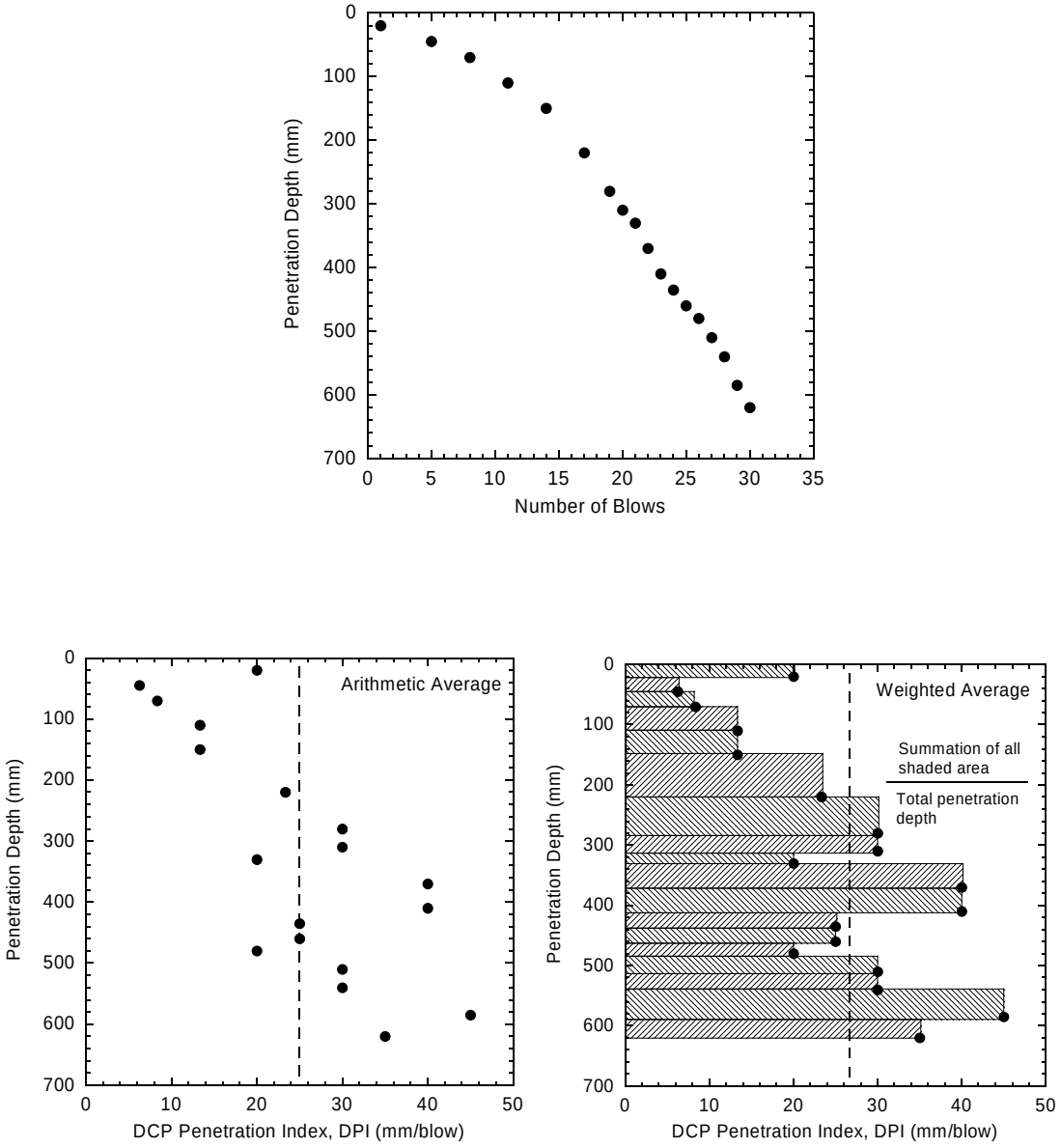

Fig. 4.1. Two methods for calculating the representative DPI value.

depends on the size of the cone, soil type, soil density, stress state, and the contrast in properties of adjacent layers (Konrad and Lachance 2001). The weighted average DPI was calculated over various DCP penetration depths, from the surface to 76, 152, 229, 305, and 381 mm, in the analyses to identify the most representative depth in correlating DPI with SSG stiffness. The only exception was the chemically stabilized soils, where the maximum penetration depth was limited by the thickness of the stabilized layer (i.e., 305 mm). As these selected penetration depths over which the DPI was calculated were generally well within a layer, the DPI obtained is considered to have negligible influence from an interface. It has been shown that vertical confinement (i.e., due to rigid pavement structure or upper granular/cohesive layers) and rod friction (i.e., due to a collapse of the granular material on the rod surface during penetration) may affect DPI values (Livneh et al. 1995). These effects were not an issue in this investigation, because the current study involved only subgrade and subbase evaluation during construction such that the DCP tests were performed directly on the exposed surface of these materials.

4.2 Results of SSG and DCP Measurements

SSG stiffness, DCP penetration index (DPI), dry unit weight, and water content were respectively measured using the SSG, DCP, and NDG along the centerline of the roadway at twelve highway construction sites in Wisconsin. In addition to the highway construction sites, the SSG stiffness and dry unit weight were also measured using the SSG and the sand cone test on the cap over a sludge lagoon, MMSD project. The soil samples were also collected from each site for moisture content determination.

The range of SSG stiffness (in MN/m), DPI (in mm/blow), dry unit weight (in kN/m^3) and water content (in percent) for various test materials from each site is provided in Appendix A. The box plot, along with the sample size and average value, represents 50% of the data with the median value of the variable. The top and bottom of the box mark the limits of ±25% of the variable. The lines extending from the top and bottom of each box mark the minimum and maximum values within the data set that fall within an acceptable range. Any value outside of this range is an outlier, which is shown as an individual point. Note again that the DPI was obtained using the weighted average method. These average DPI values were calculated from the ground surface to the certain depth of interest, i.e., 76, 152, 229, 305, and 381 mm. In the case of chemical stabilized soils, the maximum depth of interest extended to 305 mm (i.e., thickness of base layer). Depending on the test location and type of material at which the measurement was made, the DPI might not be obtained at those depths.

4.2.1 SSG Stiffness

Fig. 4.2(a) and (b) respectively illustrate the SSG stiffness of the earthen materials including granular and fine-grained soils from eleven highway construction sites in Wisconsin. These earthen materials had the overall mean stiffness ranged from 1.1 to 9.3 MN/m, depending solely upon the compaction state and material type. For granular soils, most sites indicated fairly high stiffness. The minimum and maximum stiffness were observed at USH 2 and STH 154, respectively. Note that USH 2 is located in Bayfield County, north of Wisconsin where the soils in this area are known to exhibit very unusual, i.e., bad engineering properties. For fine-grained soils, the highest mean stiffness of about 7.3 was measured at STH 100, because the subgrade had been re-

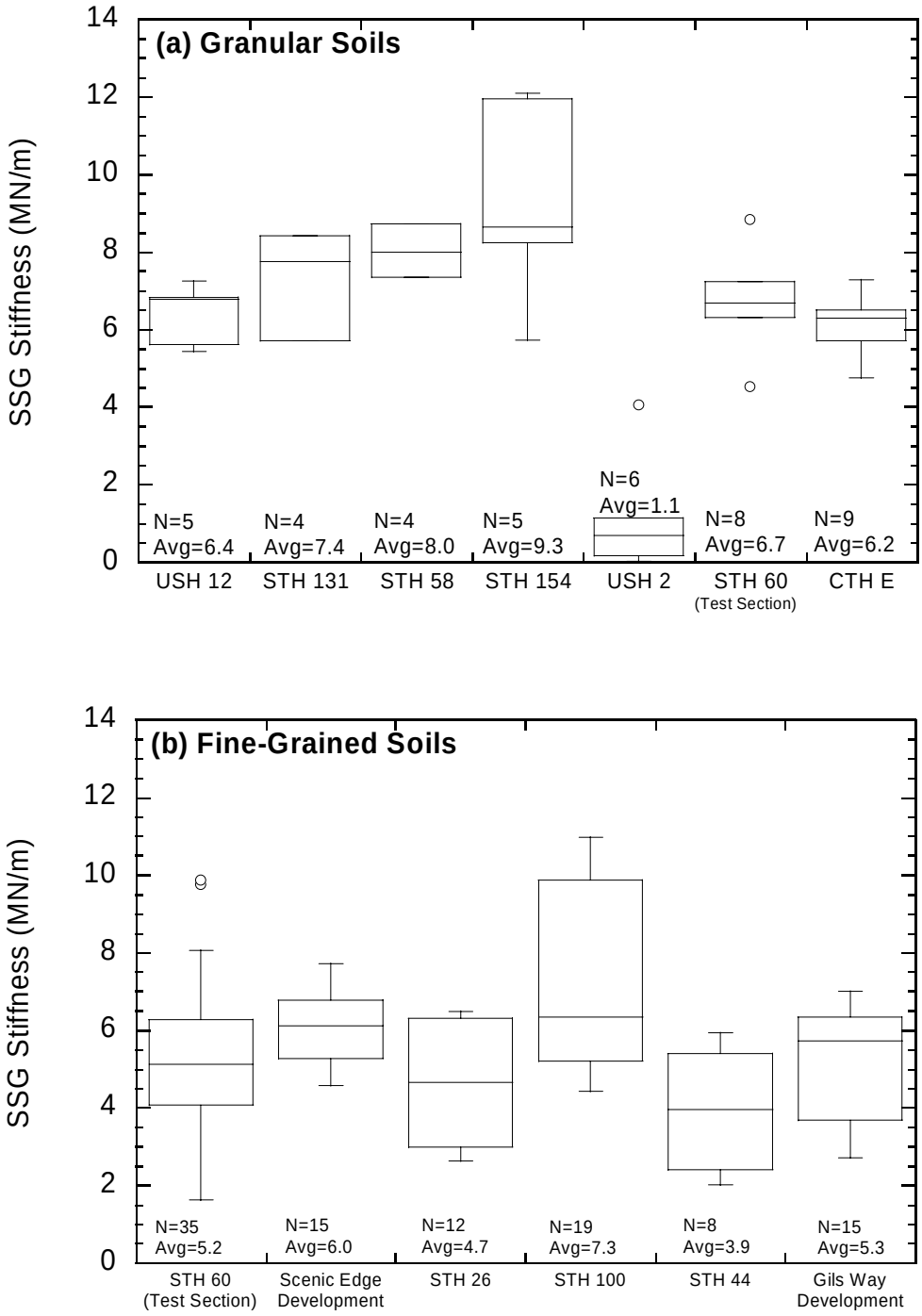

Fig. 4.2. SSG stiffness of granular soils (a) and fine-grained soils (b).

compacted prior to the test. The mean stiffness at other sites was, however, lower as none of them was compacted.

The SSG stiffness of three types of industrial by-products (i.e., bottom ash, foundry sand, and foundry slag) used as alternative soft subgrade reinforcement methods and a cap material (i.e., wood chip-soil mixture) used as a lightweight working platform is shown in Fig. 4.3. Among these by-products, the foundry sand has highest mean stiffness of about 7.7 MN/m. The mean stiffness of foundry slag and bottom ash was about 3.1 and 3.9 MN/m, respectively. The stiffness of the cap material at the sludge lagoon test site, MMSD project was very low with the mean stiffness of only 2.4 MN/m. Note that the stiffness of the cap material at some measurement locations was so small that the SSG could not register any stiffness value as the sensors in the device became overloaded.

The SSG stiffness of chemically stabilized soils including fly ash-stabilized soils and lime-stabilized soils is shown in Fig. 4.4(a) to (c). The stiffness of fly ash-stabilized soils was measured at different curing periods. Fig. 4.4(a) and (b) respectively show stiffness of the fly ash-stabilized soils from two highway construction sites: STH 60 test section and Scenic Edge development in Wisconsin. The mean stiffness of fly ash-stabilized soils during early curing period (less than 3 days) ranged from 13.1 to 14.4 MN/m and after 7- to 11-day curing period, it was increased to be about 15 to 16.5 MN/m (Fig. 4.4(a)). The mean stiffness after 24-hour and 8-day curing periods was 11.9 and 13.1 MN/m, respectively (Fig. 4.4(b)). These results indicated that the stiffness increased with increasing curing periods. For lime-stabilized soils at Gils Way development (Fig. 4.4(c)), the stiffness measurements were conducted before and after the stabilizing soil with lime. The mean stiffness before and after the liming process were about 5.3 and 9.5 MN/m, respectively. Similar to the fly ash-stabilized soils, the stiffness significantly increased after stabilizing soils with lime.

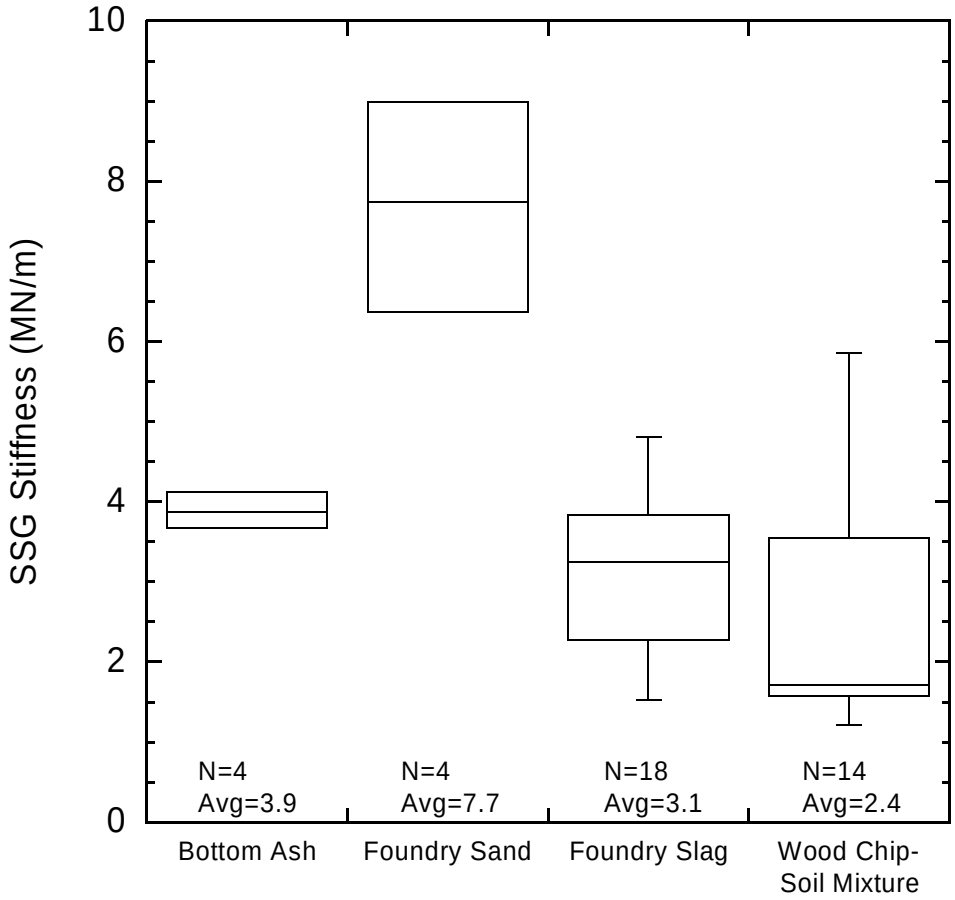

Fig. 4.3. SSG stiffness of industrial by-products and cap material.

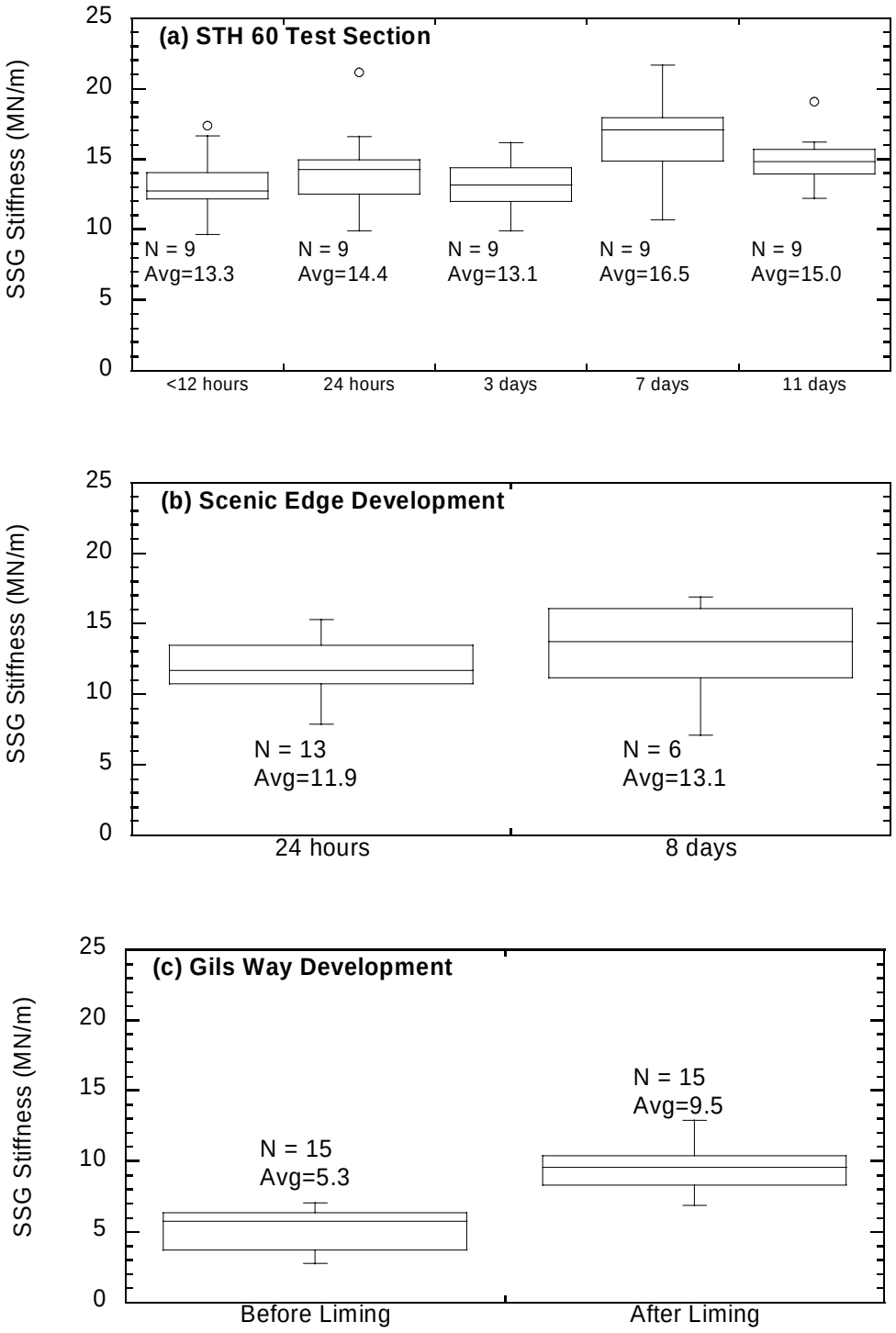

Fig. 4.4. SSG stiffness of chemically stabilized soils: fly ash-stabilized soil (a)-(b) and lime-stabilized soils (c).

Table 4.1 summarizes the results of SSG measurement made. The mean SSG stiffness of various materials is also illustrated graphically in Fig. 4.5. Fly ash-stabilized soils have the highest mean stiffness, which increases with time of curing. For the lime-stabilized soil, the mean stiffness after liming is nearly twice that of the untreated subgrade. These results clearly indicate that the SSG can be used to monitor increase in stiffness due to stabilization reactions. The stiffness of wood chips-soil mixture, which was not compacted deliberately, is the lowest of all materials. In general, the granular earthen materials including breaker run are stiffer than fine-grained earthen materials. Among three types of industrial by-products, foundry sand has the highest stiffness with bottom ash and foundry slag having nearly half its stiffness.

4.2.2 DCP Penetration Index (DPI)

The weighted average of DPI over the whole depth of penetration (less than 75 cm) for granular and fine-grained soils from eleven highway construction sites are shown in Fig. 4.6(a) and (b), respectively. For granular soils, the mean DPIs ranged from 18.8 to 64.8 mm/blow as shown in Fig. 4.6(a). The STH 131 and CTH E soils had considerably wide DPI range, while the USH 2 had the narrowest DPI range. The reason that the STH 131 and CTH E soils showed large DPI variation might be because some DCP data were obtained at greater depths of penetration (i.e., deeper than 75 cm).

For fine-grained soils, the mean DPIs ranged from 28.7 to 83 mm/blow as shown in Fig. 4.6(b). Results indicated that the STH 26 soils had the widest DPI range, whereas the STH 100 soils had the narrowest range. This might be an indication of non-uniformity in the soils. The STH 26 soils had not yet been re-compacted prior to the test and thus results in large DPI variation (i.e., non-uniform soil) and high mean DPI value (i.e., weak soil). On the other hand, the STH 100 soils had been re-compacted and thus results in small DPI variation (i.e., more uniform soil) and low average DPI value (i.e., strong soil). In general, the mean DPIs for fine-grained soils were approximately 54.6 to 65.8 mm/blow.

Table 4.1. Results of SSG Measurement: SSG Stiffness (MN/m)

Material Type	No. of Tests[a]	Mean[b]	Standard Deviation	Standard Error	Maximum	Minimum
Natural Earthen						
Granular	41	6.3	2.68	0.42	12.1	0.0
Fine-grained	104	5.6	1.91	0.19	11.0	1.6
Industrial By-Products						
Bottom Ash	4	3.9	0.20	0.10	4.1	3.7
Foundry Sand	4	7.7	1.07	0.54	9.0	6.4
Foundry Slag	18	3.1	1.03	0.24	4.8	1.5
Fly Ash-Stabilized Soils						
24 hours	22	12.9	2.85	0.67	21.1	7.9
7-8 days	15	15.1	3.75	0.97	21.7	7.1
Lime-Stabilized Soils						
Before Liming	15	5.3	1.44	0.37	7.0	2.7
After Liming	15	9.5	1.59	0.41	12.9	6.8
Cap Material						
Wood Chip-Soil Mixture	14	2.5	1.49	0.40	5.9	1.2

[a] corresponding to total number of test locations in the material category, [b] mean of SSG stiffness for total number of test locations in the material category.

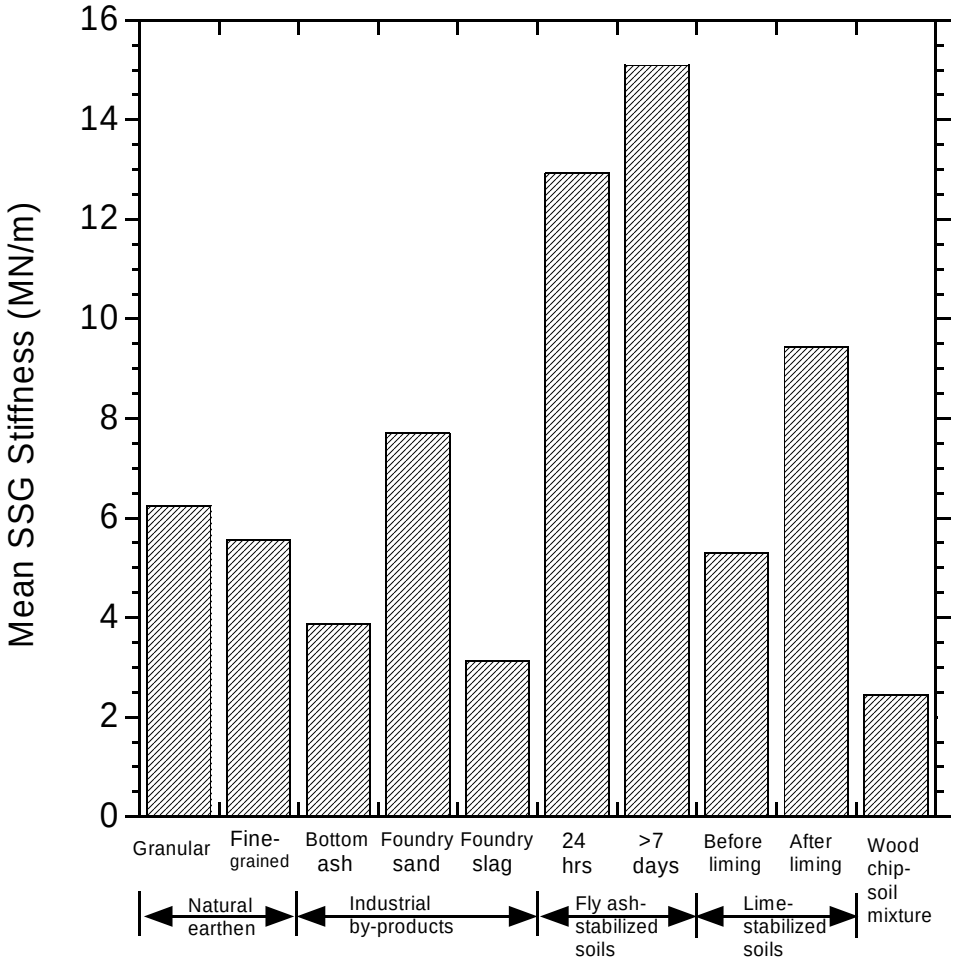

Fig. 4.5. Mean SSG stiffness of various materials.

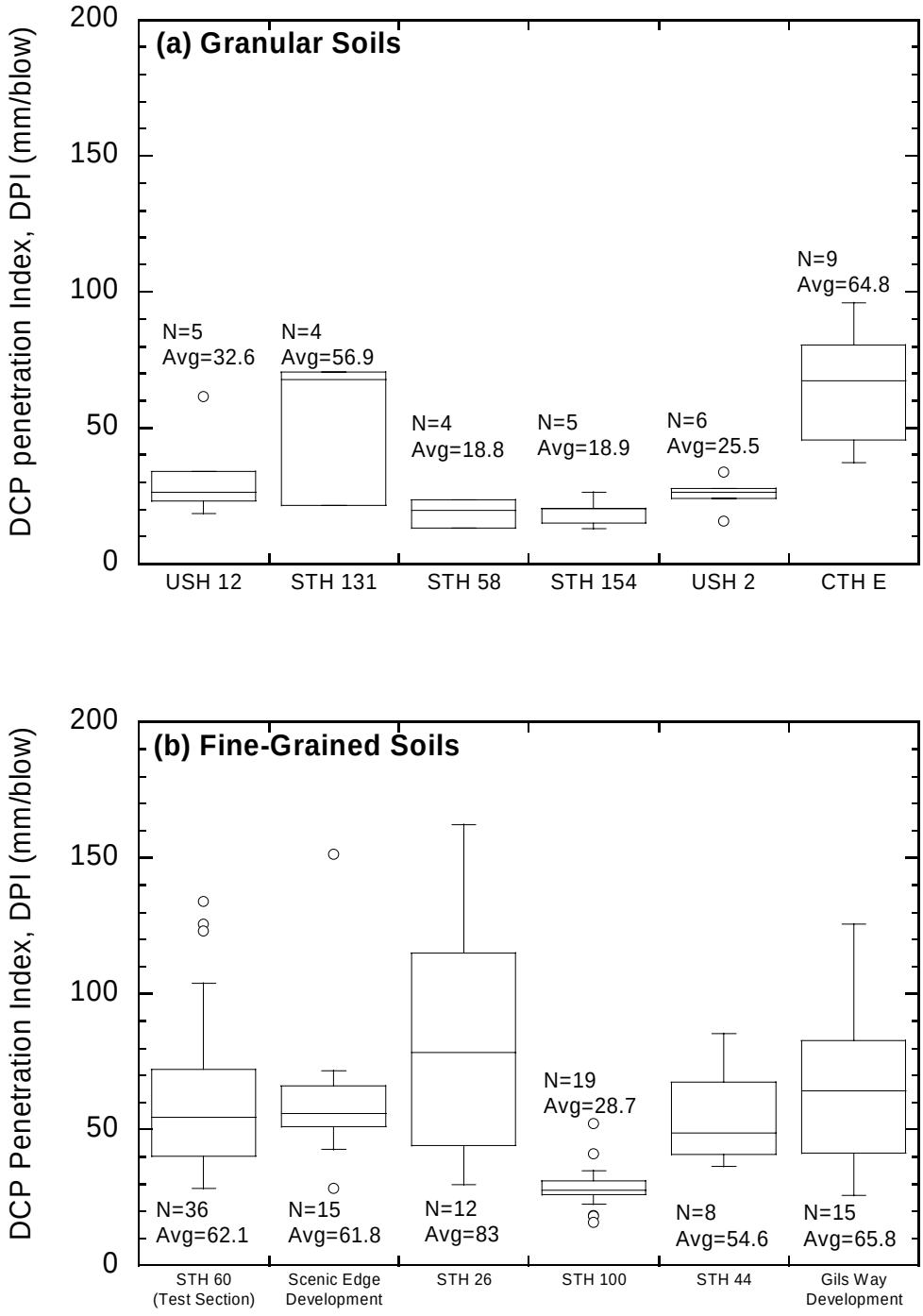

Fig. 4.6. DPI over the whole depth of penetration (less than 75 cm) for granular soils (a) and fine-grained soils (b).

Fig. 4.7 shows the weighted average DPIs of industrial by-products. Results indicated that the foundry sand had the highest mean DPI of 48.9 mm/blows, whereas the bottom ash had the smallest mean DPI of 25.5 mm/blow. The foundry slag had intermediate mean DPI of 30.5 mm/blow.

The weighted average DPI of chemically stabilized soils, i.e., fly ash-stabilized soils and lime-stabilized soils, are shown in Fig. 4.8(a) to (c). For the fly ash-stabilized soils at STH 60 test section (Fig. 4.8(a)), the DPIs were obtained at 3- and 11-day curing periods. The mean DPI measured at 11 days (12.7 mm/blow) were lower than those measured at 3-day curing period (15.1 mm/blow). This indicated that the penetration resistance, which is proportional to the shear strength, of fly ash-stabilized soils increased with increasing curing period. The increase in shear strength of the fly ash-stabilized soils at Scenic Edge development due to stabilization reactions was not as clear as that at STH 60 test section (Fig. 4.8(b)). This might be because of too small number of DCP data. For the lime-stabilized soils at Gils Way development (Fig. 4.8(c)), unfortunately no DPI data was available prior to the liming applications. The mean DPI of soil after lime treatment was about 15.7 mm/blow.

Table 4.2 summarizes the results of DCP measurement made. The mean DPI of various materials is also illustrated graphically in Fig. 4.9. Dynamic cone penetration is controlled primarily by the strength of a material and therefore DPI (amount of penetration per blow) is inversely proportional to shear strength. The patterns exhibited by the DPI, in general, parallel those of the SSG in Fig. 4.5 with some exceptions. For example, by comparing the relative stiffness and strength of industrial by-products and fine-grained soils, the DPI of the three types of industrial by-products indicates that bottom ash is the strongest unlike the case for stiffness where foundry sand is the stiffest. In addition, fine-grained soils are one of the weakest has the lowest strength but its stiffness is not the lowest among all materials. Data in Table 4.1 and 4.2 indicate that the standard error associated with DPI is considerably larger than that of the SSG stiffness.

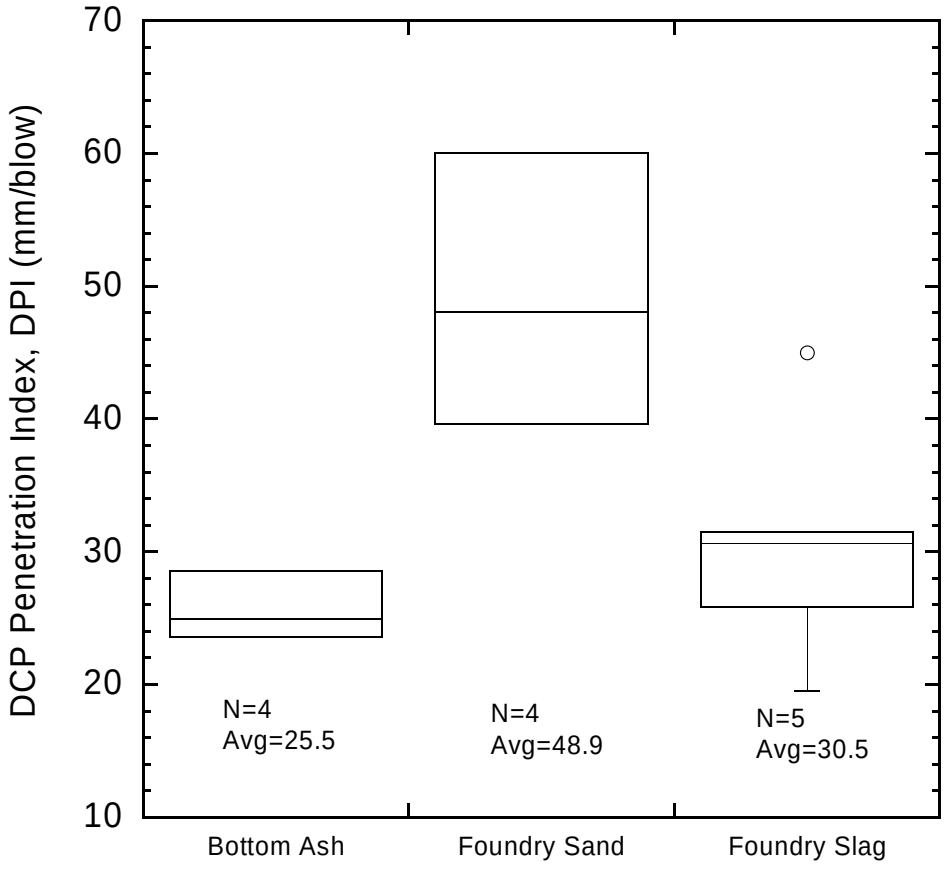

Fig. 4.7. DPI over the whole depth of penetration (less than 75 cm) of industrial by-products.

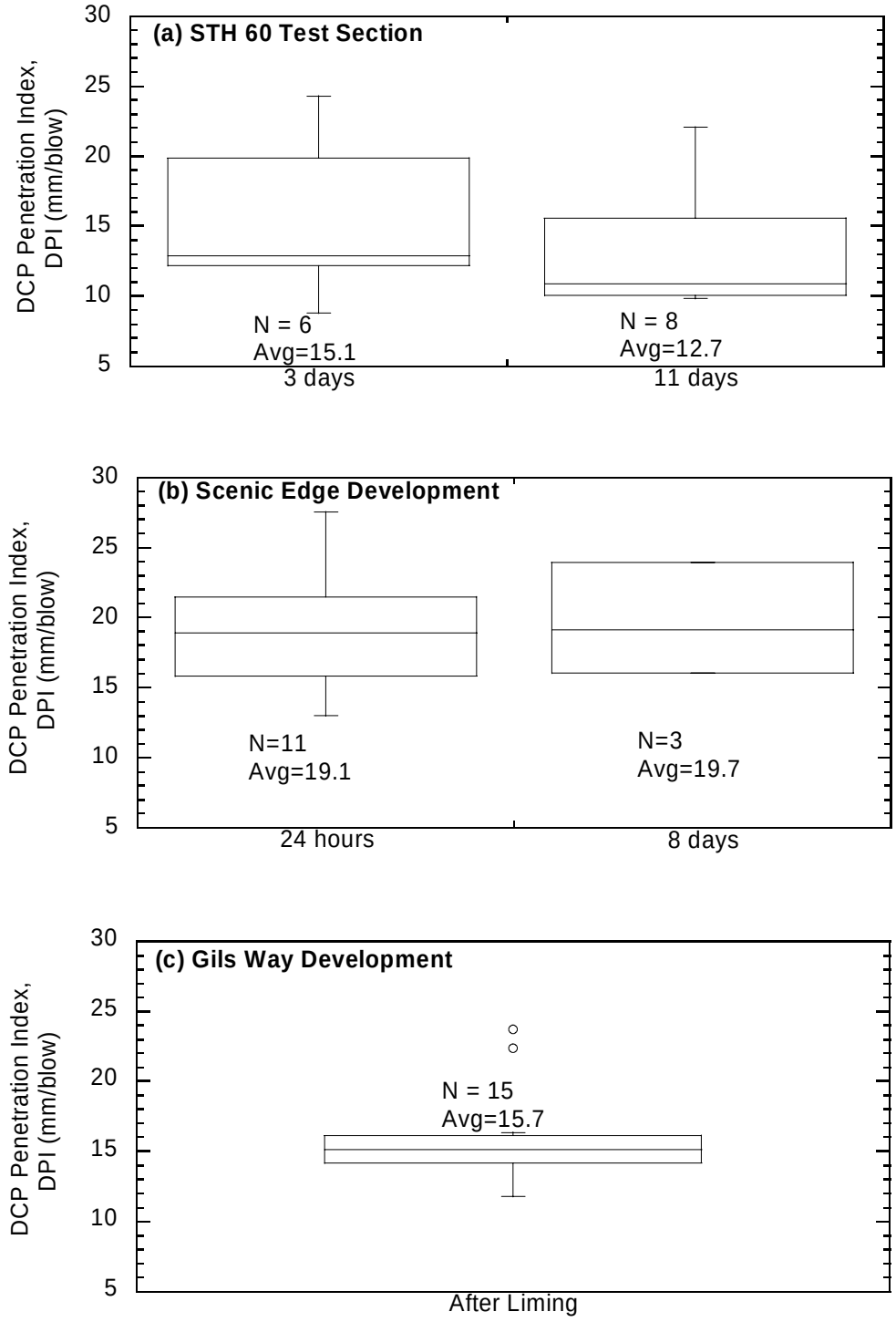

Fig. 4.8. DPI over the whole depth of penetration (less than 75 cm) of chemically stabilized soils: fly ash-stabilized soils (a)-(b) and lime-stabilized soils (c).

Table 4.2. Results of DCP Measurement: DCP Penetration Index (DPI)[a] (mm/blow)

Material Type	No. of Tests[b]	Mean[c]	Standard Deviation	Standard Error	Maximum	Minimum
Natural Earthen						
Granular	33	39.3	24.17	4.21	96.0	12.8
Fine-grained	105	58.4	30.03	2.93	162.0	15.9
Industrial By-Products						
Bottom Ash	4	25.5	2.34	1.17	28.6	23.6
Foundry Sand	4	48.9	8.55	4.27	60.1	39.6
Foundry Slag	5	30.5	9.42	4.20	45.0	19.5
Fly Ash-Stabilized Soils						
24 hours	11	19.1	4.17	1.26	27.5	13.0
8-11 days	11	14.6	5.13	1.55	23.9	9.8
Lime-Stabilized Soils						
After Liming	15	15.7	3.27	0.85	23.7	11.8

Note: DCP tests were not performed on lime-stabilized soils-before liming and wood chip-soil mixture, [a] DPI was calculated by weighted average over the whole depth of penetration (typically less than 75 cm), [b] corresponding to total number of test locations in the material category, [c] mean of weighted average DPI for total number of test locations in the material category

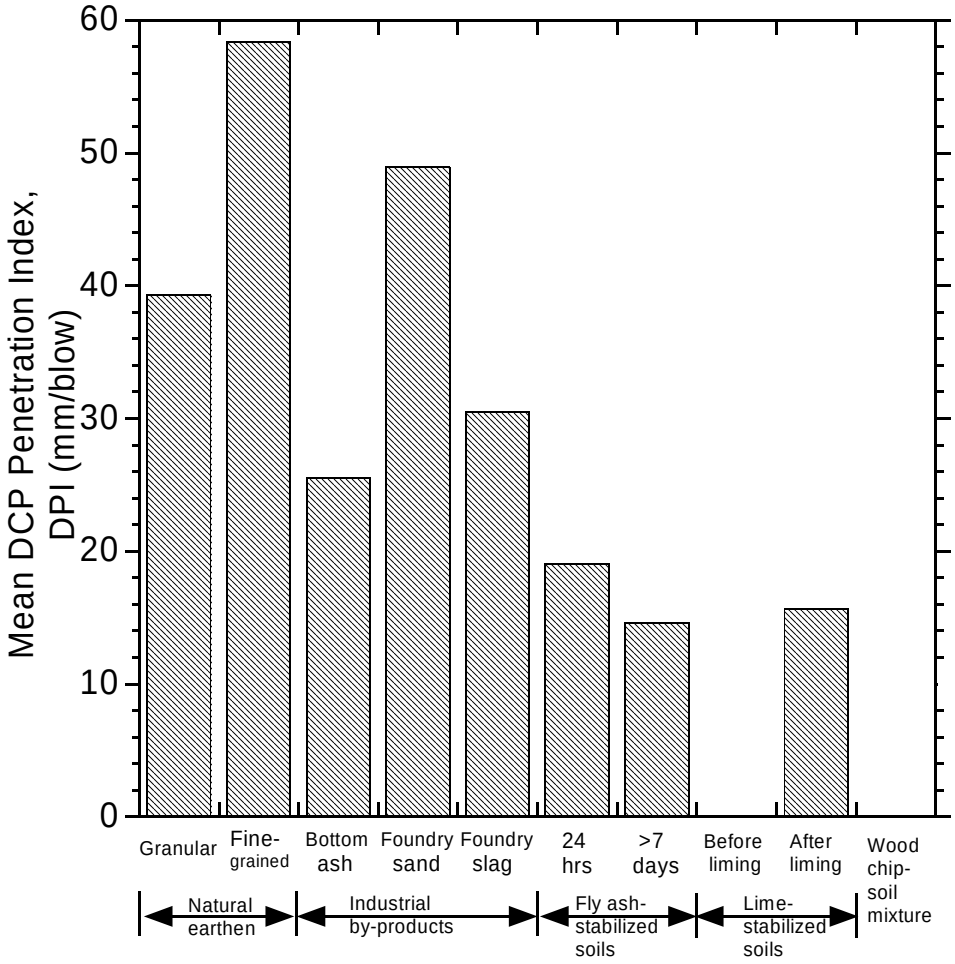

Fig. 4.9. Mean of weighted average DPI of various materials.

4.3 Correlation between SSG Stiffness and Dry Unit Weight/Water Content

The SSG stiffness is plotted against the dry unit weight for various materials in Fig. 4.10. Since the mechanical properties of fly ash-stabilized soils are insensitive to dry unit weight and water content and the USH 2 soils are known as unusual materials, they were excluded from the correlation in this analysis. Even though, there is a considerable scatter in data, a general relationship between the SSG stiffness and dry unit weight for different materials is discernable as shown in Fig. 4.11. The stiffness increased with dry unit weight. This is in agreement with the findings of others (Motan and Edil 1982, Chen et al. 1999a, Yesiller et al. 2000). However, if the data for each group is scrutinized individually, it appears that stiffness depends only partially on dry unit weight since a given material with the same dry unit weight under the same stress conditions still may have highly different stiffnesses depending on moisture content. Because of this reason, the correlation for each individual data set would not be significantly better than the general trend and scatter shown in Fig. 4.11 even if individual data sets were larger.

Water content was determined both using a nuclear density gauge (NDG) and gravimetric measurements on oven-dried samples in the laboratory. Fig. 4.12 illustrates the comparison between laboratory and NDG water content. The NDG test tends to underestimate the water content of clayey soils and foundry slag. The relationship between stiffness and water content is shown in Fig. 4.13 and Fig. 4.14. To discern the effect of water content on stiffness, the natural earthen materials were classified into two main categories: (1) predominantly coarse-grained, i.e., sandy soils (SC, SC-SM, and SP-SM) and (2) predominantly fine-grained, i.e., clayey soil (CL) according to the Unified Soil Classification System (USCS). The other materials including industrial by-products (i.e., foundry sand, foundry slag, and bottom ash), fly ash-stabilized soils, and cap material (i.e., wood chip-soil mixture) were treated separately. The stiffness-NDG water content and the stiffness-laboratory water content relationships for the sandy soils (SC, SC-SM, and SP-SM) are illustrated in Fig. 4.13(a) and Fig. 4.13(b), respectively. The results indicate that the relationship exhibits two patterns as shown in Fig. 4.13(a). The maximum stiffness occurs at a water content of about 5%. The stiffness decreases for water contents higher and lower than this critical value. However, this pattern is not as clear with the laboratory water content (Fig. 4.13(b)).

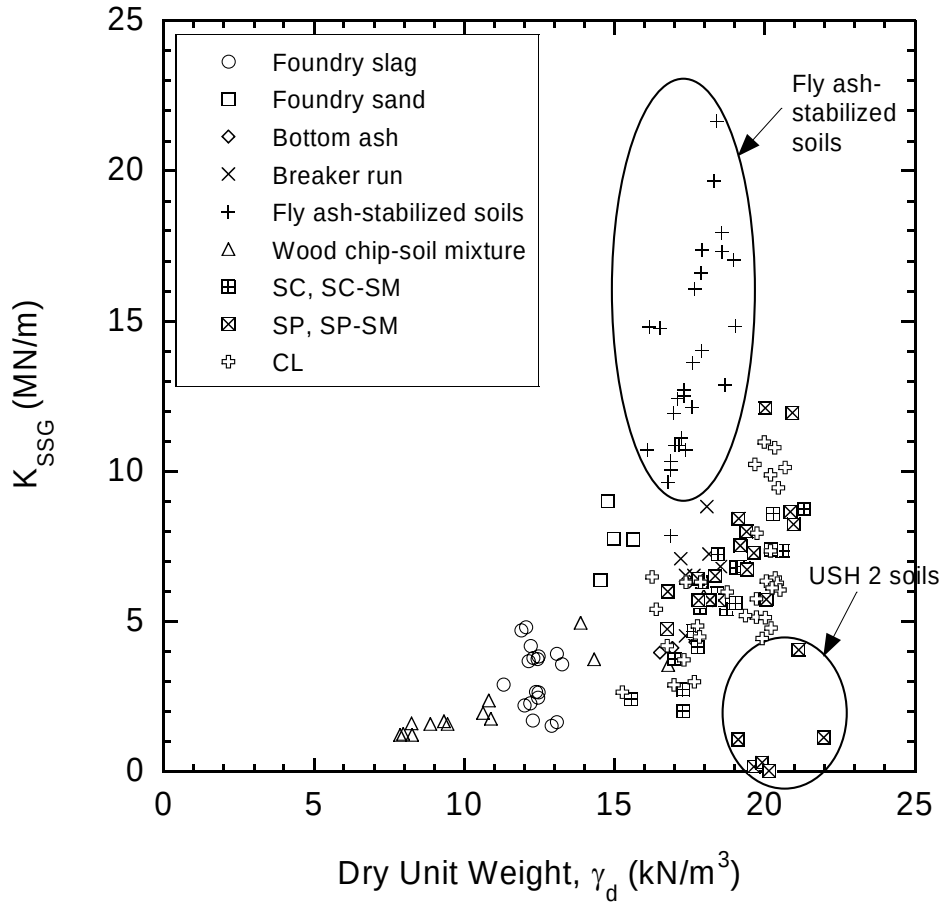

Fig. 4.10. SSG stiffness vs. dry unit weight relationship for various materials.

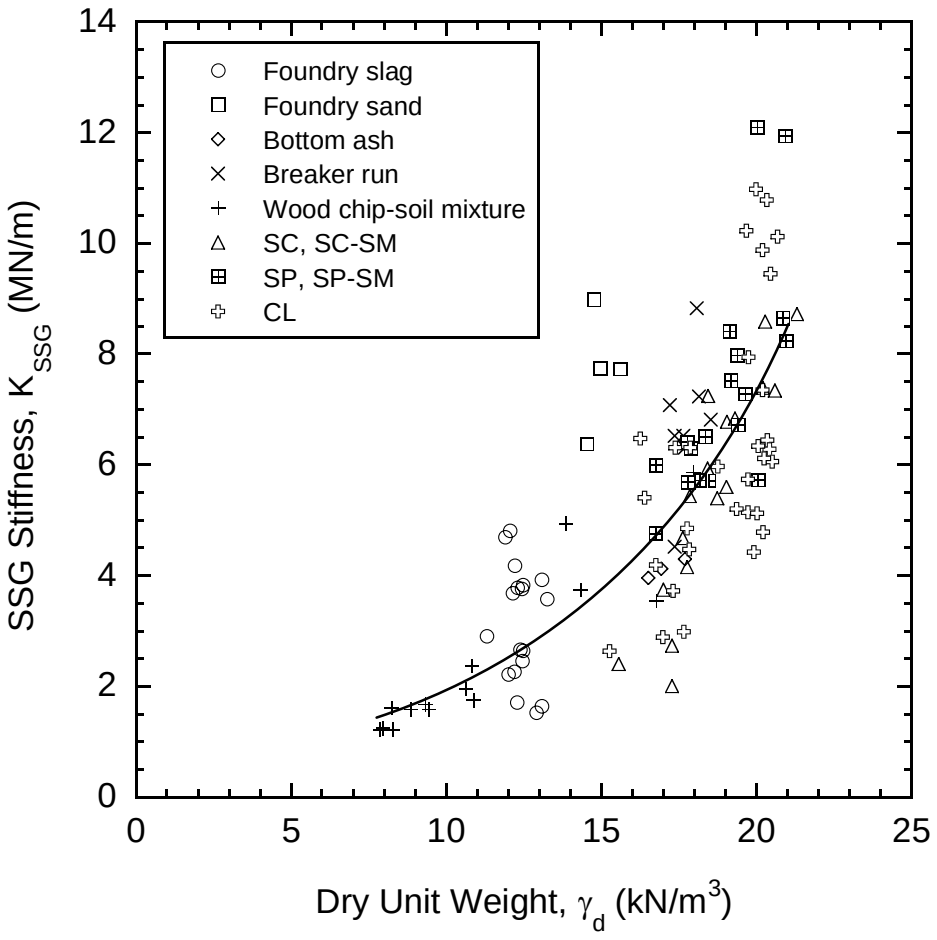

Fig. 4.11. General relationship between SSG stiffness and dry unit weight.

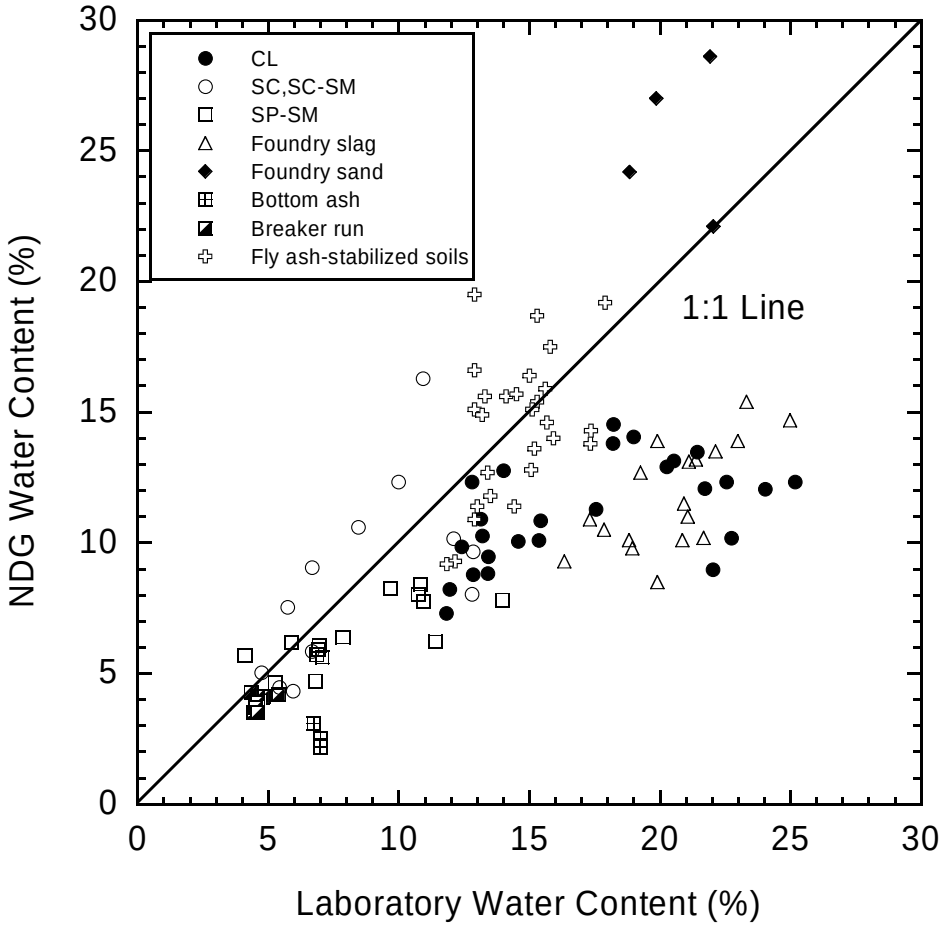

Fig. 4.12. Comparison between laboratory and NDG water content.

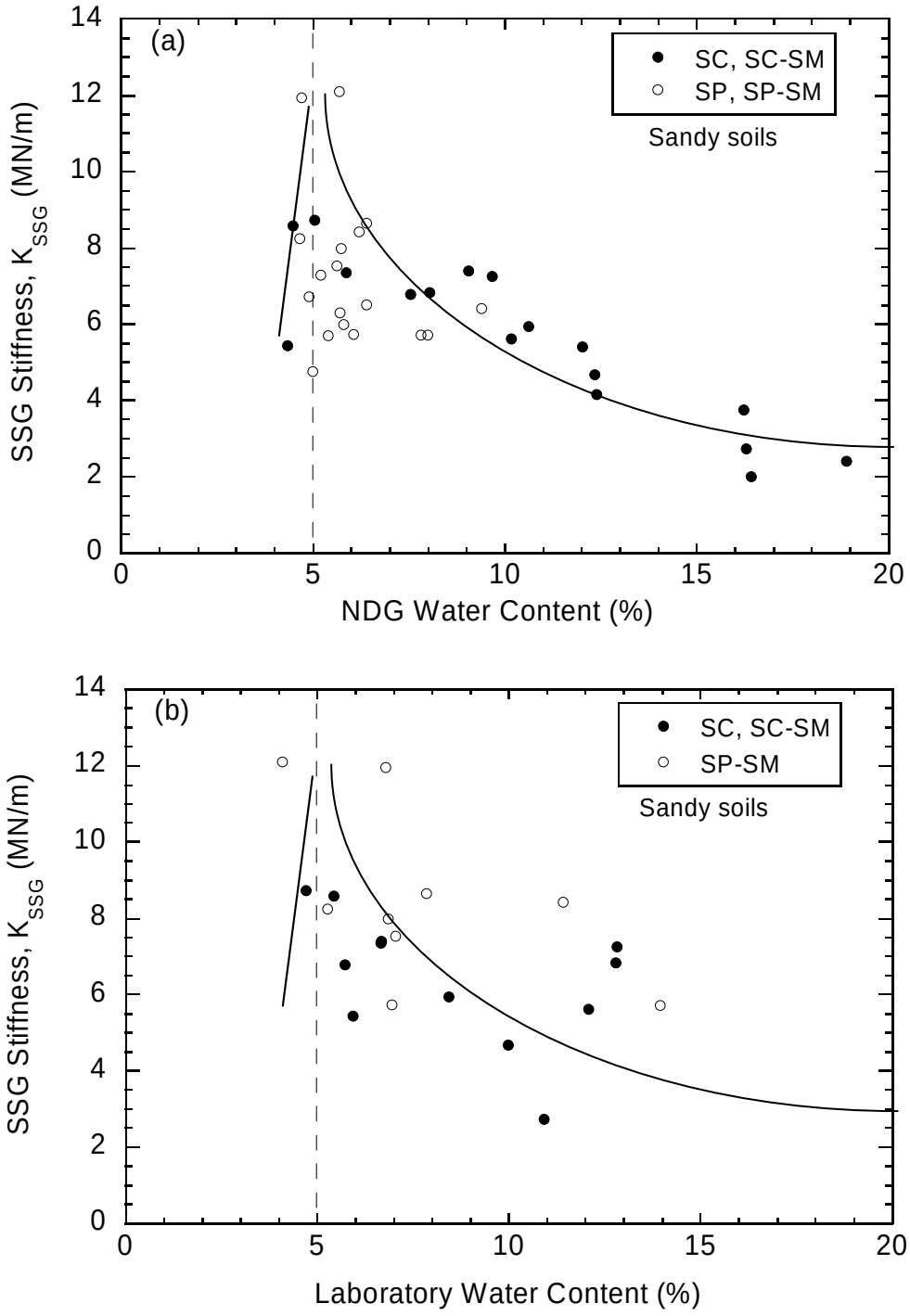

Fig. 4.13. SSG stiffness vs. NDG water content relationship (a) and SSG stiffness vs. laboratory water content relationship (b) for the sandy soils.

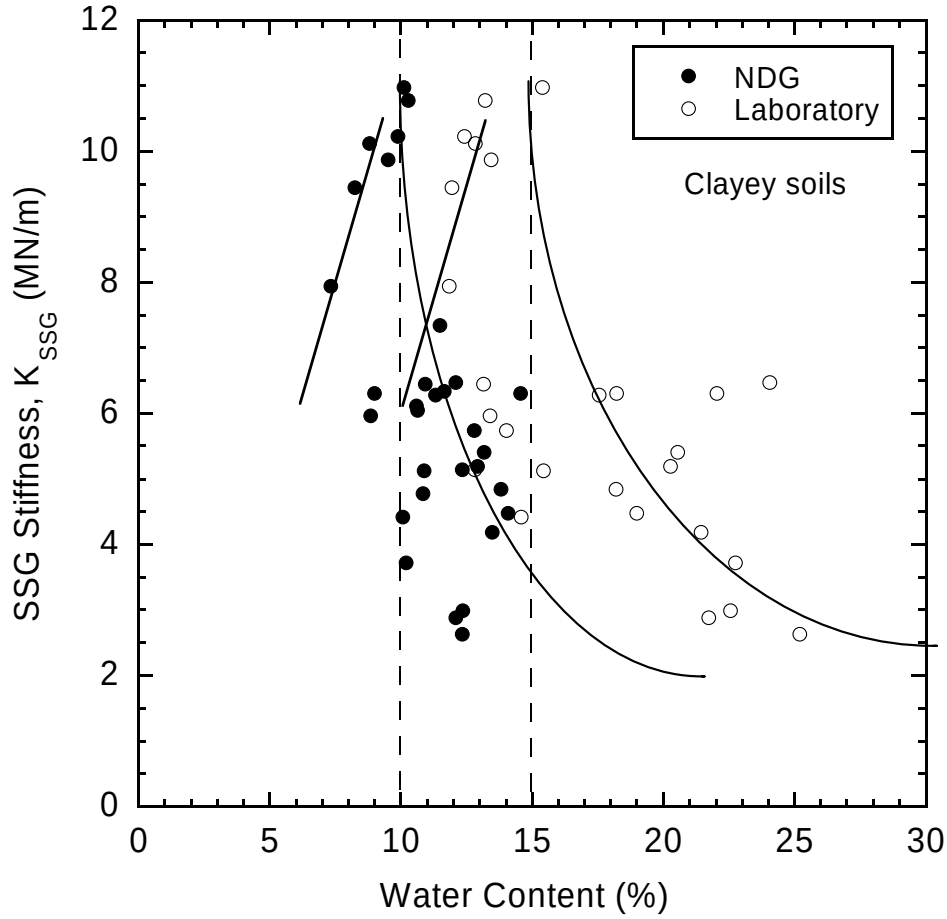

Fig. 4.14. SSG stiffness vs. water content relationship for the clayey soils.

For the clayey soils (CL), a similar trend was also observed as illustrated in Fig. 4.14. The maximum stiffness occurs at about 10% NDG water content and about 15% laboratory water content. This difference is attributable to underestimation of water content by the NDG for CL soils as shown in Fig. 4.12. The observed behavior is consistent with the behavior reported first by Edil et al. (1981) and Motan and Edil (1982) as well as others (Wu et al. 1984, Qian et al. 1993, Yuan and Nazarian 2003) for both granular and cohesive soils.

The stiffness-NDG water content and the stiffness-laboratory water content relationships for industrial by-products, breaker run, fly ash-stabilized soils, and cap material are shown in Fig. 4.15(a) and (b). These materials exhibited no such pattern (i.e., nearly insensitive to the change in water content and stiffness).

Since it becomes clear that the water content or dry unit weight alone does not control stiffness, the SSG stiffness is also regressed with both water content and dry unit weight. A three-dimension (3-D) relationship of SSG stiffness (K_{SSG}), water content (w), and dry unit weight (γ_d) is examined based on three categories: (1) sandy soils including SC, SC-SM, and SP-SM, (2) clayey soils (CL), and (3) all sandy and clayey soils combined. The relationship obtained for sandy soils is best expressed by the following equation:

$$K_{SSG} = -6.77 - 0.25w + 0.82\gamma_d \quad (4.3)$$

The multiple linear regression of this relationship has coefficient of determination (R^2) of 0.74 and standard error (S_e) of 1.34. The relationship obtained for clayey soils is best expressed by the following equation:

$$K_{SSG} = -0.32 - 0.44w + 0.61\gamma_d \quad (4.4)$$

The multiple linear regression of this relationship has R^2 = 0.43 and S_e = 1.83. Finally, in the case of all sandy and clayey soils combined, the relationship obtained is best expressed by the following equation:

$$K_{SSG} = -4.48 - 0.28w + 0.72\gamma_d \quad (4.5)$$

The multiple linear regression of this relationship has R^2 = 0.57 and S_e = 1.60. For all these three categories, the significance of individual coefficients was tested using

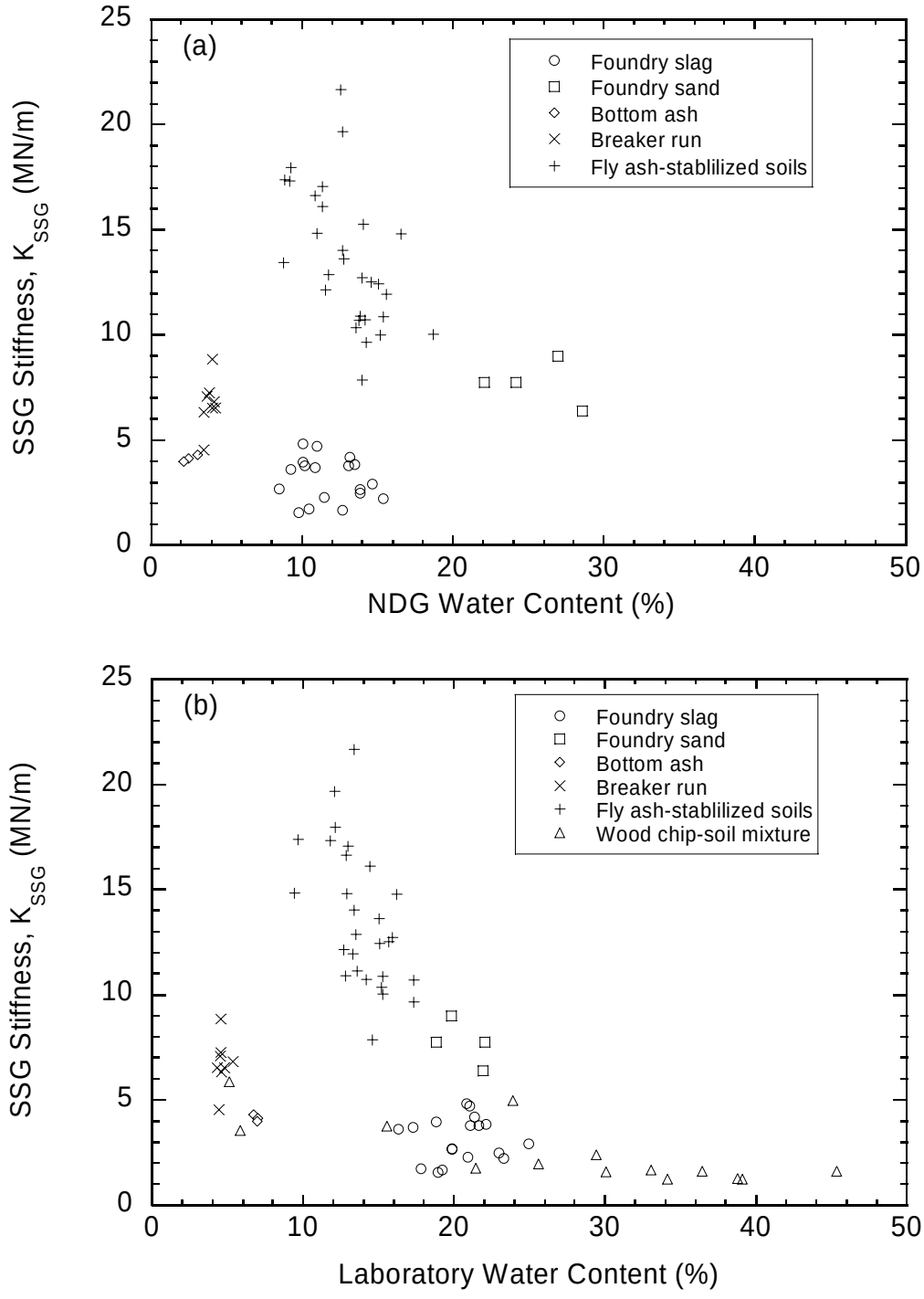

Fig. 4.15. SSG stiffness vs. NDG water content relationship (a) and SSG stiffness vs. laboratory water content relationship (b) for industrial by-products, breaker run, fly ash-stabilized soils, and cap material.

t-test. At a confidence level of 95%, both of the estimated coefficients are significant, i.e., t-statistic > 1.96 or p-value < 0.05.

4.4 Correlation between DPI and Dry Unit Weight/Water Content

DPI, which is regarded to be inversely proportional to shear strength, was also investigated in terms of dry unit weight and water content. The weighted average of DPI was determined at different penetration depths: 76, 152, 229, and 305 mm and plotted in semi-logarithmic scale against dry unit weight and water content as shown in Fig. 4.16 to Fig. 4.23. Note again that two probe depths, 203 mm and 305 mm, were used for the nuclear density tests. The DPI-dry unit weight relationship (Fig. 4.16 to Fig. 4.19) suggests that DPI decreases (or shear strength increases) with increasing dry unit weight. There is a significant dispersion of the DPI vs. dry unit weight data. Although the data for some of the individual materials suggest that DPI decreases (or shear strength increases) with increasing dry unit weight, there is no apparent trend when all of the data are considered.

The DPI-nuclear density gauge (NDG) water content and DPI-laboratory water content relationships are presented in Fig. 4.20 to Fig. 4.23, respectively. A trend of increasing DPI with increasing water content is discernable for materials containing fine fractions. In other words, shear strength, which is also directly related to commonly used California Bearing Ratio (CBR), decreases with increasing water content. The average DPIs determined at these depths, in general, exhibited a similar pattern. These observations are in agreement with the well-established strength-water content relationship for soils (Turnbull and Foster 1956, Seed and Chan 1959, Black 1962, and Motan and Edil 1982). The mechanical properties of fly ash-stabilized soils again are shown to be insensitive to dry unit weight and water content.

Similar to stiffness, the water content or dry unit weight alone does not control strength, the strength index in term of weighted average DPI over a DCP penetration depth of interest is regressed with both water content and dry unit weight. A three-dimension (3-D) relationship of DPI over a 229-mm penetration depth, water content (w), and dry unit weight (γ_d) is examined based on three categories: (1) sandy soils including SC, SC-SM, and SP-SM, (2) clayey soils (CL), and (3) all sandy and clayey soils

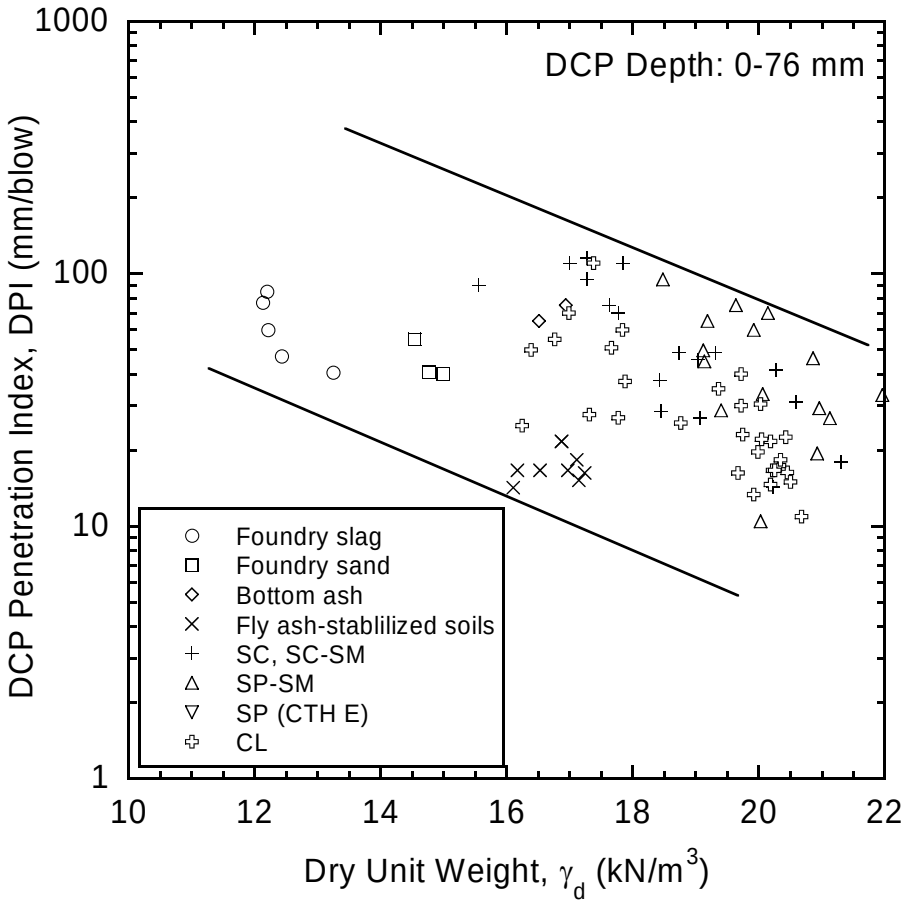

Fig. 4.16. Weighted average DPI at 76 mm vs. dry unit weight relationship for various materials.

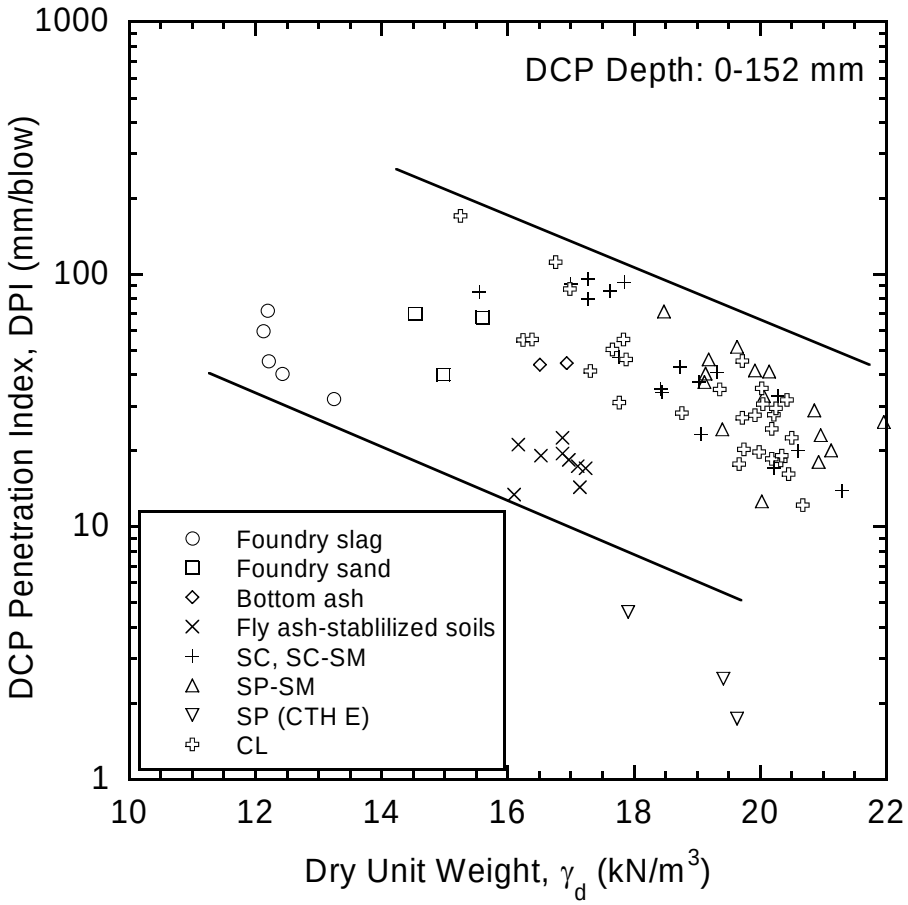

Fig. 4.17. Weighted average DPI at 152 mm vs. dry unit weight relationship for various materials.

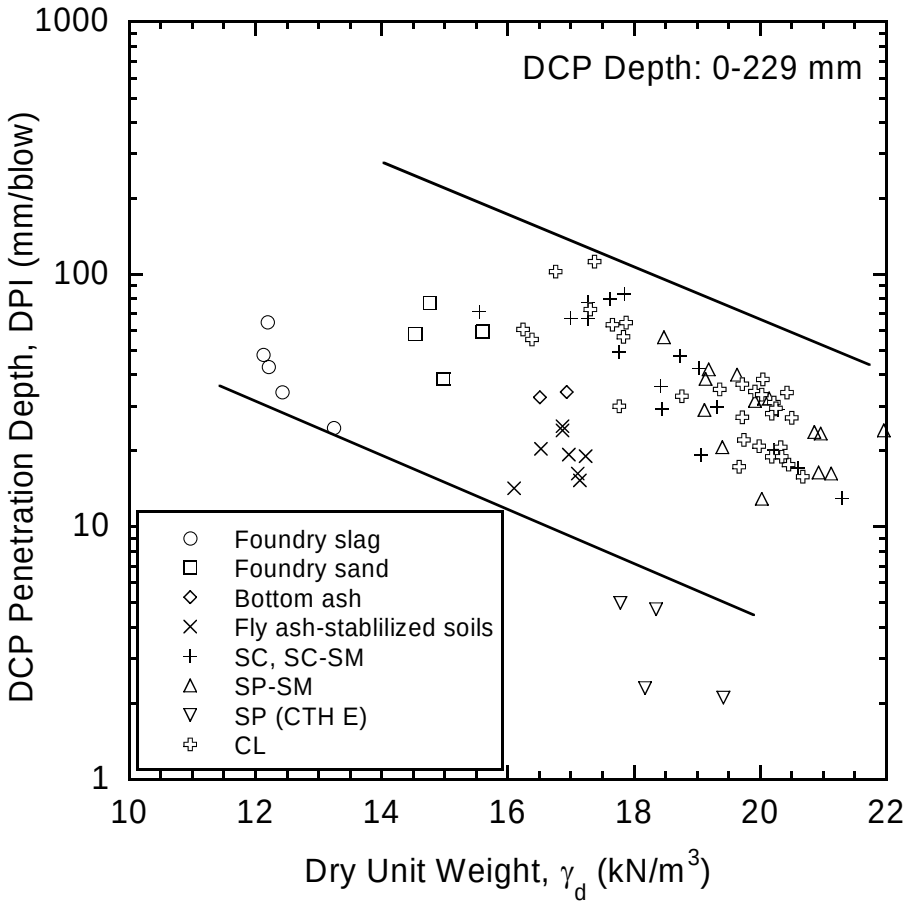

Fig. 4.18. Weighted average DPI at 229 mm vs. dry unit weight relationship for various materials.

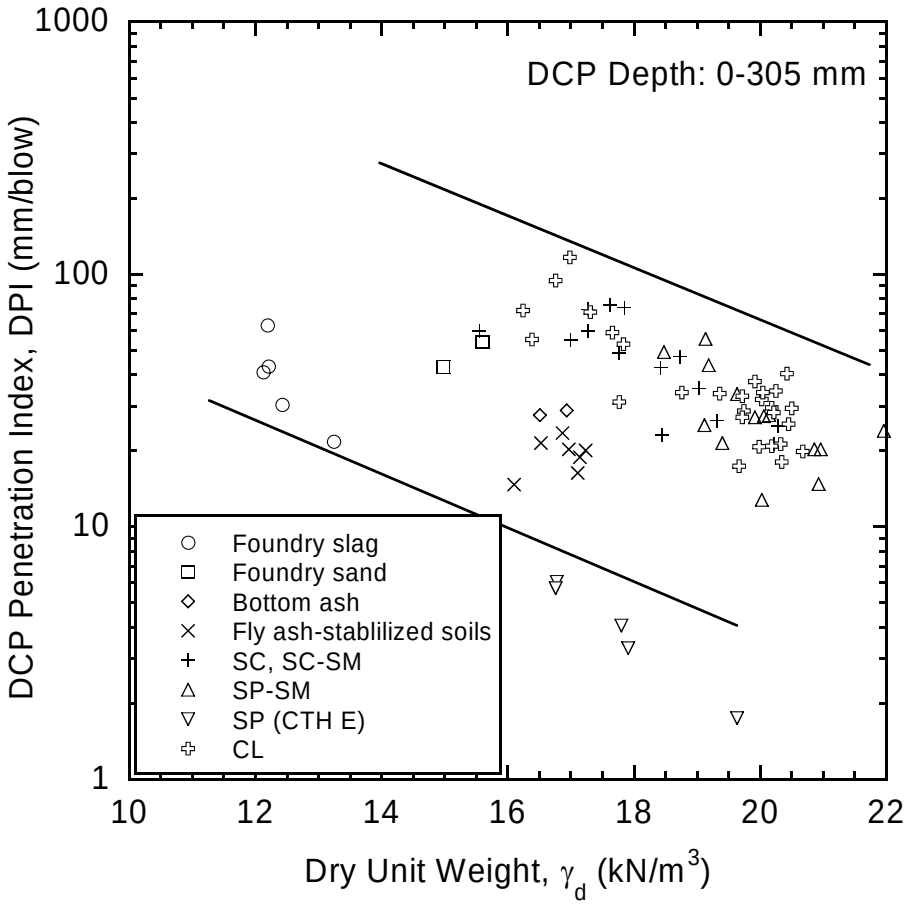

Fig. 4.19. Weighted average DPI at 305 mm vs. dry unit weight relationship for various materials.

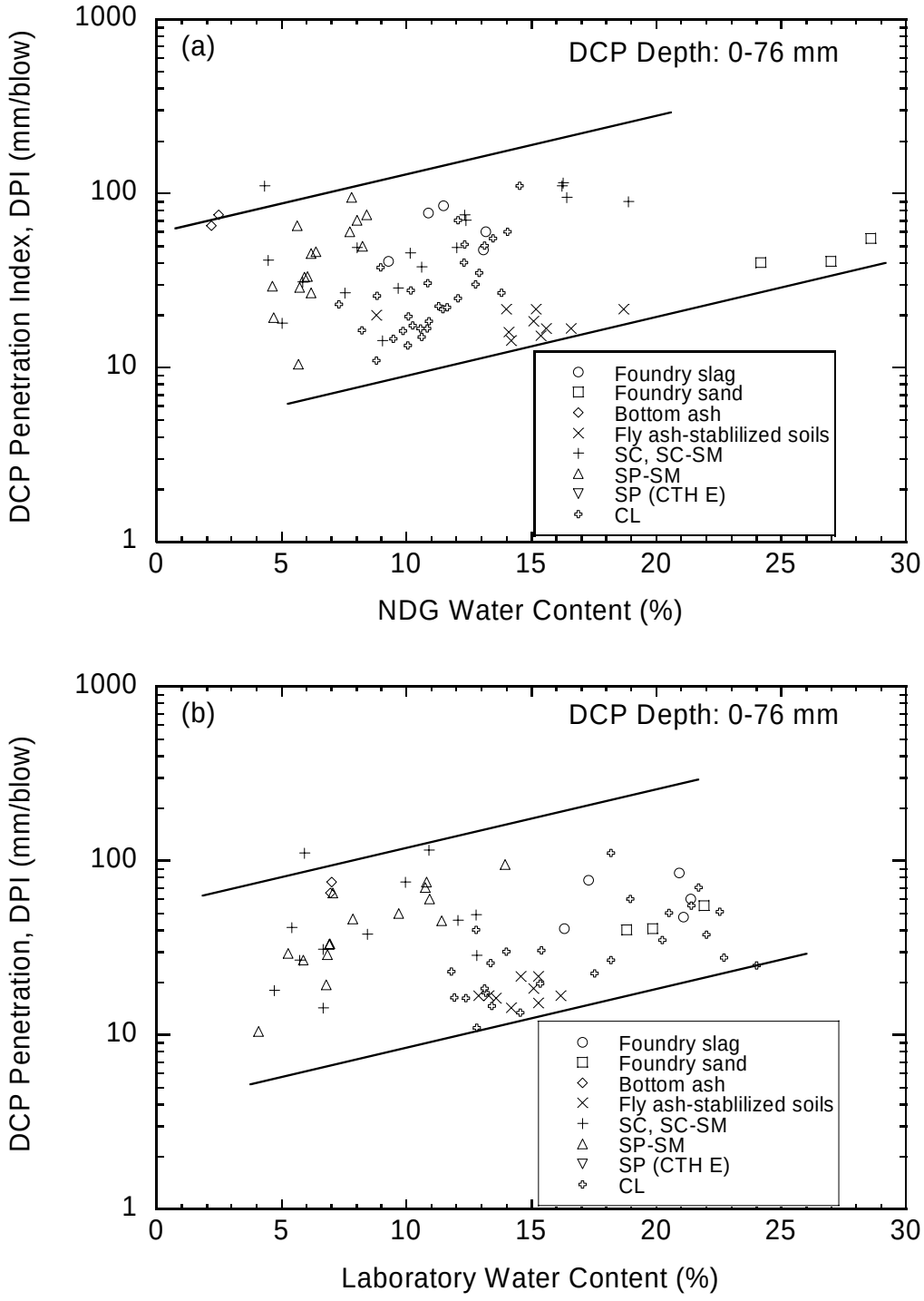

Fig. 4.20. Weighted average DPI at 76 mm vs. NDG water content relationship (a) and weighted average DPI at 76 mm vs. laboratory water content relationship (b) for various materials.

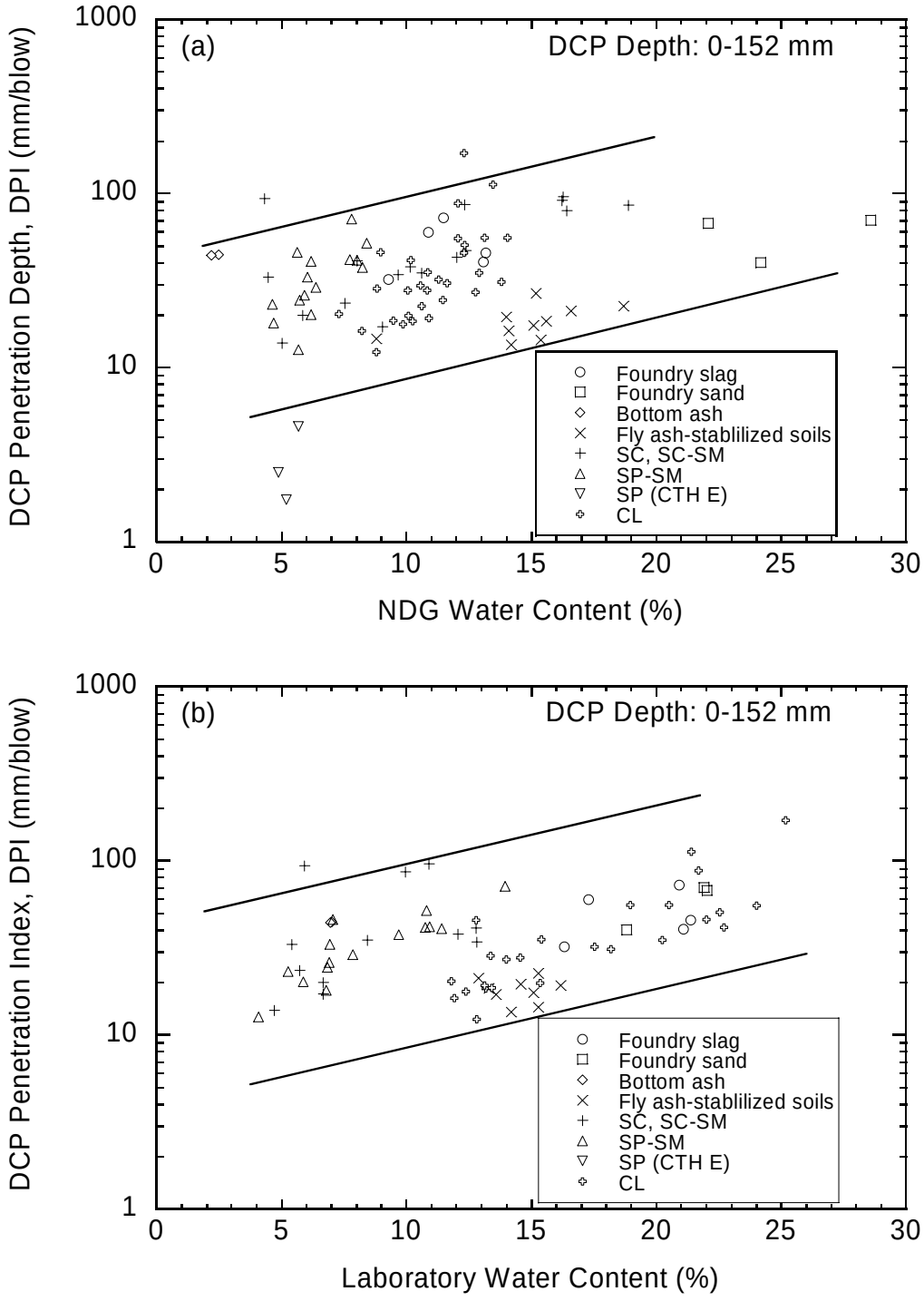

Fig. 4.21. Weighted average DPI at 152 mm vs. NDG water content relationship (a) and weighted average DPI at 152 mm vs. laboratory water content relationship (b) for various materials.

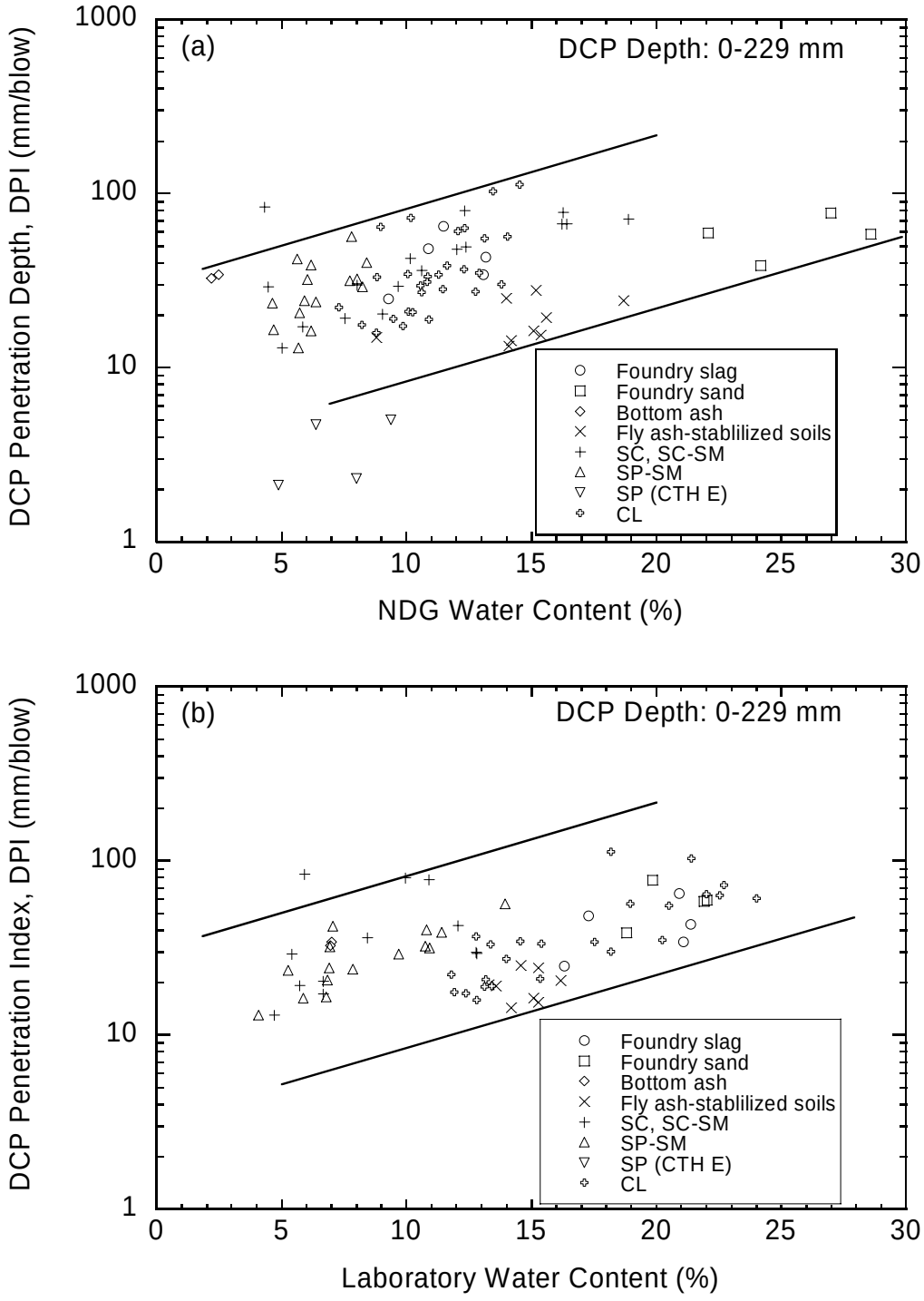

Fig. 4.22. Weighted average DPI at 229 mm vs. NDG water content relationship (a) and weighted average DPI at 229 mm vs. laboratory water content relationship (b) for various materials.

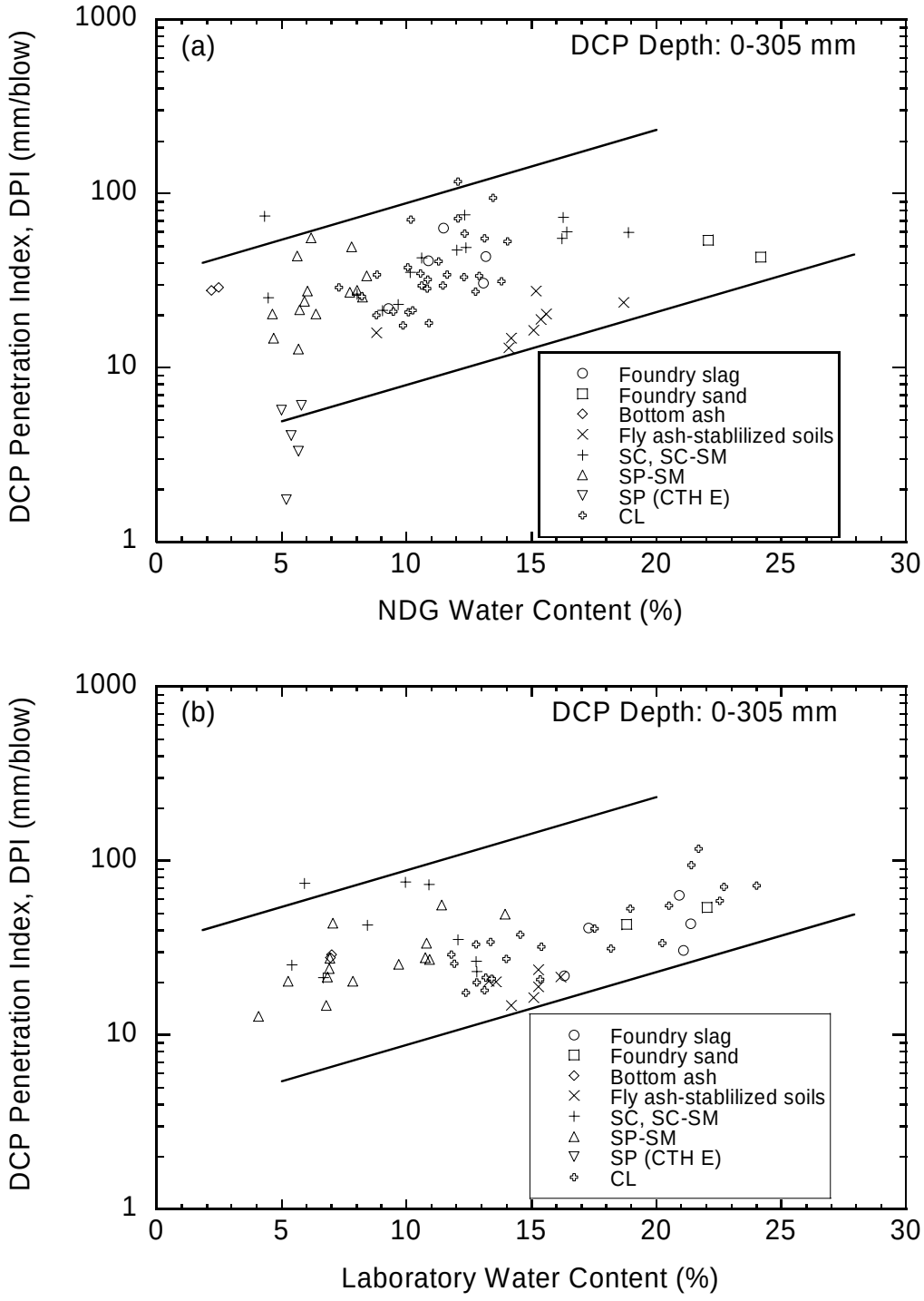

Fig. 4.23. Weighted average DPI at 305 mm vs. NDG water content relationship (a) and weighted average DPI at 305 mm vs. laboratory water content relationship (b) for various materials.

combined. The relationship obtained for sandy soils is best expressed by the following equation:

$$DPI = 338.50 - 0.86w - 15.28\gamma_d \quad (4.6)$$

The multiple linear regression of this relationship has coefficient of determination (R^2) of 0.73 and standard error (S_e) of 12.0. The relationship obtained for clayey soils is best expressed by the following equation:

$$DPI = 242.96 + 2.62w - 12.12\gamma_d \quad (4.7)$$

The multiple linear regression of this relationship has R^2 = 0.66 and S_e = 14.77. Finally, in the case of all sandy and clayey soils combined, the relationship obtained is best expressed by the following equation:

$$DPI = 290.35 + 0.20w - 13.21\gamma_d \quad (4.8)$$

The multiple linear regression of this relationship has R^2 = 0.67 and S_e = 13.58. For all these three categories, the significance of individual coefficients was tested using t-test. At a confidence level of 95%, only the estimated coefficients of dry unit weight is significant, i.e., t-statistic > 1.96 or p-value < 0.05. This might be an indication that the strength index in term of DPI value is more dependent on dry unit weight than the water content; however, additional studies are required to better understand the relationship.

4.5 Correlation between SSG Stiffness and DPI

The correlation of SSG stiffness to DPI is examined based on six material categories: (1) natural earthen materials (both granular and fine-grained soils), (2) granular materials (natural soils, bottom ash, and foundry slag), (3) fine-grained (cohesive) soils, (4) fly ash-stabilized soils, (5) fine-grain materials including fly ash-stabilized soils, and (6) all materials combined including foundry sand. Breaker run is not included because the DCP cannot be performed on this material. Foundry sand exhibits both granular and fine-grained material behavior, so it is only included only in category 6. Table 4.3 summarizes the results of the linear regression analyses between SSG stiffness and log DPI in these material categories. Only those tests that were conducted at the same location are included in the analysis. The coefficient of determination (R^2) examined from the correlations of weighted average DPI calculated over varying DCP penetration depths for all material categories is summarized in Table 4.4. The best relationship for each category is presented as follows:

4.5.1 Natural Earthen Materials

Fig. 4.24 shows the correlation between the SSG stiffness and DPI for natural earthen materials including granular and fine-grained soils. The best correlations (i.e., highest R^2) were obtained when DPI was averaged over a DCP penetration depth of 152 mm. Note that the STH 60 test section and CTH E soils were excluded from the correlation since the measurements were not performed at the exact location. The USH 2 soils were also excluded from the correlation since the soil at this site was known to exhibit very unusual. The relationship is best expressed by the following equation:

$$K_{SSG} = -7.5\log(DPI) + 17.9 \quad (4.9)$$

where K_{SSG} is the SSG stiffness in MN/m and DPI is the DCP penetration index in millimeters per blow. The linear regression of SSG stiffness on average DPI calculated over 152-mm DCP penetration depth has $R^2 = 0.60$ and a standard error (S_e) = 1.44. This error suggests that SSG stiffness can be estimated ± 2.87 from DPI.

Table 4.3. Parameters of Linear Regression Analysis for SSG Stiffness (MN/m) vs. log DPI (mm/blow) Relationship

Material Category	No. of Points	Intercept	Slope	R^2	Standard Error	P-Value
Natural Earthen	79	17.9	-7.5	0.60	1.44	0.00
Granular	27	19.3	-8.3	0.55	1.73	0.00
Fine-Grained Soils	52	17.1	-7.1	0.64	1.28	0.00
Fly Ash-Stabilized Soils	36	26.4	-11.1	0.47	1.92	0.00
Fine-Grained + Fly Ash-Stabilized Soils	89	26.7	-12.7	0.75	2.16	0.00
All Combined (include Foundry Sand)	119	25.6	-12.0	0.72	2.15	0.00

Note: DPI was calculated by weighted average over a penetration depth of 152 mm from the surface except for fly ash-stabilized soils where it was averaged over a penetration depth of 229 mm.

Table 4.4. Coefficient of Determination (R^2) Examined from the Correlations between SSG Stiffness and Weighted Average DPI Calculated over Varying DCP Penetration Depths for all Material Categories

Material Category	Name	DCP Depth (mm)				
		0-76	0-152	0-229	0-305	0-381
Granular + Fine-grained	Natural	0.43	0.6	0.49	0.45	0.26
Granular	Natural (w/ USH 2+CTH E)	0.39*	0.16	0.10	0.07	0.03
	Natural	0.43	0.46	0.47	0.50*	0.20
	Natural+B.ash+F.slag	0.56	0.55	0.49	0.38	0.02
	Natural+B.ash+F.slag+F.sand	0.54	0.45	0.27	0.29	0.05
Fine-grained	Natural (w/ STH60 test section)	0.33	0.38	0.31	0.34	0.26
	Natural	0.43	0.64	0.51	0.53	0.42
	Natural+Fly ash	0.64	0.75	0.73	0.77*	NA
	Natural+Fly ash+F.sand	0.64	0.73	0.70	0.76*	NA
Fly ash-stabilized soils	Fly ash	0.45	0.40	0.47	0.38	NA
All materials combined	All materials	0.61	0.45	0.35	0.31	NA
	w/o CTH E	0.61	0.60	0.52	0.53	NA
	w/o USH 2+CTH E	0.61	0.65	0.59	0.62	NA
	w/o STH60 test section +USH 2+ CTH E	0.64	0.72	0.65	0.68	NA

*Some DPI values were not available
NA = not applicable

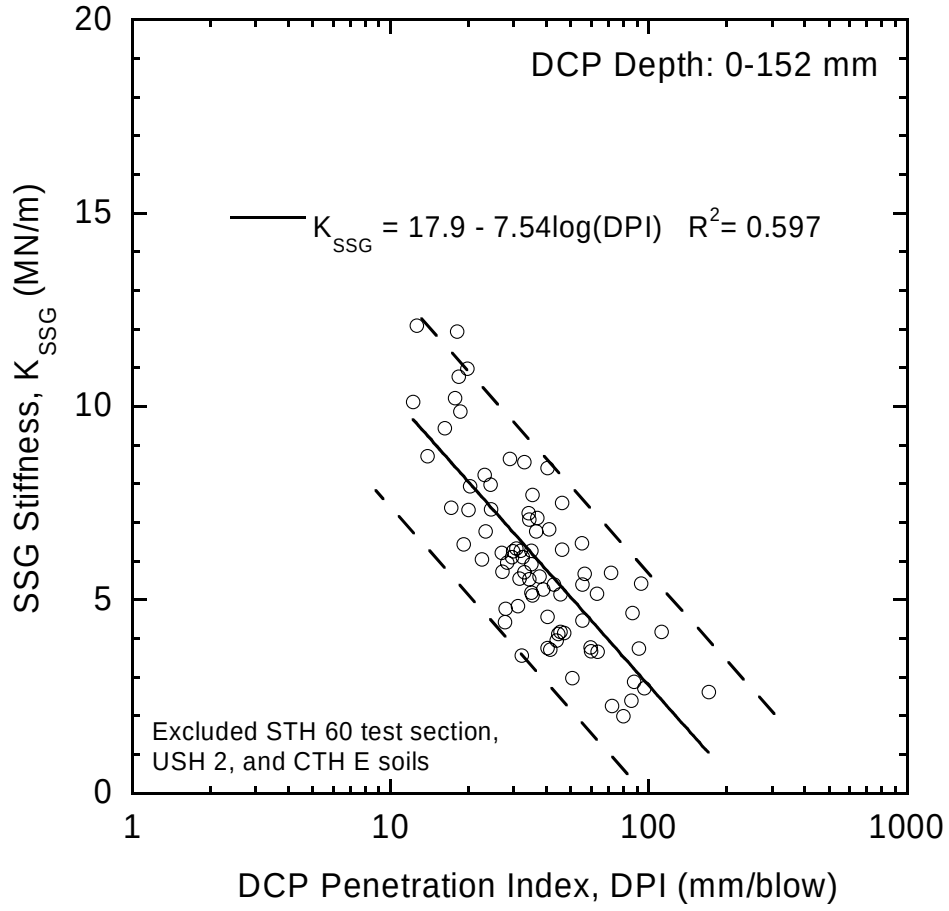

Fig. 4.24. Best correlation between SSG stiffness and DPI for natural earthen materials including granular and fine-grained soils.

4.5.2 Granular Materials

Fig. 4.25 shows the correlation between the SSG stiffness and DPI for granular materials including natural soils, bottom ash, and foundry slag. It is also important to note that foundry sand exhibits both granular and fine-grained material behavior (i.e., foundry sand exhibits granular-like material when it dries and fine-grained-like material when it wets). However, its inclusion in granular material categories reduces the quality of correlation. Without foundry sand, the best correlation was obtained when DPI was averaged over DCP penetration depths of 76 and 152 mm (Fig. 4.25(a) and (b)). With the same reason as natural earthen materials category, the USH 2 and CTH E soils were excluded from the correlation. The relationship is best expressed by the following equations:

For 76-mm DCP penetration depth,

$$K_{SSG} = -7.1\log(DPI) + 18.1 \quad (4.10)$$

For 152-mm DCP penetration depth,

$$K_{SSG} = -8.3\log(DPI) + 19.3 \quad (4.11)$$

The linear regression of SSG stiffness on average DPI calculated over 76- and 152-mm DCP penetration depths has R^2 = 0.56 and 0.55, respectively and S_e = 1.71 and 1.73, respectively. This error suggests that SSG stiffness can be estimated ± 3.42 and ± 3.45 from DPI for 76- and 152-mm DCP penetration depths, respectively.

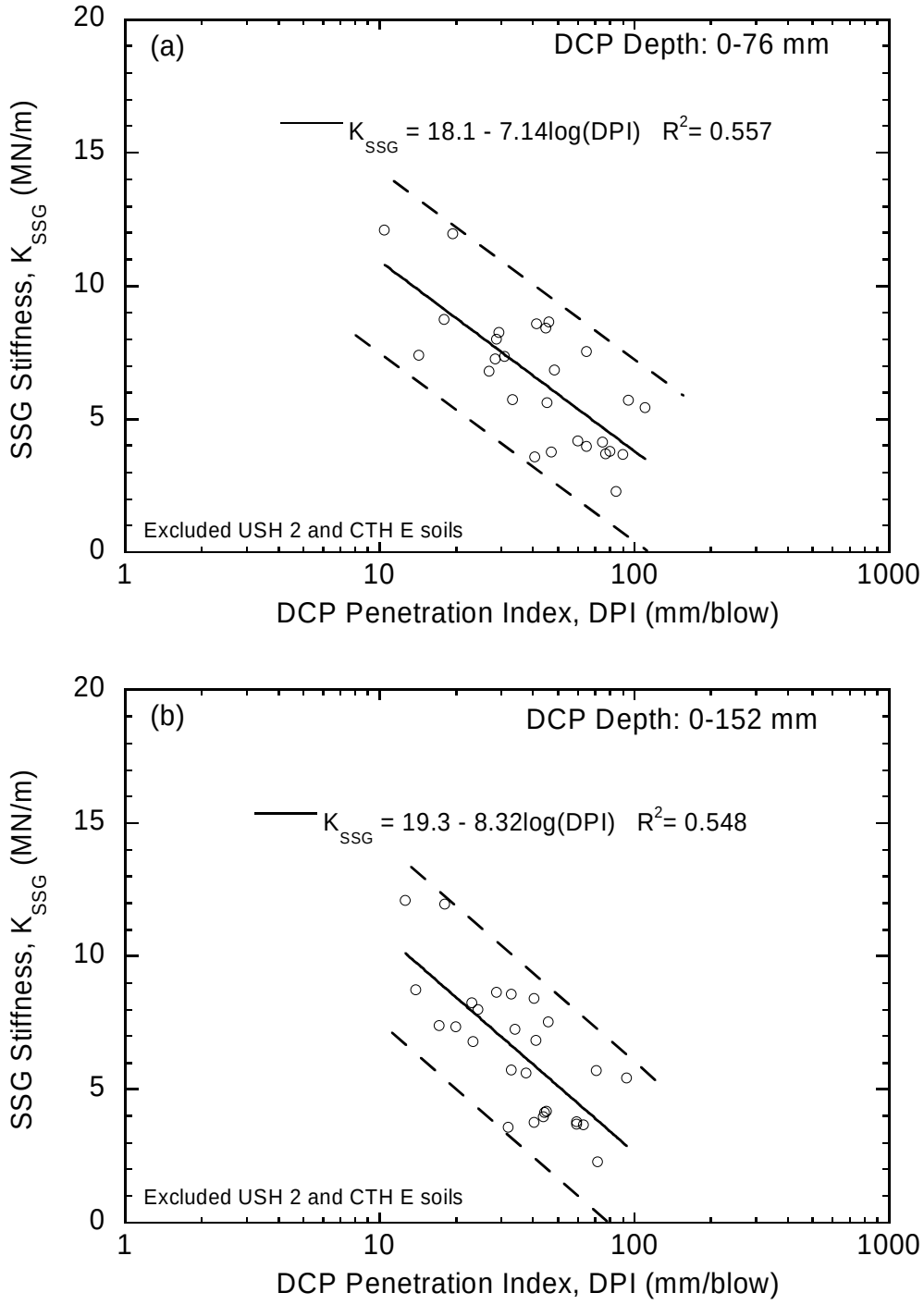

Fig. 4.25. Best correlation between SSG stiffness and DPI for granular materials including natural soils, bottom ash, and foundry slag.

4.5.3 Fine-Grained Soils

Fig. 4.26 shows the correlation between the SSG stiffness and DPI for fine-grained soils. The best correlation was obtained when DPI was averaged over a DCP penetration depth of 152 mm. The STH 60 test section soils were excluded from the correlation since the measurements were not made at the exact location. The relationship is best expressed by the following equation:

$$K_{SSG} = -7.1\log(DPI) + 17.1 \quad (4.12)$$

The linear regression of SSG stiffness on average DPI calculated over 152-mm DCP penetration depth has R^2 = 0.64 and S_e = 1.28. This error suggests that SSG stiffness can be estimated ± 2.55 from DPI.

4.5.4 Fly ash-Stabilized Soils

Fly ash-stabilized soils from two test sites: STH 60 test section and Scenic Edge development were used in the analysis. Fig. 4.27 shows the SSG stiffness-DPI correlation for fly ash-stabilized soils. The best correlation was obtained when DPI was averaged over a DCP penetration depth of 229-mm. This might be due to the fact that at this depth fly ash and subgrade soils were mixed well forming the homogeneous layer and thus improve the quality of correlation. The relationship is best expressed by the following equation:

$$K_{SSG} = -11.1\log(DPI) + 26.4 \quad (4.13)$$

The linear regression of SSG stiffness on average DPI calculated over 229-mm DCP penetration depth has R^2 = 0.47 and S_e = 1.92. This error suggests that SSG stiffness can be estimated ± 3.84 from DPI.

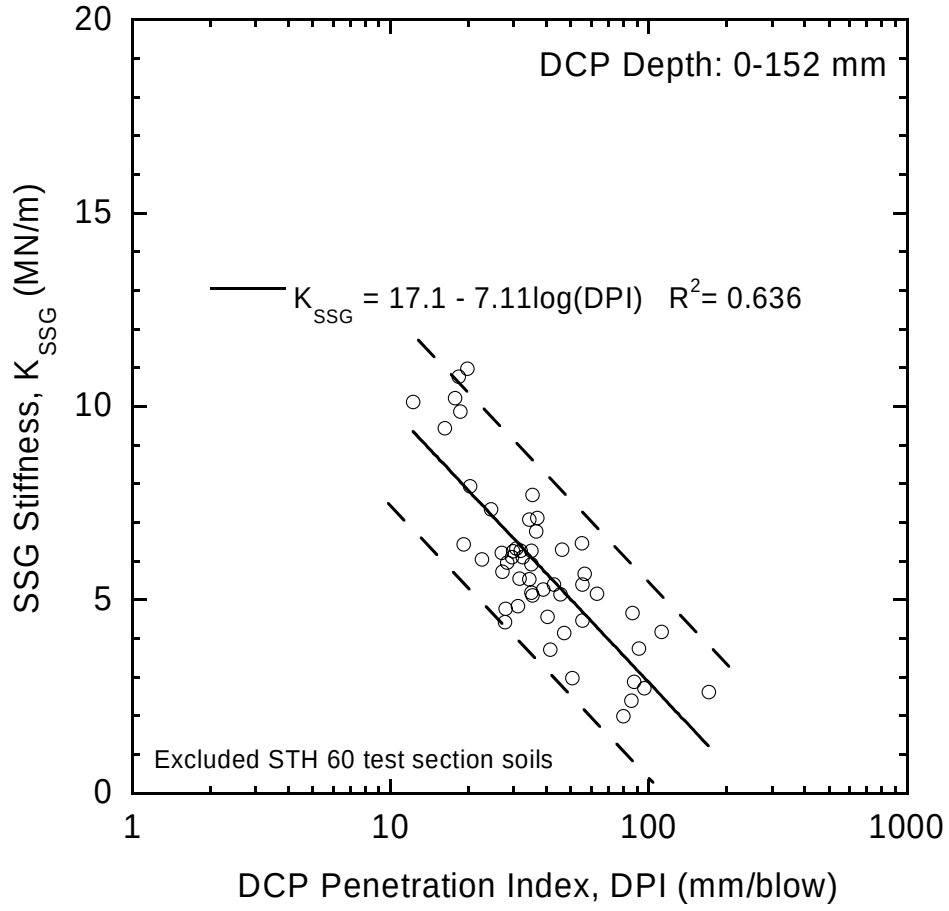

Fig. 4.26. Best correlation between SSG stiffness and DPI for fine-grained soils.

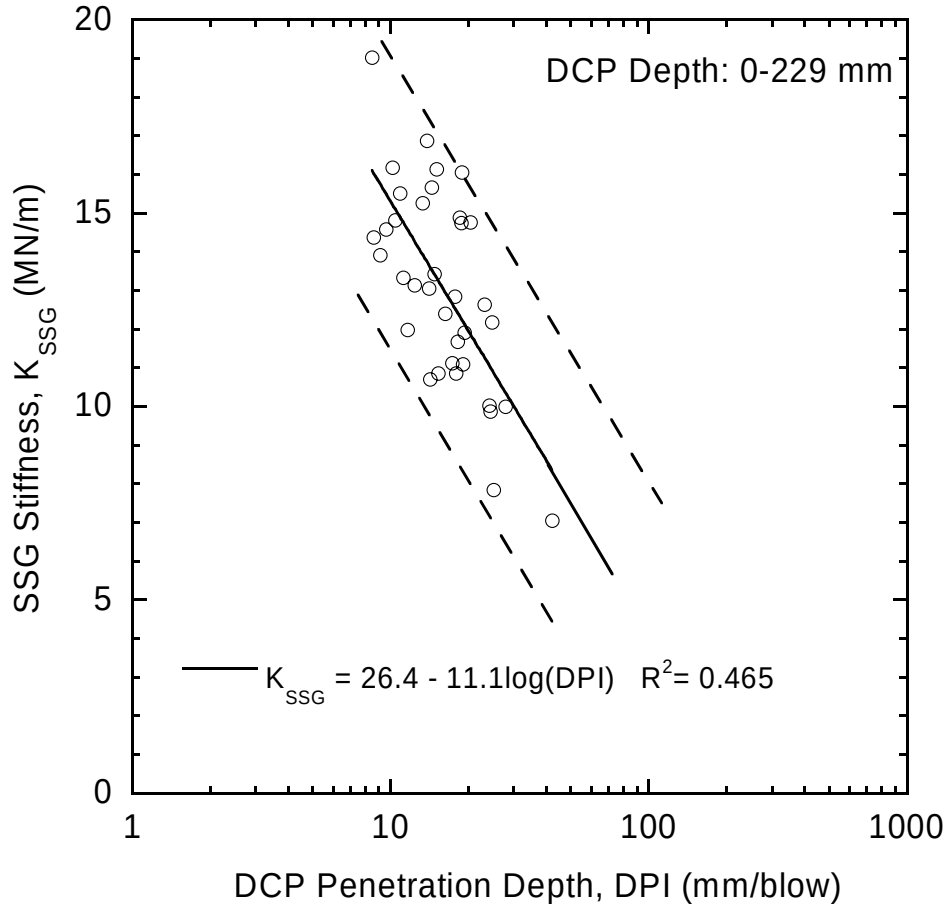

Fig. 4.27. Best correlation between SSG stiffness and DPI for fly ash-stabilized soils.

4.5.5 Fine-Grained Materials Including Fly Ash-Stabilized Soils

Fig. 4.28 shows the correlation between the SSG stiffness and DPI for fine-grained materials including fly ash-stabilized soils. Similar to granular materials, the inclusion of foundry sand in this category reduces the quality of correlation. The best correlation was obtained when DPI was averaged over DCP penetration depths of 152 mm and without the foundry sand. The STH 60 test section soils were excluded from the correlation since the measurements were not made at the exact location. The relationship is best expressed by the following equation:

$$K_{SSG} = -12.7 \log(DPI) + 26.7 \quad (4.14)$$

The linear regression of SSG stiffness on average DPI calculated over 152-mm DCP penetration depth has R^2 = 0.75 and S_e = 2.16. This error suggests that SSG stiffness can be estimated ± 4.32 from DPI.

4.5.6 All Materials Combined

All materials from all test sites were combined in the analysis. Fig. 4.29 shows the SSG stiffness-DPI correlation for all materials combined. The best correlation was obtained when DPI was averaged over DCP penetration depths of 152 mm. The STH 60 test section and CTH E soils were excluded from the correlation since the measurements were not made at the exact location. The USH 2 soils were also excluded from the correlation since their behavior was known to be very unusual. The relationship is best expressed by the following equation:

$$K_{SSG} = -12.0 \log(DPI) + 25.6 \quad (4.15)$$

The linear regression of SSG stiffness on average DPI calculated over 152-mm DCP penetration depth has R^2 = 0.72 and S_e = 2.15. This error suggests that SSG stiffness can be estimated ± 4.30 from DPI.

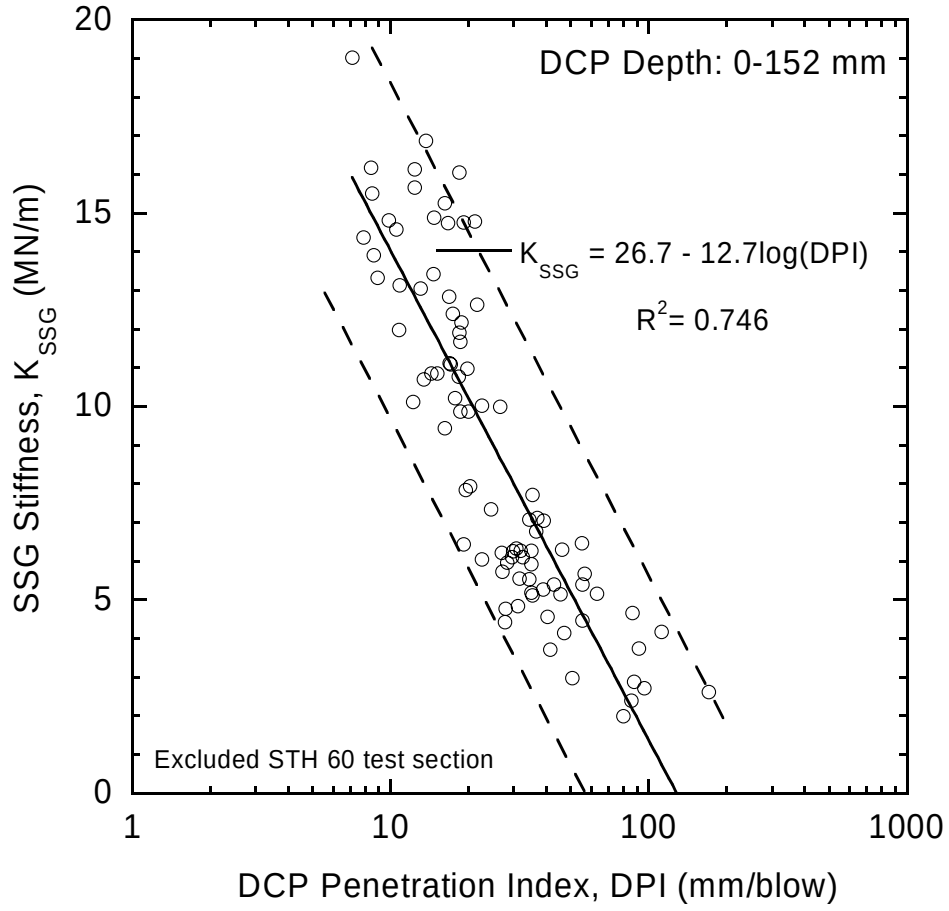

Fig. 4.28. Best correlation between SSG stiffness and DPI for fine-grained materials including fly ash-stabilized soils.

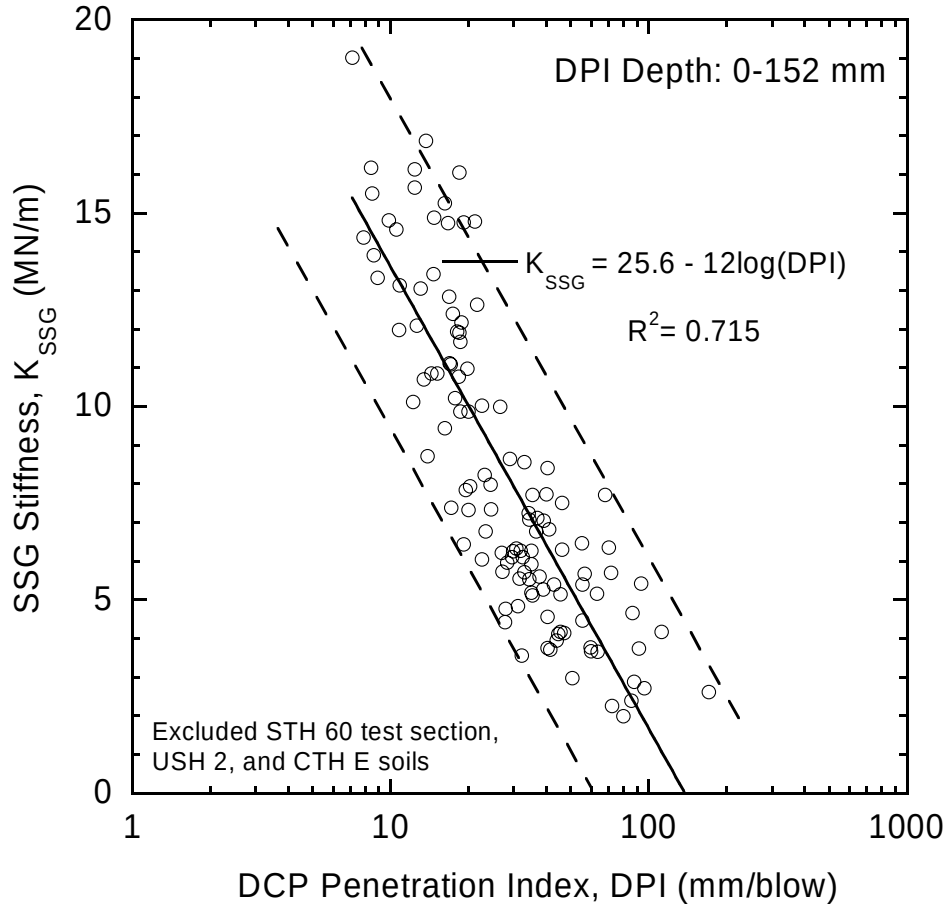

Fig. 4.29. Best correlation between SSG stiffness and DPI for all materials combined.

For all material categories in Table 4.3 except category 4 (i.e., fly ash-stabilized soils), the best correlations (i.e., highest R^2) were obtained when DPI was averaged over a DCP penetration depth of 152 mm after examining correlations of average DPI calculated over varying DCP penetration depths. The best correlation for fly ash-stabilized soils, however, was obtained when DPI was averaged over a DCP penetration depth of 229-mm. The SSG stiffness is related to DPI in a simple linear semi-logarithmic relationship. The dispersion of the data as shown in Fig. 4.24 to Fig. 4.29 is explainable to a degree by the fact that although stiffness and strength are related in a general sense, there is not always a one-to-one relationship as demonstrated in Fig. 4.5 and Fig. 4.9. Nonetheless, the SSG stiffness and DPI correlate well with an R^2 of 0.72.

4.6 Effect of SSG Depth of Measurement Significance on SSG Stiffness and DPI Correlation

To avoid the dead zone in SSG measurements (less than 125 mm) in granular soils according to Sawangsuriya et al. (2002), the depth of measurement significant of the SSG was selected to be ranged from 125 to 381 mm. To investigate this effect, the correlation between SSG stiffness and DPI was examined within this range. The arithmetic average DPI was calculated over a series of DCP penetration depths: 76-229 mm, 76-381 mm, 125-229 mm, and 125-381 mm for granular materials. Table 4.5 summarizes the coefficient of determination (R^2) examined from the correlations between SSG stiffness and arithmetic average DPI calculated over a series of DCP penetration depths: 76-229 mm, 76-381 mm, 125-229 mm, and 125-381 mm. In particular, the correlations between the SSG stiffness and DPI for granular materials including natural soils, bottom ash, and foundry slag) at these penetration depths are shown in Fig. 4.30 to Fig. 4.33. Note that the arithmetic average method was employed to calculate the representative DPI value for a given penetration depth of interest since the weighted average method cannot be applied in this case. In all cases, the best correlation was obtained when the USH 2 soils were not included in the correlation due to their unusual behavior. The CTH E soils were also excluded from the correlation since the measurements were not performed at the exact location.

Results indicated that the best correlation was obtained when DPI was averaged over DCP penetration depths of 76-229 mm as shown in Fig. 4.30. The coefficient of determination (R^2) was obtained to be 0.41; however, it was smaller than that obtained when the effect of dead zone was not considered. This might be partly due to the difference in method used to calculate the representative DPI value for a specified DCP penetration depth.

Table 4.5. Coefficient of Determination (R^2) Examined from the Correlations between SSG Stiffness and Weighted Average DPI Calculated over a Series of DCP Penetration Depths: 76-229 mm, 76-381 mm, 125-229 mm, and 125-381 mm for Granular Materials

Material Category	Name	DCP Depth (mm)			
		76-229	76-381	125-229	125-381
Granular	Natural (w/ USH 2+CTH E)	0.07	0.02	0.00	0.00
	Natural	0.29	0.25	0.21	0.21
	Natural+B.ash+F.slag	0.41	0.30	0.19	0.13
	Natural+B.ash+F.slag+F.sand	0.25	0.23	0.11	0.06

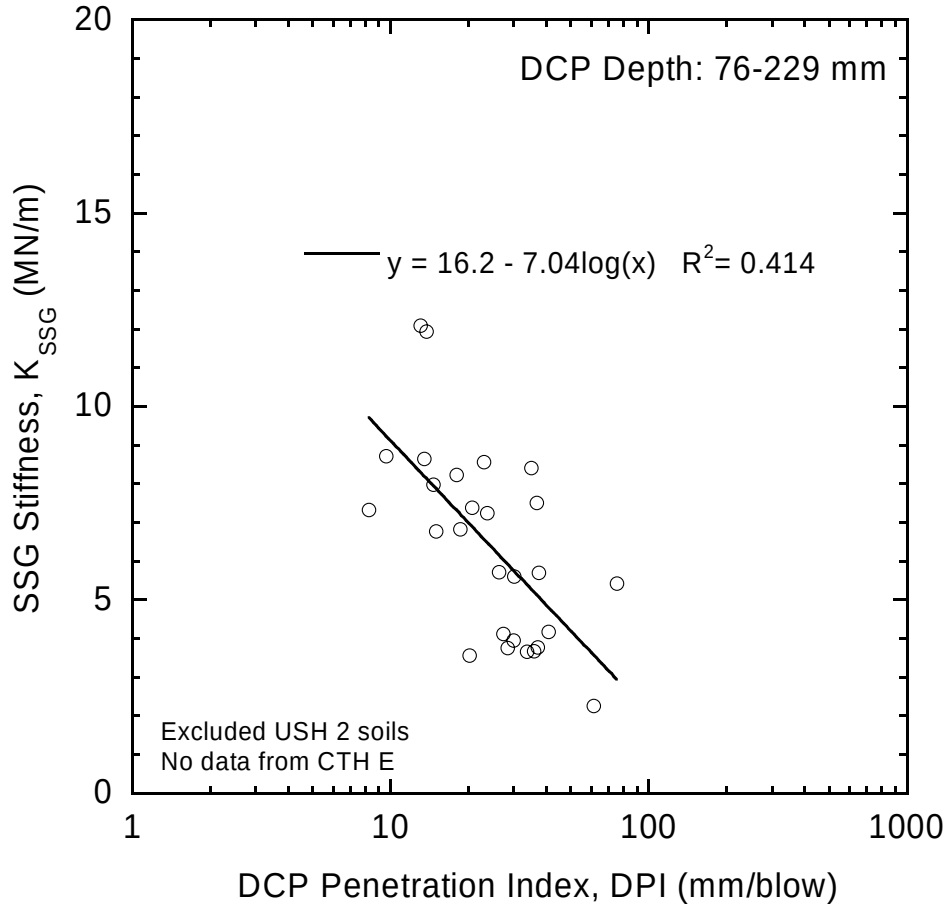

Fig. 4.30. Correlation between SSG stiffness and arithmetic average DPI calculated over a DCP penetration depth of 76-229 mm for granular materials (i.e., natural soils, bottom ash, and foundry slag).

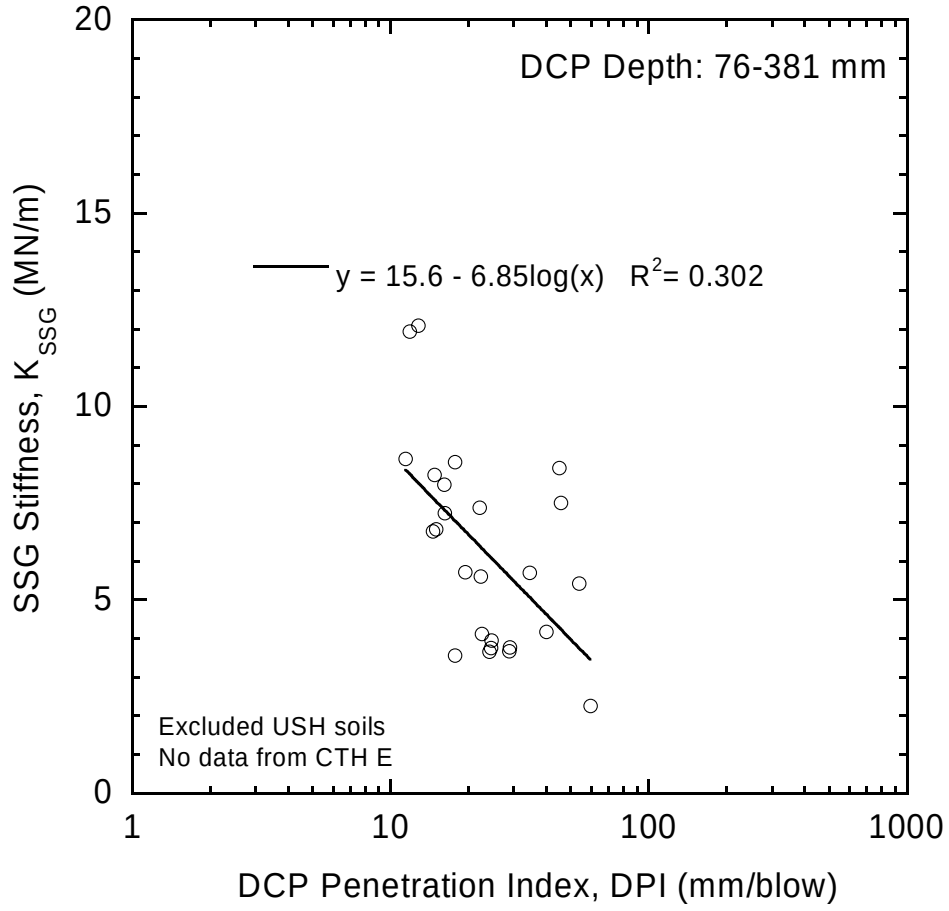

Fig. 4.31. Correlation between SSG stiffness and arithmetic average DPI calculated over a DCP penetration depth of 76-381 mm for granular materials (i.e., natural soils, bottom ash, and foundry slag).

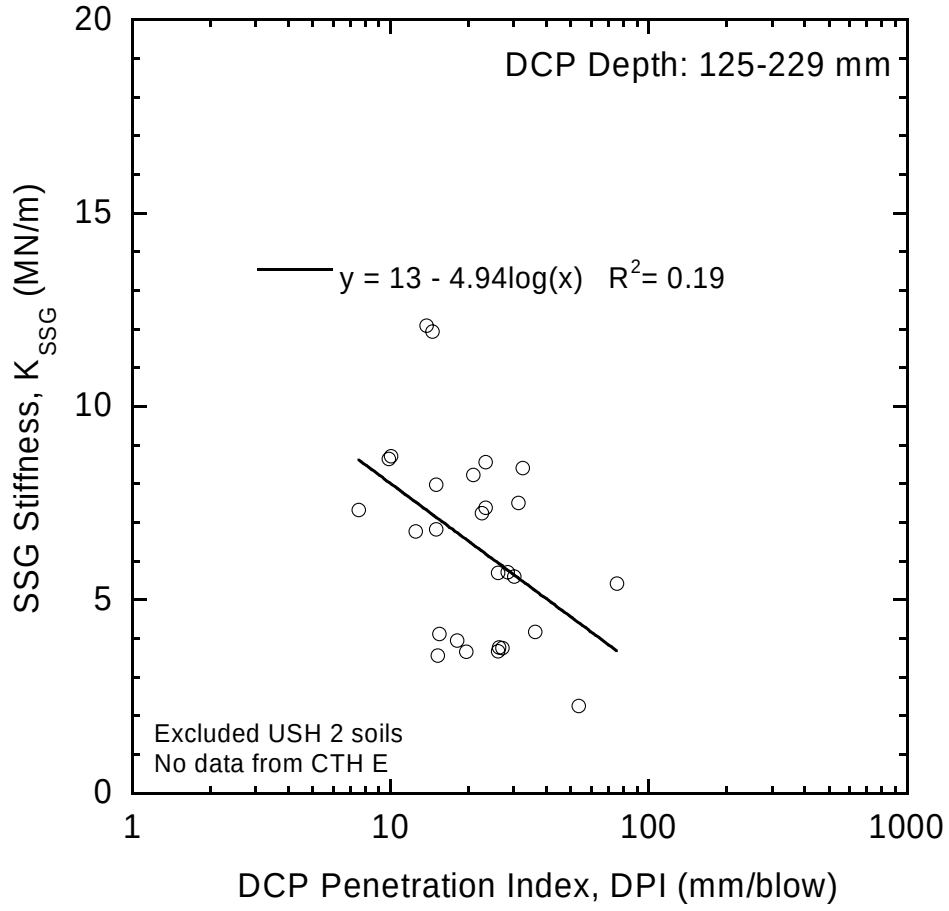

Fig. 4.32. Correlation between SSG stiffness and arithmetic average DPI calculated over a DCP penetration depth of 125-229 mm for granular materials (i.e., natural soils, bottom ash, and foundry slag).

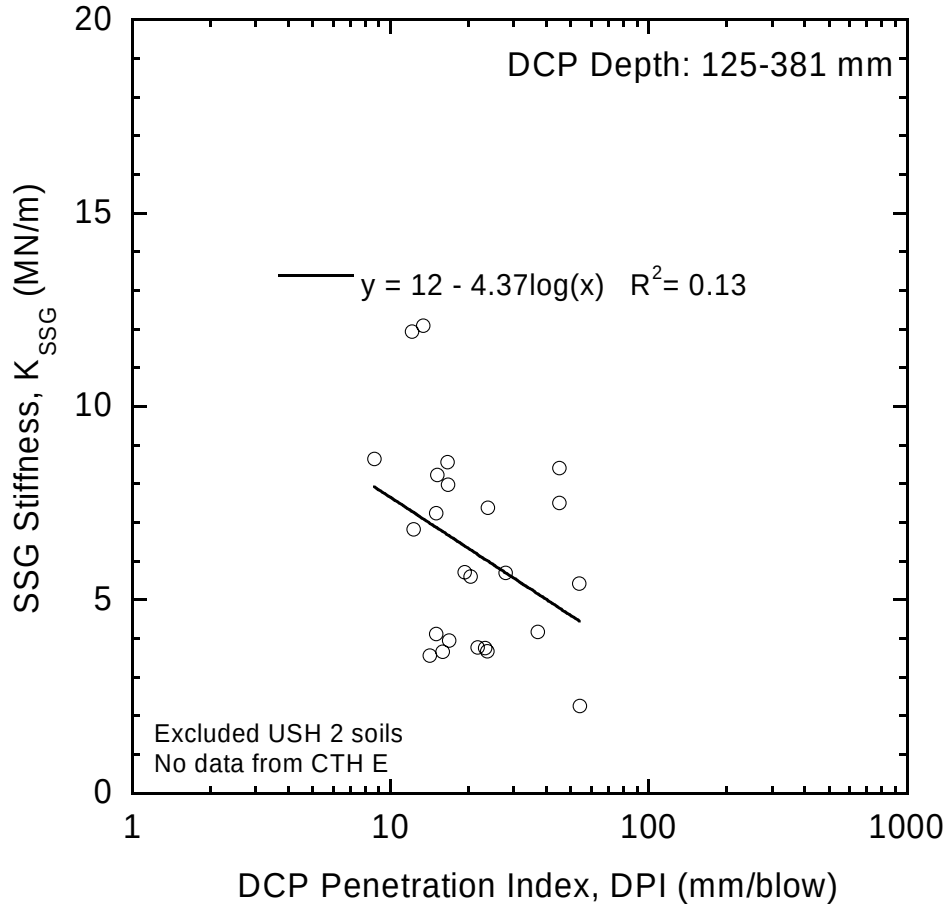

Fig. 4.33. Correlation between SSG stiffness and arithmetic average DPI calculated over a DCP penetration depth of 125-381 mm for granular materials (i.e., natural soils, bottom ash, and foundry slag).

4.7 Effect of State of Compaction on SSG Stiffness and DPI Correlation

Effect of state of compaction on the SSG stiffness and DPI correlation is also important in the analysis. The natural subgrade soils from two test sites with similar soil properties and classification were selected to investigate this effect on the SSG stiffness and DPI correlation. The STH 26 and STH 100 sites respectively represent the non-compacted and compacted soils. The stiffness and shear strength (which is inversely proportional to DPI) of the STH 26 soils were much smaller than the STH 100 soils as shown in Fig. 4.2(b) and Fig. 4.6(b). Fig. 4.34 and Fig. 4.35 respectively show the SSG stiffness and DPI correlation obtained when DPI was averaged over DCP penetration depths of 152 mm and 229 mm for compacted subgrade soils (i.e., at STH 100) and for non-compacted subgrade soils (i.e., at STH 26). The results indicated that the state of compaction has a significant effect on the SSG stiffness and DPI correlation. The coefficient of determination (R^2) obtained from STH 100 was about 0.65 and 0.69 when DPI was averaged over DCP penetration depths of 152 mm and 229 mm, respectively. On the other hand, the value of R^2 obtained from STH 26 was about 0.32 and 0.01 when DPI was averaged over DCP penetration depths of 152 mm and 229 mm, respectively. Therefore, a better correlation was obtained after the natural subgrade soils were compacted probably due to more uniform conditions, which result in reduction of the dispersion of the data and thus improve the quality of correlation between SSG stiffness and DPI.

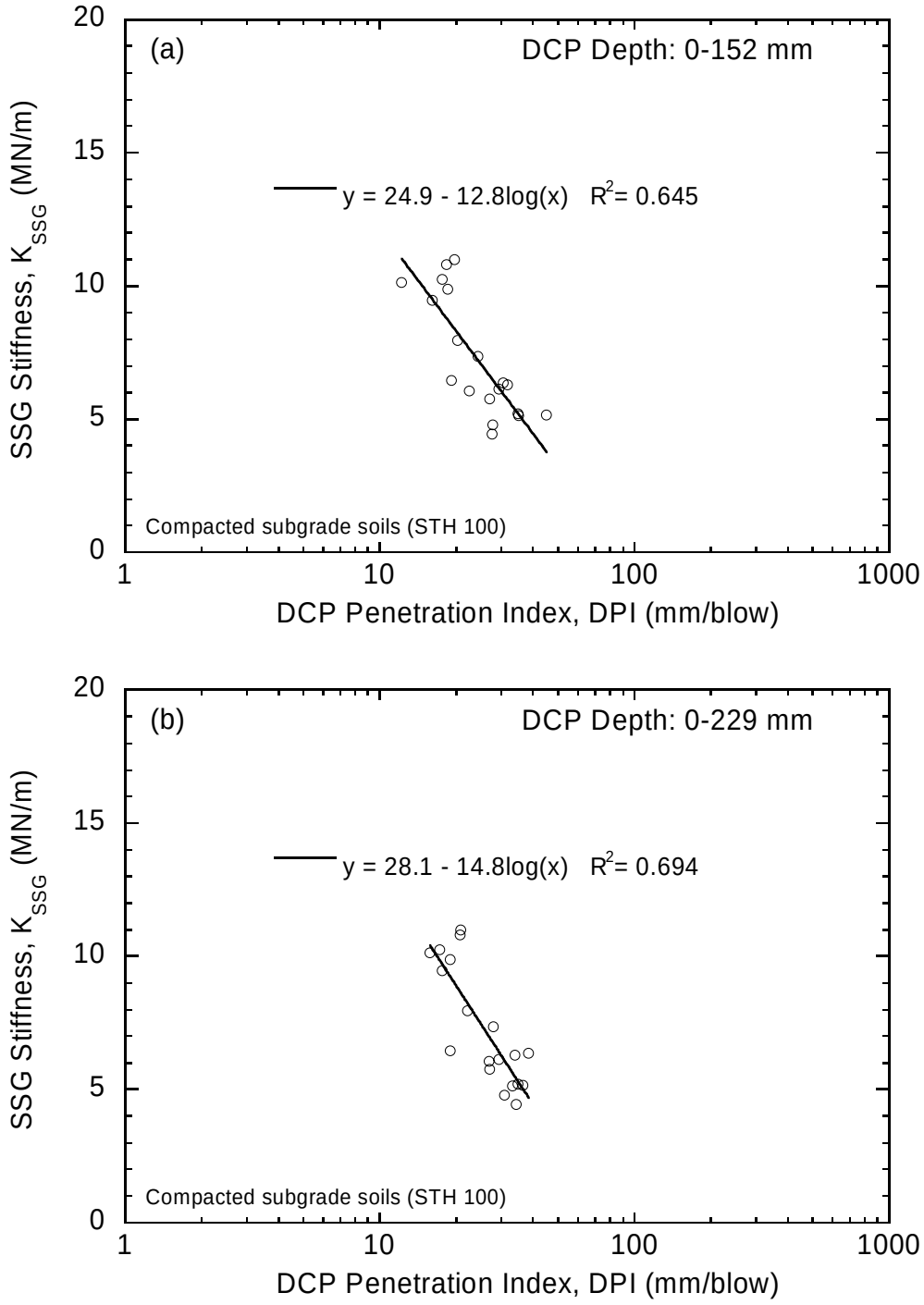

Fig. 4.34. Correlation between SSG stiffness and weighted average DPI over DCP penetration depths of 152 mm (a) and 229 mm (b) for compacted subgrade soils.

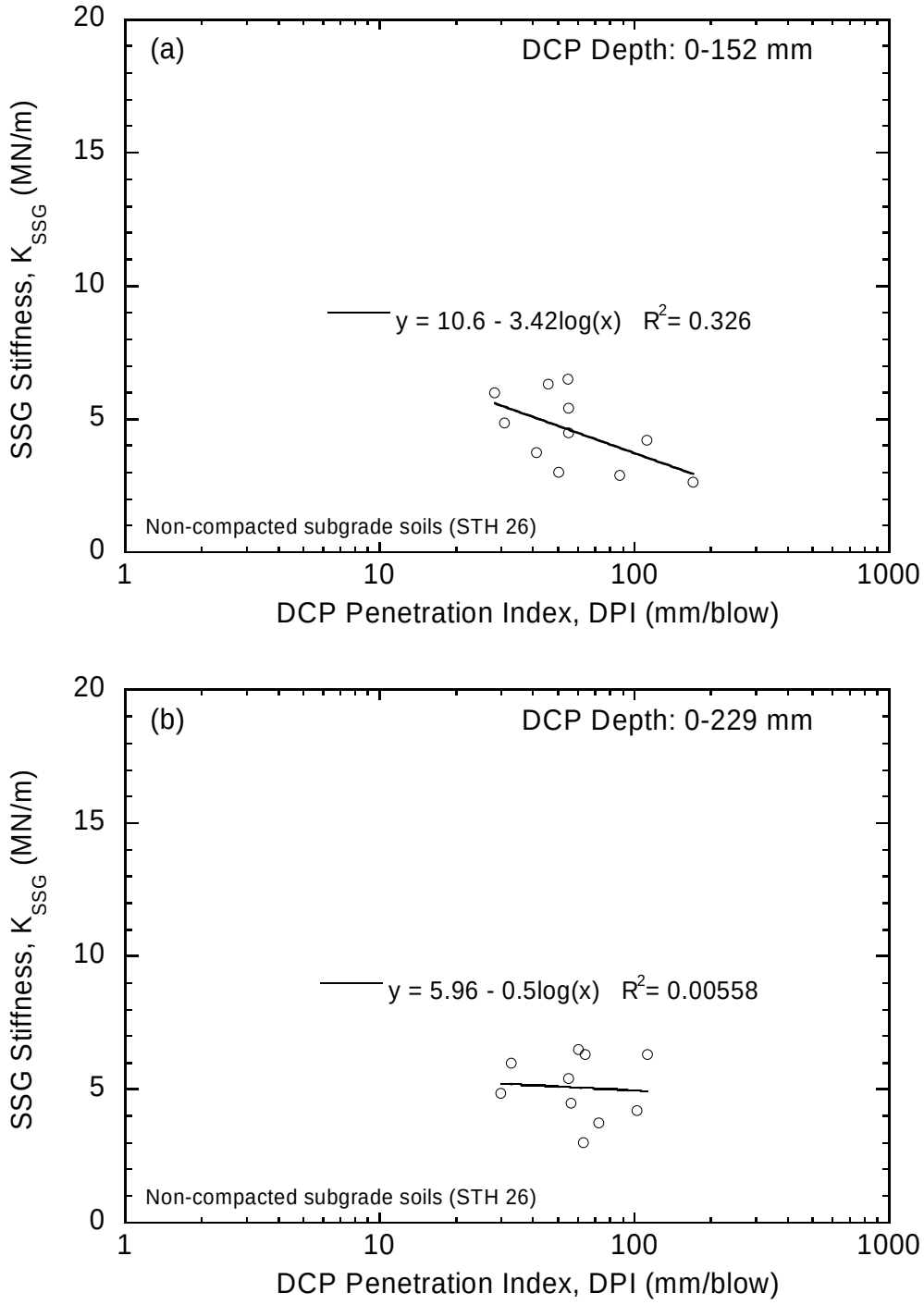

Fig. 4.35. Correlation between SSG stiffness and weighted average DPI over DCP penetration depths of 152 mm (a) and 229 mm (b) for non-compacted subgrade soils.

4.8 Correlation between Elastic Modulus and CBR

After a simple linear semi-logarithmic relationship between SSG stiffness (K_{SSG}) and DPI values was determined (i.e., K_{SSG} = 25.6-12 log DPI) based on direct regression from the actual measured data for all materials combined (Fig. 4.29), such a correlation can be further developed to become a more meaningful and useful equation, which can be used in the design of pavements. To accomplish this, the measured K_{SSG} is converted to SSG modulus (E_{SSG}) of the materials using Eq. (2.2). For a certain type of material involved, the values of Poisson's ratio (ν) can be selected according to their typical values suggested in Table 2.2. Values for ν of the granular soils including foundry slag and bottom ash were assumed to be 0.40. For fly ash-stabilized soils and fine-grained soils including foundry sand, ν values of 0.25 and 0.35 were used. Similarly, the weighted average DPI value obtained from the DCP can be also converted to California bearing ratio (CBR) of the materials using the well-established correlation given in Eq. (2.8) with the coefficients α and β of 2.46 and -1.12, respectively. Fig. 4.36 illustrates a plot of calculated E_{SSG} against CBR from the DCP. The regression equation obtained is expressed as follows:

$$E_{SSG} = 18.77 \times CBR^{0.63} \quad R^2 = 0.74 \tag{4.16}$$

where the units of E_{SSG} and CBR are MPa and percent, respectively. It can be seen that a unique relationship exists between E_{SSG} and CBR, regardless of soil type and site, although the coefficient of correlation of Eq. (4.16) is inherently dependent on the coefficient of correlation of Eq. (2.8). The results of SSG tests and DCP tests are expected to be affected by the same factors (i.e., relating the two test results directly excludes the influence of water content, dry density, and other basic indices). Furthermore, such a relationship is not affected by change in pavement condition and is also applicable to both the as-compacted and post-construction states. This equation yields almost identical values to those obtained from the equation given by Powell et al. (1984), i.e., Eq. (2.9). Fig. 4.37 illustrates the comparison between moduli from the SSG (E_{SSG}) and those from the DCP (E_{DCP}) using the regression equations given in Eq. (2.8) and Eq. (2.9). Remarkably good agreement is obtained with an independent widely used approach.

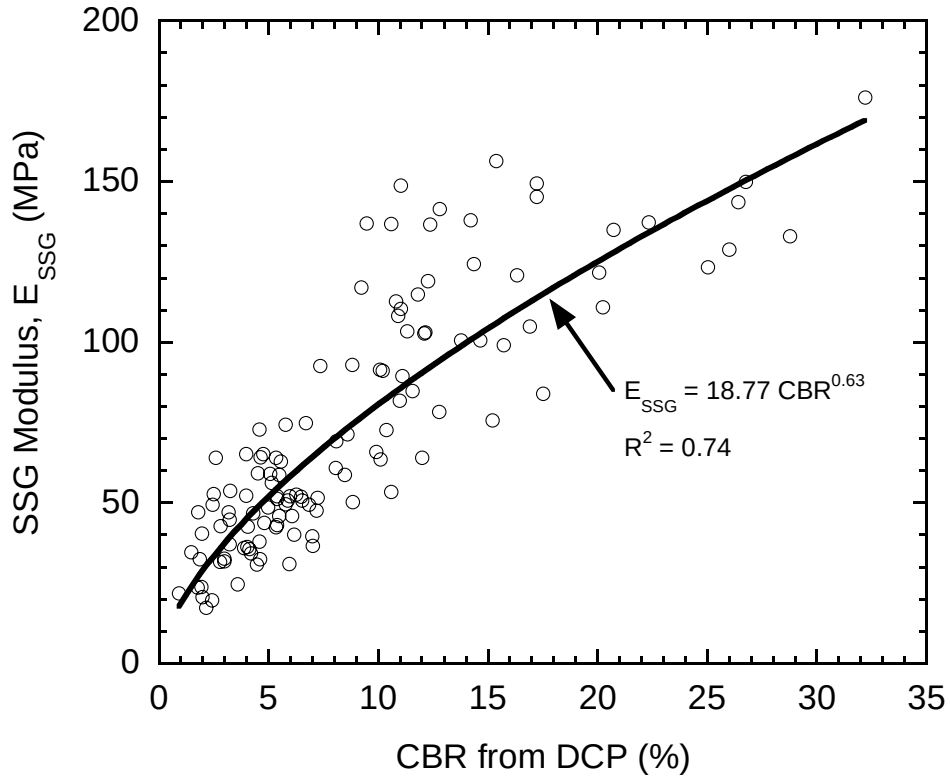

Fig. 4.36. Correlation between modulus from the SSG and CBR from the DCP.

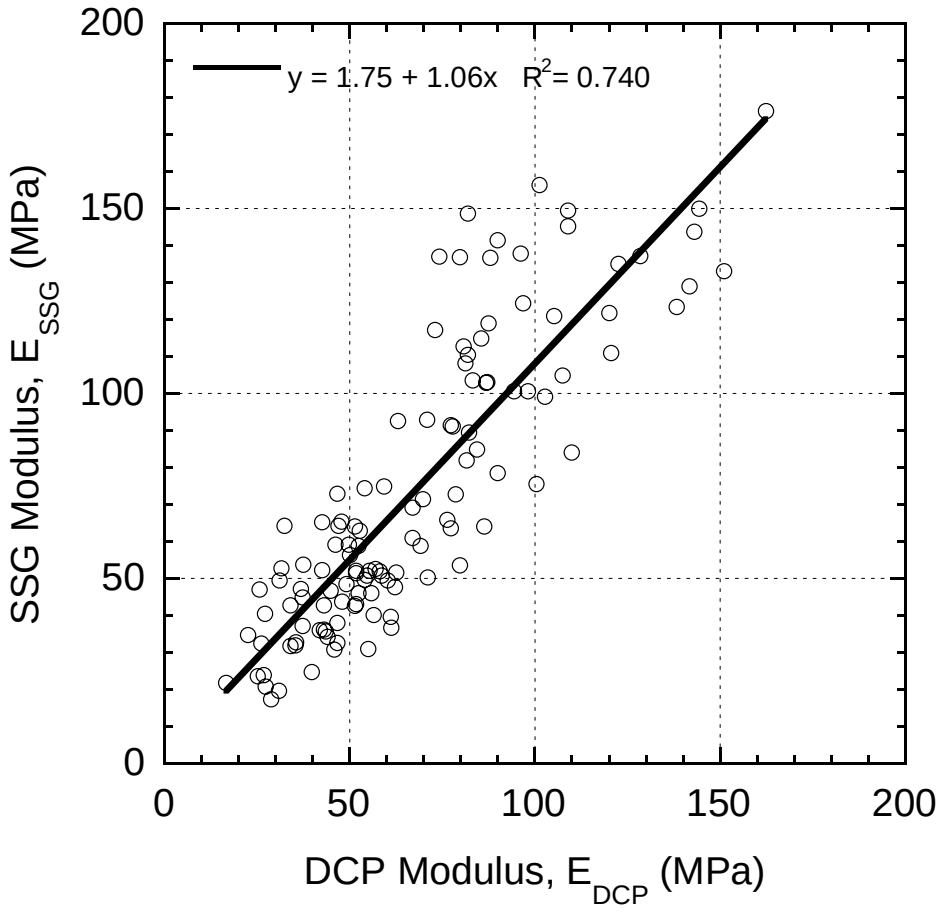

Fig. 4.37. Comparison between moduli from the SSG and those from the DCP.

A regression equation obtained in this study is also compared with that obtained from different in-situ tests including the FWD, LWD, and plate load tests, as shown in Fig. 4.38. The equations obtained for the FWD, LWD, and plate load test are given by Chen et al. (1999a), Livneh and Goldberg (2001), and Konrad and Lachance (2001), respectively. Note also that the parameter DPI in Eq. (2.11) and Eq. (2.12) can be converted to CBR using Eq. (2.8) with the coefficients α and β of 2.46 and -1.12, respectively. The comparison results suggest that the regression equation obtained in this study is best correlated to the equation given by Powell et al., i.e., Eq. (2.9), established between modulus and CBR (Powell et al. 1984). Within the CBR values ranging from 0 to 20%, the FWD and LWD (on sand) tests, respectively, provide the highest and lowest E for a given CBR. The relationship from the plate load test is in between the curve of Eq. (2.9) and LDW test (on sand). The suggested equation by AASHTO (1993) gives the highest modulus when the CBRs are greater than 10%. Large deviation from the other modulus tests is observed at relatively high CBRs as well. Using Fig. 4.38, the modulus can be estimated for any pavement condition if CBR is obtained for the corresponding condition. It is perhaps not surprising that the modulus given in Eq. (2.9) by Powell et al. and the SSG modulus given in Eq. (4.16) as developed in this study as a function of CBR agree well. The reason might be that both moduli were adjusted to realistic strain amplitude and stress levels from those corresponding to the wave propagation technique. According to Powell et al., their moduli were adjusted to strain amplitude and stress level in pavements from those corresponding to the wave propagation technique. In the case of the SSG, it was shown by Sawangsuriya et al. (2003) that the SSG modulus corresponds to strain amplitudes larger than the strain amplitudes of the wave propagation technique, even though the SSG induces strain amplitudes comparable to that of the wave propagation technique. In fact, the stress and strain levels induced by the SSG are 2 kPa and less than 10^{-3}%, respectively. It has also been shown that a somewhat reduced modulus is reported by the internal computation of the SSG device (Sawangsuriya et al. 2003).

To verify the power model given in Eq. (4.16), field measurement data from another two test sites were plotted onto the developed power model and Powell's equation as shown in Fig. 4.39. The test sites were a section of State Trunk Highway

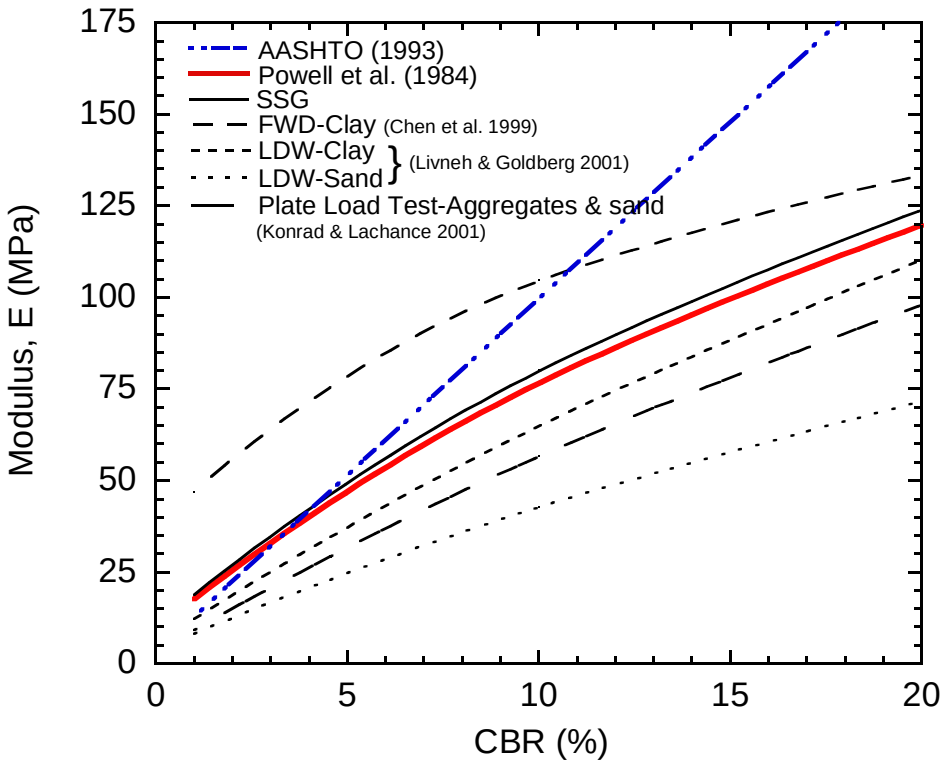

Fig. 4.38. E-CBR relationship of different methods.

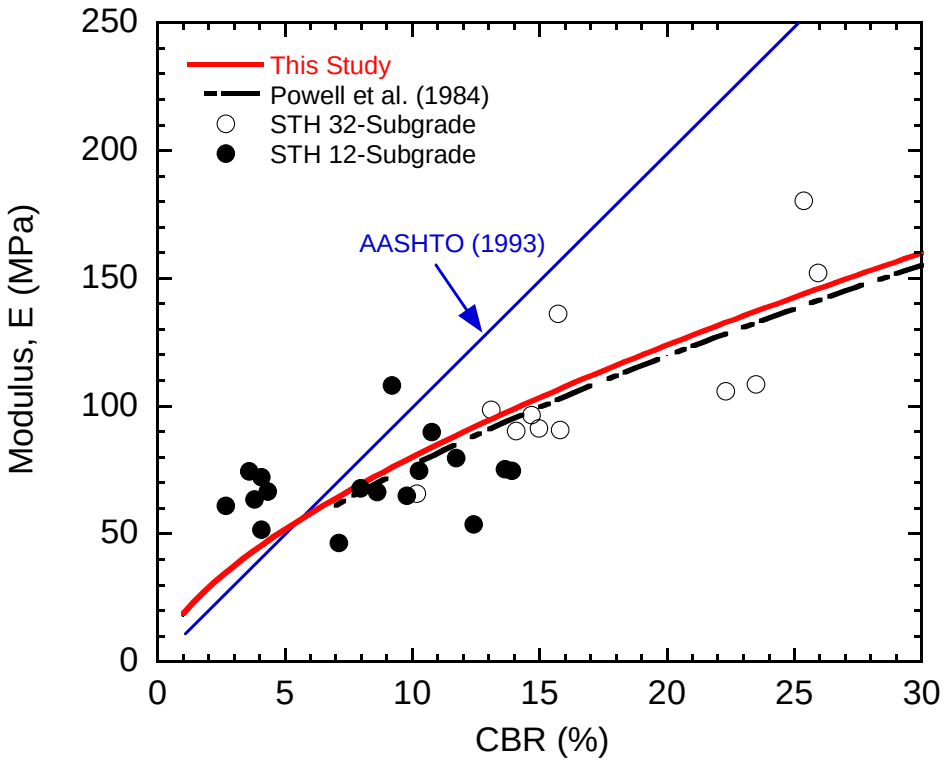

Fig. 4.39. Comparison of predicted subgrade moduli at STH 32, WI.

(STH) 32 located in Port Washington and a section of STH 12 located between Cambridge and Fort Atkinson, both in Wisconsin. The SSG and DCP data from these sites were obtained recently and were not included in the development of Eq. (4.16). The predominant subgrade soil of STH 32 is clayey sand classified as SC and A-4(0) according to the Unified Soil Classification System (USCS) and the AASHTO classification system, respectively. The predominant subgrade soil of STH 12 comprises lean clay with sand (CL or A-6(15)) and clayey sand with gravel (SC or A-2-6(0)). Results show that both the developed model (Eq. (4.16)) and Powell's equation fit reasonably well to the data set from STH 12 and STH 32 and thus Eq. (4.16) appears to be useful for estimating the subgrade modulus. Additionally, the equation suggested by AASHTO (1993) overestimates the subgrade modulus for soils with relatively high CBRs.

4.9 Correlation between Modulus Test and Unconfined Compression Test

In addition to the correlation with CBR from the DCP, the modulus from the SSG can be correlated with the strength from the conventional unconfined compression test. Lee et al. (1995) suggested an empirical correlation between the modulus from resilient modulus test (AASHTO T274-82) (E_{RM}) and the stress causing 1% axial strain ($S_{u1.0\%}$) in conventional unconfined compressive test (ASTM D2166) for the cohesive soils sampled from five in-service subgrades. The relationship is as follows:

$$E_{RM} = 10{,}748.4 + 5{,}744.9 S_{u1.0\%} - 48 S_{u1.0\%}^{2} \quad (4.17)$$

where the units of E_{RM} and $S_{u1.0\%}$ are both in kPa. Note that the E_{RM} values used to develop Eq. (4.17) are at axial deviator stress ($\sigma_1 - \sigma_3$) of 41.4 kPa and confining stress (σ_3) of 20.7 kPa. $S_{u1.0\%}$ was found to have the best correlations with E_{RM}, compared with other variables (i.e., in-service water content and dry density) and was chosen as a predictor variable instead of the unconfined compressive strength because its strain level is comparable with those of the resilient modulus test and the stresses at smaller axial strains may have larger error due to incorrect readings or imperfect contact between the specimen and top cap (Lee et al. 1995).

In this study, the moduli from the SSG (E_{SSG}) conducted on subgrade soils at STH 60 (test section) are correlated with the $S_{u1.0\%}$ values from the conventional unconfined compression test. Unconfined compression tests were conducted following ASTM D2166 on undisturbed specimens (50 mm in diameter and 100 mm high) trimmed from the tube samples. The test was performed using a strain rate of 2% per min and the stress at about 1% axial strain was reported. A regression analysis was conducted to obtain a relationship between E_{SSG} and $S_{u1.0\%}$ and the coefficient of determination (R^2) for this relationship is 0.64. A plot of E against $S_{u1.0\%}$ was made as shown in Fig. 4.40 in order to compare the correlation results obtained with Eq. (4.17). At a similar $S_{u1.0\%}$, the E_{SSG} value is higher than E_{RM} obtained from Eq. (4.17) and as $S_{u1.0\%}$ increases, the difference between E_{SSG} and E_{RM} also increases. This difference may be attributed to the fact that the E_{RM} values used in Eq. (4.17) are at higher stress and hence higher corresponding strain levels, whereas the E_{SSG} are measured at much lower stress-strain levels (Sawangsuriya et al. 2003).

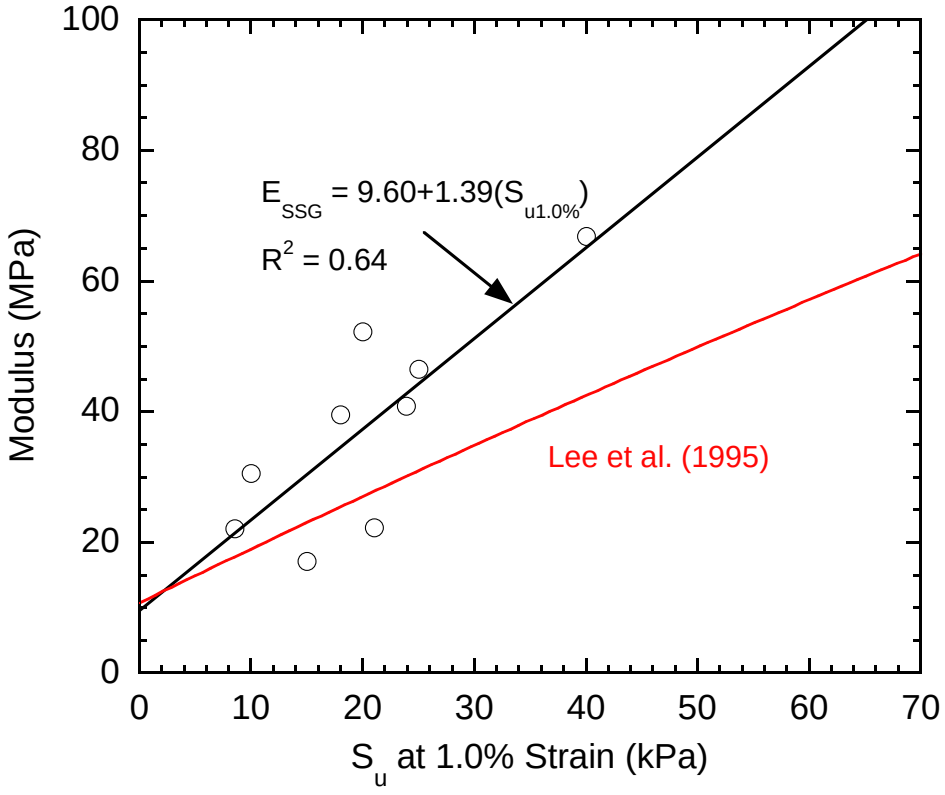

Fig. 4.40. Relationship between E and $S_{u1.0\%}$ for undisturbed subgrade soils at STH 60 (test section), WI.

CHAPTER FIVE
EARTHWORK QUALITY CONTROL

5.1 Compaction Quality Control

Subgrade soils from seven highway construction sites in Wisconsin, namely STH 100, STH 26, STH 44, USH 12, STH 131, STH 58, and STH 154, were monitored in terms of their stiffness, dry unit weight, and moisture content. The subgrade soils consisted of predominantly granular natural earthen materials with fines content (percent passing No 200 sieve, 0.075 mm size) up to 35% (USCS designations of SC, SC-SM, SP-SM) and also predominantly fine-grained soils with fines content greater than 59% (USCS designations of CL). Some of the soils were tested after they were compacted in the field (i.e., STH 100 and USH 12, STH 131, STH 58, and STH 154) and some were in natural uncompacted state (i.e., STH 26 and STH 44).

Fig. 5.1 shows the relationship of the state of density (i.e., relative compaction, RC defined as the ratio of the field dry unit weight divided by the laboratory maximum standard Proctor dry unit weight) to the deviation of moisture content from the respective optimum moisture content ($w\text{-}w_{opt}$) for the natural subgrade soils tested. Typical compaction specifications call for RC ≥ 95%. Most of the RC of field compacted soils are from 90 to 112.5% with moisture contents dry of the optimum moisture content, whereas uncompacted soils (all CL soils) in their natural state exhibit low dry densities and much wider moisture contents including some wet of the optimum. Furthermore, RC decreases with increasing $w\text{-}w_{opt}$. Fig. 5.2 and 5.3 respectively shows the variation of SSG stiffness (K_{SSG}) with $w\text{-}w_{opt}$ and the variation of DPI weighted average over a DCP penetration depth of 152 mm with $w\text{-}w_{opt}$ for the natural subgrade soils. Strong dependency of stiffness and strength parameters on moisture content is evident as K_{SSG} varies from 2 to 12 MN/m and DPI varies from 10 to 110 mm/blow for a moisture content deviation of about ±8% of the optimum moisture content. The compacted soils have moisture contents mostly dry of optimum. Of course, there are other factors that may affect stiffness such as dry density, texture, and soil fabric and they cause the spread in K_{SSG} and DPI for a given moisture content.

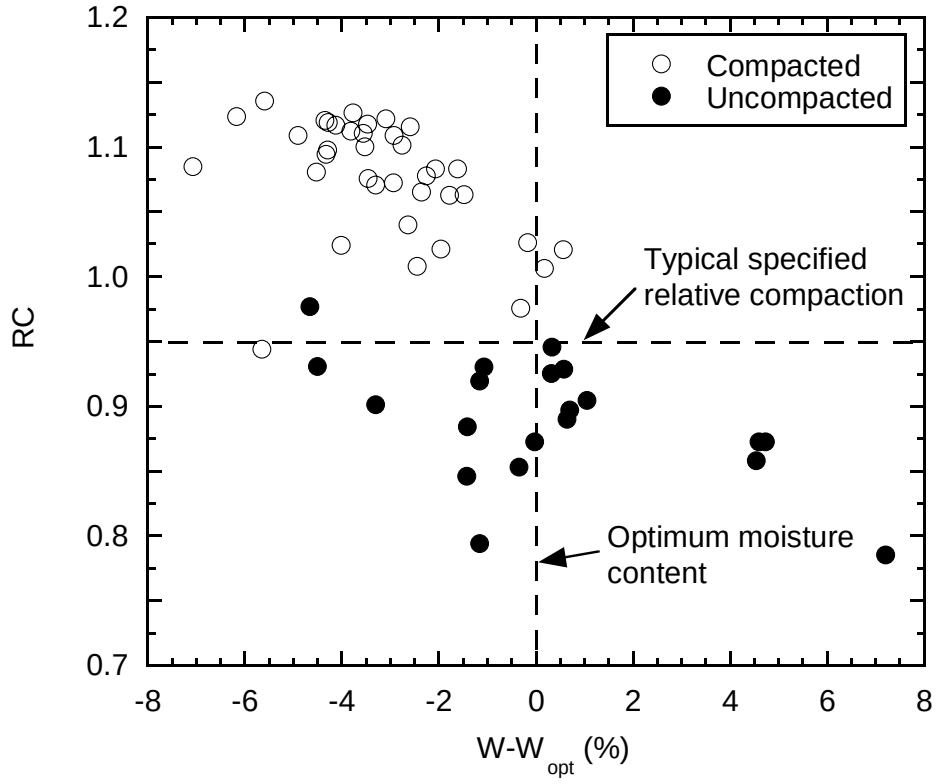

Fig. 5.1. Relative compaction vs. deviation of moisture content from the optimum moisture content for natural earthen materials.

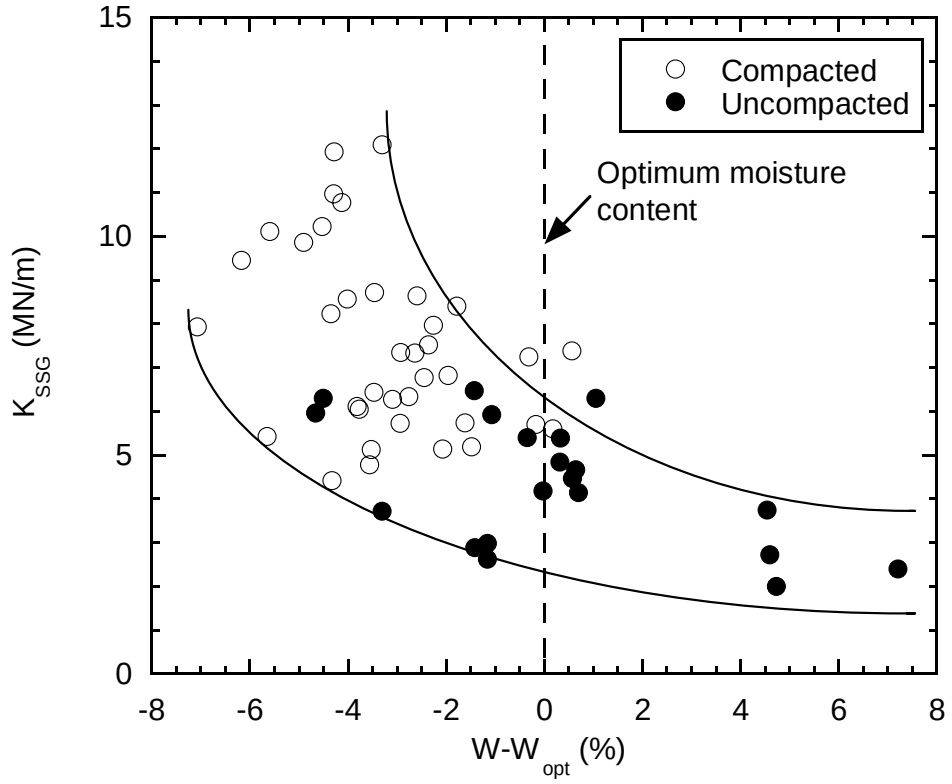

Fig. 5.2. SSG stiffness vs. moisture content variance for natural earthen materials.

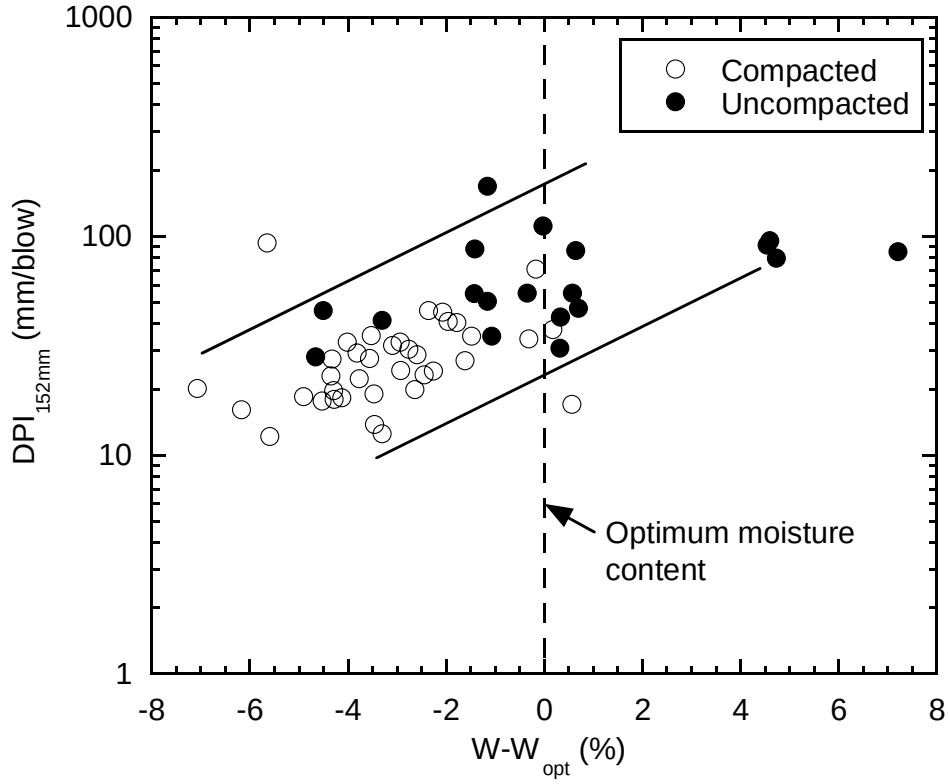

Fig. 5.3. DPI weighted average over a DCP penetration depth of 152 mm vs. moisture content variance for natural earthen materials.

In the case of subgrade soils subjected to the same state of stress (i.e., near-surface), moisture content and dry unit weight of a test soil play significant role on its stiffness and strength parameters and their effects are hard to uncouple. To account for the effect of moisture content, K_{SSG} and DPI weighted average over a DCP penetration depth of 152 mm is divided by $(w\text{-}w_{opt})$. These normalized stiffness and strength parameters are plotted versus RC in Fig. 5.4 and Fig. 5.5, respectively. The normalized stiffness and strength parameters vary very little with relative compaction for compacted soils with an average value of -2.4 and -8.35, respectively, which can be used to estimate K_{SSG} and DPI of a wide variety of properly compacted soils. A larger variation is observed for uncompacted soils perhaps due to their more complex fabric. The implication of this for compacted soils with the typically rather narrow range of RC is that the effect of dry unit weight on stiffness and strength is relatively minor compared to moisture content.

According to the manufacturer, the SSG can be also used to estimate the dry unit weight from soil stiffness and an independently measured moisture content using the following analytical-empirical relationship given in Eq. 5.1 (Humboldt 1999a) and thus eliminating the need for a nuclear density gauge. Since stiffness is dependent on both moisture content and dry unit weight, the moisture content must be independently acquired in conjunction with the stiffness measurement for this purpose.

$$\gamma_d = \frac{\gamma_o}{1+1.2\left[\frac{Cw}{K_{SSG}}-0.3\right]^{0.5}} \tag{5.1}$$

where γ_o is the idealized void-free unit weight, C is a stiffness- and moisture-dependent parameter, which is defined based on a linear relationship between C and K_{SSG}/w obtained from companion stiffness, moisture content, and dry unit weight measurements, and the other terms are as defined before. Stiffness, moisture content, and dry unit weight of various materials including industrial by-products, natural earthen materials, and fly ash stabilized soils tested were used to establish such a relationship as shown in Fig. 5.6. The relationship for C in terms of K_{SSG}/w given in Fig. 5.6 for the materials tested in this investigation is comparable in slope but slightly different in intercept from

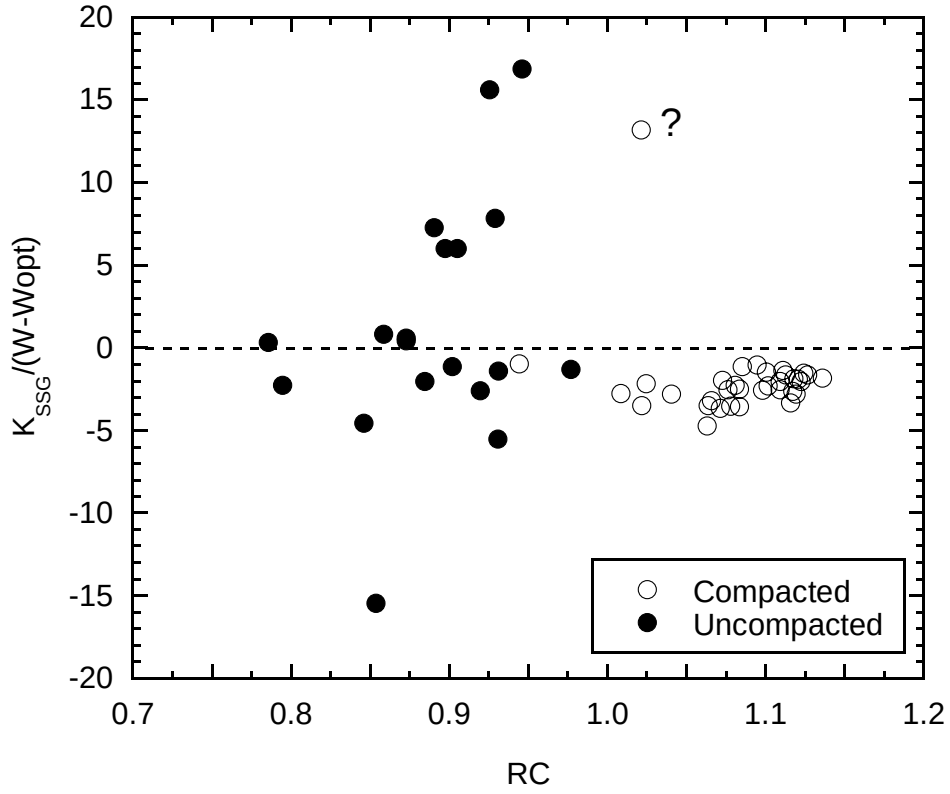

Fig. 5.4. Normalized SSG stiffness vs. relative compaction.

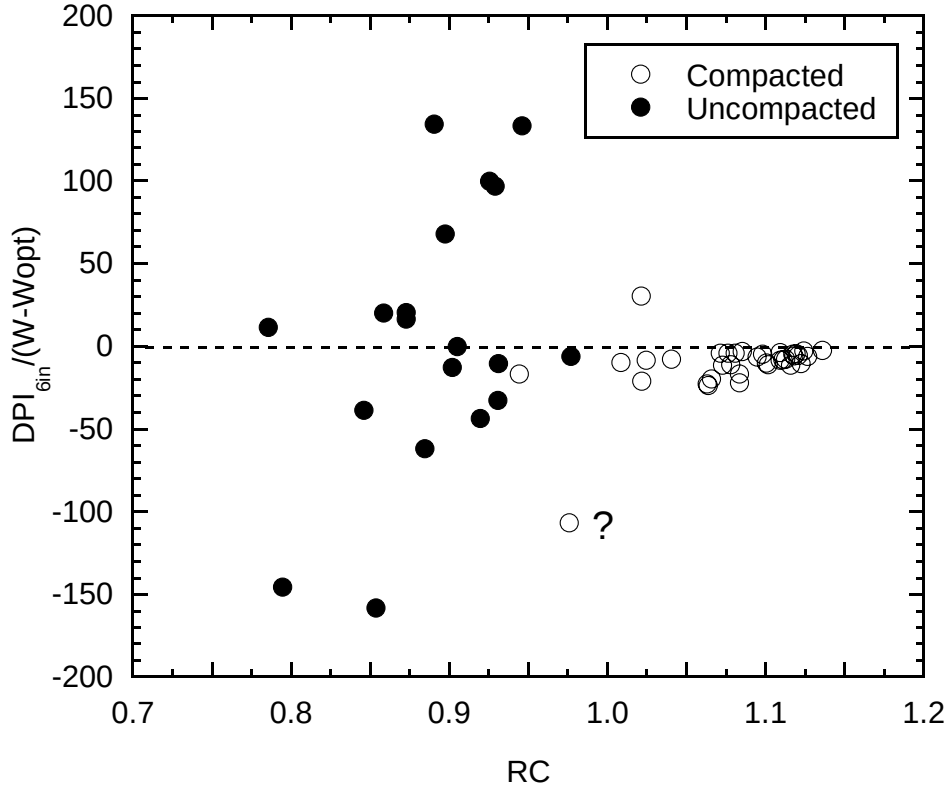

Fig. 5.5. Normalized DPI weighted average over a DCP penetration depth of 152 mm vs. relative compaction.

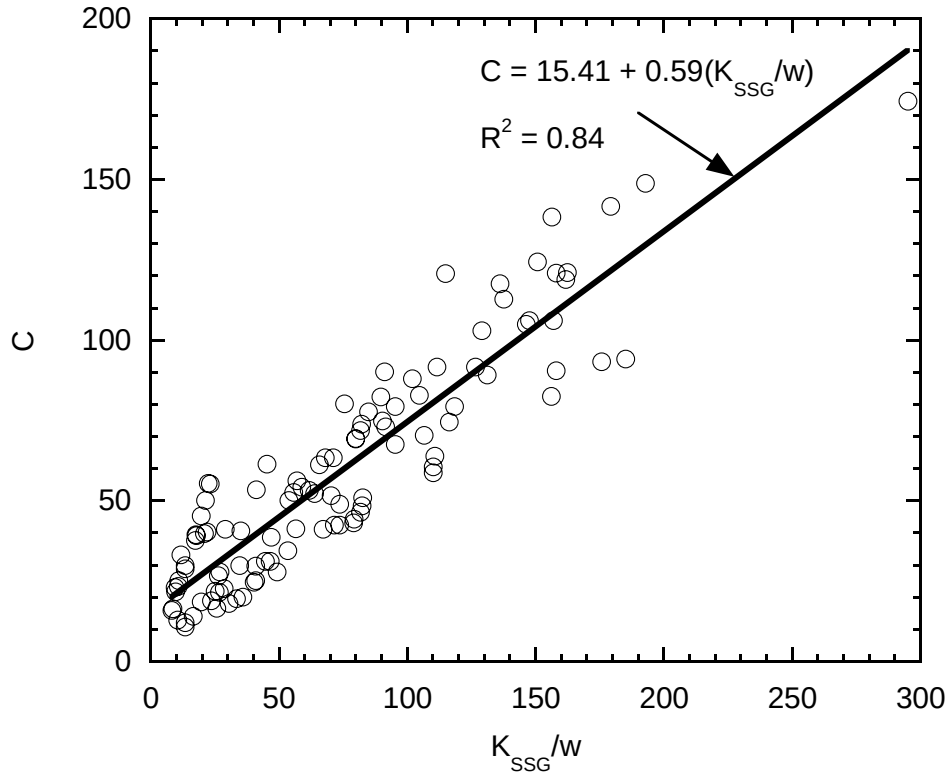

Fig. 5.6. Relationship of C and K_{SSG}/w.

the one given by Humboldt (1999a) (i.e., the intercept is 15.41 instead of 21.01). From the measured SSG stiffness, measured gravimetric moisture content, and parameter C from Fig. 5.6, the dry unit weights were estimated and compared to those measured from the nuclear density gauge in Fig. 5.7. Compared to the line of equality, all fine-grained soils have lower estimated dry unit weights than those measured using the nuclear gauge. There is a large dispersion of the data. A comparison of gravimetric moisture contents (determined by drying a sample) with those obtained from the nuclear density gauge showed that the latter being consistently lower (Fig. 4.12). This also may be contributing to the dispersion of the data. It appears that more evaluations are needed to rely solely on dry density estimated from the stiffness measurement for construction density control. However, if this approach is reliably established, SSG can replace nuclear density device as long as moisture content is also measured. The implementation of Moisture Gauge along with SSG may be considered as a promising means for the moisture content determination in the field.

5.2 Design Parameter Control

In general, either the stiffness or strength of compacted earthwork is needed for design. In subgrade and subbase layers for pavement systems, typical structural property used is resilient modulus (elastic modulus under repetitive loading) and/or California Bearing Ratio (CBR). Modulus of soils can be assessed by a variety of methods (Table 2.1) and it varies with confining stress and strain amplitude. For design, a modulus corresponding to the stress and strain amplitude as well as the moisture state expected under the operating conditions is needed. SSG stiffness can be converted to an elastic modulus obtained near-surface at the moisture conditions prevailing during the measurement with an assumption of Poisson's ratio. It is therefore not a modulus necessarily can be used directly in design. However, it can be used to control the structural uniformity of the earthwork and can be also viewed as an index of design modulus. In other words, the SSG stiffness or modulus can be indirectly employed as to control mechanical property for the design.

Laboratory tests were performed to establish the general relationship of the SSG modulus with the moduli obtained from other tests on a dry sand and presented on a

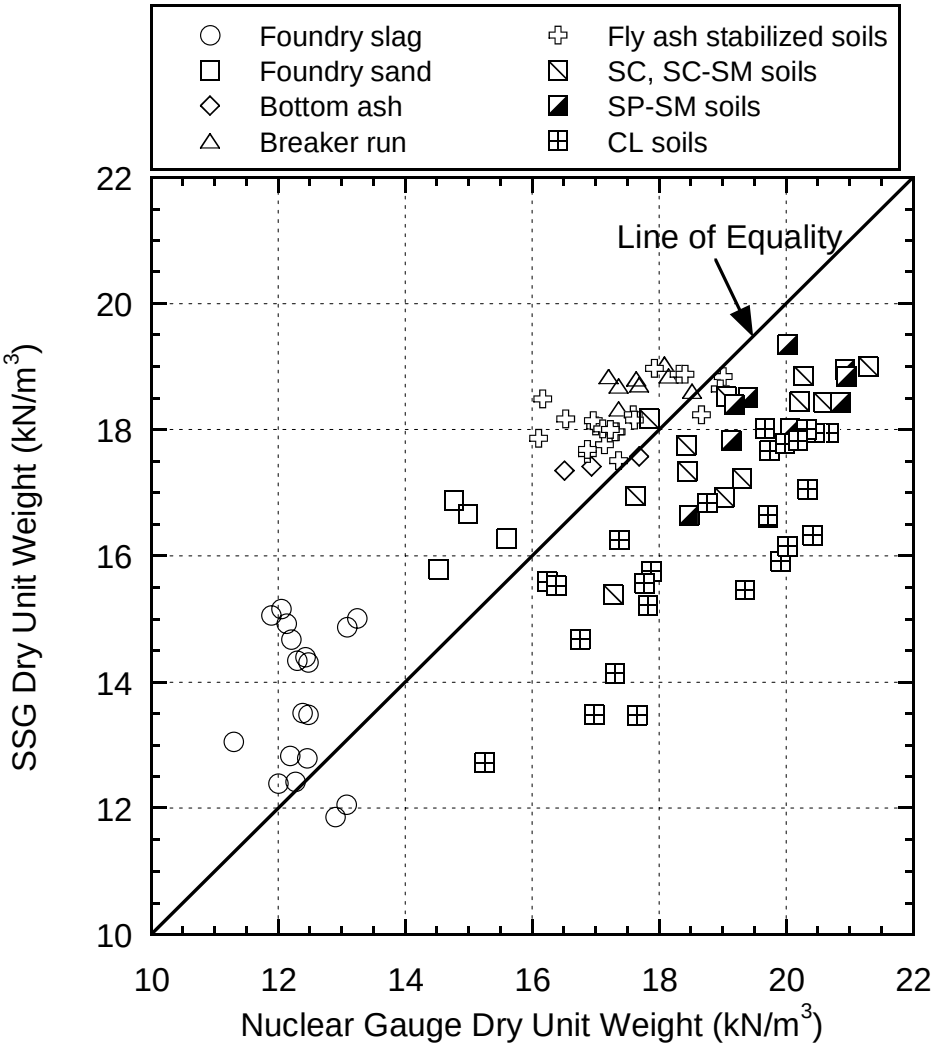

Fig. 5.7. Comparison of dry unit weight from the SSG and the nuclear gauge.

modulus degradation curve in Fig. 5.8 (Sawangsuriya et al. 2003). These moduli were determined at the same stress level (confining pressure of 2.6 kPa) over a range of strain amplitudes. The relationship of the SSG modulus to other moduli and particular to the resilient modulus can be seen. Using the modulus degradation curve, the SSG modulus can be adjusted to the modulus at any desired strain level and using the theory stress effects can be taken into account. Alternatively, a modulus ratio can be determined between the SSG modulus and the design modulus on the basis of laboratory tests. Knowing the modulus ratio, the design modulus can be reasonably determined from the measured SSG modulus (Sawangsuriya et al. 2004). In addition to the modulus variation due to differences in stress and strain levels, one must make the necessary reductions in modulus due to local climatic (i.e., moisture) effects to arrive a design value.

A relationship between the shear strength of soils in term of the CBR and K_{SSG} (Fig. 5.9) can be given as follows:

$$CBR = 0.59K_{SSG}^{1.23}; \ R^2 = 0.74 \qquad (5.2)$$

Using such a relationship, the SSG stiffness can be directly converted to a design CBR and vice versa. Consequently, the CBR value can be used indirectly to control the design soil strength, which is more important during the construction stage. Note that this CBR value can be either obtained in the laboratory or by using the dynamic cone penetrometer (DCP) such that there exists a widely accepted correlation between the DCP penetration index (DPI) and CBR (Webster et al. 1992, Livneh et al. 1995).

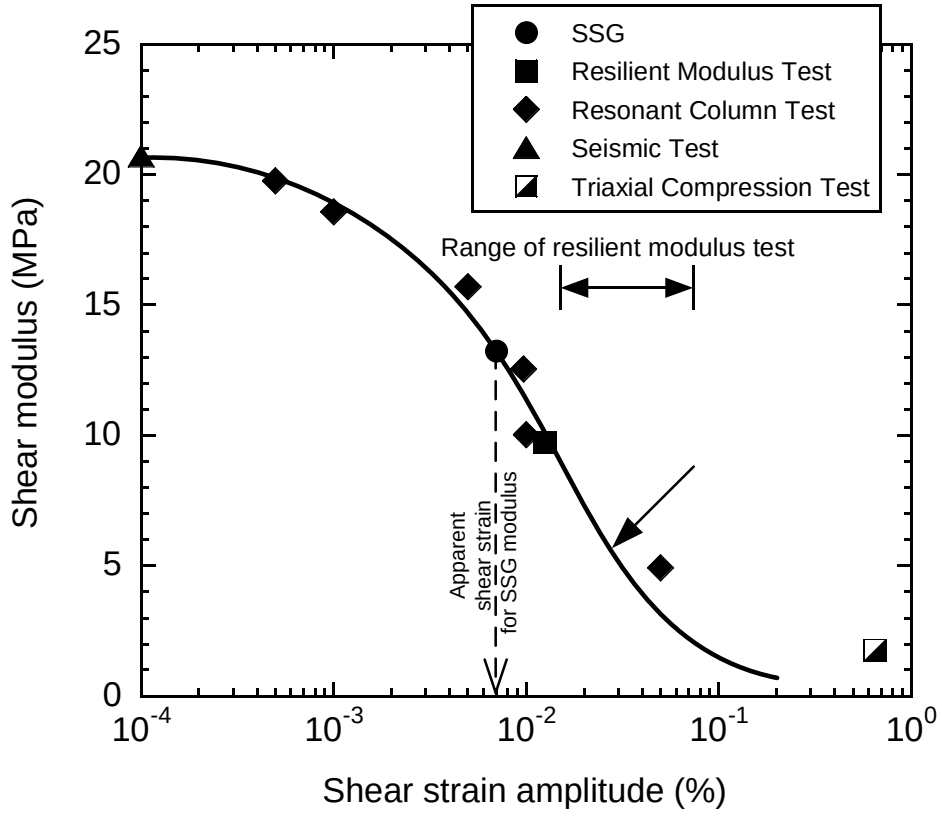

Fig. 5.8. Modulus from different tests (Sawangsuriya et al. 2003).

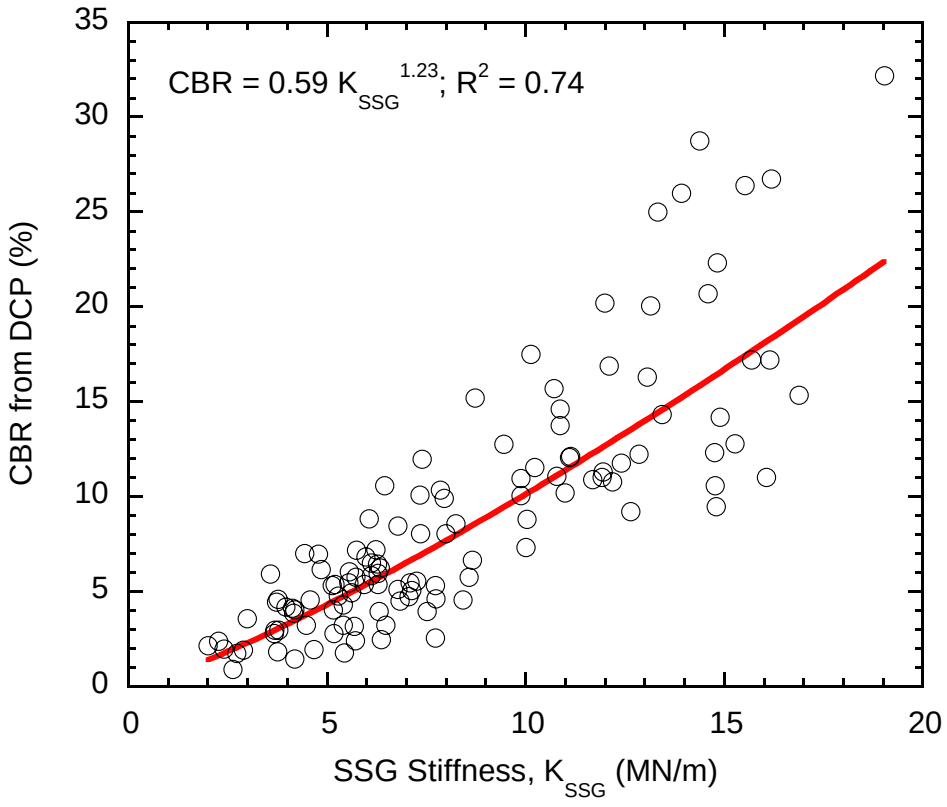

Fig. 5.9. Relationship between CBR and SSG stiffness.

CHAPTER SIX
CONCLUSIONS

SSG and DCP survey data of natural earthen materials, industrial by-products, chemically stabilized soils, and other materials from thirteen construction sites around the state of Wisconsin are presented along with their correlation with each other as well as with density, moisture content and other properties obtained from traditional tests. The data display considerable dispersion characteristic of the conditions and sampling sizes typical during construction. SSG provides in-place near-surface soil stiffness averaged over a zone, whereas DCP provides individual points of an index of in situ shear strength expressed as DCP penetration index (DPI) as a function of depth. Therefore, each fundamentally relates to a different material property and is presented in a spatially different manner. To deal with the latter issue, weighted average of DPI over depth of measurement is employed to obtain a representative strength index of the material. This approach provided better correlations than the arithmetic average.

The dependency of SSG stiffness and DPI strength index on dry unit weight and water content is obscured by large dispersion of the data although individual material appears to follow a pattern consistent with those expected from other research on stiffness and strength. However, it is also clear that dry unit weight or water content alone does not control stiffness or strength. It is also noted that the standard error associated with DPI is considerably larger than that of the SSG stiffness, reflective of the nature of the two tests.

A simple linear semi logarithmic relationship is observed between SSG stiffness and DPI. DPI weighted average over a DCP penetration depth of 152 mm yields the highest coefficient of determination and also yields a statistically significant relationship between the SSG stiffness and DPI for most materials. This depth is consistent with the significant depth of measurement for the SSG as shown in previous studies. The relationship is indicative of the fact that although there is not always a one-to-one relationship, stiffness and strength are related in a general sense.

The study indicates that either or both devices show good potential for future use in the pavement and subgrade property evaluation during construction phase. The in situ

stiffness and strength properties of various materials can be rapidly and directly monitored in companion with the conventional compaction control tests (e.g., nuclear density or laboratory moisture content samples) during earthwork construction. Stiffness and strength are material properties that are needed in different phases of highway design, i.e., for long-term pavement performance and during-construction working platform support and stability, respectively. The experience with recycled and reclaimed materials as well as chemically stabilized soils is limited compared to natural earthen materials in terms of moisture-density relationships and the related mechanical behavior. Direct monitoring of stiffness and strength of these new materials using these two devices also appears to be as effective as in natural earthen materials.

Use of the convenient SSG and DCP in conjunction with conventional moisture-density measurements enhances quality control during earthwork construction by achieving more uniform structural property and aids developing a design modulus. SSG stiffness normalized by the deviation of compaction moisture content from the optimum moisture content is remarkably constant around a value equal to -2.4 for compacted natural earthen materials. Similarly, the DCP penetration index normalized by the deviation of compaction moisture content from the optimum moisture content is around a constant of -8.4 for compacted natural earthen materials. In addition, there is potential for using SSG alone with an independent moisture measurement for both density and stiffness control with further evaluation.

Practical implications of the use of SSG and DCP for both structural property assessment and earthwork quality control for pavement materials are described in Appendix C with appropriated examples.

REFERENCES

Allbright, R. L. (2002), "Evaluation of the Dynamic Cone Penetrometer and its Correlations with Other Field Instruments," M.S. Thesis, Department of Civil and Environmental Engineering, University of Wisconsin-Madison, WI.

Black, W. P. M. (1962), "A Method of Estimating the California Bearing Ratio of Cohesive Soils from Plasticity Data," *Geotechnique*, pp. 271-282.

Chen, D-H., Wang, J-N., and Bilyeu, J. (2001), "Application of the Dynamic Cone Penetrometer in Evaluation of Base and Subgrade Layers," *Transportation Research Record 1764*, TRB, National Research Council, Washington, D.C., pp. 1-10.

Chen, D-H., Wu, W., He, R., Bilyeu, J., and Arrelano, M. (1999a), "Evaluation of In Situ Resilient Modulus Testing Techniques," *Recent Advances in the Characterization of Transportation Geo-Materials, Geotechnical Special Publication No. 86*, ASCE, pp. 1-11.

Chen, J., Hossain, M., and LaTorella, T. M. (1999b), "Use of Falling Weight Deflectometer and Dynamic Cone Penetrometer in Pavement Evaluation," *Transportation Research Record 1655*, TRB, National Research Council, Washington, D.C., pp. 145-151.

Chua K. M. (1988), "Determination of CBR and Elastic Modulus of Soils Using a Portable Pavement Dynamic Cone Penetrometer," *Proceedings of the First International Symposium on Penetration*, Orlando, Florida, pp. 407-414.

Claessen, H. I. M., Valkering, C. P., and Ditsmarch, R., (1976), "Pavement Evaluation with the Falling Weight Deflectrometer," *Proceedings of the Association of Asphalt Pavement Technologists*, Minneapolis, MN.

Edil, T. B. and Aydilek, A. H. (2001), "Geotechnics of Capping Very Soft Wastes," *Proceedings of the Thirteenth International Conference on Soil Mechanics and Geotechnical Engineering*, Istanbul, Turkey, Vol. 3, pp. 1903-1906.

Edil, T. B., Benson, C. H., Bin-Shafique, S., Tanyu, B. F., Kim, W-H., and Senol, A. (2002), "Field Evaluation of Construction Alternatives for Roadway Over Soft Subgrade," *Transportation Research Record 1786*, TRB, National Research Council, Washington, D.C., pp. 36-48.

Edil, T. B., Motan, S. E., and Toha, F. X. (1981), "Mechanical Behavior and Testing Methods of Unsaturated Soils," *Laboratory Shear Strength of Soil, ASTM STP 740*, West Conshohocken, PA., pp. 114-129.

Egorov, K. E. (1965), "Calculation of Bed for Foundation with Ring Footing," *Proceedings of the 6th International Conference of Soil Mechanics and Foundation Engineering*, Vol. 2, pp. 41-45.

Fiedler, S. A., Main, M., and DiMillio, A. F. (2000), "In-place Stiffness and Modulus Measurement," *Proceedings of Sessions of ASCE Specialty Conference on Performance Confirmation of Constructed Geotechnical Facilities*, Geotechnical Special Publication No. 94, pp. 365-376.

Fiedler, S. A., Nelson, C. R., Berkman, E. F. and DiMillio, A. F. (1998), "Soil Stiffness Gauge for Soil Compaction Control," *Public Roads*, U.S. Department of Transportation, Federal Highway Administration, Vol. 61, No. 4.

Fleming, P. R. (1998), "Recycled Bituminous Planings as Unbound Granular Materials for Road Foundations in the UK," *Fifth International Conference on the Bearing Capacity of Roads and Airfields*, Vol. 3, pp. 1581-1590.

Fleming, P. R., Lambert, J. P., Frost, M. W., and Rogers, C. D. F. (2000), "In-situ Assessment of Stiffness Modulus for Highway Foundations during Construction," *Proceedings of the 9th International Conference on Asphalt Pavements*, Copenhagen, Denmark, 15 pp.

Harison, J. A. (1987), "Correlation between California Bearing Ratio and Dynamic Cone Penetrometer Strength Measurement of Soils," *Proceeding of Institute of Civil Engineers*, Part 2, 83, pp. 833-844.

Heukelom, W. and Foster, C. R. (1960), "Dynamic Testing of Pavements," *Journal of the Soil Mechanics and Foundations Division,* ASCE, 86, No. SM1, pp. 1-28.

Hoffman, O. J-M., Guzina, B. B., and Drescher, A. (2004), "Stiffness Estimates Using Portable Deflectometers," *Transportation Research Record 1869*, TRB, National Research Council, Washington, D.C., pp 59-66.

Hoffman, M. S. and Thompson, M. R. (1981), "Nondestructive Testing of Flexible Pavements: Field Testing Program Summary," *Report No. UILU-ENG-2003*, Illinois Department of Transportation, Springfield, IL.

Holtz, R. D. and Kovacs, W. D. (1981), An Introduction to Geotechnical Engineering, Prentice-Hall, Englewood Cliffs, NJ.

Huang, Y. H. (1993), Pavement Analysis and Design, Prentice-Hall, Englewood Cliffs, NJ.

Humboldt Mfg. Co. (1999a), *Report Estimating Dry Density from Soil Stiffness and Moisture Content*, Norridge, IL.

Humboldt Mfg. Co. (1999b), *Humboldt Soil Stiffness Gauge (GeoGauge) User Guide: Version 3.3*, Norridge, IL.

Jones, R. (1958), "In Situ Measurements of the Dynamic Properties of Soil by Vibration Methods," *Geotechnique*, , 8, No.1, pp. 1.

Kleyn, E. G. (1975), "The Use of the Dynamic Cone Penetrometer (DCP)," Transvaal Roads Department, *Report No. 2/74*, South Africa.

Kleyn E. G., Maree J. H. and Savage P. F. (1982), "Application of a Portable Pavement Dynamic Cone Penetrometer to Determine In Situ Bearing Properties of Road Pavement Layers and Subgrades in South Africa," *Proceedings of the 2nd European Symposium on Penetration Testing*, Amsterdam, Netherland, pp. 277-282.

Konrad, J.-M. and Lachance D. (2001), "Use of In Situ Penetration Tests in Pavement Evaluation" *Canadian Geotechnical Journal*, Vol. 38, No. 5, pp. 924-935.

Lee, W., Bohra, N. C., Altschaeffl, A.G., and White, T. D. (1995), "Resilient Modulus of Cohesive Soils and the Effect of Freeze-Thaw," *Canadian Geotechnical Journal*, 32, pp. 559-568.

Lenke, L. R., McKeen, R. G., and Grush, M. (2001), "Evaluation of a Mechanical Stiffness Gauge for Compaction Control of Granular Media," *Report NM99MSC-07.2*, New Mexico State Highway and Transportation Department, Albuquerque, NM.

Lenke, L. R., McKeen, R. G., and Grush, M. P. (2003), "Laboratory Evaluation of the GeoGauge for Compaction Control," *Transportation Research Record 1849*, TRB, National Research Council, Washington, D.C., pp. 20-30.

Livneh, M. (1987), "Validation of Correlations between a Number of Penetration Tests and In Situ California Bearing Ratio Tests," *Transportation Research Record 1219*, TRB, National Research Council, Washington, D.C., pp. 56-67.

Livneh, M. and Goldberg, Y. (2001), "Quality Assessment during Road Formation and Foundation Construction: Use of Falling-Weight Deflectometer and Light Drop Weight," *Transportation Research Record 1755*, TRB, National Research Council, Washington, D.C., pp. 69-77.

Livneh, M., Ishao, I., and Livneh, N. A. (1995), "Effect of Vertical Confinement on Dynamic Cone Penetrometer Strength Values in Pavement and Subgrade Evaluations," *Transportation Research Record 1473*, TRB, National Research Council, Washington, D.C., pp. 1-8.

Livneh, M. and Livneh, N. A. (1994), "Subgrade Strength Evaluation with the Extended Dynamic Cone Penetrometer," *Proceedings of the 7th International Congress International Association of Engineering Geology*, Part 1, Lisbon, Portugal, pp. 219.

Lytton, R. L. (1989), "Backcalculation of Layer Moduli- State of the Art," Nondestructive Testing of Pavements and Backcalculation of Moduli, ASTM STP 1026, A. J. Bush III and G. Y. Baladi, Eds., American Society for Testing and Materials, Philadelphia, PA, pp. 7-38.

Mayne, P. W., Christopher, B. R., and DeJong, J. (2001), *Manual on Subsurface Investigations*, National Highway Institute Publication No. FHWA NHI-01-031, FHWA, Washington, D.C.

McElvaney, J. and Djatnika, B. I. (1991), "Strength Evaluation of Lime-Stabilized Pavement Foundations Using the Dynamic Cone Penetrometer," *Australian Road Research*, 21, No. 1, pp. 40-52.

Motan, S. E. and Edil, T. B. (1982), "Repetitive-Load Behavior of Unsaturated Soils," *Transportation Research Record 872*, TRB, National Research Council, Washington, D.C., pp. 41-48.

Müller, C. (2003), "The light falling weight device: a new and innovative compaction testing method –theory and practice," M.S. Thesis, Institute for Ground Engineering and Soil Mechanics, Vienna University of Technology, Austria.

Nazarian, S. and Stokoe, K. H., II (1987), "In Situ Determination of Elastic Moduli of Pavements Systems by Special-Analysis-of-Surface-Waves Method (Theoretical Aspects)," *Research Report 437-2*, Center for Transportation Research, The University of Texas at Austin, Austin, TX.

Nazarian, S., Yuan, D., and Baker, M. R. (1994), "Automation of SASW Method," *Dynamic Geotechnical Testing II, ASTM STP 1213*, Philadelphia, PA, pp. 88-100.

Newcomb, P. E. and Birgisson, B. (1999), "Measuring In Situ Mechanical Properties of Pavement Subgrade Soils," *Synthesis of Highway Practice 278*, Transportation Research Board, National Research Council, Washington, D.C.

Newcomb, D. E., Chadbourn, B. A., VanDeusen, D. A., and Burnham, T. R. (1996), "Initial Characterization of Subgrade Soils and Granular Base Materials at the Minnesota Road Research Project," *MN/RC 96-19*, 149 pp.

Pidwerbesky, B. (1997), "Prediction Rutting in Unbound Granular Base Courses from Loadman and Other In Situ Non-Destructive Tests," *Road and Transport Research*, Vol. 6, No. 3, September, pp. 16-25.

Pinard, M. I. (1998), "Innovative Compaction Techniques for Improving the Bearing Capacity of Roads and Airfields," *Fifth International Conference on the Bearing Capacity of Roads and Airfields*, Vol. 3, pp. 1471-1480.

Powell, W. D., Potter, J. F., Mayhew, H. C., and Nunn, M. E. (1984), "The Structural Design of Bituminous Roads," *TRRL Laboratory Report 1132*, Transportation and Road Research Laboratory, Crowthorne, Berkshire, 62 pp.

Qian, X., Gray, D. H., and Woods, R. D. (1993), "Voids and Granulometry: Effects on Shear Modulus of Unsaturated Sands," Journal of Geotechnical Engineering, Vol. 119, No. 2, pp. 295-314.

Rix, G. J. and Stokoe, K. H., II (1989), "Stiffness Profiling of Pavement Subgrades," *Transportation Research Record*, No. 1235, Washington, D.C., pp. 1-9.

Saarenketo, T., Scullionm, T., and Kolisoja, P. (1998), "Moisture Susceptibility and Electrical Properties of Base Course Aggregates," *Fifth International Conference on the Bearing Capacity of Roads and Airfields*, Vol. 3, pp. 1401-1410.

Sanchez-Salinero, I., Roesset, J. M., Shao, K., Stokoe, K. H., II, and Rix, G. J. (1987), "Analytical Evaluation of Variables Affecting Surface Wave Testing of Pavements," *Transportation Research Record 1136*, Washington, D.C., pp. 132-144.

Sawangsuriya, A., Bosscher, P. J., and Edil T. B. (2002), "Laboratory Evaluation of the Soil Stiffness Gauge," *Transportation Research Record 1808*, TRB, National Research Council, Washington, D.C., pp. 30-37.

Sawangsuriya, A., Edil, T. B., and Bosscher, P. J. (2003), "Relationship between Soil Stiffness Gauge Modulus and Other Test Moduli for Granular Soils," *Transportation Research Record 1849*, TRB, National Research Council, Washington, D.C., pp. 3-10.

Sawangsuriya, A., Edil, T. B., and Bosscher, P. J. (2004), "Assessing Small-Strain Stiffness of Soils Using the Soil Stiffness Gauge," *Proceedings of the 15th Southeast Asian Geotechnical Conference*, Bangkok, Thailand, pp. 101-106.

Scala A. J. (1956), "Simple Methods of Flexible Pavement Design Using Cone Penetrometers," *New Zealand Engineering*, 11, No. 2, pp. 34-44.

Seed, H. B. and Chan, C. K. (1959), "Structure and Strength Characteristics of Compacted Clays," *Journal of the Soil Mechanics and Foundations Division*, Vol. 85, No. SM5, pp. 87-128.

Siekmeier, J. A., Young, D., and Beberg, D. (1999), "Comparison of the Dynamic Cone Penetrometer with Other Tests during Subgrade and Granular Base

Characterization in Minnesota," *Nondestructive Testing of Pavements and Back Calculation of Moduli, ASTM STP 1375*, West Conshohocken, PA, pp. 175-188.

Smith, R. E. and Lytton, R. L. (1984), "Synthesis Study of Nondestructive Testing Devices for Use in Overlay Thickness Design of Flexible Pavement," *Report No. FHWA/RD-83/097*, Federal Highway Administration, Washington, D. C.

Syed, I. and Scullion, T. (1998), "In-Place Engineering Properties of Recycled and Stabilized Pavement Layers," *Fifth International Conference on the Bearing Capacity of Roads and Airfields*, Vol. 3, pp. 1619-1630.

Tanyu, B. F., Kim, W. H., Edil, T. B. and Benson, C. H. (2003) **"**Comparison of Laboratory Resilient Modulus with Back-Calculated Elastic Moduli from Large-Scale Model Experiments and FWD Tests on Granular Materials**,"** *Resilient Modulus Testing for Pavement Components, ASTM STP 1437*, G. N. Durham, A. W. Marr, and W. L. De Groff, Eds., ASTM, West Conshohocken, PA, pp. 191-208.

Turnbull, W. J. and Foster, C. R. (1956), "Stabilization of Materials by Compaction," *Journal of the Soil Mechanics and Foundations Division*, Vol. 82, No. SM2, pp. 934(1)-934(23).

van Niekerk, A. A., Houben, L. J. M., and Molenaar, A. A. A. (1998), "Estimation of Mechanical Behavior of Unbound Road Building Materials from Physical Material Properties," *Fifth International Conference on the Bearing Capacity of Roads and Airfields*, Vol. 3, pp. 1221-1233.

Van Vuuren, D. J. (1969), "Rapid Determination of CBR with the Portable Dynamic Cone Penetrometer," *The Rhodesian Engineer*, Vol. 7, No.5, pp. 852-854.

Webster, S. L., Grau, R. H., and Williams, T. P. (1992), "Description and Application of Dual Mass Dynamic Cone Penetrometer," *Instruction Report GL-92-3*, U.S. Army Engineers Waterways Experimental Station, Vicksburg, MS, 17 pp.

Wright, S. G., Stokoe, K. E., II, and Roesset, J. M. (1994), "SASW Measurements at Geotechnical Sites Overlaid by Water," *Dynamic Geotechnical Testing II, ASTM STP 1213*, Philadelphia, PA, pp. 39-57.

Wu, S., Gray, D. H., and Richart, F. E., Jr. (1984), "Capillary Effects on Dynamic Modulus of Sands and Silts," *Journal of Geotechnical Engineering*, Vol. 110, No. 9, pp. 1188-1203.

Wu, W., Arellano, M., Chen, D-H., Bilyeu, J., and He, R. (1998), "Using a Stiffness Guage as an Alternative Quality Control Device in Pavement Construction," Texas Department of Transportation, Austin, TX, 17 pp.

Yesiller, N., Inci, G., and Miller, C. J. (2000), "Ultrasonic Testing for Compacted Clayey Soils," *Advances in Unsaturated Geotechnics, Geotechnical Special Publication No. 99,* ASCE, pp. 54-68.

Yuan D. and Nazarian S. (2003), "Variation in Moduli of Base and Subgrade with Moisture," *TRB Annual Meeting (in CD-ROM),* 15 pp.

APPENDIX A:

Field Measurement Results from Each Test Site

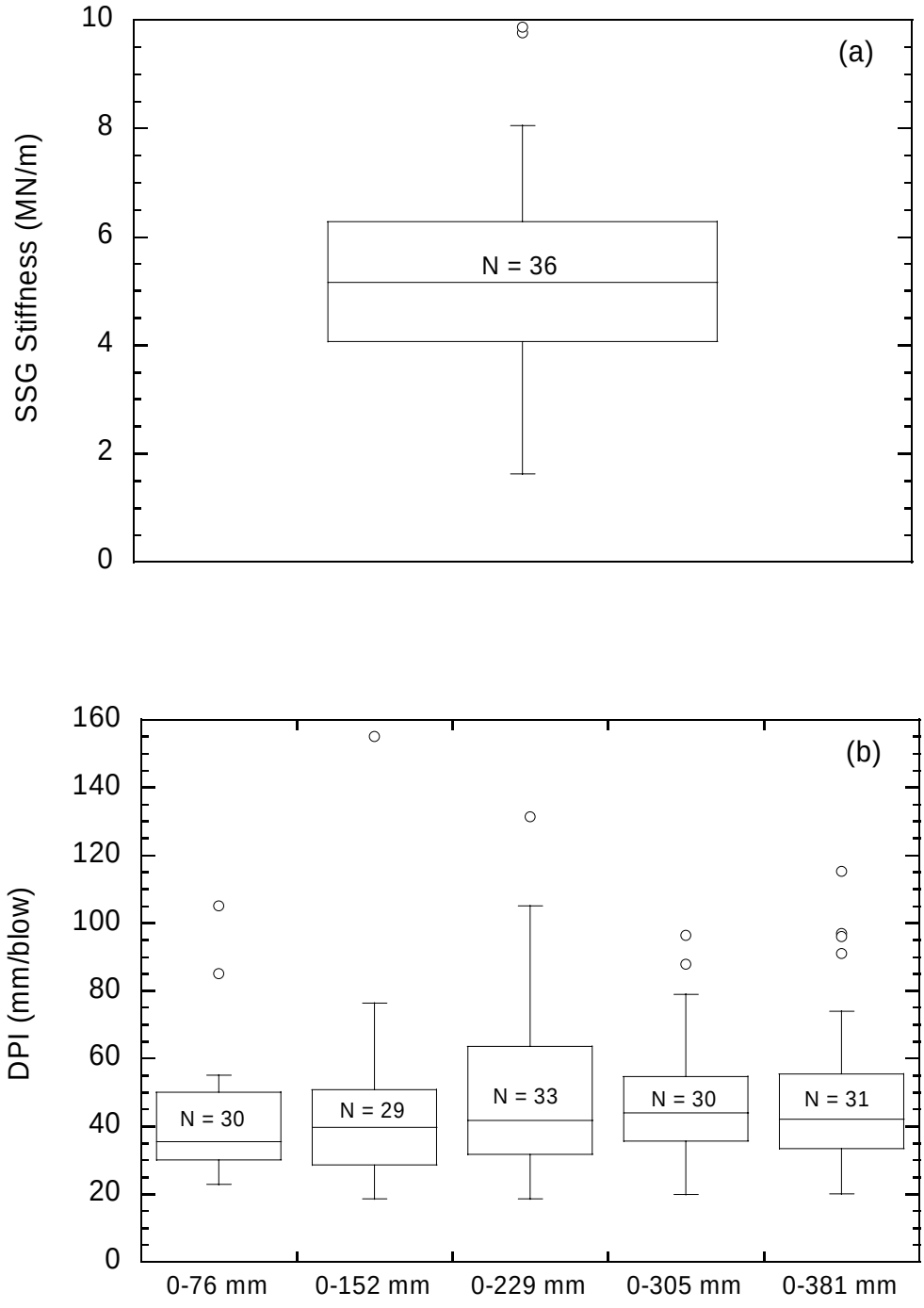

Fig. A-1. STH 60 test section: CL-ML (a) SSG stiffness and (b) DCP penetration index (DPI).

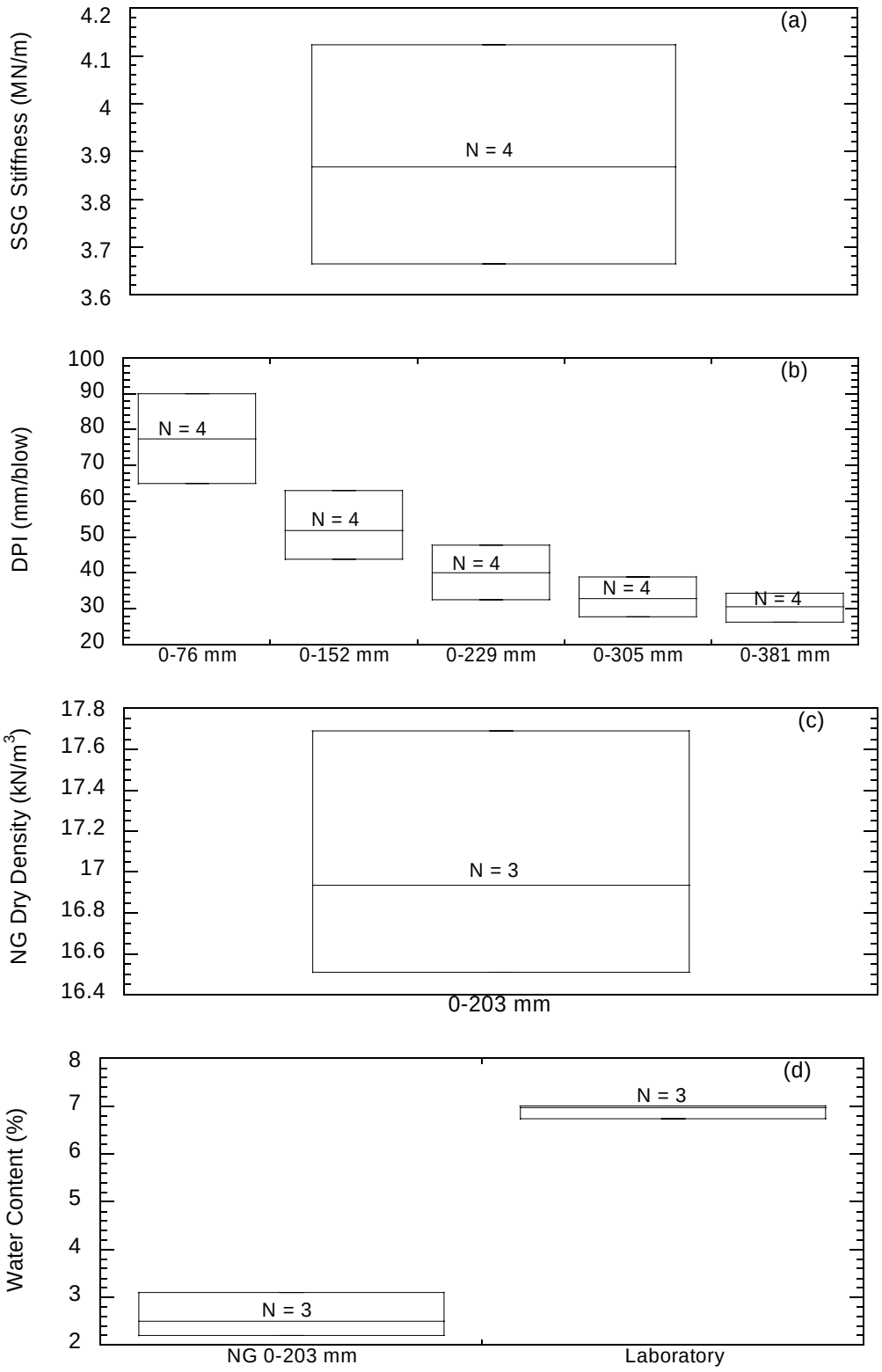

Fig. A-2. STH 60 test section: bottom ash (a) SSG stiffness, (b) DCP penetration index (DPI), (c) nuclear gauge (NG) dry density, and (d) water content.

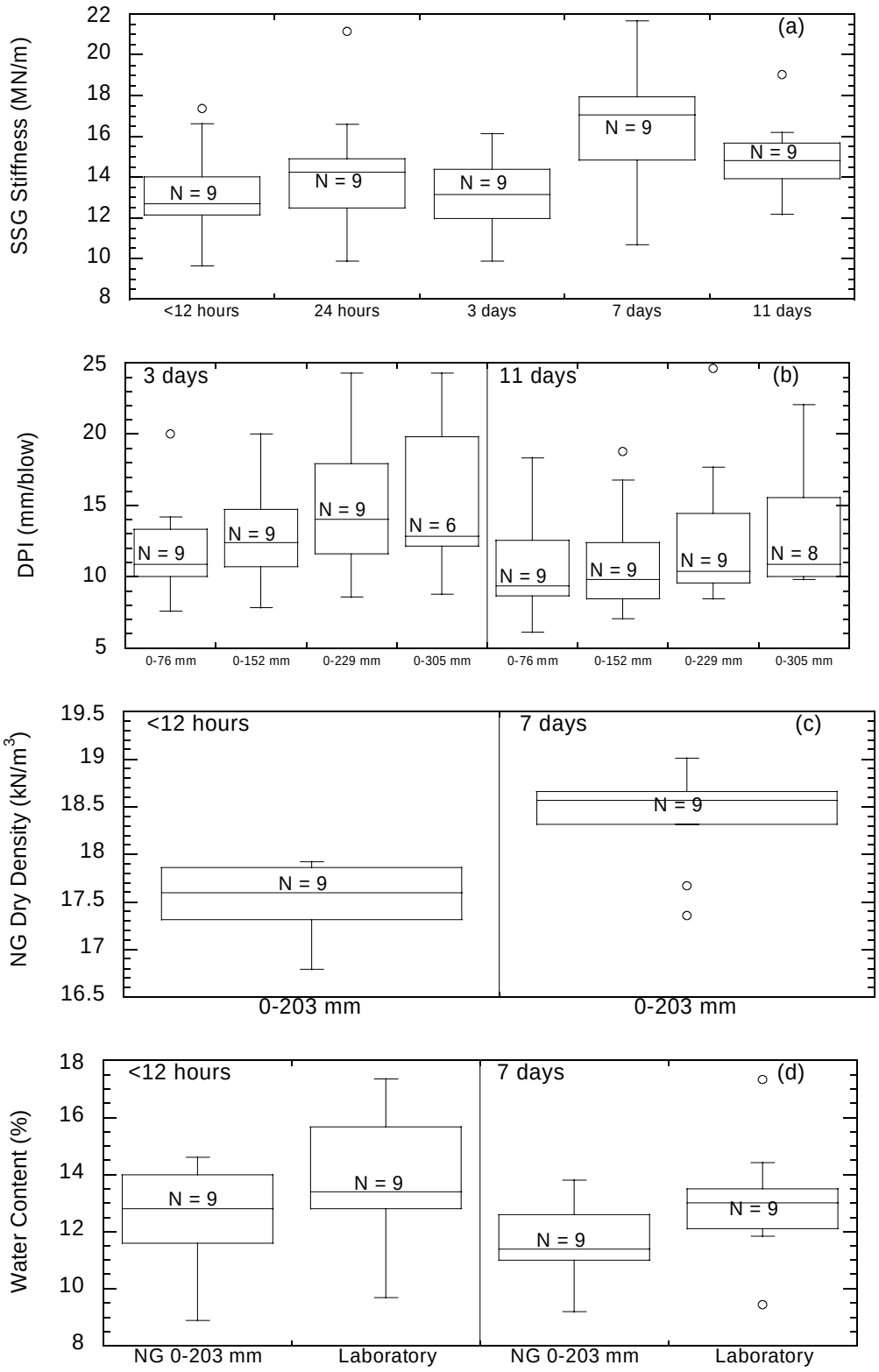

Fig. A-3. STH 60 test section: fly ash-stabilized soils (a) SSG stiffness, (b) DCP penetration index (DPI), (c) nuclear gauge (NG) dry density, and (d) water content.

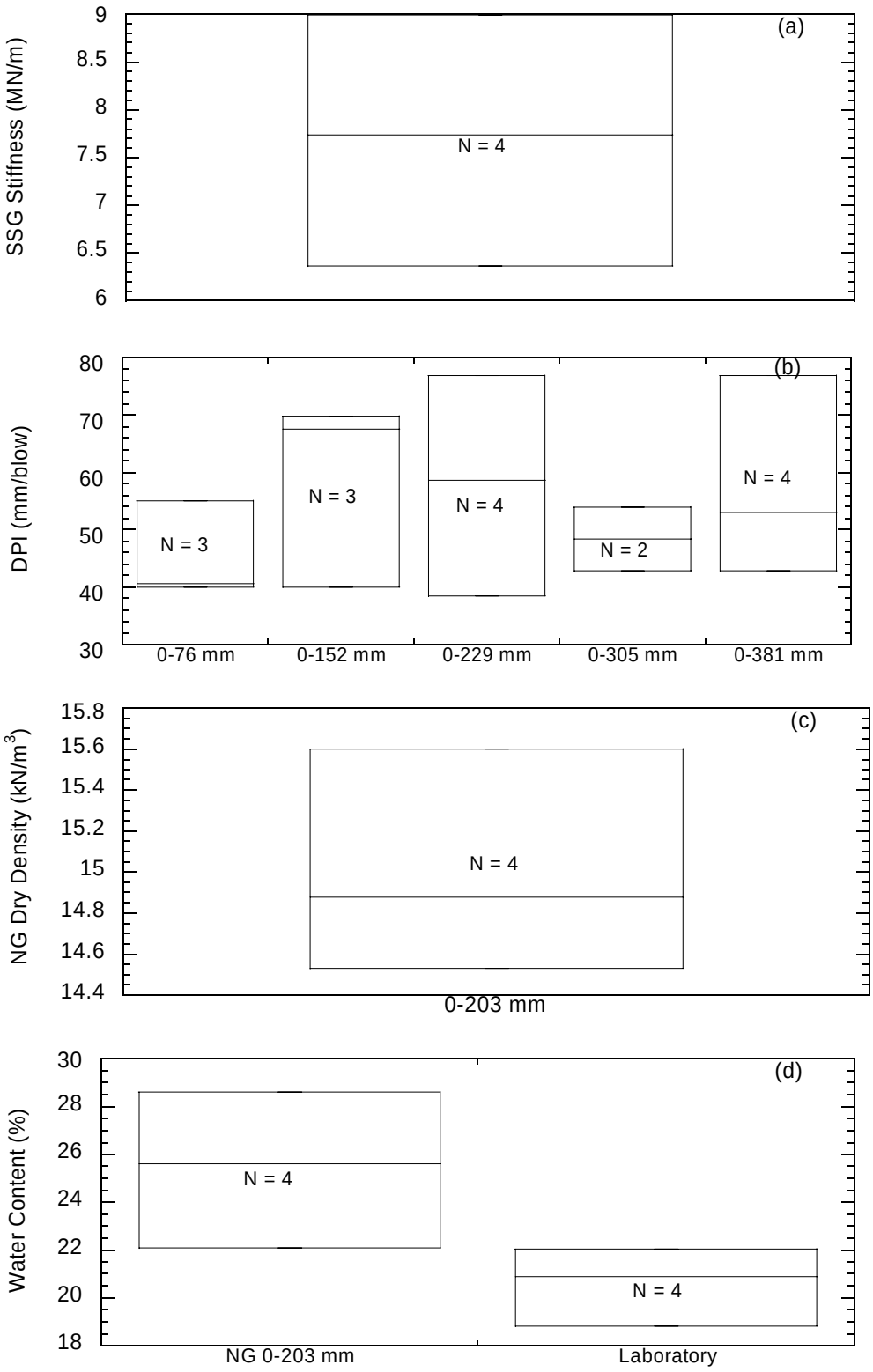

Fig. A-4. STH 60 test section: foundry sand (a) SSG stiffness, (b) DCP penetration index (DPI), (c) nuclear gauge (NG) dry density, and (d) water content.

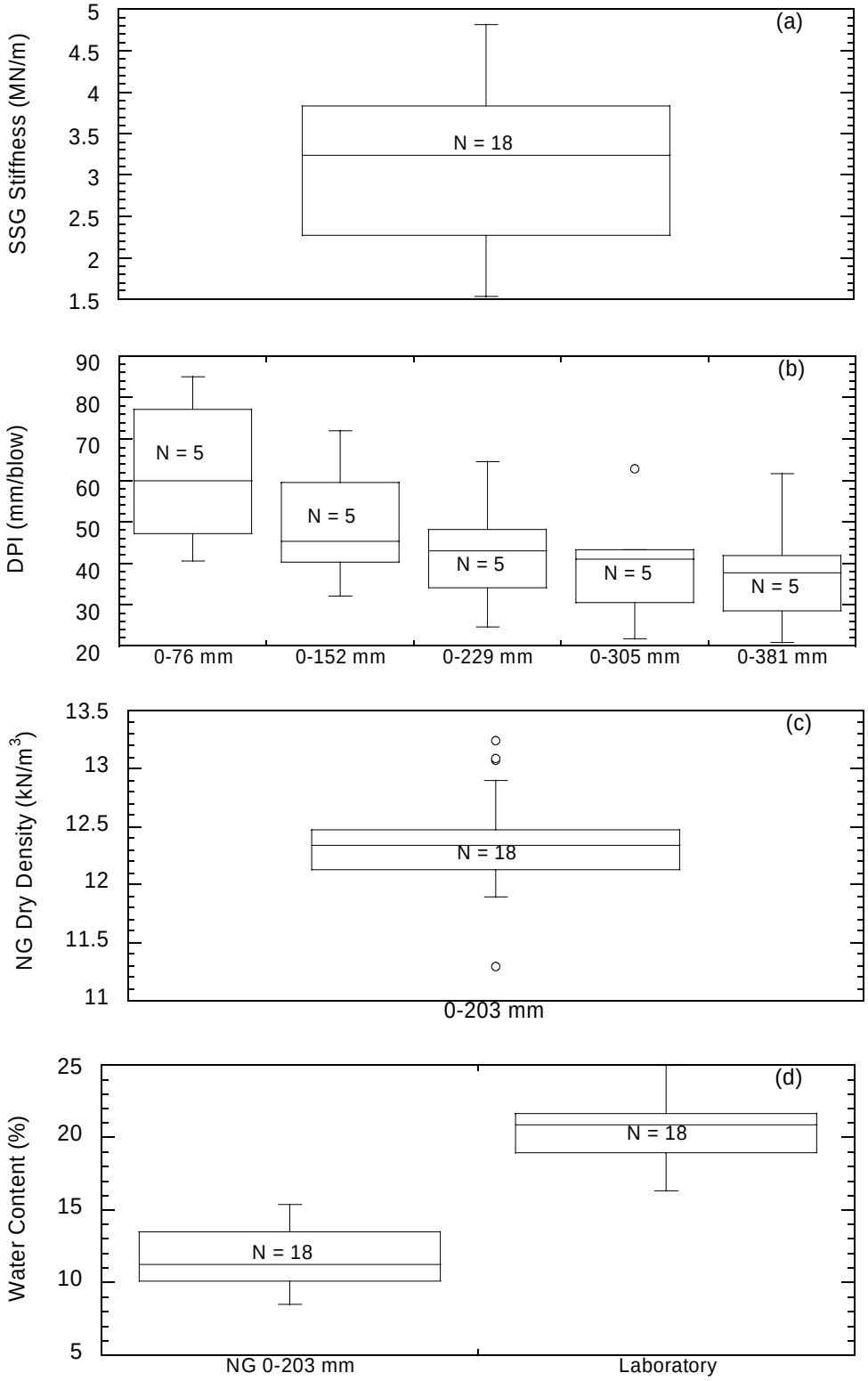

Fig. A-5. STH 60 test section: foundry slag (a) SSG stiffness, (b) DCP penetration index (DPI), (c) nuclear gauge (NG) dry density, and (d) water content.

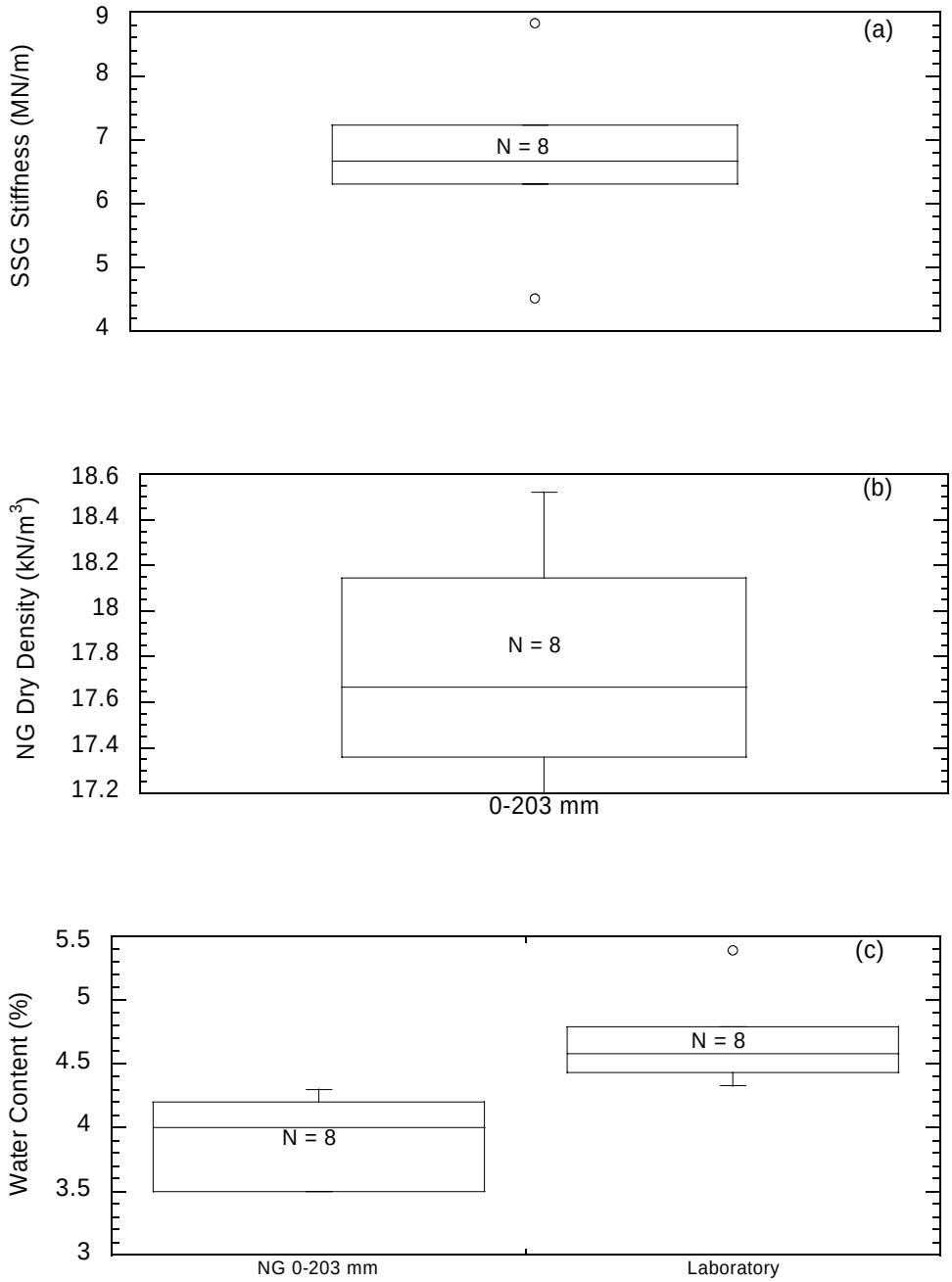

Fig. A-6. STH 60 test section: breaker run (a) SSG stiffness, (b) nuclear gauge (NG) dry density, and (c) water content.

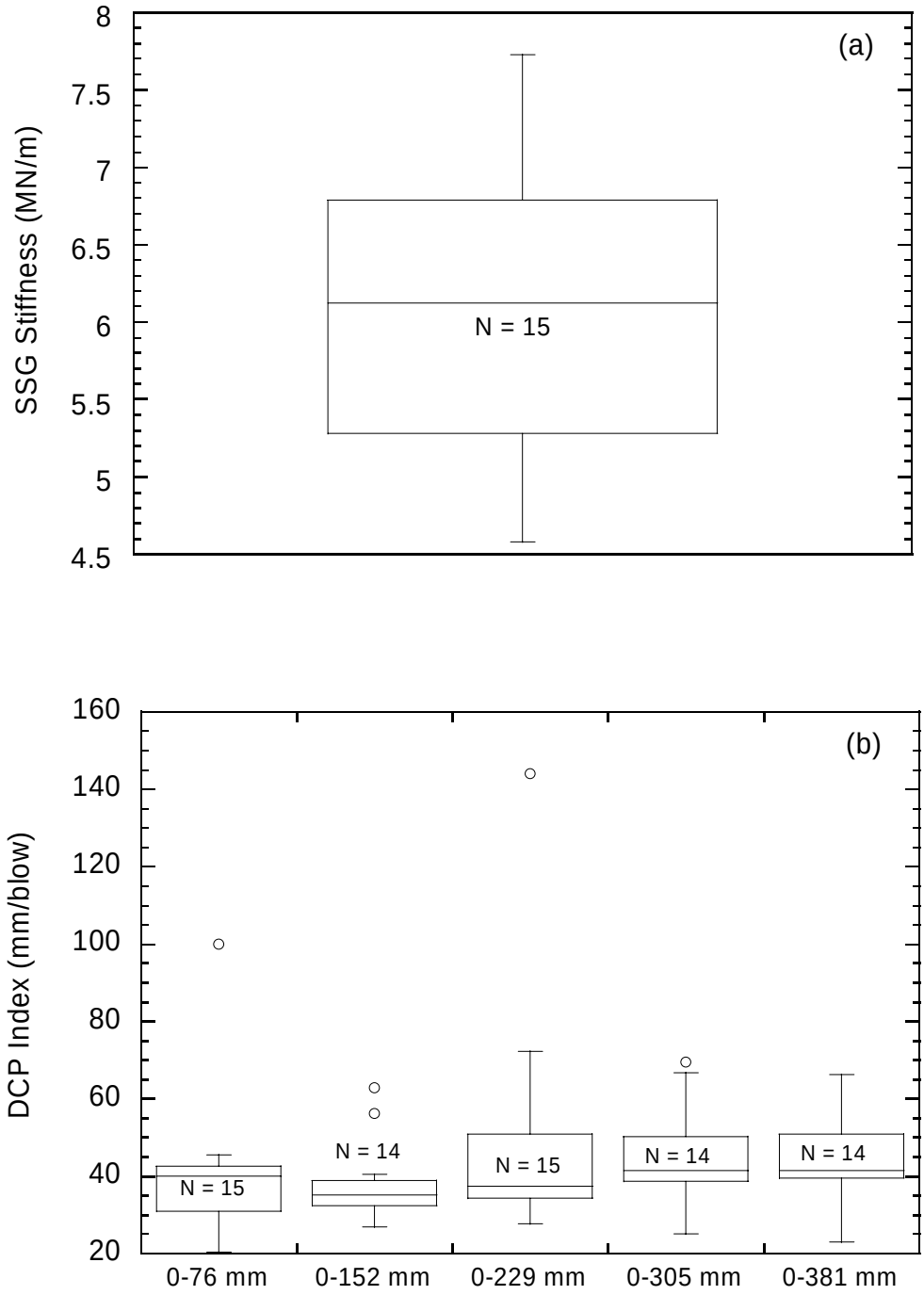

Fig. A-7. Scenic Edge development: CL (a) SSG stiffness and (b) DCP penetration index (DPI).

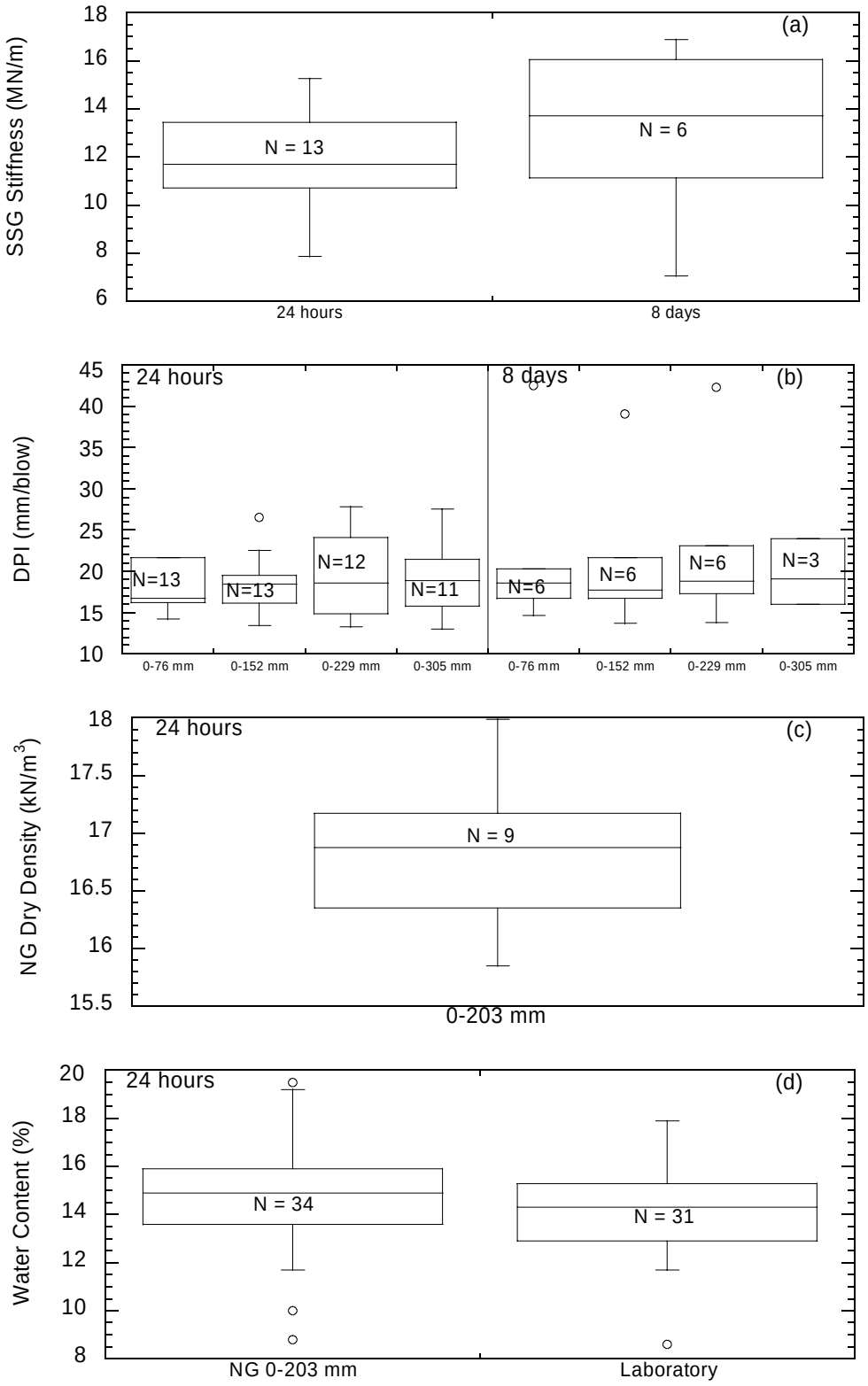

Fig. A-8. Scenic Edge development: fly ash-stabilized soils (a) SSG stiffness, (b) DCP penetration index (DPI), (c) nuclear density (NG) dry density, and (d) water content.

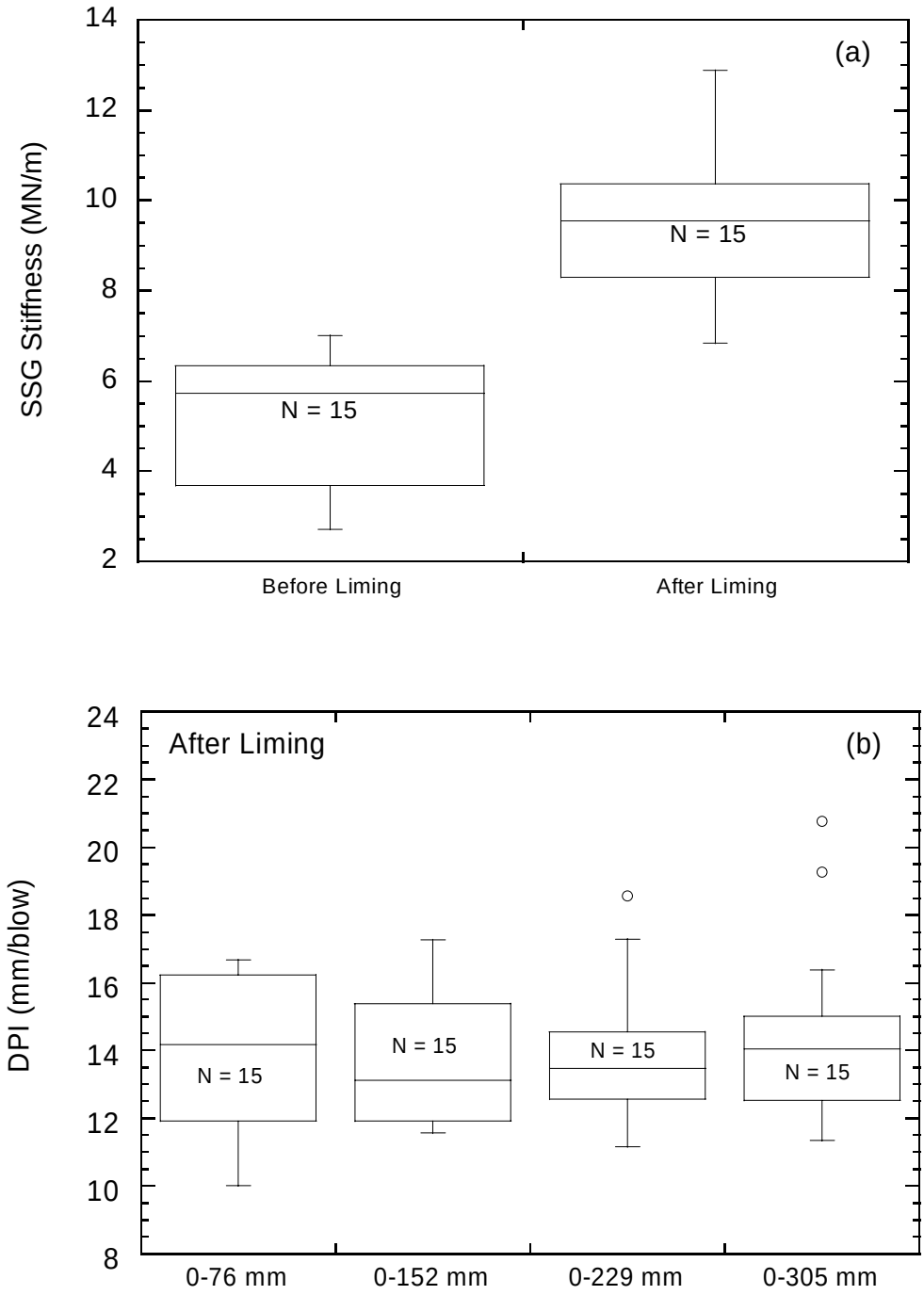

Fig. A-9. Gils Way development: before and after liming (a) SSG stiffness and (b) DCP penetration index (DPI).

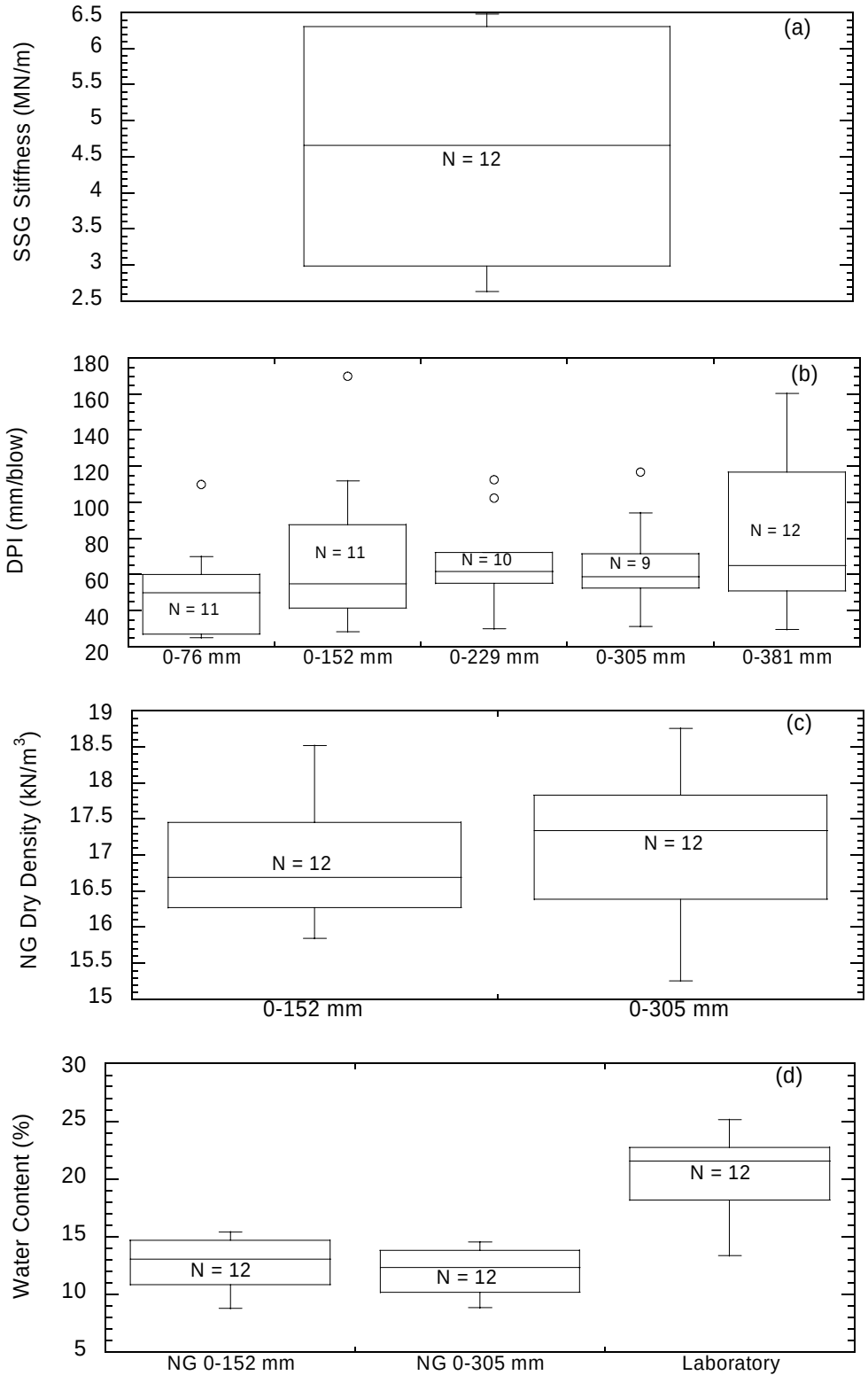

Fig. A-10. STH 26: CL (a) SSG stiffness, (b) DCP penetration index (DPI), (c) nuclear gauge (NG) dry density, and (d) water content.

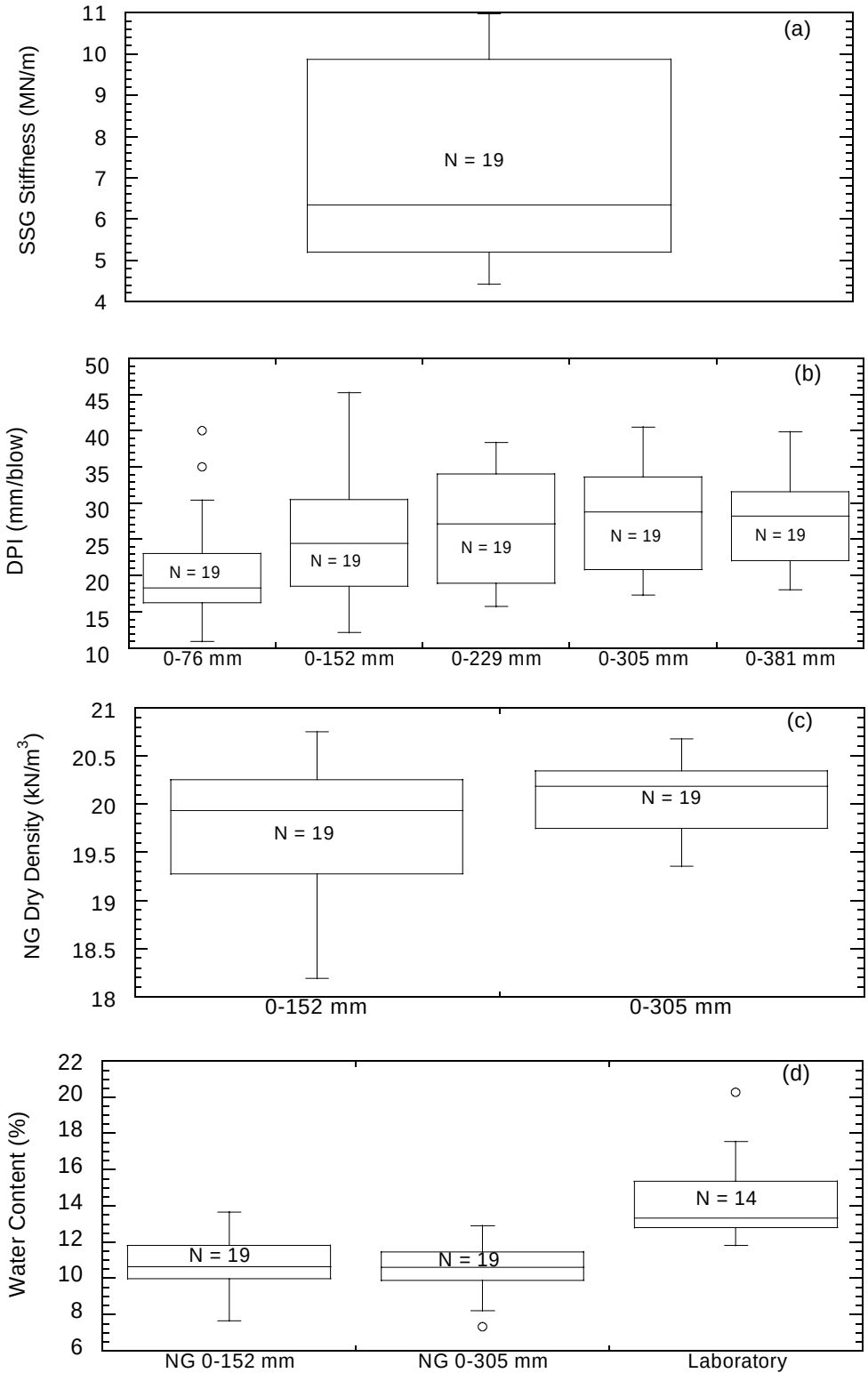

Fig. A-11. STH 100: CL (a) SSG stiffness, (b) DCP penetration index (DPI), (c) nuclear gauge (NG) dry density, and (d) water content.

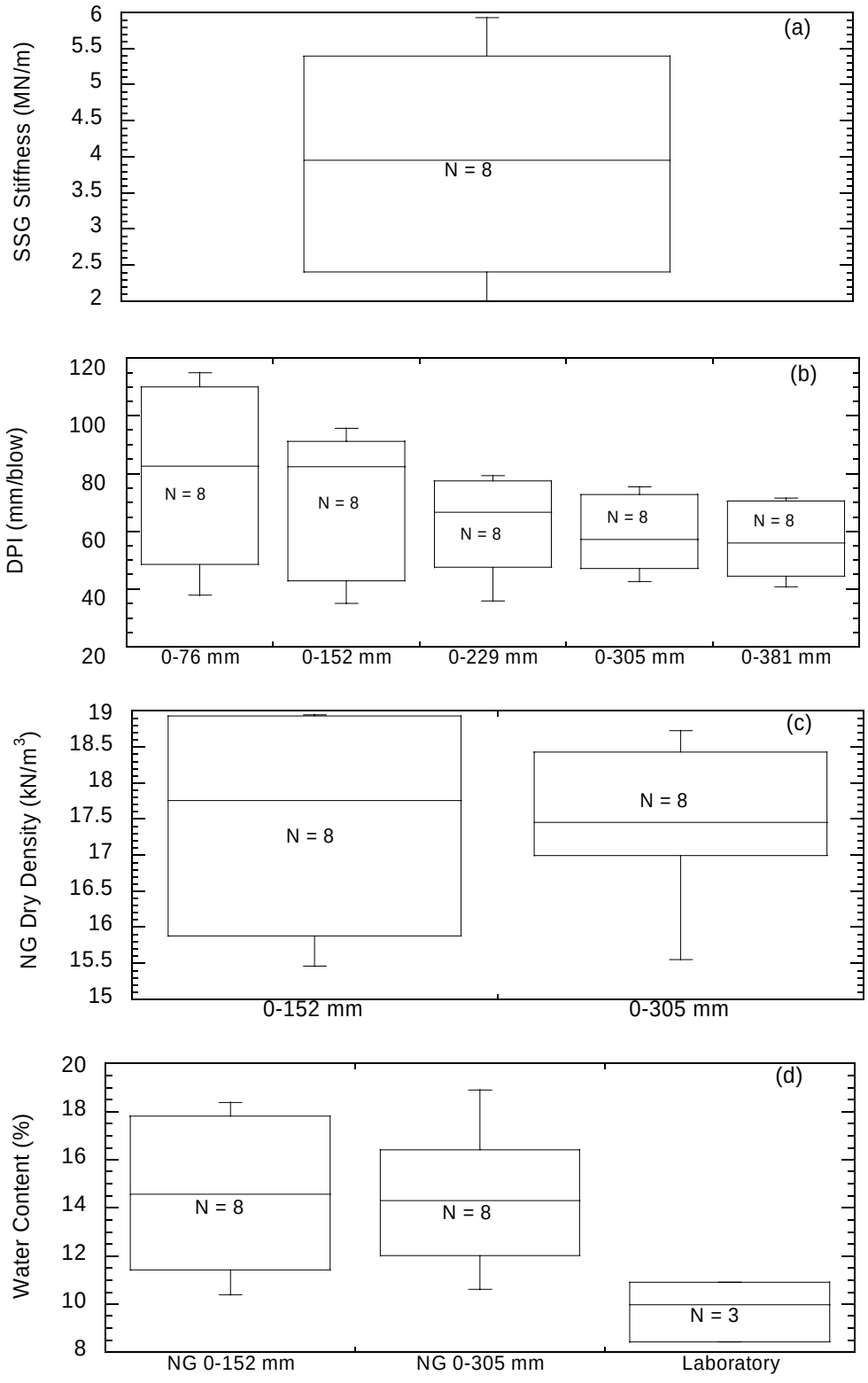

Fig. A-12. STH 44: SC-SM (a) SSG stiffness, (b) DCP penetration index (DPI), (c) nuclear density (NG) dry density, and (d) water content.

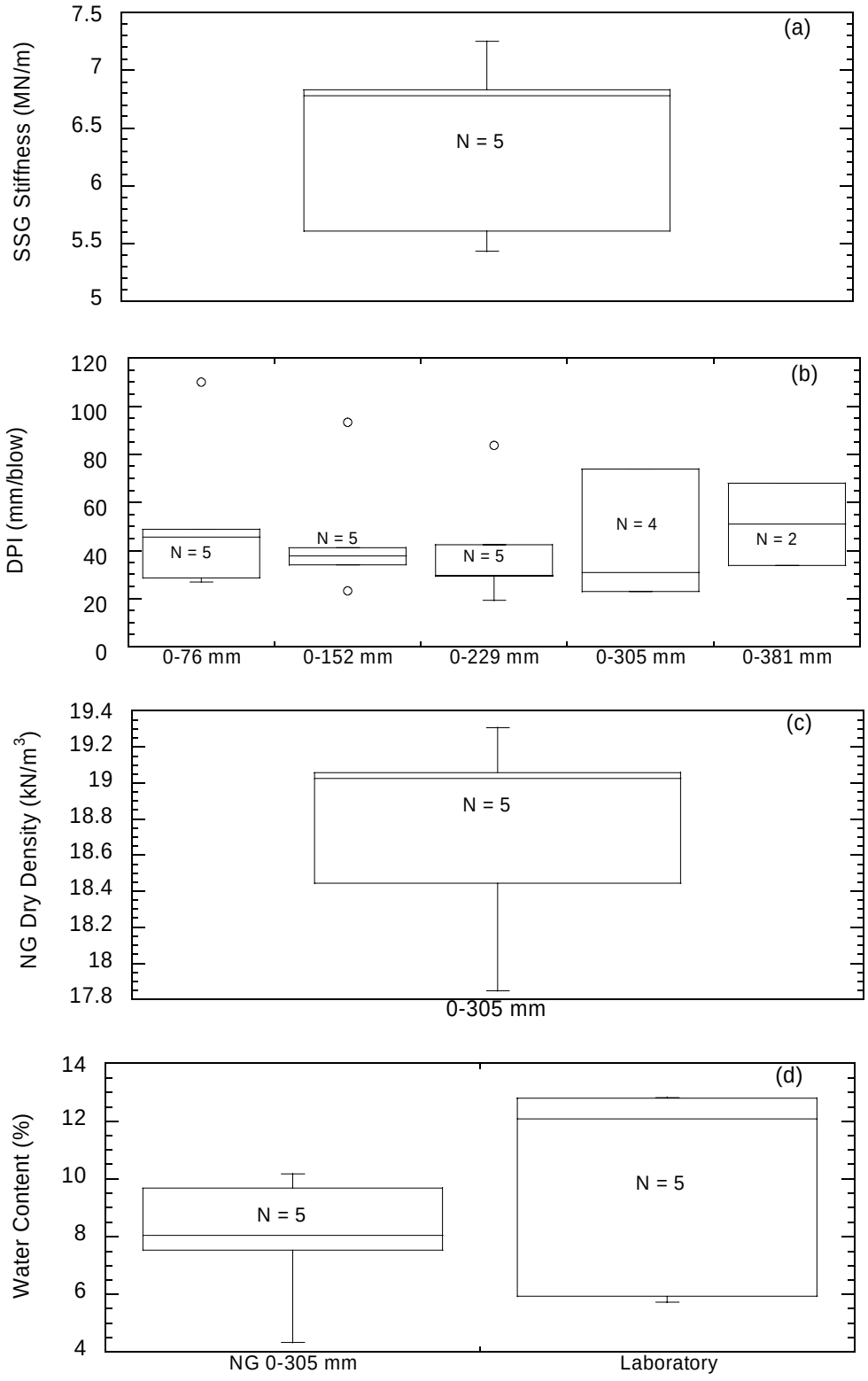

Fig. A-13. USH 12: SC (a) SSG stiffness, (b) DCP penetration index (DPI), (c) nuclear density (NG) dry density, and (d) water content.

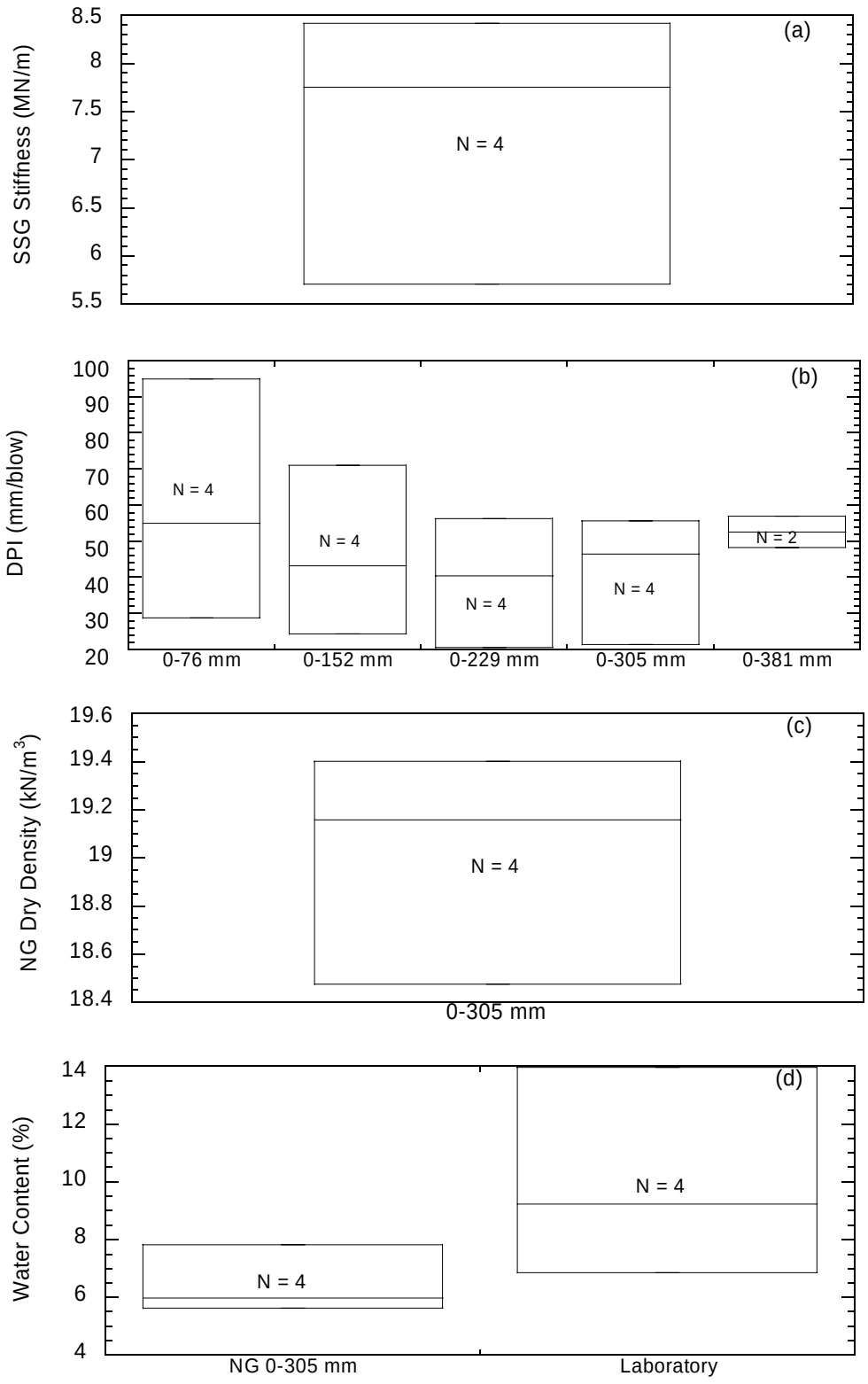

Fig. A-14. STH 131: SP-SM (a) SSG stiffness, (b) DCP penetration index (DPI), (c) nuclear gauge (NG) dry density, and (d) water content.

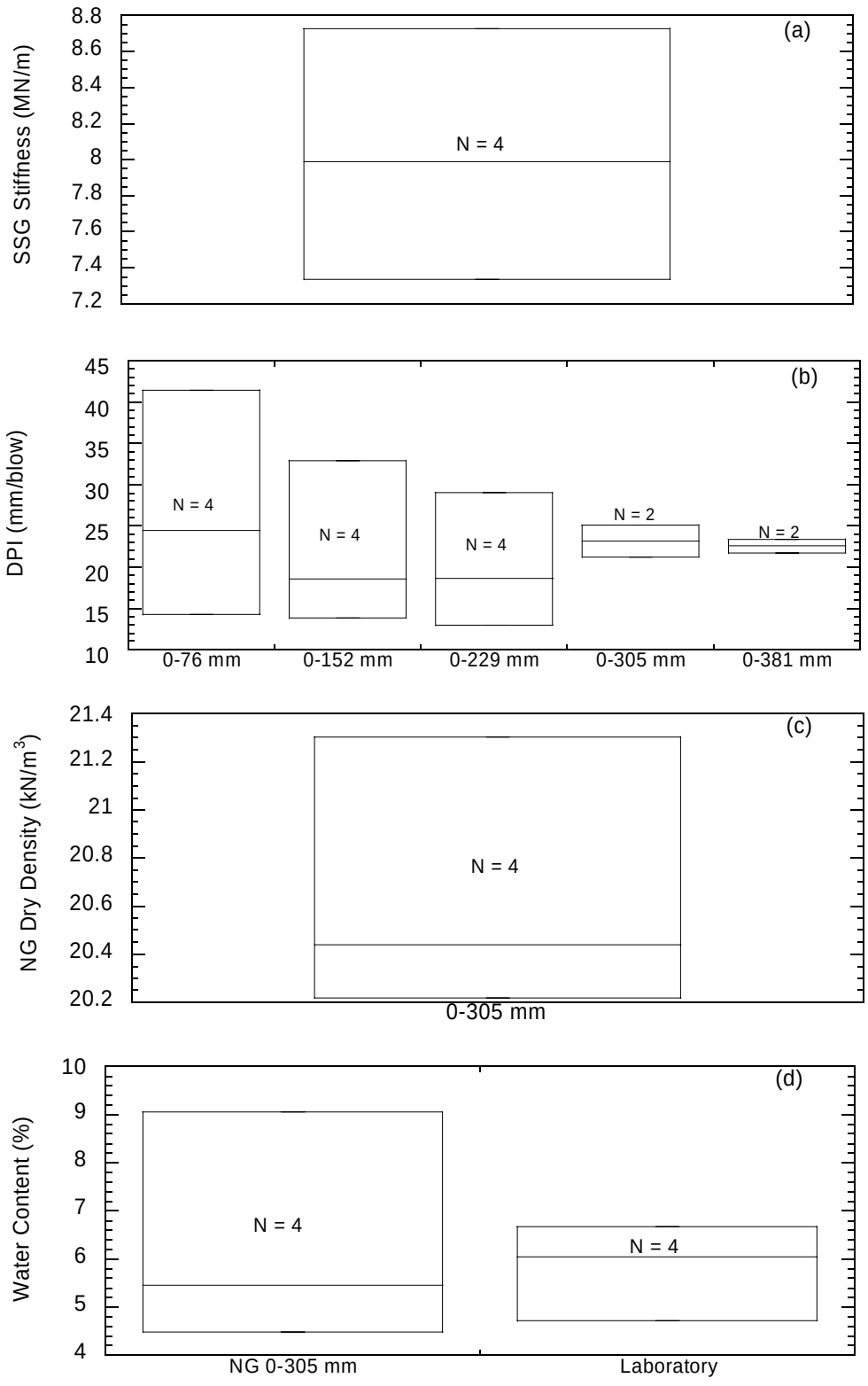

Fig. A-15. STH 58: SC (a) SSG stiffness, (b) DCP penetration index (DPI), (c) nuclear density (NG) dry density, and (d) water content.

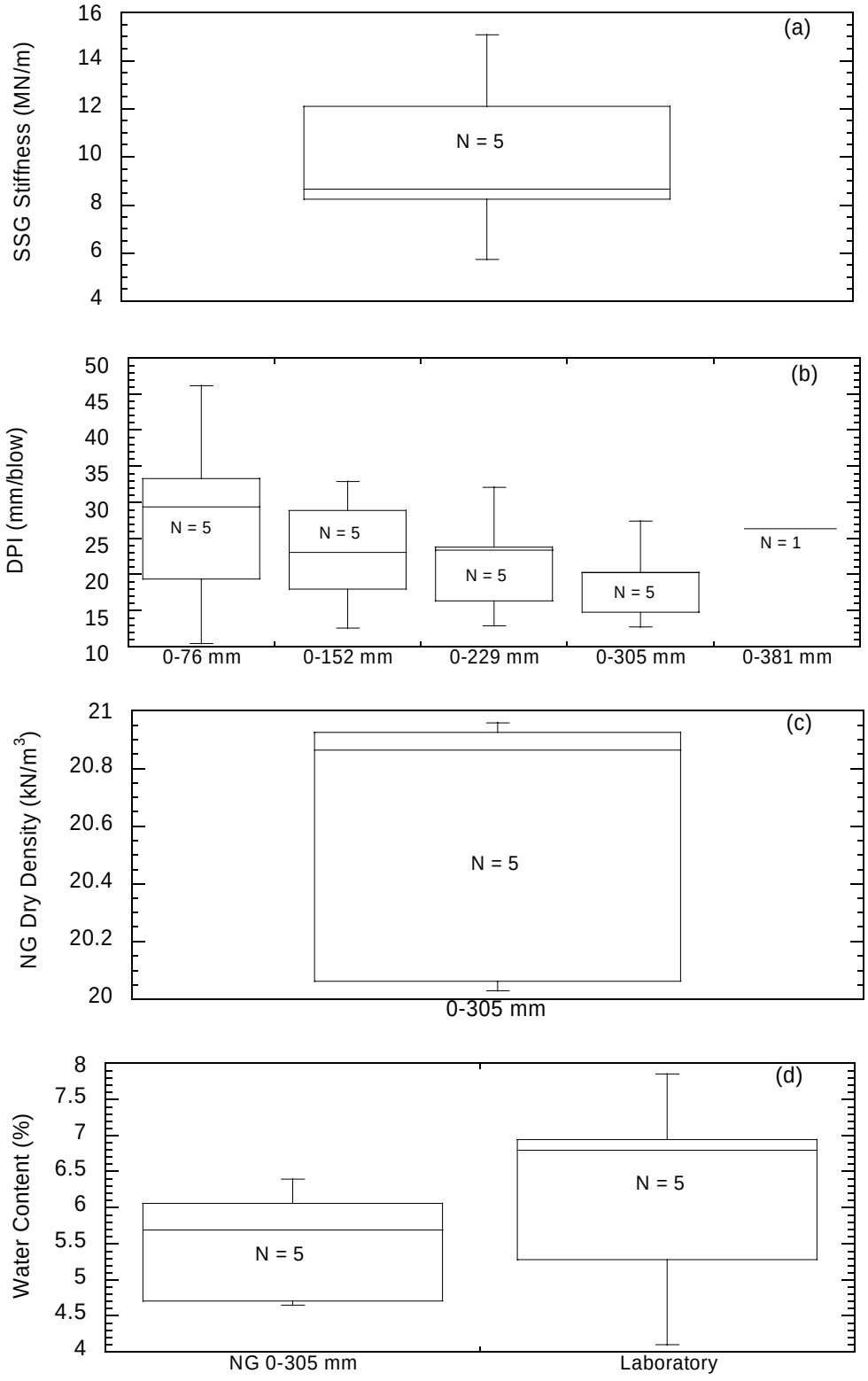

Fig. A-16. STH 154: SP-SM (a) SSG stiffness, (b) DCP penetration index (DPI), (c) nuclear gauge (NG) dry density, and (d) water content.

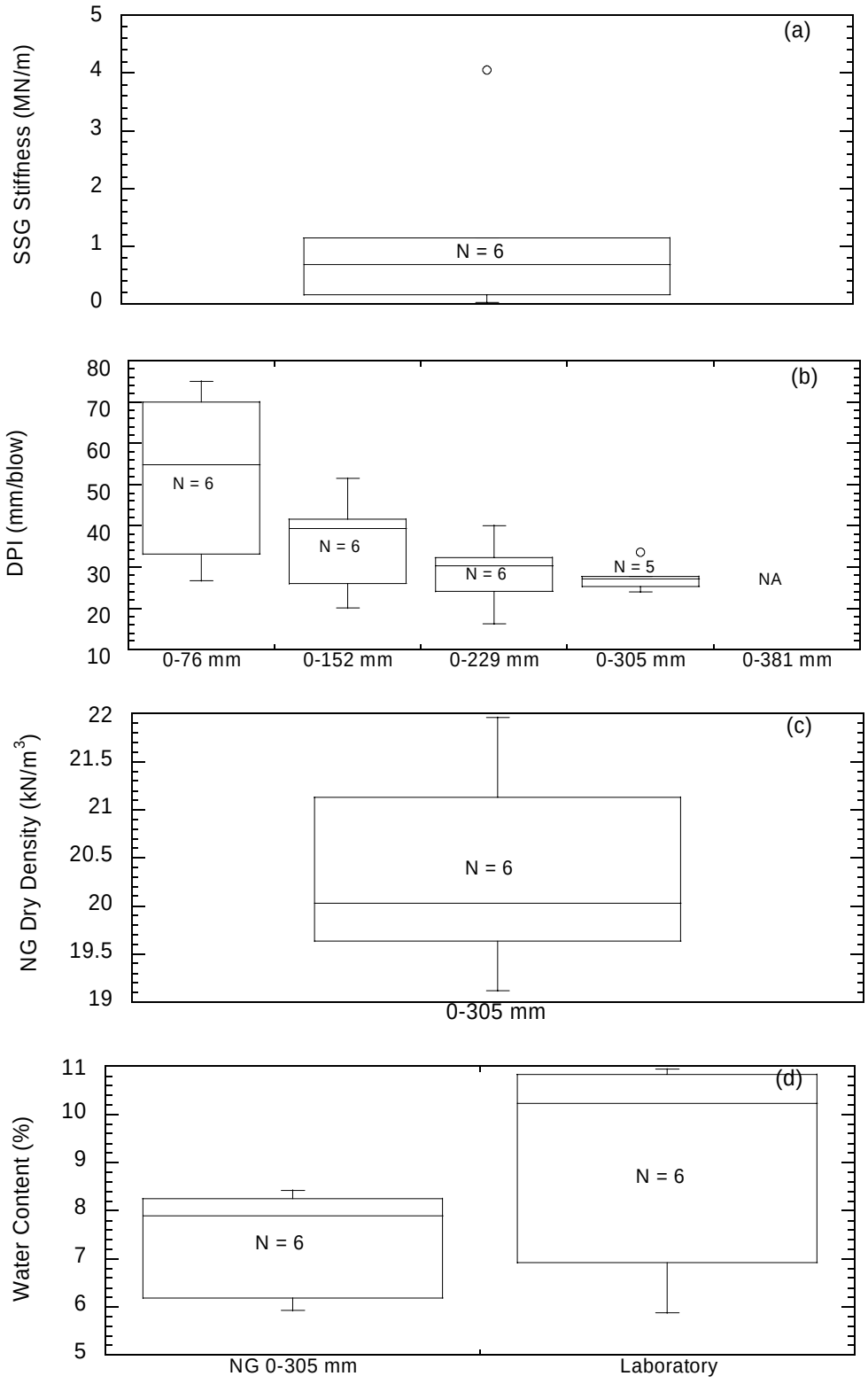

Fig. A-17. USH 2: SP-SM (a) SSG stiffness, (b) DCP penetration index (DPI), (c) nuclear gauge (NG) dry density, and (d) water content.

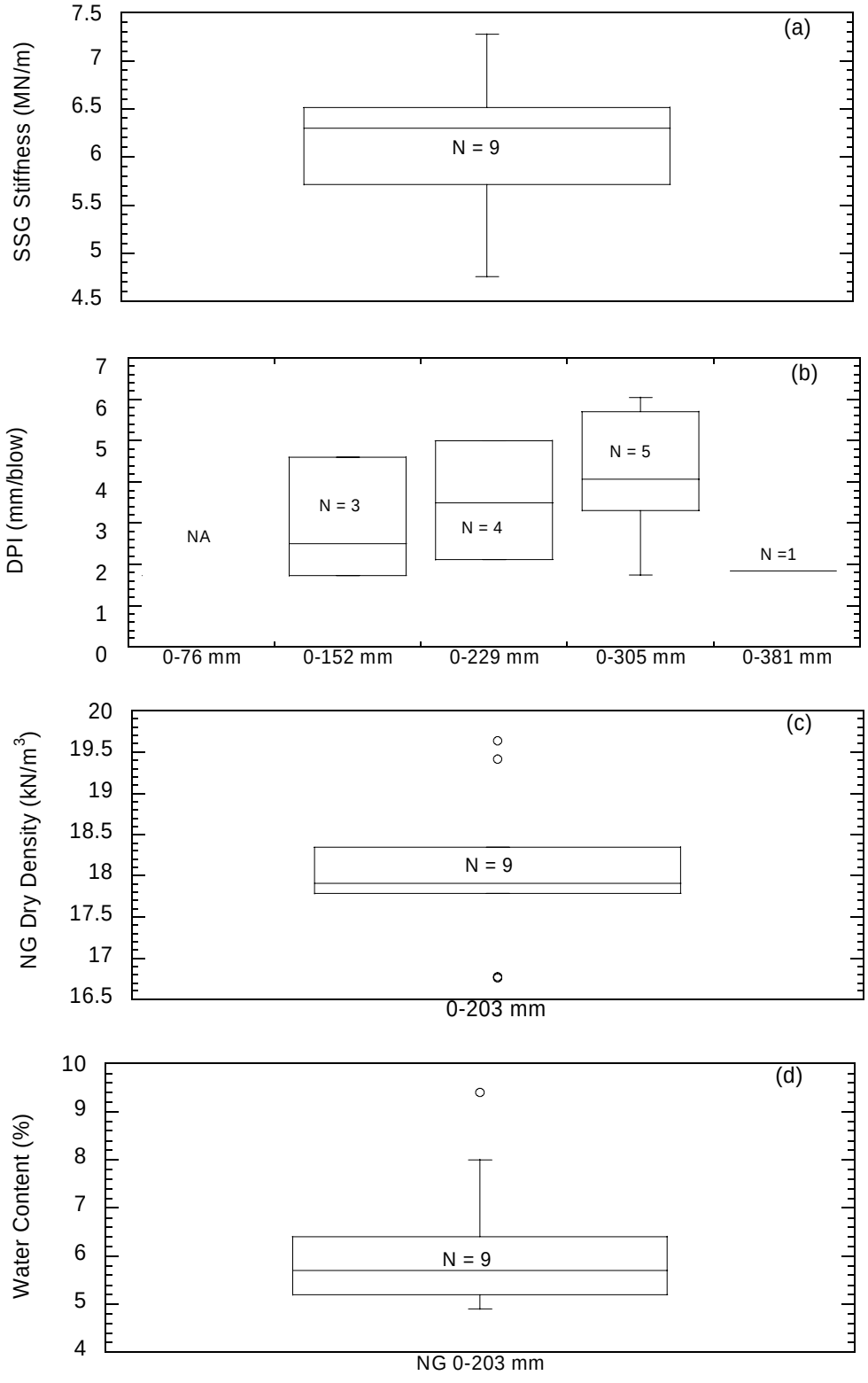

Fig. A-18. CTH E: SP (a) SSG stiffness, (b) DCP penetration index (DPI), (c) nuclear gauge (NG) dry density, and (d) water content.

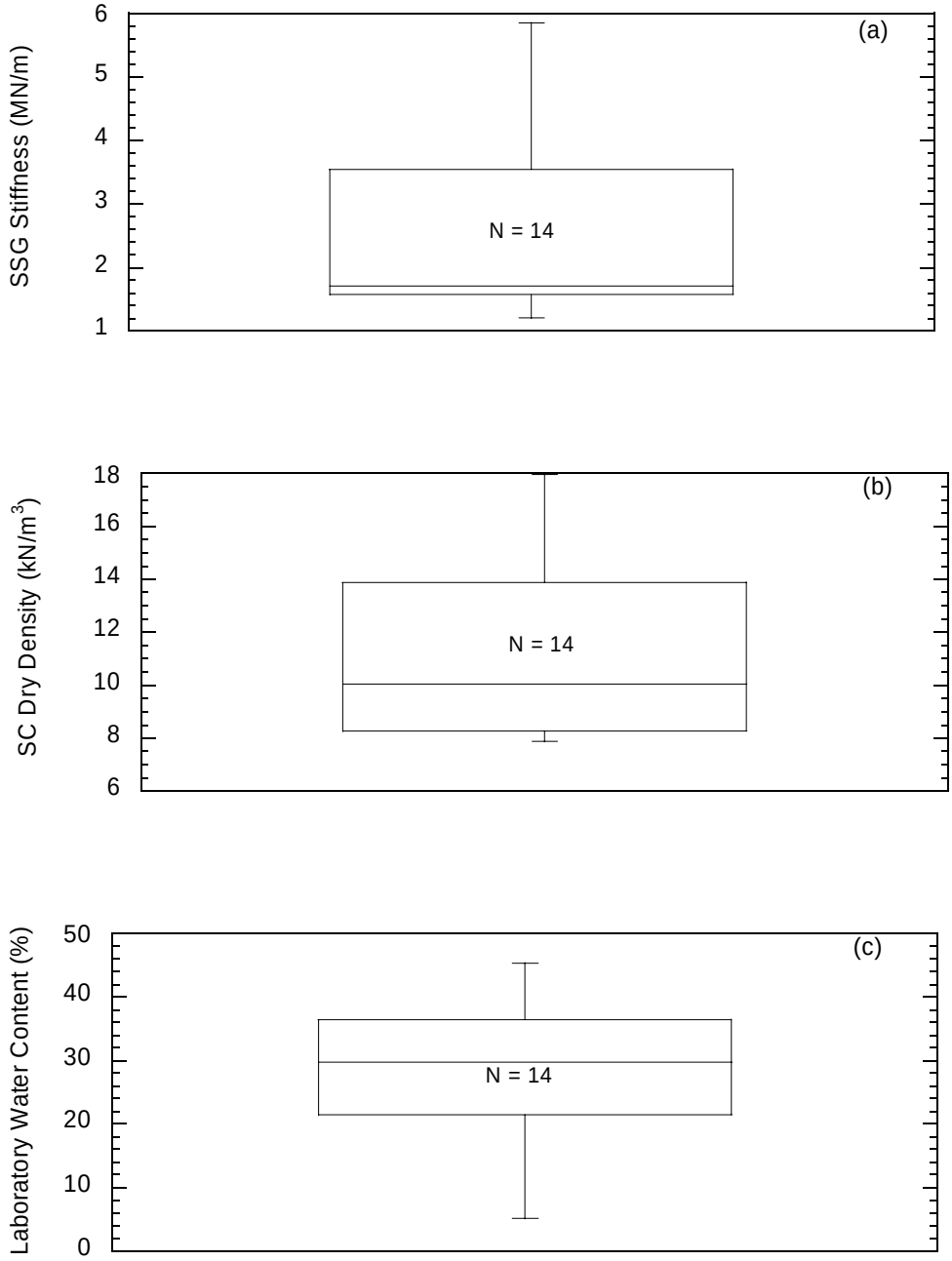

Fig. A-19. MMSD project: cap material (a) SSG stiffness, (b) sandcone (SC) dry density, and (c) laboratory water content.

APPENDIX B:

Statistical Analysis

Guideline for Statistical Analysis of the SSG Stiffness and DPI Correlation

1) Categorize the field measurement data (i.e., SSG stiffness and DCP penetration index) on the basis of material types. Create plots of the data for each material type and DCP penetration depth. Then, *coefficient of determination* (R^2) can be determined.
2) Assume a high R^2 signifies a useful regression equation and that a low R^2 signifies the opposite. In addition, high R^2 indicates that the observed relation between independent and dependent variables is true and can be used to predict new conditions.
3) Take only possible relations (i.e., high R^2 from 1) into consideration.
4) Fit a simple linear regression equation for any possible relations. Transformation of the data is also required if the relations is nonlinear. Use the significant level of 95% to obtain the p-value and/or F statistic, etc. Determine if a regression with either high or low R^2 is statistically significant at 95% level of confidence.
5) If the regression has a high R^2 and is statistically significant at 95% level of confidence*, then go to 6). For high R^2 without statistically significant relationship, the variation of the data might be checked by using the box plots so that a prediction range is to be examined (see also 6). For a low R^2 but statistically significant relationship, other regression models should be considered to fit the data (see also 7). For a low R^2 without statistically significant relationship, the relation for that particular set of data cannot be established. It is also important for all cases to check for the residual and the normal quantile plots in order to assure the IIDN$(0,\sigma^2)$ assumptions.

*__Note__: *It generally is good news if R^2 is large and also statistically significant, but it does not assure a useful equation, especially if the equation is to be used for prediction. One reason is that R^2 is not expressed on the same scale as the dependent variable. A particular equation may explain a large proportion of the variability in the dependent variable, thus have a high R^2, yet unexplained variability may be too large for useful prediction. It is not possible to tell from the magnitude of R^2 how accurate the predictions will be. The value of R^2 decreases with a decrease in the range of variation of the independent variable (x), other things being equal, and assuming the correct model is being fitted to the data.*

6) In order for the fitted equation to be regarded as a satisfactory predictor, the observed F ratio (regression mean square/residual mean square) should exceed not merely the selected percentage point of the F distribution, but several times the selected percentage point. As a rule-of-thumb, unless the observed F for overall regression exceeds the chosen test percentage point by at least a factor of four, and preferably more, the regression is unlikely to be of practical value for prediction purposes.
7) If R^2 does not tell all that is needed about how well a model fits the data and how good the model may be for prediction, additional statistical analyses can be of useful:
    a. Graphics reveal information in data, examine the data and the proposed model graphically.

b. Use the standard error of the estimate computed from the variance of the predicted value, this indicates the precision with which the model estimates the value of the dependent variable. This statistic is used to compute intervals as the following:
    i. Confident interval for the dependent variable
    ii. Prediction interval for the dependent variable
    iii. Confident interval around a parameter in a model (i.e., a regression coefficient)

8) Since the repeat measurements (i.e., replications) are not available, there is no need to consider the pure error and the lack-of-fit in this analysis.

Reference: Berthouex, P. M. and Brown, L. C. (2002), Statistics for Environmental Engineers, Lewis Publishers, pp. 345-352.

Linear Regression Analysis: Natural Earthen Materials

SUMMARY OUTPUT

Regression Statistics	
Multiple R	0.7726
R Square	0.5969
Adjusted R Square	0.5917
Standard Error	1.4360
Observations	79.0000

ANOVA

	df	*SS*	*MS*	*F*	*Significance F*
Regression	1.0000	235.1155	235.1155	114.0144	0.0000
Residual	77.0000	158.7861	2.0622		
Total	78.0000	393.9016			

	Coefficients	*Standard Error*	*t Stat*	*P-value*	*Lower 95%*	*Upper 95%*	*Lower 95.0%*	*Upper 95.0%*
Intercept	17.8626	1.1179	15.9785	0.0000	15.6365	20.0886	15.6365	20.0886
X Variable 1	-7.5363	0.7058	-10.6778	0.0000	-8.9417	-6.1308	-8.9417	-6.1308

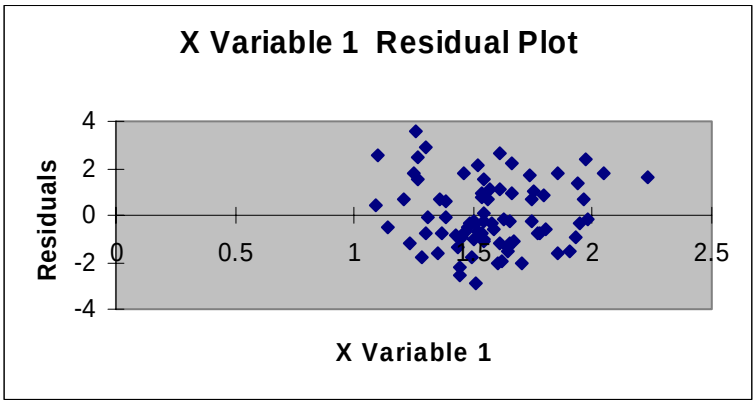

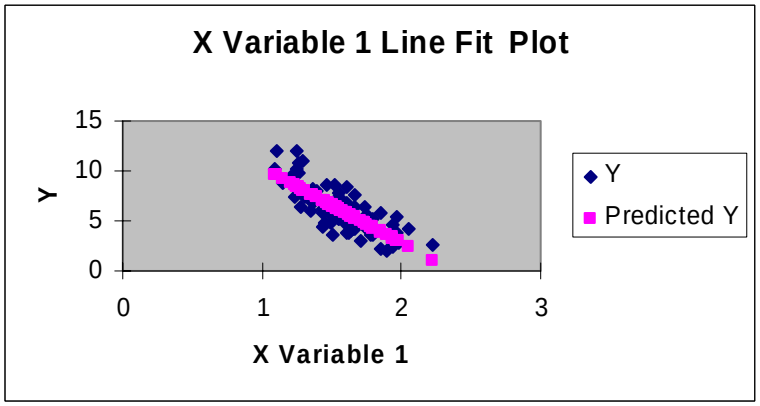

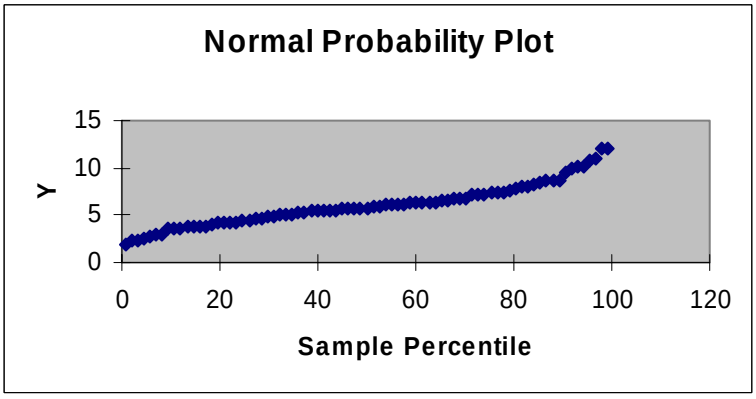

Fig. B-1. Residual, linear regression, normal quantile plots for natural earthen materials.

Linear Regression Analysis: Granular Materials-76-mm DCP Penetration Depth

SUMMARY OUTPUT

Regression Statistics	
Multiple R	0.7461
R Square	0.5567
Adjusted R Square	0.5389
Standard Error	1.7090
Observations	27.0000

ANOVA

	df	*SS*	*MS*	*F*	*Significance F*
Regression	1.0000	91.6862	91.6862	31.3904	0.0000
Residual	25.0000	73.0209	2.9208		
Total	26.0000	164.7070			

	Coefficients	*Standard Error*	*t Stat*	*P-value*	*Lower 95%*	*Upper 95%*	*Lower 95.0%*	*Upper 95.0%*
Intercept	18.0770	2.1071	8.5789	0.0000	13.7373	22.4168	13.7373	22.4168
X Variable 1	-7.1430	1.2749	-5.6027	0.0000	-9.7687	-4.5173	-9.7687	-4.5173

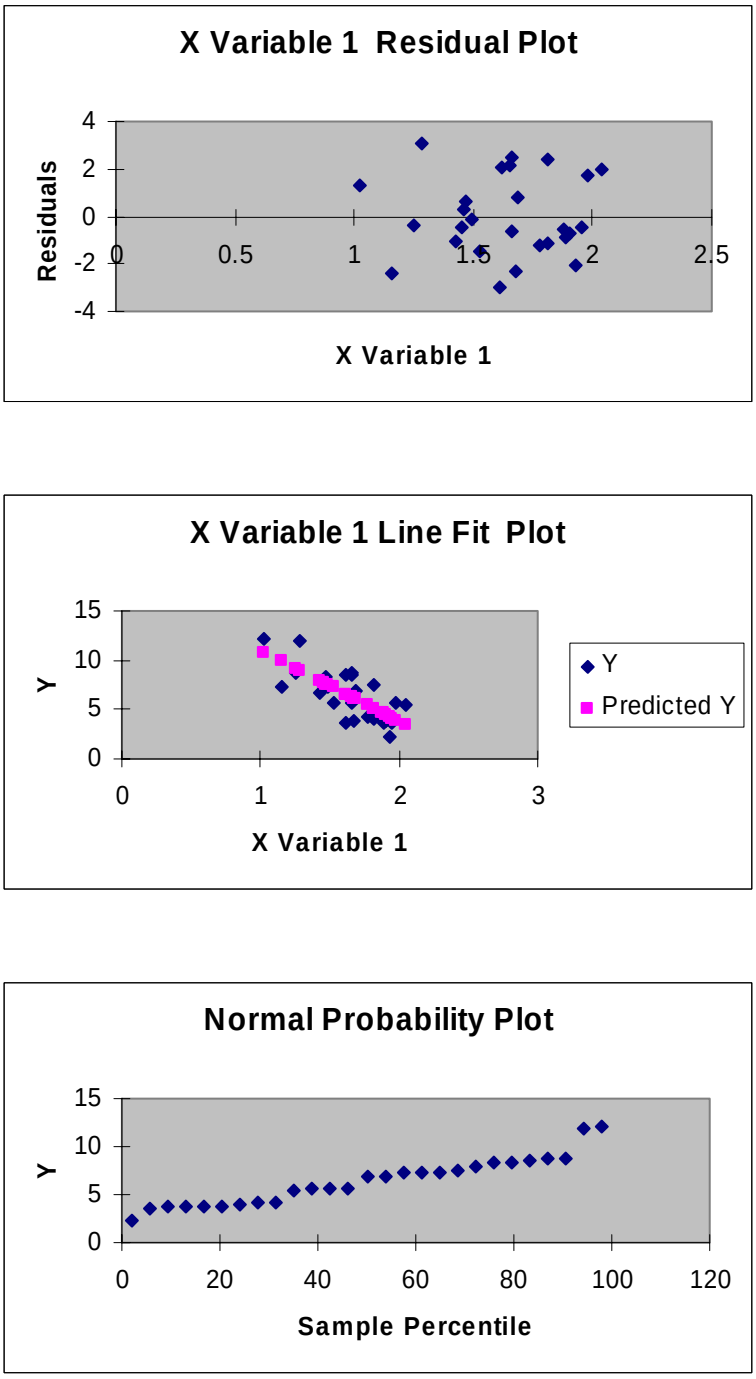

Fig. B-2. Residual, linear regression, normal quantile plots for granular materials- 76-mm DCP penetration depth.

Linear Regression Analysis: Granular Materials-152-mm DCP Penetration Depth

SUMMARY OUTPUT

Regression Statistics	
Multiple R	0.7403
R Square	0.5481
Adjusted R Square	0.5300
Standard Error	1.7255
Observations	27.0000

ANOVA

	df	*SS*	*MS*	*F*	*Significance F*
Regression	1.0000	90.2726	90.2726	30.3195	0.0000
Residual	25.0000	74.4345	2.9774		
Total	26.0000	164.7070			

	Coefficients	*Standard Error*	*t Stat*	*P-value*	*Lower 95%*	*Upper 95%*	*Lower 95.0%*	*Upper 95.0%*
Intercept	19.2792	2.3596	8.1707	0.0000	14.4196	24.1388	14.4196	24.1388
X Variable 1	-8.3248	1.5119	-5.5063	0.0000	-11.4386	-5.2111	-11.4386	-5.2111

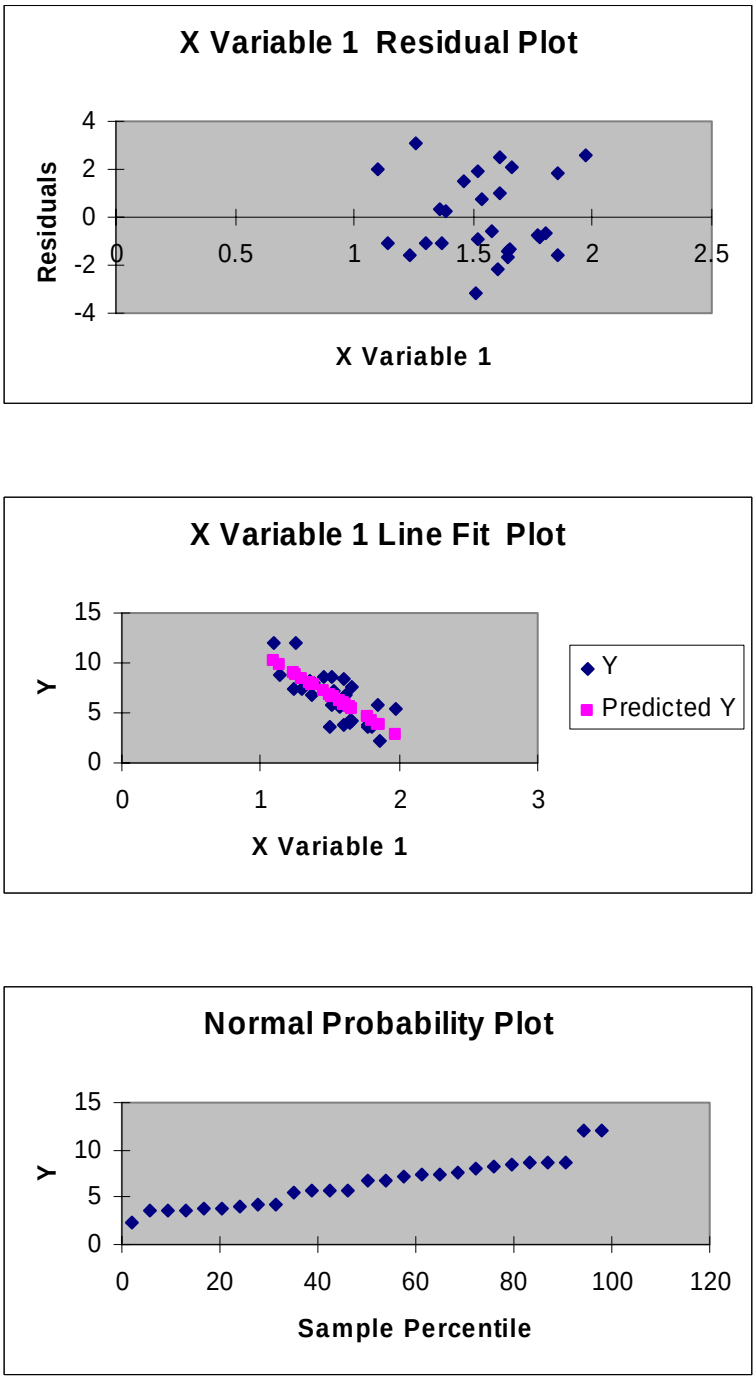

Fig. B-3. Residual, linear regression, normal quantile plots for granular materials- 152-mm DCP penetration depth.

Linear Regression Analysis: Fine-Grained Soils

SUMMARY OUTPUT

Regression Statistics	
Multiple R	0.7976
R Square	0.6361
Adjusted R Square	0.6288
Standard Error	1.2760
Observations	52.0000

ANOVA

	df	*SS*	*MS*	*F*	*Significance F*
Regression	1.0000	142.3173	142.3173	87.4040	0.0000
Residual	50.0000	81.4134	1.6283		
Total	51.0000	223.7307			

	Coefficients	*Standard Error*	*t Stat*	*P-value*	*Lower 95%*	*Upper 95%*	*Lower 95.0%*	*Upper 95.0%*
Intercept	17.0832	1.2133	14.0803	0.0000	14.6463	19.5201	14.6463	19.5201
X Variable 1	-7.1078	0.7603	-9.3490	0.0000	-8.6348	-5.5807	-8.6348	-5.5807

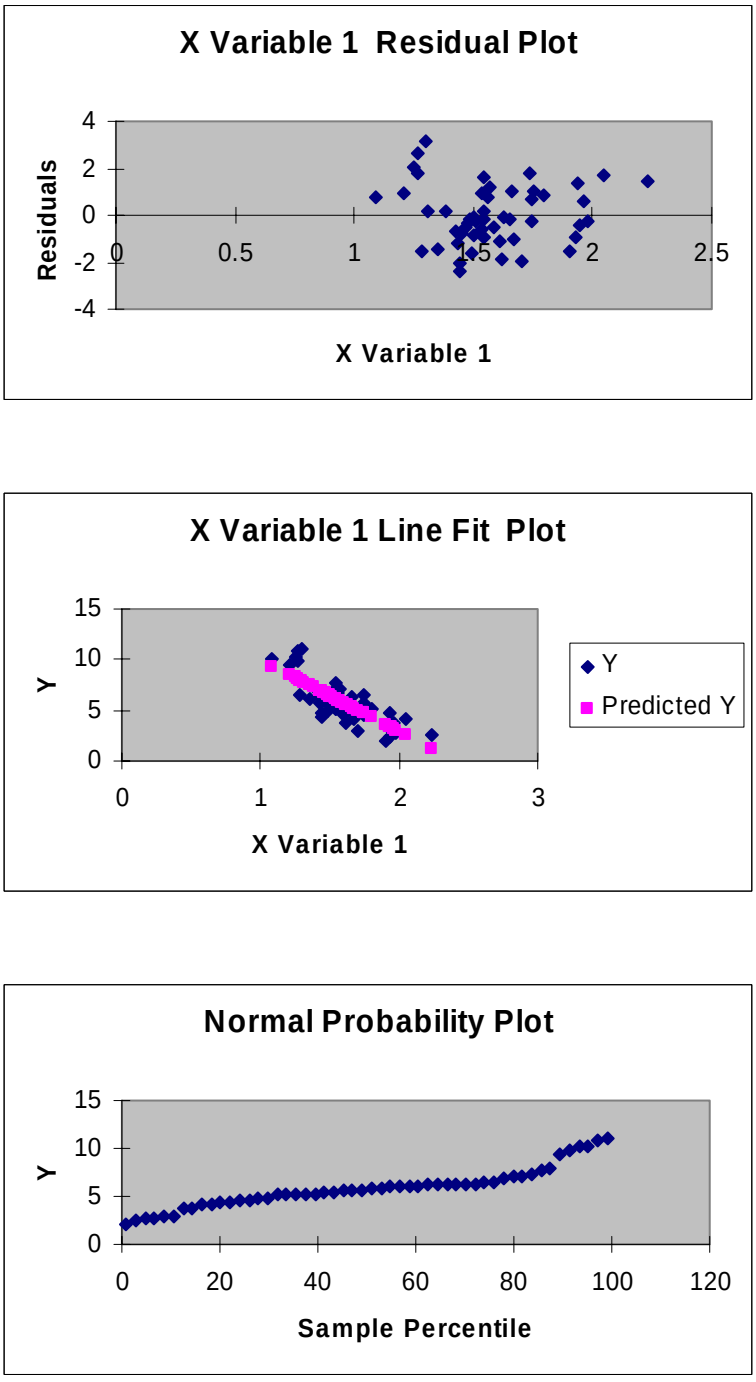

Fig. B-4. Residual, linear regression, normal quantile plots for fine-grained soils.

Linear Regression Analysis: Fly Ash-Stabilized Soils

SUMMARY OUTPUT

Regression Statistics	
Multiple R	0.6821
R Square	0.4653
Adjusted R Square	0.4496
Standard Error	1.9175
Observations	36.0000

ANOVA

	df	*SS*	*MS*	*F*	*Significance F*
Regression	1.0000	108.7960	108.7960	29.5891	0.0000
Residual	34.0000	125.0144	3.6769		
Total	35.0000	233.8104			

	Coefficients	*Standard Error*	*t Stat*	*P-value*	*Lower 95%*	*Upper 95%*	*Lower 95.0%*	*Upper 95.0%*
Intercept	26.4056	2.4702	10.6898	0.0000	21.3856	31.4256	21.3856	31.4256
X Variable 1	-11.1022	2.0410	-5.4396	0.0000	-15.2500	-6.9544	-15.2500	-6.9544

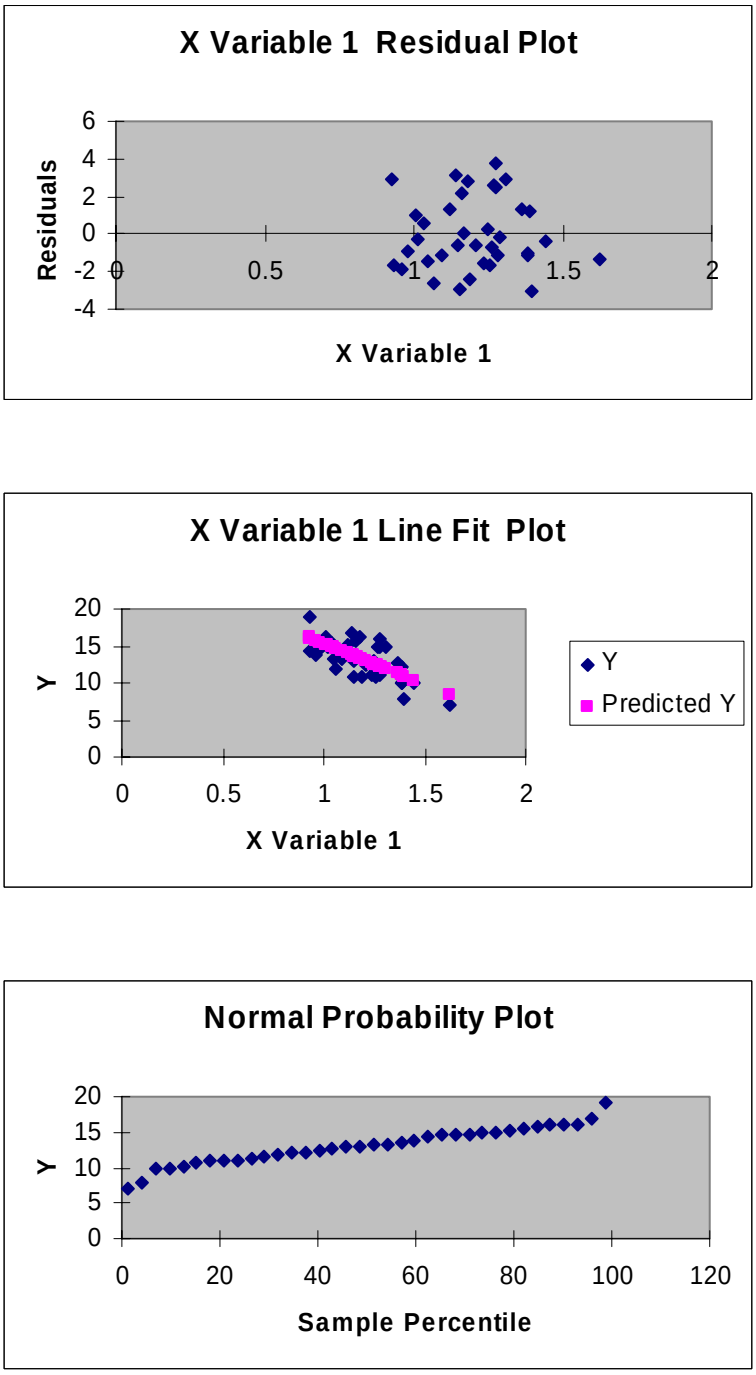

Fig. B-5. Residual, linear regression, normal quantile plots for fly ash-stabilized soils.

Linear Regression Analysis: Fine-Grained + Fly Ash-Stabilized Soils

SUMMARY OUTPUT

Regression Statistics	
Multiple R	0.8640
R Square	0.7465
Adjusted R Square	0.7436
Standard Error	2.1605
Observations	89.0000

ANOVA

	df	*SS*	*MS*	*F*	*Significance F*
Regression	1.0000	1195.8226	1195.8226	256.1809	0.0000
Residual	87.0000	406.1059	4.6679		
Total	88.0000	1601.9286			

	Coefficients	*Standard Error*	*t Stat*	*P-value*	*Lower 95%*	*Upper 95%*	*Lower 95.0%*	*Upper 95.0%*
Intercept	26.6980	1.1364	23.4937	0.0000	24.4393	28.9567	24.4393	28.9567
X Variable 1	-12.6634	0.7912	-16.0057	0.0000	-14.2360	-11.0908	-14.2360	-11.0908

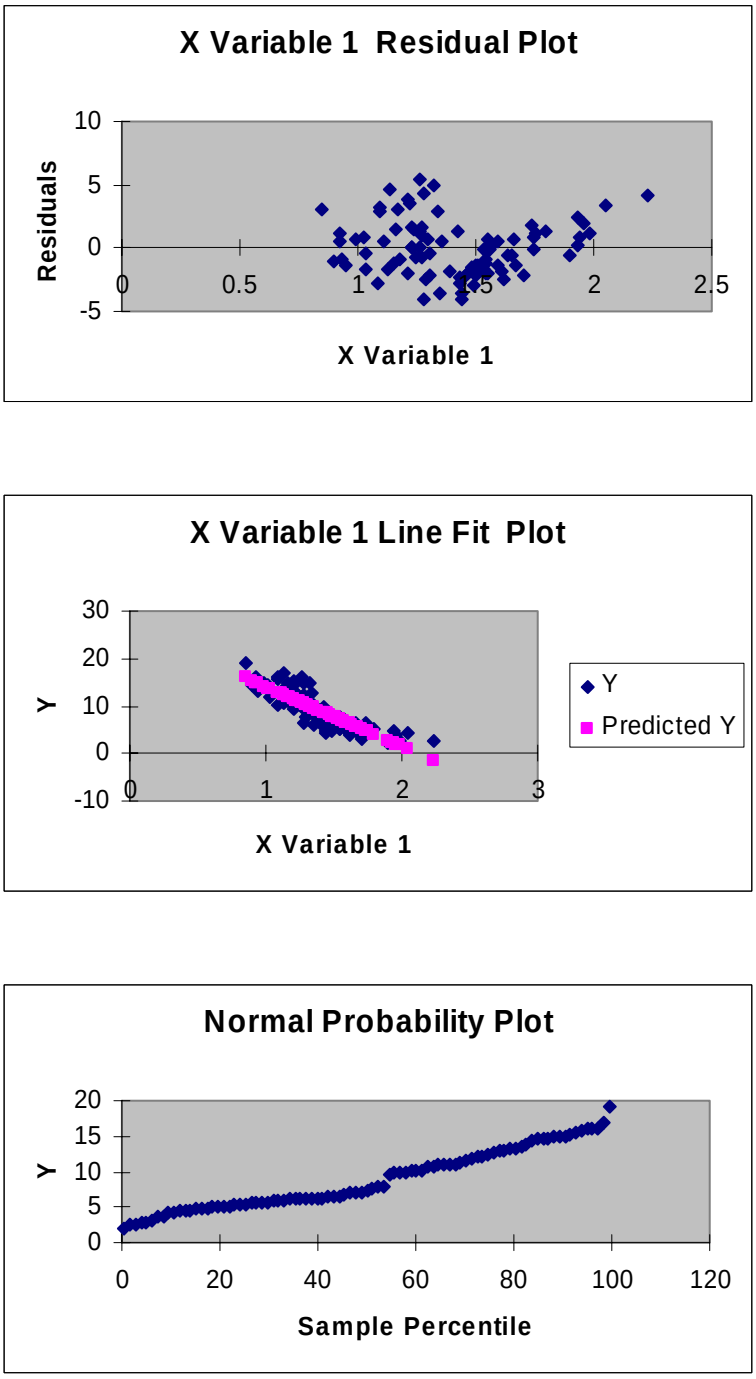

Fig. B-6. Residual, linear regression, normal quantile plots for fine-grained + fly ash-stabilized soils.

Linear Regression Analysis: All Materials Combined (include Foundry Sand)

SUMMARY OUTPUT

Regression Statistics	
Multiple R	0.8453
R Square	0.7145
Adjusted R Square	0.7121
Standard Error	2.1515
Observations	119.0000

ANOVA

	df	*SS*	*MS*	*F*	*Significance F*
Regression	1.0000	1355.4460	1355.4460	292.8290	0.0000
Residual	117.0000	541.5692	4.6288		
Total	118.0000	1897.0152			

	Coefficients	*Standard Error*	*t Stat*	*P-value*	*Lower 95%*	*Upper 95%*	*Lower 95.0%*	*Upper 95.0%*
Intercept	25.5759	1.0297	24.8394	0.0000	23.5367	27.6151	23.5367	27.6151
X Variable 1	-11.9505	0.6984	-17.1122	0.0000	-13.3335	-10.5674	-13.3335	-10.5674

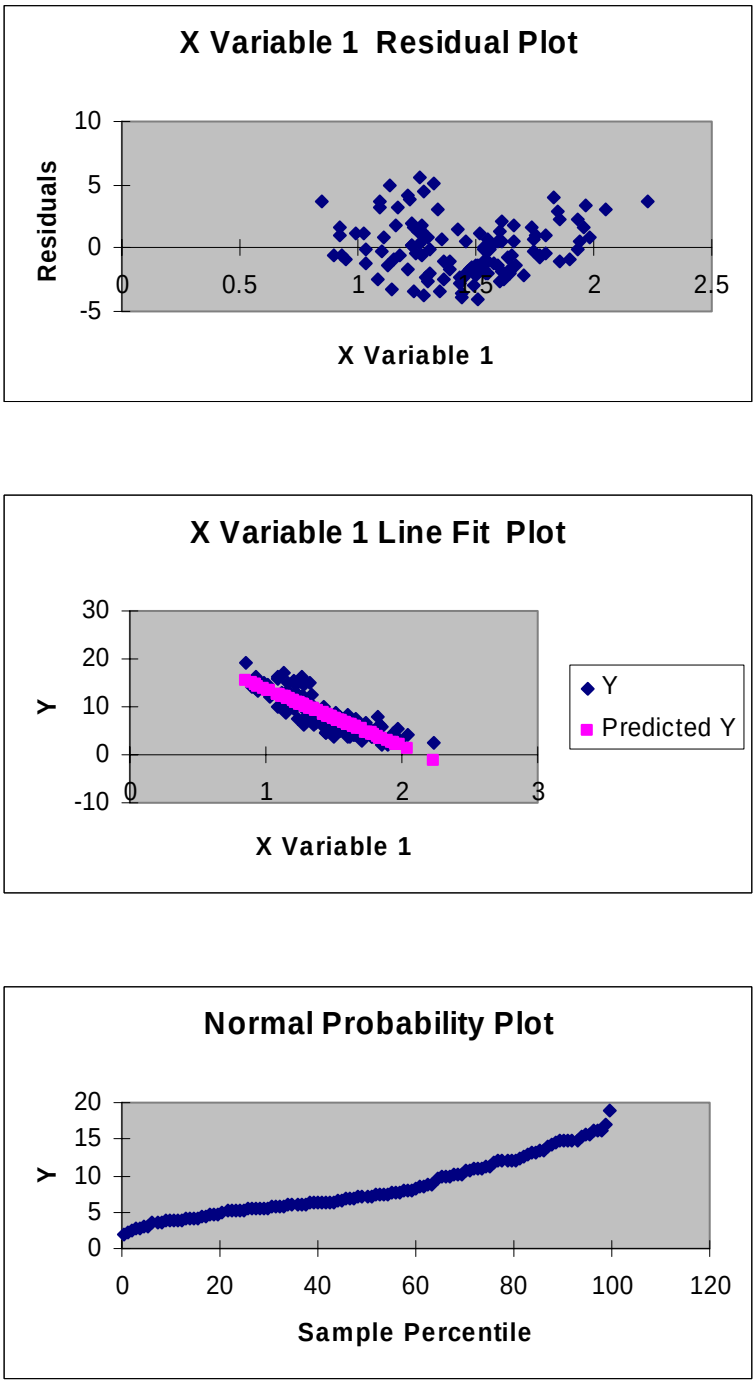

Fig. B-7. Residual, linear regression, normal quantile plots for all materials combined (include foundry sand).

APPENDIX C:

Practical Implications of SSG and DCP for Highway Construction Quality Evaluation

"PRACTICAL IMPLICATIONS OF SSG AND DCP FOR HIGHWAY CONSTRUCTION QUALITY EVALUATION"

This section provides recommendations for the implementation of the soil stiffness gauge (SSG) and the dynamic cone penetrometer (DCP) in practice. Two key practical issues are recommended on the basis of the findings from the study and are summarized as follows:

1) Structural properties assessment

Either or both the SSG and the DCP can be effectively utilized in the highway construction projects for assessing the structural properties such as soil stiffness and strength of various earthen materials used for base, subbase, and subgrade.

Based on the theory of elasticity, the SSG stiffness can be converted to an equivalent Young's modulus if Poisson's ratio of the given materials is known or assumed. This equivalent Young's modulus can, in turn, be related to resilient modulus, which is typically required in the mechanistic design of pavement structures. The relationship between the equivalent Young's modulus obtained from the SSG and the resilient modulus is represented by the so-called strain-dependent modulus degradation curve (i.e., a plot of modulus versus strain amplitude). Since the confining stress and strain levels are two important factors affecting the modulus of materials, under a given confining stress, the equivalent Young's modulus of the SSG at smaller strains can be adjusted to the resilient modulus at larger strains using the strain-dependent modulus degradation curve. This strain dependent modulus degradation curve can be either experimentally obtained or estimated from the equations proposed in the literature. For granular materials, the strain-dependent modulus degradation curve is significantly affected by the confining stress. However, in the case of non-granular materials, the plasticity index is a significant factor.

The DCP provides an index of strength in term of DCP penetration index (DPI). Its correlation with California bearing ratio (CBR) is widely accepted and well established. This CBR value is a parameter that has been used in design of pavements and is also related to the Young's modulus as well as the resilient modulus. Therefore,

by measuring stiffness and strength properties using either or both the SSG and the DCP, the outcome will essentially provide the relevant structural properties and thus the design parameters.

Although the resilient modulus can be estimated base on the procedure described above, a direct approach can be also taken. In the direct approach, resilient modulus test would be performed on the materials of the same density and moisture content in the field where the SSG and (or) DCP measurements are made. A direct correlation between the SSG stiffness and (or) DPI and resilient modulus would be established.

2) Earthwork quality control

The SSG and DCP can be used in conjunction with conventional moisture-density measurements in order to enhance the quality control during earthwork construction. The ultimate goals of this practice are to achieve more uniform structural property and to help developing a design modulus. For this purpose, the stiffness and/or strength needs to be respectively measured using the SSG and the DCP plus a moisture content measurement (e.g., from the nuclear moisture gauge or moisture samples). The study indicated that when the SSG stiffness or the DPI is normalized by the deviation of the compaction moisture content from the optimum moisture content, remarkably constant numbers, around a value equal to -2.4 and -8.4, respectively are obtained for compacted natural earthen materials where the range of relative compaction is typically rather narrow. This implies that for compacted soils, the effect of dry unit weight on stiffness and strength is relatively minor compared to moisture content. Consequently, the study recommends that the use of the SSG and the DCP for earthwork quality control has some promise and can be done by measuring the SSG stiffness and/or the DPI along with an independent moisture content measurement. These measurements, especially with the SSG, are rapid and convenient. Therefore, many more measurements can be made to establish the uniformity of earthwork.

Example 1: Fine-Grained Plastic Soils

Compacted subgrade soils at STH 100, Milwaukee, WI are lean clay with sand (CL or A-6(9)) with the plasticity index (PI) of 14 and specific gravity (G_s) of 2.74. The maximum dry unit weight ($\gamma_{d,\ max}$) and optimum moisture content (w_{opt}) based on the standard Proctor compaction test are respectively 18.2 kN/m^3 and 14.4 %. The SSG and DCP were employed to assess the structural properties (stiffness and strength) of this subgrade in conjunction with the conventional moisture-density measurements (e.g. nuclear gauge). All tests were performed at the same location (within approximately 0.3 m). The measurement results from one station are obtained as follows:

- SSG stiffness (K_{SSG}) = 7.4 MN/m
- Weighed average DCP penetration index (DPI) calculated over a penetration depth of 152 mm from the surface ($DPI_{152\ mm}$) = 24.4 mm/blow
- Moisture content (w) = 11.5 %
- Dry unit weight (γ_d) = 20.2 kN/m^3

Methods and Procedures

1) Structural properties assessment

By using Eq. (2.2), the equivalent Young's modulus from the SSG (E_{SSG}) can be calculated as:

$$E_{SSG} = \frac{K_{SSG}(1-\nu^2)}{1.77 \cdot R}$$

From Table 2.2, Poisson's ration (ν) is assumed to be 0.4. The outside radius (R) of the ring-shaped foot of the SSG is 57.15 mm.

Thus,

E_{SSG} = 61 MPa

E_{SSG} needs to be converted to shear modulus for use in modulus degradation curve. From $E_{SSG} = 2 \cdot G_{SSG}(1+\nu)$, G_{SSG} is equal to 21.8 MPa.

The confining stress that exists in the upper regions of the subgrade of a typical flexible highway pavement is relatively small, i.e., normally less than 34.5 kPa (5 psi) (Thompson and Robnett 1979). The average confining stress is therefore selected to be 20 kPa (3 psi)

for a typical pavement at the subgrade level. The resilient modulus for design would correspond to this confining stress. The average confining stress in the zone of measurement under the SSG however is approximately 2.6 kPa (0.38 psi) (Sawangsuriya et al. 2003). In addition, typical shear strain levels of the resilient modulus and the SSG fall between 10^{-4} and 10^{-3} (about 10^{-2} % to 10^{-1}%) and between 10^{-5} and 10^{-4} (about 10^{-3} % to 10^{-2}%), respectively (Sawangsuriya et al., 2005). Therefore, a correction due to the differences in confining stress and strain levels under the SSG operation and the pavement system must be made. To do that, the strain-dependent modulus degradation curve can be used. In general, the strain-dependent modulus degradation curve is represented by the plot of normalized shear modulus (G/G_{max}) versus the shear strain amplitude (γ).

Ishibashi and Zhang (1993) suggested the following unified formula for the strain-dependent modulus degradation curve (also referred to normalized modulus reduction curve) for plastic and non-plastic soils as follows:

$G/G_{max} = K(\gamma, I_p)\ \sigma_o^{m(\gamma,\ Ip)}$

where

$$K(\gamma, I_p) = 0.5\left[1 + \tanh\left\{\ln\left(\frac{0.000102 + n(I_p)}{\gamma}\right)^{0.492}\right\}\right]$$

$$m(\gamma, I_p) = 0.272\left[1 - \tanh\left\{\ln\left(\frac{0.000556}{\gamma}\right)^{0.4}\right\}\right]e^{-0.0145I_p^{1.3}}$$

$$n(I_p) = \begin{cases} 0.0 \quad \text{for} \quad I_p = 0 \\ 3.37\times10^{-6} I_p^{1.404} \quad \text{for} \quad 0 < I_p \le 15 \\ 7.0\times10^{-7} I_p^{1.976} \quad \text{for} \quad 15 < I_p \le 70 \\ 2.7\times10^{-5} I_p^{1.115} \quad \text{for} \quad I_p > 70 \end{cases}$$

For convenience, Table C-1 is provided for use of the Ishibashi & Zhang equation.

Table C-1. Numerical results for use of the Ishibashi & Zhang equation.

PI	K_{RM}	K_{SSG}	m_{RM}	m_{SSG}	$R_{\sigma o}$	R_{γ}	$R_{\sigma o}R_{\gamma}$
0	0.173	0.669	0.1669	0.0299	1.602	0.390	0.625
10	0.150	0.629	0.1249	0.0224	1.423	0.323	0.460
14	0.219	0.729	0.1066	0.0191	1.351	0.390	0.526
20	0.345	0.835	0.0818	0.0147	1.260	0.505	0.636
30	0.537	0.918	0.0499	0.0090	1.151	0.661	0.761
40	0.670	0.951	0.0289	0.0052	1.085	0.756	0.820
50	0.758	0.968	0.0160	0.0029	1.046	0.814	0.852
60	0.817	0.977	0.0085	0.0015	1.024	0.854	0.874
70	0.857	0.983	0.0044	0.0008	1.013	0.882	0.893
80	0.874	0.985	0.0022	0.0004	1.006	0.892	0.897
90	0.887	0.987	0.0011	0.0002	1.003	0.902	0.904
100	0.898	0.988	0.0005	0.0001	1.001	0.910	0.912

Note: $\gamma_{SSG} = 5x10^{-5}$; $\gamma_{RM} = 5x10^{-4}$; $R_{\sigma_o} = \frac{20^{m_{RM}}}{2.6^{m_{SSG}}}$; $R_{\gamma} = \frac{K_{RM}}{K_{SSG}}(20)^{m_{RM}-m_{SSG}}$

For soils with plasticity index (PI or I_p) = 14 and σ_o = 2.6 and 20 kPa respectively for the SSG and the pavement system, the modulus degradation curves are shown in Fig. C-1.

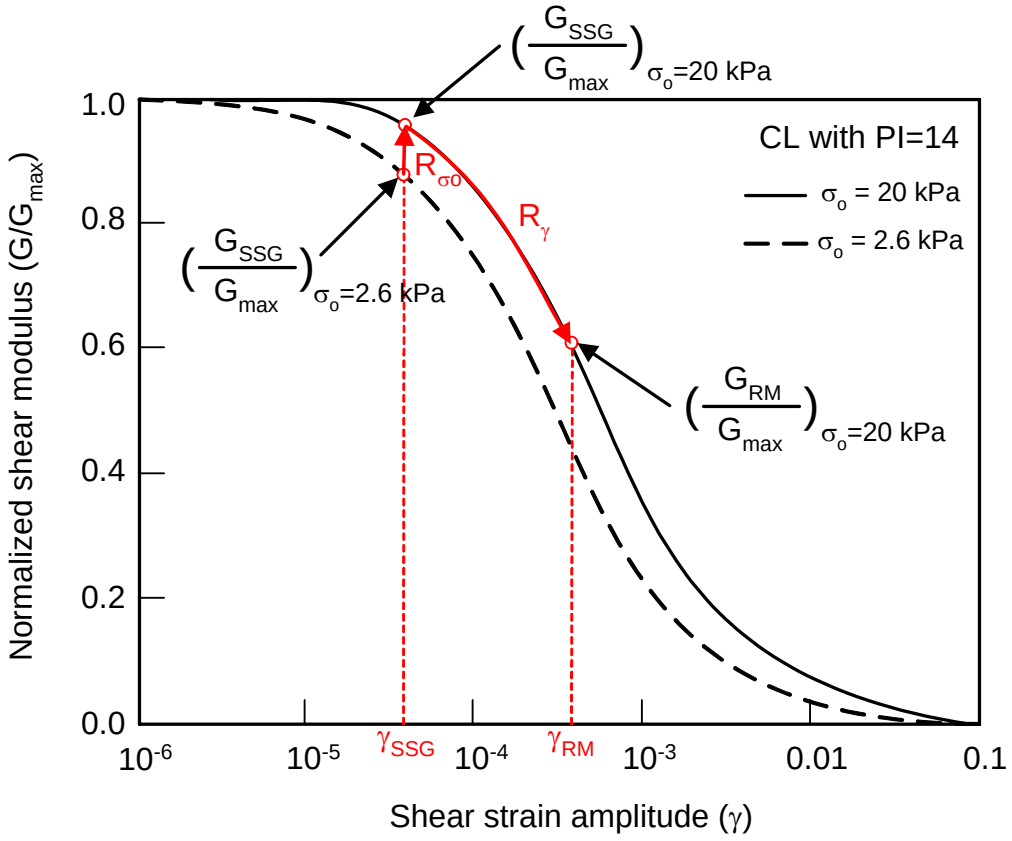

Fig. C-1. Strain-dependent modulus degradation curves for CL with PI = 14.

A proposed modulus correction equation that takes into account the differences in stress and strain levels can be expressed as:

$$G_{RM} = G_{SSG} \times R_{\sigma_o} \times R_{\gamma}$$

The equation is checked for its validity,

$$G_{RM} = G_{SSG} \times \left(\frac{G_{RM}}{(G_{max})_{RM}} \times \frac{(G_{max})_{SSG}}{G_{SSG}} \right) \times \left(\frac{G_{RM}}{G_{max}} \times \frac{G_{max}}{G_{SSG}} \right)$$

Ratio (no unit)

If measured G_{SSG} = **21.8** MPa (E_{SSG} = 61 MPa) under σ_o = 2.6 kPa, using a modulus correction equation and correction factors obtained in Table C-1, G_{RM} = **11.5** MPa (E_{RM} = 32 MPa) under σ_o = 20 kPa.

Additionally, the equivalent Young's modulus can also be obtained from the weighed average DPI calculated over a penetration depth of 152 mm from the surface ($DPI_{152\ mm}$). Two approaches can be used. In the first approach, the DPI value is correlated to K_{SSG} using Eq. (4.15):

$$K_{SSG} = -12.0 \log(DPI) + 25.6$$

Hence, K_{SSG} = 9.0 MN/m. Then, using Eq. (2.2), E_{SSG} is obtained to be 74.7 MPa.

In the second approach, the DPI value is converted to the California bearing ratio (CBR) using Eq. (2.8):

$$\log(CBR) = 2.46 - 1.12 \log(DPI)$$

Hence, CBR = 8.0. Then using Eq. (4.16),

$$E_{SSG} = 18.77 \times CBR^{0.63}$$

Hence, E_{SSG} = 69.6 MPa.

Finally, a procedure similar to the aforementioned procedure can be repeated to correct this value for confining stress and strain level to obtain the equivalent resilient modulus in the pavement system. Since DPI does not directly measure stiffness but correlated

empirically, it is recommended only as a substitute to SSG when DCP is the only test available.

2) Earthwork quality control

Typical compaction specifications call for a specific relative compaction (RC) ≥ 95%. The reason for this is to ensure that the void space is kept to a practical minimum to limit water content changes due to post-construction environmental conditions. Ultimately, it is the water content that impacts the structural properties and needs to be limited after construction. For use of SSG and DPI for earthwork quality control, a specified normalized stiffness ($K_{SSG}/(w-w_{opt})$) or normalized strength ($DPI/(w-w_{opt})$) for a properly-compacted subgrade must fall within -5 to 0 and -10 to 0, respectively.

For the fine-grained plastic soil described above, the field measurements indicated that γ_d, w, K_{SSG}, and DPI_{152mm} were 20.2 kN/m^3, 11.5%, 7.4 MN/m, and 24.4 mm/blow, respectively. Remembering that the standard Proctor $\gamma_{d,\ max}$ = 18.2 kN/m^3 and w_{opt} = 14.4% for this soil, the RC ($\gamma_d/\gamma_{d,\ max}$) is determined to be 110%. The deviation of moisture content from the respective optimum moisture content ($w-w_{opt}$) is calculated to be -2.9% (i.e, at dry side of optimum water content). Then, $K_{SSG}/(w-w_{opt})$ and $DPI_{152mm}/(w-w_{opt})$ are obtained as -2.6 and -8.4, respectively. Therefore, the compaction control meets the specifications.

Example 2: Granular Industrial By-Product

The working platform at a section of STH 60, near Lodi, WI, consists of granular bottom ash which is an industrial by-product. It is a well-graded coarse-grained sand-like materials classified as SW or A-1-b(0) with a specific gravity (G_s) of 2.65. The maximum dry unit weight ($\gamma_{d,\,max}$) based on the standard Proctor compaction test (ASTM D 698) and the vibratory table (ASTM D 4253) is 15.1 and 13.7 kN/m^3, respectively. The SSG and DCP were employed to assess the structural properties (stiffness and strength) of this material in conjunction with the conventional moisture-density measurements (e.g. nuclear gauge). All tests were performed at the same location (within approximately 0.3 m). Three to four measurements were performed and the average values were obtained as follows:

- SSG stiffness (K_{SSG}) = 3.9 MN/m
- Weighed average DCP penetration index (DPI) calculated over a penetration depth of 152 mm from the surface ($DPI_{152\,mm}$) = 52.7 mm/blow
- Dry unit weight (γ_d) = 17.1 kN/m^3
- Moisture content (w) = 2.6 %

Methods and Procedures

1) Structural properties assessment

By using Eq. (2.2), the equivalent Young's modulus obtained from the SSG (E_{SSG}) can be calculated as:

$$E_{SSG} = \frac{K_{SSG}(1-\nu^2)}{1.77 \cdot R}$$

From Table 2.2, Poisson's ration (ν) is assumed to be 0.35. The outside radius (R) of the ring-shaped foot of the SSG is 57.15 mm.

Thus,

E_{SSG} = 52.7 MPa

Since $E_{SSG} = 2 \cdot G_{SSG}(1+\nu)$, G_{SSG} becomes 19.5 MPa.

The average bulk stress estimated at the mid-depth of the working platform layer is approximately 31 kPa (4.5 psi) (Tanyu et al., 2003). The average confining stress (1/3 of the bulk stress) is therefore selected to be 10.3 kPa (1.5 psi). Similar to Example 1, in order to adjust E_{SSG} at smaller strains to the resilient modulus (E_{RM}) at larger strains, the strain-dependent modulus degradation curve is used.

From Table C-1, the K_{RM}, K_{SSG}, m_{RM}, and m_{SSG} values for I_p = 0 are 0.173, 0.669, 0.1669, and 0.0299. For the SSG confining stress of 2.6 kPa and the pavement confining stress of 10.3 kPa, the correction factors are calculated as $R_{\sigma o}$= 1.43 and R_{γ}= 0.36. Note for this case, $R_{\sigma_o} = \frac{10.3^{m_{RM}}}{2.6^{m_{SSG}}}$ and $R_{\gamma} = \frac{K_{RM}}{K_{SSG}}(10.3)^{m_{RM}-m_{SSG}}$. Therefore, G_{RM} is obtained as 10 MPa (E_{RM} = 26.9 MPa) from G_{SSG} of 19.5 MPa (E_{SSG} = 52.7 MPa).

2) Earthwork quality control

The compaction characteristics of granular materials and their structural properties are not as sensitive to moisture content changes as the fine-grained plastic soils. Therefore, the modulus corresponding to the specified density can be directly used to monitor earthwork quality.

References

Ishibashi, I. and Zhang, X. (1993), "Unified Dynamic Shear Moduli and Damping Ratios of Sand and Clay," *Soils and Foundations*, Vol. 33, No. 1, pp. 182-191.

Sawangsuriya, A., Bosscher, P. J., and Edil, T. B. (2005), "Alternative Testing Techniques for Modulus of Pavement Bases and Subgrades," Proceeding of the 13th Annual Great Lakes Geotechnical and Geoenvironmental Engineering Conference, Milwaukee, WI (in press).

Sawangsuriya, A., Edil, T. B., and Bosscher, P. J. (2003), "Relationship between Soil Stiffness Gauge Modulus and Other Test Moduli for Granular Soils," *Transportation Research Record 1849*, TRB, National Research Council, Washington, D.C., pp. 3-10.

Tanyu, B. F., Kim, W. H., Edil, T. B. and Benson, C. H. (2003), **"**Comparison of Laboratory Resilient Modulus with Back-Calculated Elastic Moduli from Large-Scale Model Experiments and FWD Tests on Granular Materials**,"** *Resilient Modulus Testing for Pavement Components, ASTM STP 1437*, G. N. Durham, A. W. Marr, and W. L. De Groff, Eds., ASTM, West Conshohocken, PA, pp. 191-208.

Thompson, M. R. and Robnett, Q. L. (1979), "Resilient Properties of Subgrade Soils," *Transportation Engineering Journal*, Vol. 105, No. TE1, pp. 71-89.

APPENDIX D:

Papers Written by Authors

Paper No. 02-3608

TITLE:

LABORATORY EVALUATION OF THE SOIL STIFFNESS GAUGE (SSG)

Author(s):

Auckpath Sawangsuriya
Peter J. Bosscher
Tuncer B. Edil

Department of Civil and Environmental Engineering
2210 Engineering Hall, 1415 Engineering Dr.
The University of Wisconsin-Madison, Madison, WI, 53706
sawangsuriya@students.wisc.edu, bosscher@engr.wisc.edu ,
edil@engr.wisc.edu

Paper submitted for presentation and publication at the

Transportation Research Board
81st Annual Meeting
January 13-17, 2002
Washington, D.C.

LABORATORY EVALUATION OF THE SOIL STIFFNESS GAUGE (SSG)

By Auckpath Sawangsuriya, Peter J. Bosscher, and Tuncer B. Edil

Abstract: A new alternative geotechnical field testing device called the soil stiffness gauge or SSG (also known as GeoGauge™) exhibits particular promise for monitoring insitu soil stiffness during construction quality control. However, there has been only limited research on this device regarding its characteristics and limitations. This study presents the results of laboratory testing and a finite-element analysis (FEA) of the SSG. Based on the FEA and the SSG measurement in the test box, the radius of measurement influence extends to 300 mm. For two-layer materials with different stiffness, the SSG starts to register the stiffness of an upper-layer material of 125 mm or thicker. The effect of the lower layer however, may continue to be present even at an upper-layer material thickness of 275 mm depending on the relative stiffness of the layer materials. Caution needs to be exercised in interpreting the results from the SSG when it is used on multi-layer systems, especially those with geosynthetic separators. The presence of a geosynthetic separator between the layers may cause a stiffness decoupling of the layers.

Key Words: soil stiffness gauge, finite-element analysis, stiffness

INTRODUCTION

The soil stiffness gauge or SSG (also known as GeoGauge™) is a portable, non-nuclear, and non-destructive field testing device that directly and rapidly measures the insitu stiffness of soils. It weights about 10 kg, is 28 cm in diameter, is 25.4 cm height, and rests on a rigid ring-shaped foot on the soil surface. The foot bears directly on the soil and supports the weight of the SSG. The force and displacement-time history are measured by two velocity sensors. According to the technical information from the manufacturer (*1*), the SSG vibrates and produces small changes in vertical force and deflections at 25 steady state frequencies between 100 to 200 Hz. The soil stiffness is determined at each frequency and its average value is displayed. The SSG stiffness can be used to directly determine Young's modulus. Due to the newness of the device, a better understanding of the characteristics and limitations of the SSG to measure these structural properties is needed.

The objective of this study (*2*) is to evaluate the recently developed SSG for measuring the insitu soil stiffness. In the laboratory testing program, the SSG was used in a test box to investigate the zone of measurement influence and the factors that influence the SSG measurement in the test box. Three types of test materials with different stiffnesses were utilized to determine their effect on the SSG. The influence of a two layered deposit and the effects of a separator were also included in this study. In addition to the laboratory testing program, the finite-element analysis (FEA) was employed to investigate the zone of influence of the SSG.

TEST MATERIALS

Three types of test materials characterized as high stiffness, intermediate stiffness, and low stiffness were used in the study. The high stiffness material is Yahara 19-mm crushed lime rock with a C_u of 2.13. The intermediate stiffness material is a medium,

uniformly-graded quartz sand classified as SP and A-3(0) according to the Unified Soil Classification System (USCS) and the American Association of State Highway and Transportation Officials (AASHTO) classification system, respectively. It has a uniformity coefficient (C_u) of 1.3 and an effective grain size (D_{10}) of 0.45 mm, D_{30} of 0.5 mm, and D_{60} of 0.6 mm. The low stiffness material is a mixture of nylon plastic beads (Zeier Plastic's product) and medium sand. A 50% by volume of sand and 50% by volume of plastic beads mixture was used in order to get the desired low stiffness material. The plastic beads have a prismatic shape and pass sieve No. 4 but are retained on sieve No. 8 with dimensions of approximately 2.5 x 2.5 x 1.5 mm.

EXPERIMENTAL SETUP IN THE TEST BOX

Lenke et al. (*3*) conducted geotechnical centrifuge model experiments of rigid circular footings at the surface of a soil mass in order to evaluate various boundary conditions including square- and circular-shaped containers with and without an energy-absorbing boundary material. Their results demonstrated the influence and importance of proper boundary geometry and energy-absorbing boundary material on the response of a vertically excited circular footing and the desirability of non-cylindrical containers to minimize reflected wave energy. In this study, various cubical-shaped container sizes were considered and modeled using the FEA program to establish reasonable dimensions of an elastic half space that would minimize reflected wave energy.

In order to test the SSG in controlled conditions, a test box was needed which would behave as a full-scale soil deposit. Proper sizing of the test box requires a balance between a large enough box to prevent dynamic reflections from the sides and bottom and a small enough box to quickly change soil types and densities. The test box was modeled using ANSYS® (*4*), a commercially available finite-element analysis program. Two types of analysis, static and dynamic, were employed in the model. In order to simplify the models and reduce the analysis time, only a quarter of the test box was modeled. In the static analysis, four different cross-sectional sizes of 3-D finite-element models ranging from 0.15 x 0.15 m to 0.6 x 0.6 m with a height of 0.3 m were selected for analysis. An annular loading area of the SSG was also simplified by an equivalent square loading area. A normal stress of approximately 27.5 kPa as produced by the self-weight of the SSG was applied to model the loading condition. Figure 1(a) shows an elevation and a plan view of the test box model for the FEA along with the boundary conditions. An 8-node brick element type was selected for all models. The material properties in these finite-element models were selected as isotropic with Young's modulus (E) of $4x10^4$ kPa and Poisson's ratio (υ) of 0.3. Figure 1(b) shows one of the finite-element models (quarter of the physical model). The maximum displacement produced by the self-weight of the SSG for different sizes of test boxes is given in Figure 2(a). The maximum displacement significantly reduced as the width of the FEA model increased and eventually became nearly constant at a box width of 0.3 m.

In the dynamic analysis, the geometry, boundary conditions, and material properties were selected to be the same as that in the static case; however, a mass density of 1.65 kNs^2/m^4 was additionally selected in the material properties. The dynamic pressure produced from the SSG of 0.24 kPa was applied in all models. Two analysis types were employed: modal and harmonic analysis. In both cases, the frequency ranged from 0 to 1,000 Hz. Figure 2(b) shows the FEA results for the dynamic case. The FEA

data with 5 different ranges of frequencies were determined using modal analysis. In the harmonic analysis, the maximum displacement response from FEA was very small such that the effect of the size of the model was not significant. On the other hand, the maximum response from the modal analysis was very large compared to that of the harmonic analysis and hence the effect of the size of the model became clearer. Similar to the static analysis, the maximum displacement response was significantly reduced as the width of test box model increased. Both Figure 2(a) and (b) indicate that the boundary effects become negligible for test box widths greater than about 0.6 m.

Based on the FEA results, a 1.2 m x 1.2 m x 1.2 m wooden box was selected. Cylindrical molds with three different sizes (0.3-m, 0.6-m, and 0.9-m in diameter) made of a woven geotextile (GT) were used to hold the test materials in the cubical test box and separate them from the energy absorbing boundary materials. The styrofoam beads and foam peanuts were placed in the space between the cylindrical mold and the container as an energy absorbing material. Figure 3 illustrates a schematic of the test box used in the laboratory experiments.

LABORATORY TESTING PROGRAM

Preliminary Testing Program

Tests were conducted to determine how stiffness changes with depth for different materials. The materials tested had 635-mm depth and 0.3 to 0.9-m diameter. A series of tests were performed to determine the appropriate dimensions of the physical model, to assess the general behavior of stiffness with depth, and to develop the test procedure.

Two sample preparation approaches, pluviation and scooping, were considered in this study. Medium sand was used to investigate the effects of sample preparation in a 0.3-m diameter mold. For the scooping method, sand was poured slowly from a scoop. Pouring was done from a position very close to the surface such that the sand grains rolled into place rather than drop or rain on the surface. For the pluvation method, the "rain-through-air" technique (*5*) was employed. The sand particles were dropped or rained from a regulator screen onto a finer screen. In this study, pegboard was used as the regulator screen to control the rate of sand and the standard sieve No. 8 was used for splitting the sand particle streams into a uniform rain. Figure 4 shows a pluviation device made for this study. It was suggested that the distance between the regulator and the finer screen be more than 150 mm in order to ensure a uniform, highly compact cohesionless soil (*5*). In this study, a distance of 200 mm was employed. The unit weight of sand deposit was determined by placing a metal cup of known volume in the sand bed during the deposition process. The cup was subsequently excavated and weighed to determine the unit weight of sand deposited in the cup. The measured unit weight of sand with the scooping and pluviation methods in this study were 16 kN/m^3 and 18 kN/m^3, respectively.

The stiffness tests were conducted using the SSG. Measurements were made in 25-mm increments of test material depth deposited in the cylindrical mold and were located at the center of the mold. The measured SSG stiffness values were recorded from the bottom to the top of the cylindrical mold. The SSG manufacturer recommends to have good contact (more than 75% contact area) between the ring-shaped foot of the SSG

and the measured surface (*1*); therefore, the surface of any test material was carefully leveled prior to each measurement.

Main Testing Program

Two main stiffness tests were proposed in this phase: the stiffness tests for the single and layered materials. The tests were performed in the 0.6-m diameter cylindrical mold in order to eliminate the effect of physical model size. Three test materials: high, intermediate, and low stiffness were prepared by the scooping method as described earlier since all of the materials could not be pluviated.

The stiffness tests for a single material were similar to those conducted in the preliminary test program. The measurements were performed at each 25-mm increment of test material depth from the bottom to the top of the mold and were conducted at the center of the mold. The measurements were made twice. If the difference between the two SSG stiffness values was larger than 5%, the test was repeated.

For layered material testing, six combinations from the three test materials (medium sand, 19-mm lime rock, and plastic beads-sand mixture) were used in this study. In each combination, one of these three test materials was used as the bottom layer deposited up to about 380 mm (where the SSG stiffness values become stable). Then one of the other two test materials was used as the upper layer. In this study, two types of separators were used between the layers: woven geotextile (GT) and thin plastic wrap sheet.

RESULTS AND ANALYSIS OF LABORATORY TESTING

Effect of Sample Preparation

The test results on medium sand comparing the two sample preparation methods, (1) pluviation (or rain-through-air) and (2) scooping, are presented in Figure 5. The difference in SSG stiffness obtained from the two methods is relatively small. It is important for the SSG measurements that the measured surface of any test materials be leveled prior to each measurement in order to ensure good contact area between the ring-shaped foot of the SSG and the measured surface. Leveling the surface by hand, however, can disturb the sand, i.e., change its density and hence its stiffness. This may have led to the small difference.

Effect of Physical Model Size

The size of the GT mold (physical model) is another factor considered in this study. Figure 6 shows three SSG stiffness curves of medium sand which were obtained in three different sizes of the GT molds: 0.3, 0.6, and 0.9-m diameter. Results indicate that a 0.3-m diameter mold has the greatest influence on stiffness. The effect of mold size is drastically reduced in the 0.6 and 0.9-m diameter molds. For the 0.3-m diameter mold, the SSG stiffness dramatically increased from negative values near the base of the mold to the maximum value of about 13 MN/m. No pronounced peak SSG stiffness is observed in the 0.6 and 0.9-m diameter molds and the maximum SSG stiffness is approximately 4 to 5 MN/m. The SSG stiffness of medium sand in 0.3-m diameter mold stabilizes at a value less than that in 0.6 and 0.9-m diameter molds. The average SSG stiffness values of medium sand are computed after they stabilize and are given in Figure

7 for each mold size. They are 2.8 and 3.8 MN/m, respectively in 0.3 and both 0.6 and 0.9-m diameter molds. The lower SSG stiffness in the 0.3-m diameter mold after stabilization might be due to the effect of soft material (i.e., foam peanuts) on the outside of the mold. However, this effect was eliminated by using a larger diameter mold. A similar result is obtained from the FEA. Thus the radius of measurement influence of the SSG is determined to be less than 0.3 m, i.e., a lateral zone of influence of 0.6 m in diameter.

Stiffness of the Test Materials

Three materials: medium sand, 19-mm crushed lime rock, and plastic beads-sand mixture, were tested in a 0.6-m diameter GT mold in order to eliminate the effect of physical model size. Results of the single material tests using these three test materials in 0.6-m diameter GT mold are graphically shown in Figure 8. The average SSG stiffness of each material was determined when the stiffness values became stable, i.e., above 380-mm height. Results show that the crushed rock has the highest average SSG stiffness of about 4.83 MN/m. The average SSG stiffness of medium sand is about 3.83 MN/m. The plastic beads-sand mixture has the lowest average SSG stiffness of about 2.39 MN/m. Therefore, crushed rock is considered as "high stiffness" material, medium sand as "intermediate stiffness" material, and plastic beads-sand mixture as "low stiffness" material.

Effect of Coupling in Coarse-Grained Materials

The SSG manufacturer states that it is important to maintain good contact area between the ring-shaped foot of the SSG and the measured surface. Further tests were conducted on crushed rock in order to investigate the effect of providing coupling using moist sand on the surface of crushed rock (as suggested by the SSG manufacturer). Figure 9 represents the effect of contact area between the ring-shaped foot of the SSG and the measured surface. The SSG stiffness of crushed rock when tested without applying the moist sand on the surface of crushed rock was essentially the same as when tested with the moist sand on the surface of crushed rock. For this reason, during subsequent testing on crushed rock, no additional moist sand was applied.

Effect of Layering and Separator

For two-layered sample tests, six types of layered systems consisting of the three test materials were established. These materials correspond to high, intermediate, and low stiffness. Tests were conducted in 0.6-m diameter GT mold. A woven GT sheet was used at the interface between these two materials. For the layered sample tests with crushed rock on medium sand and medium sand on crushed rock, the results are shown in Figure 10. For comparison, single layer measurements on the bottom layer material are also shown. In case of crushed rock on medium sand (Figure 10), SSG stiffness measured at the interface after placing the GT sheet was close to that before placing the GT sheet. No stiffness value was obtained from the SSG (the velocity sensors became overloaded) after crushed rock was deposited up to 25 mm above the interface. The average SSG stiffness of about 3 MN/m was determined from 50 to 150 mm height above the interface. SSG stiffness dramatically increased at 175 mm above the interface. Then, after 175 mm above the interface, SSG stiffness gradually increases with height. In case

of medium sand on crushed rock layered system (Figure 10), similar to the previous layered system, no stiffness value was obtained from the SSG when the sand was deposited only 25 mm above the interface. The average SSG stiffness of about 1.5 MN/m is calculated from 50 to 125 mm height above the interface. SSG stiffness dramatically increases at a height of 150 mm above the interface. Results of these two tests show that the GT separation sheet did not provide stiffness coupling at the interface between the two materials. The stiffness significantly decreased after placing the GT sheet.

Further study on the reason why stiffness dramatically decreases when the GT sheet is placed at the interface was investigated by conducting a test with medium sand on crushed rock but without the GT sheet. Figure 11 shows the results of this test. During the filling of the mold, the SSG stiffness greatly increased after 25 mm of medium sand was placed above the interface,. Then as the height of medium sand (the upper layer material) increased, the SSG stiffness continued to decrease. However, the results are different during the emptying of the mold. SSG stiffness during filling was much higher than that during emptying. It is obvious that SSG stiffness values are affected in a zone from the interface to 100 mm height above the interface. However, SSG stiffness during filling and emptying is comparable above that height. Without a separator, mixing of the materials occurs, thus a separator was used in all subsequent tests.

Consequently, two tests were conducted, one with crushed rock and the other one with plastic beads-sand mixture on medium sand with a thin plastic wrap sheet at the interface as shown in Figure 12. Results show that SSG stiffness at the interface of these two materials after placing the plastic wrap on medium sand became essentially the same as that before placing the plastic wrap. In case of crushed rock on medium sand, the SSG measures the stiffness of medium sand, the bottom layer material, from the interface up to 125 mm height above the plastic wrap interface. Then, the SSG starts to register the stiffness of crushed rock, the upper layer material, and hence the SSG stiffness increases with height.

Another series of layered sample tests with crushed rock at the bottom and medium sand and plastic beads-sand mixture at the top were performed using a thin plastic wrap sheet as the separator as shown in Figure 13. The crushed rock used in this test had medium sand mixed into it therefore its stiffness is reduced from that of the clean crushed rock. SSG stiffness at the interface in these tests was close to that before placing the plastic wrap. Similar to the previous layered sample tests (with the medium sand at the bottom), the SSG measures the stiffness of crushed rock, the bottom layer material, up to about 125 mm height above the interface. Thereafter, SSG stiffness decreases until it reached the stiffness of medium sand, the upper layer material. In case of plastic beads-sand mixture on crushed rock, SSG stiffness starts to decrease immediately at the interface and continues to decrease until it reaches the stiffness of plastic beads-sand mixture at about 250 mm above the interface.

The results of a third series of layered sample tests with medium sand and crushed rock on the plastic beads-sand mixture (50:50 by volume) with a thin plastic wrap sheet as the separator are given in Figure 14. SSG stiffness at the interface and up to about 100 to 125 mm height above the interface is essentially the same as the SSG stiffness of plastic beads-sand mixture, the bottom layer material. After that height, SSG stiffness of

both systems tends to increase with height. The use of thin plastic wrap sheet at the interface produced a better coupling between the test materials while providing separation between them in contrast to the GT sheet which produced a loss in coupling. It should be noted that the effect of the lower layer continues to be present in some cases (Figures 12 to 14) even at an upper-layer material thickness of 275 mm (the size limit of the test box) depending on the relative stiffness of the layer materials.

CONCLUSIONS

The main objective of this study was to evaluate aspects of the soil stiffness gauge (SSG) as a potential alternative geotechnical field testing device for measuring the insitu soil stiffness. In order to understand the SSG measurement characteristics and limitations, a laboratory investigation was conducted. In the laboratory experiments, the zone of measurement influence and the effect of significant factors on measurements were determined. For this purpose, the measurements were made in a test box with energy absorbing boundary materials. In order to investigate the boundary effects, three different sizes of the cylindrical molds made of a woven geotextile were made. The ANSYS® finite-element analysis (FEA) program was employed to model and validate the size of the test box as well as to investigate the zone of influence of the SSG. Three main test materials with varying stiffnesses were utilized in this study.

Based on the FEA and the SSG measurement in the test box, the radius of measurement influence extends to 300 mm. For two-layer materials with different stiffness, the SSG starts to register the stiffness of an upper-layer material of 125 mm or thicker. The effect of the lower layer however, may continue to be present even at an upper-layer material thickness of 275 mm depending on the relative stiffness of the layer materials. Caution needs to be exercised in interpreting the results from the SSG when it is used on multi-layer systems, especially those with geosynthetic separators. The presence of a geosynthetic separator between the layers may cause a stiffness decoupling of the layers.

ACKNOWLEDGEMENT

This research was funded by the Wisconsin Department of Transportation and the United States Department of Transportation in the interest of information exchange. The material or information presented/published/reported is the result of research done under the auspices of the Department and Wisconsin Highway Research Program (WHRP). The Research Section within the Department's Division of Infrastructure Management, under the direction of the Department and WHRP, manages the research program of the Department, including review and approval of final publications endorsed by the Department. However, the content of this presentation/publication/report reflects the views of the author, who is responsible for the correct use of brand names, and for the accuracy, analysis and any inferences drawn from the information or material presented/published/reported. WisDOT and FHWA (US DOT) assume no liability for its contents or use thereof. This presentation/publication/report does not endorse or approve any commercial product, even though trade names may be cited, does not reflect official views or policies of the Department or FHWA (US DOT), and does not constitute a standard specification or regulation of the Department or FHWA.

REFERENCES

1. Humboldt Mfg. Co. (1999), "Soil Stiffness Gauge (GeoGauge) User Guide," Version 3.3, November.

2. Sawangsuriya, A. (2001), "Evaluation of the Soil Stiffness Gauge," M.S. Thesis, University of Wisconsin-Madison, Department of Civil and Environmental Engineering, Madison, WI.

3. Lenke, L. R., Pak, R. Y. S., and Ko, H-Y (1991), "Boundary Effects in Modeling Foundations Subjected to Vertical Excitation," Proc. International Conference Centrifuge, Balkema, Rotterdam, pp. 473-480.

4. ANSYS® (2000), Swanson Analysis Systems (SAS), Inc.

5. Bosscher, P. J. and Gray, D. H. (1986), "Soil Arching in Sandy Slopes," Journal of Geotechnical Engineering, ASCE, Vol. 112, No. 6, pp. 626-645.

LIST OF FIGURES

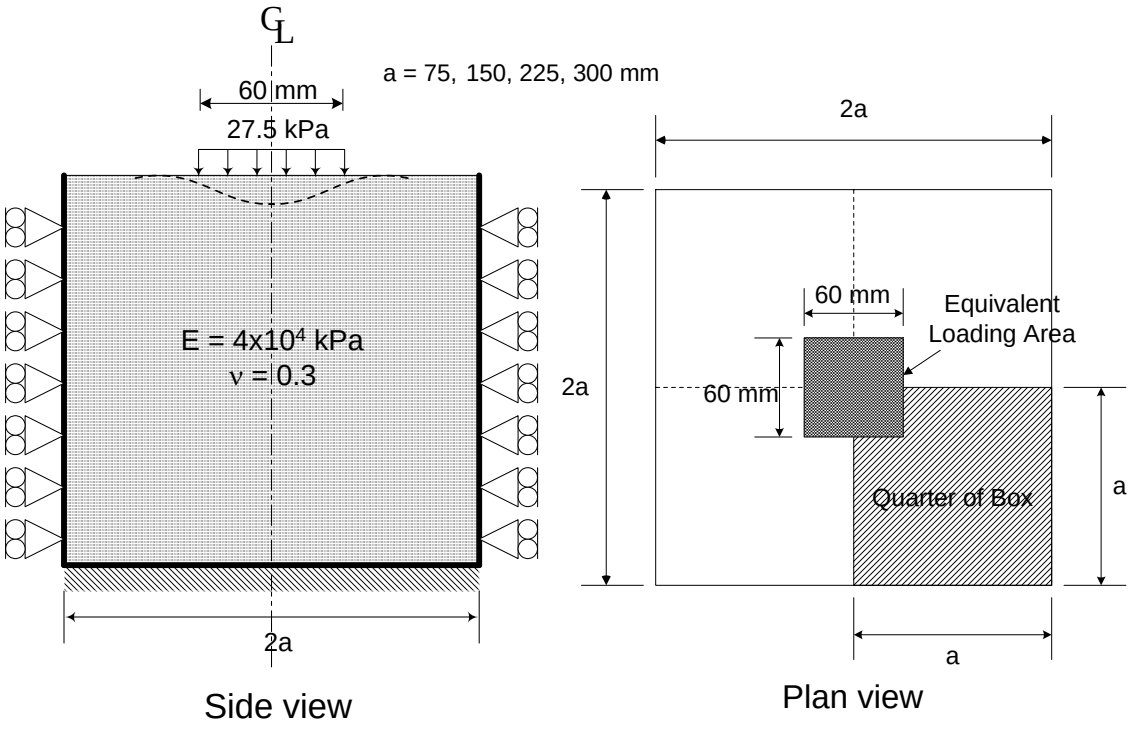

(a)

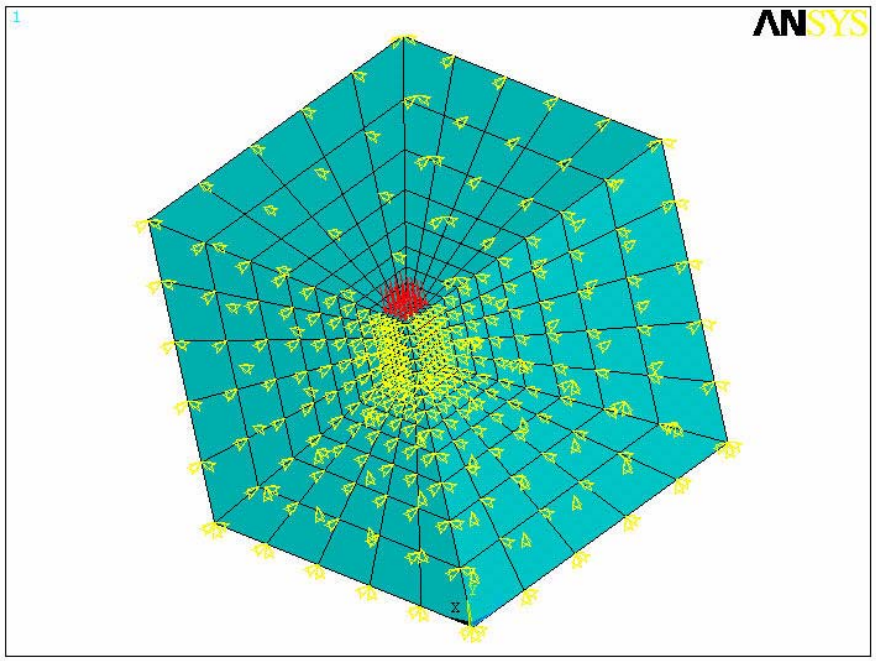

(b)

FIGURE 1 (a) An elevation and a plan view of test box model in FEA and (b) a finite-element model with the boundary condition.

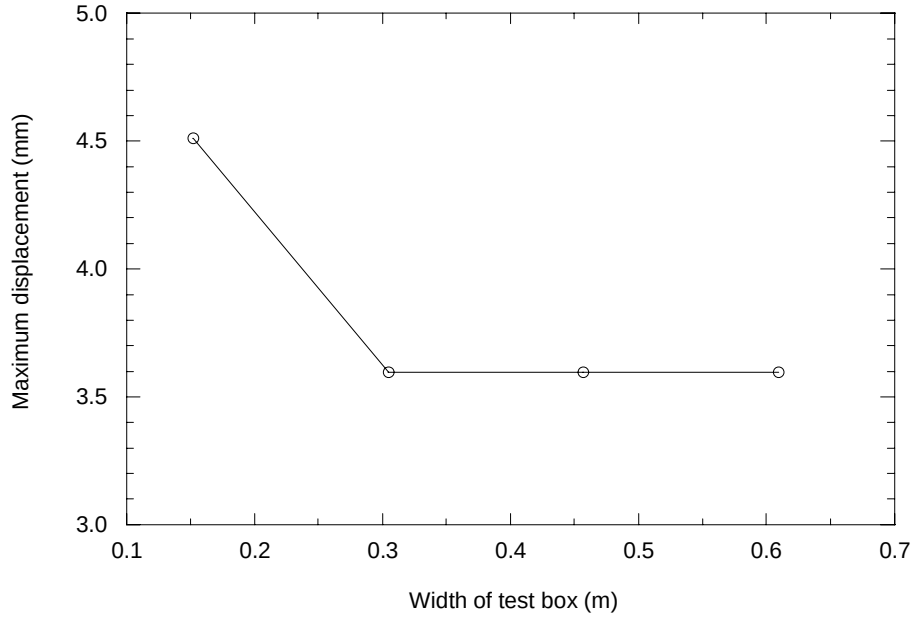

(a)

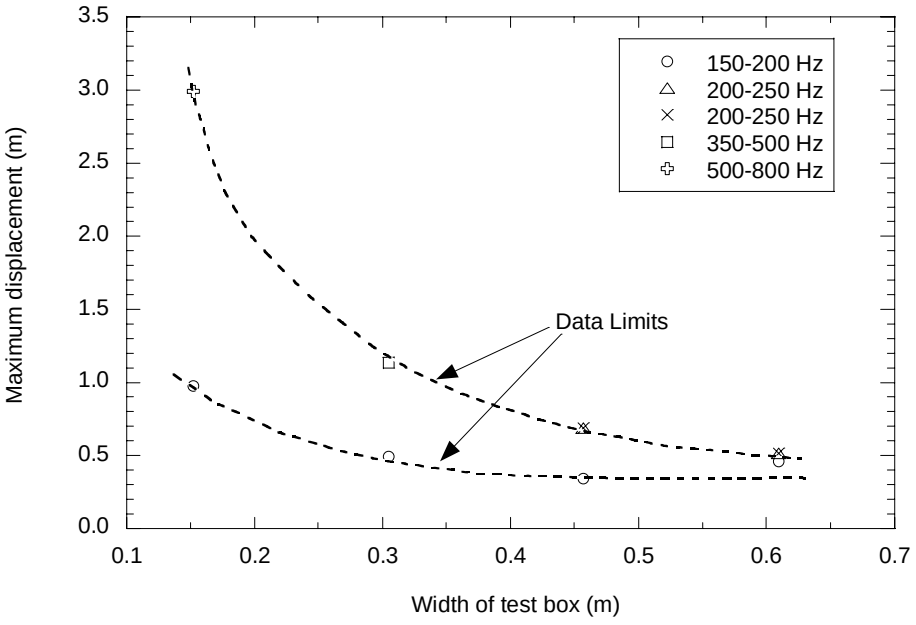

(b)

FIGURE 2 Maximum displacement as a function of test box width for (a) static and (b) dynamic FEA analysis.

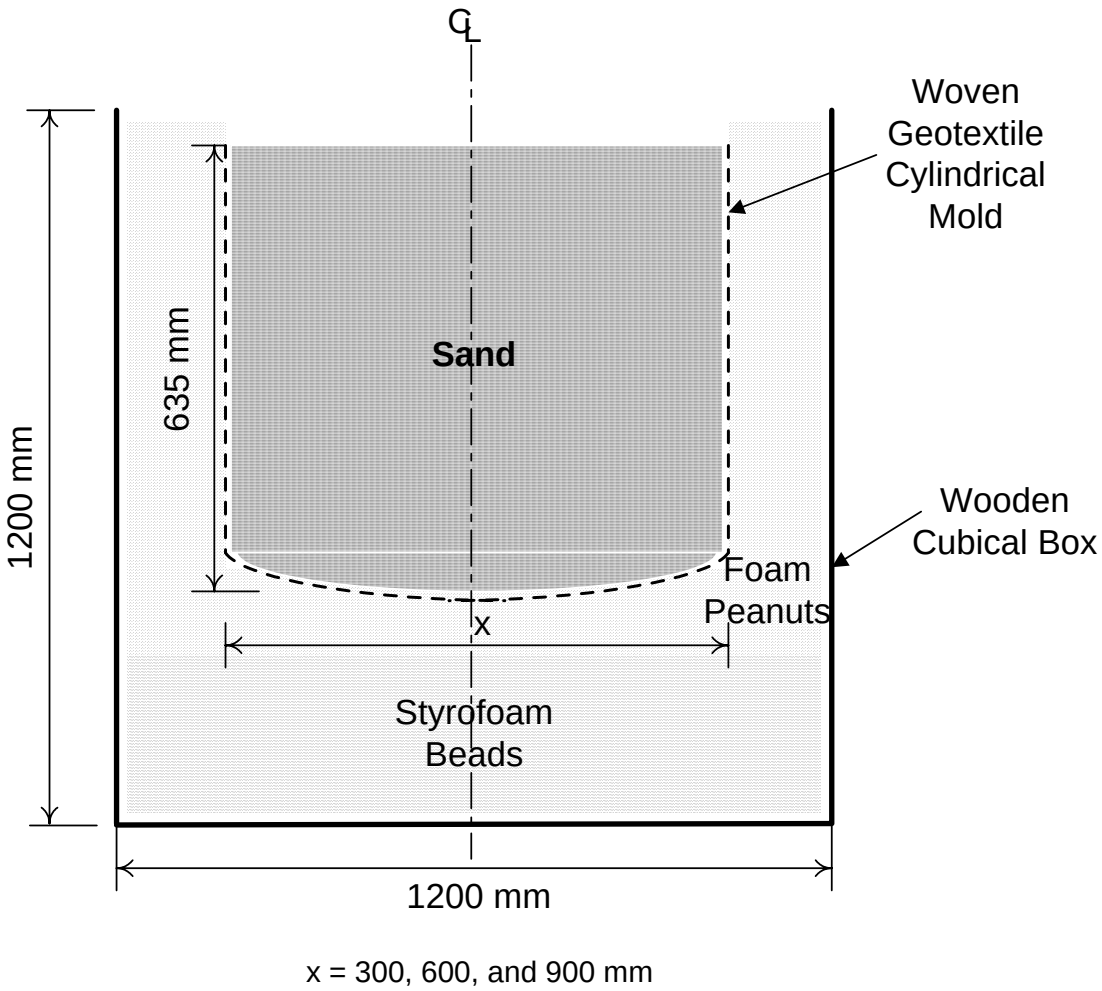

FIGURE 3 Schematic of the test box.

FIGURE 4 Pluviation device.

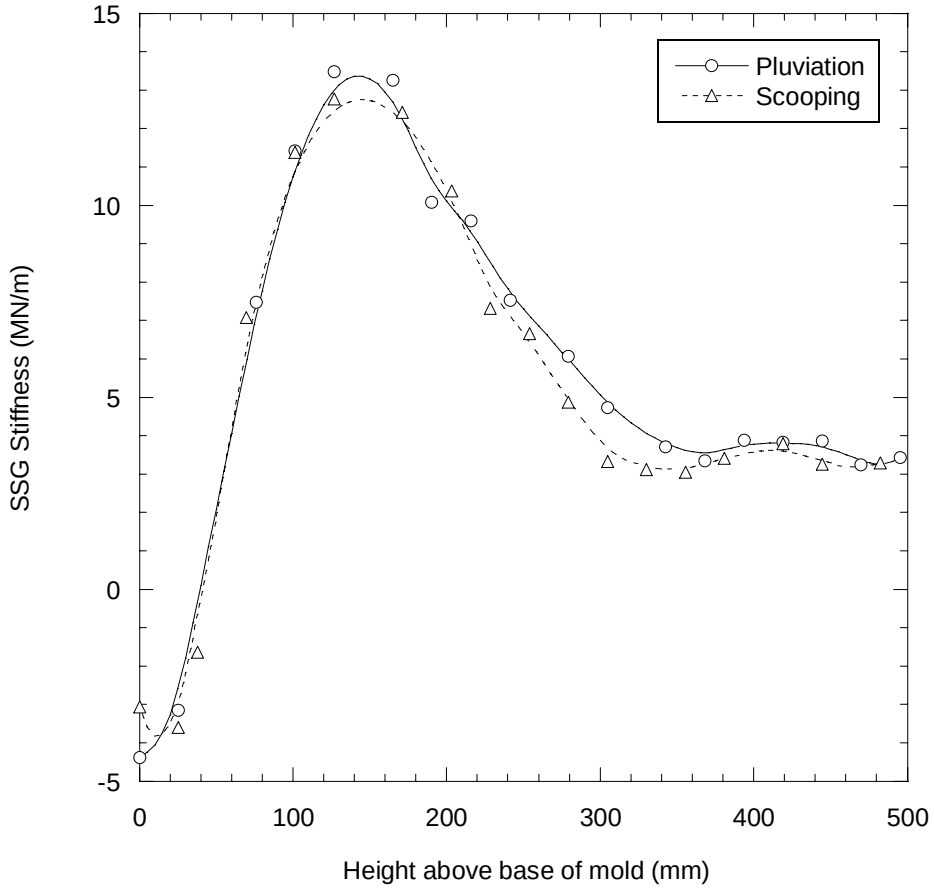

FIGURE 5 SSG stiffness test results in 0.3-m diameter mold of two sample preparation methods, pluviation and scooping.

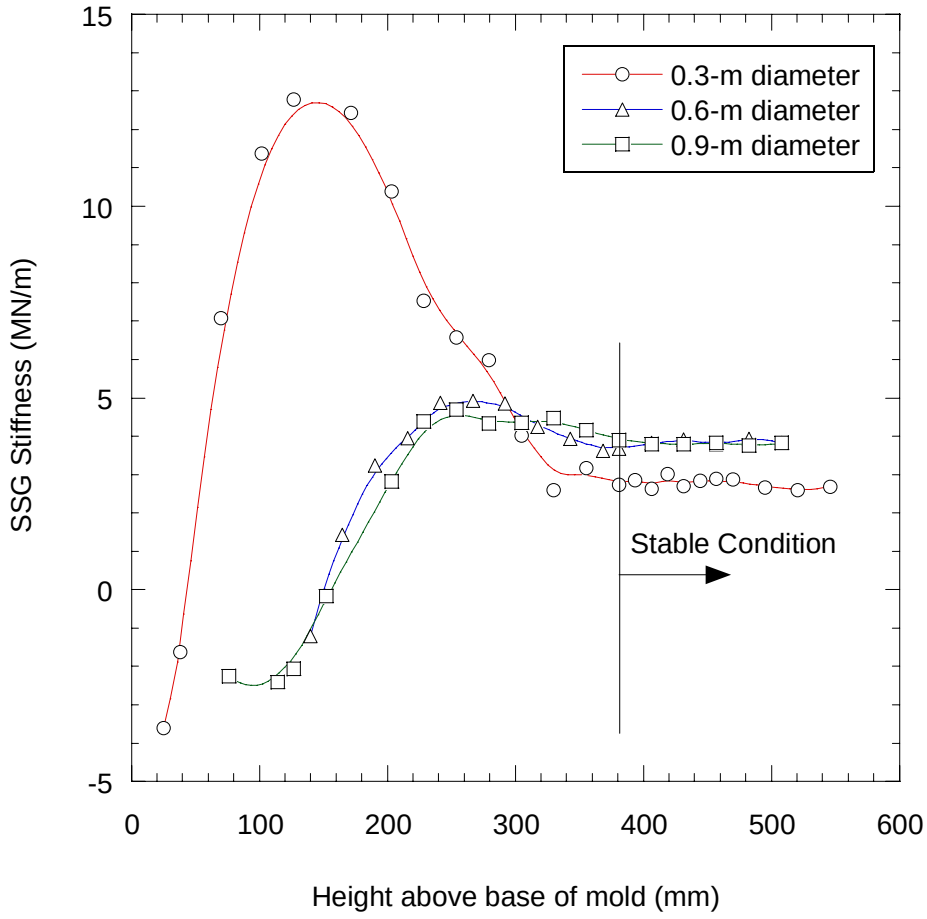

FIGURE 6 SSG stiffness of medium sand in 0.3, 0.6, and 0.9-m diameter molds.

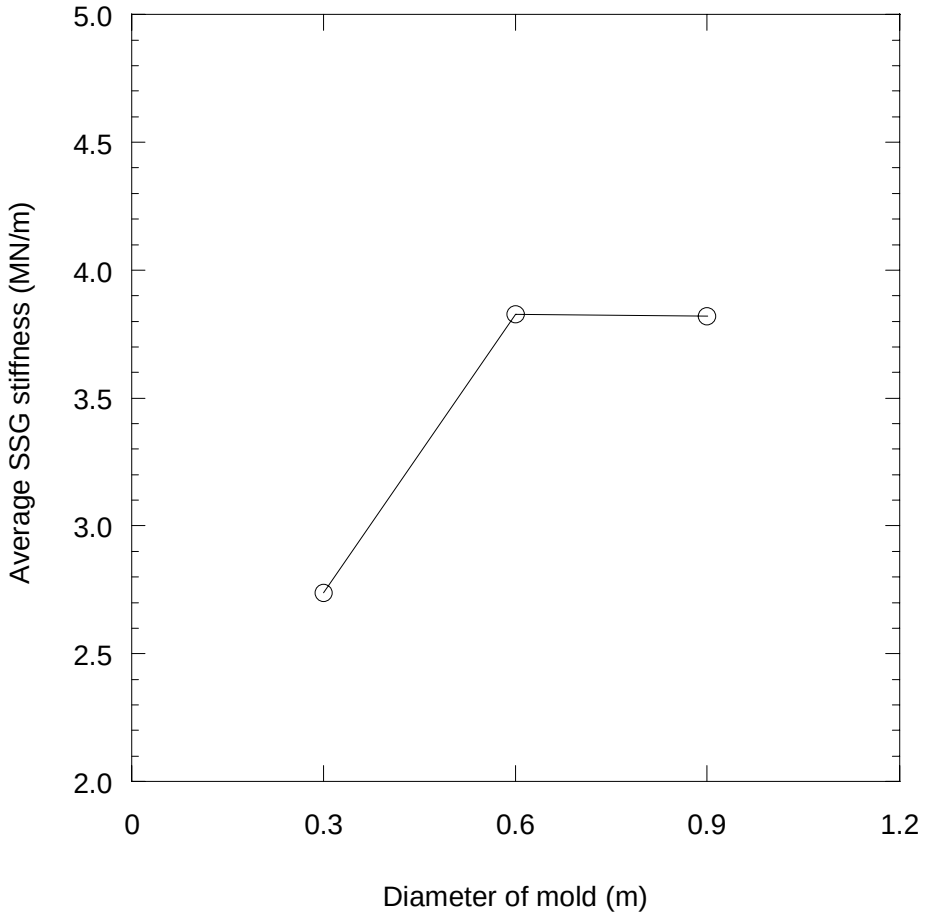

FIGURE 7 Effects of mold sizes (physical models) on SSG stiffness test.

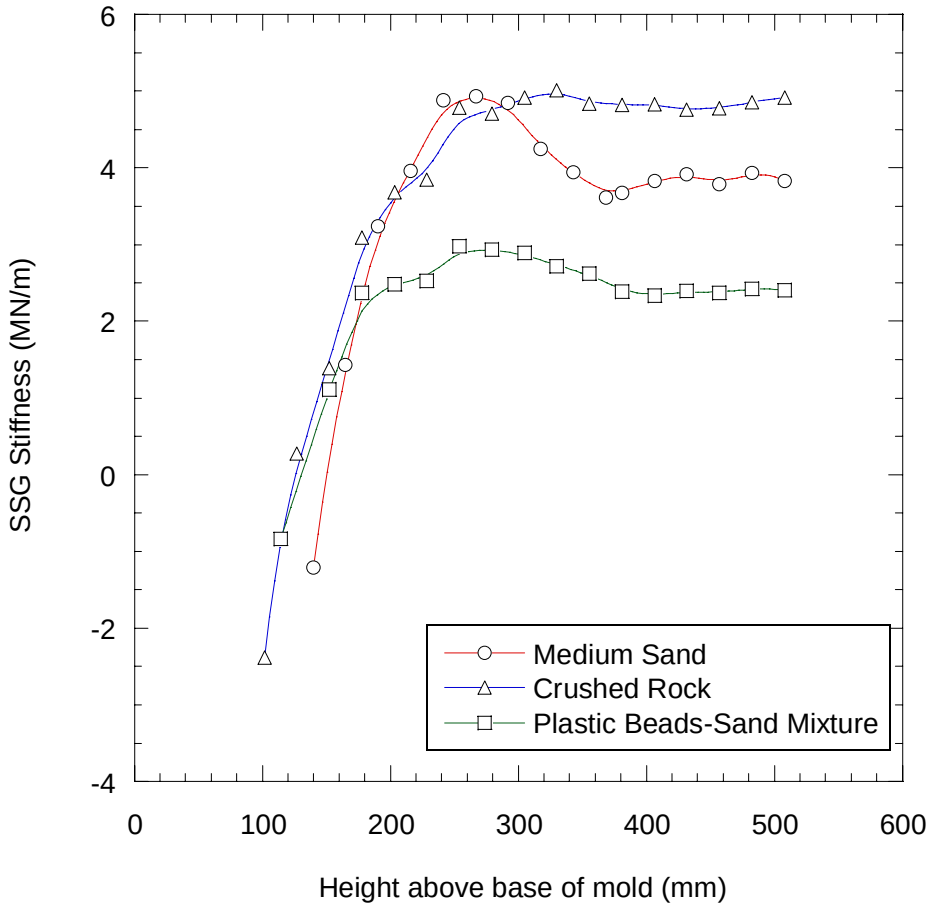

FIGURE 8 SSG stiffness of medium sand, crushed rock, and plastic beads-sand mixture in 0.6-m diameter mold.

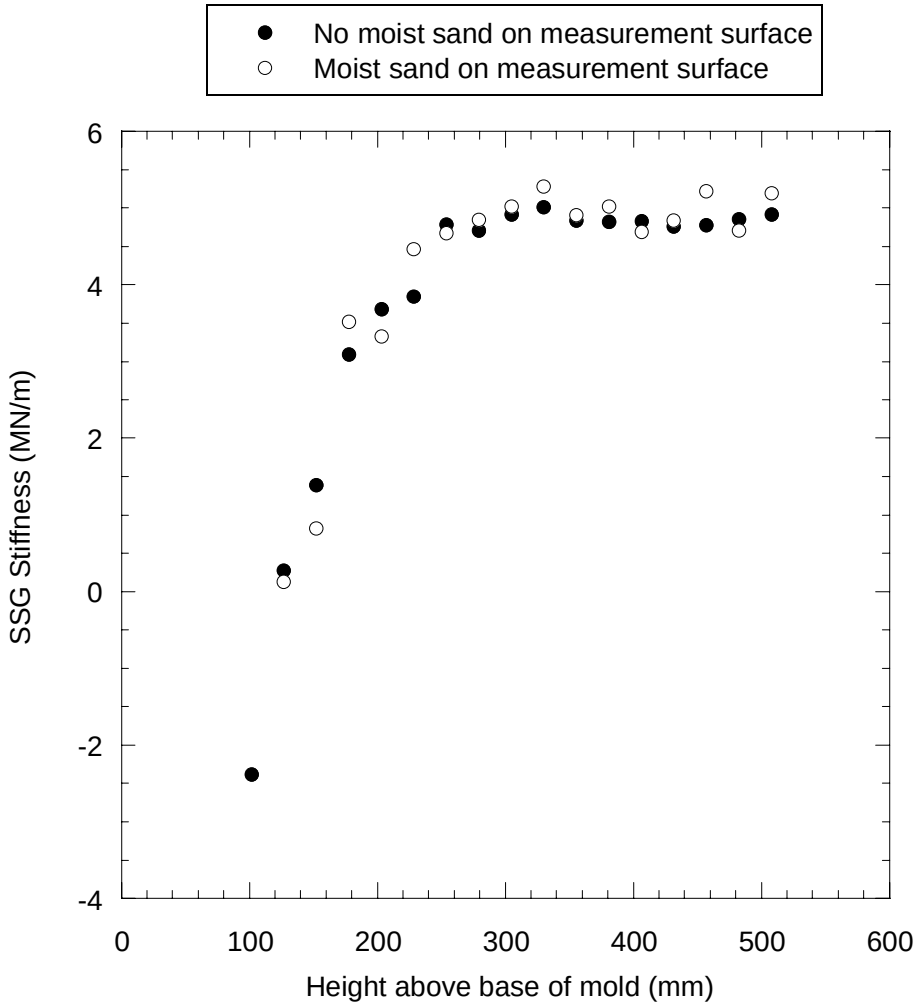

FIGURE 9 Effect of providing coupling using moist sand on the surface of crushed rock.

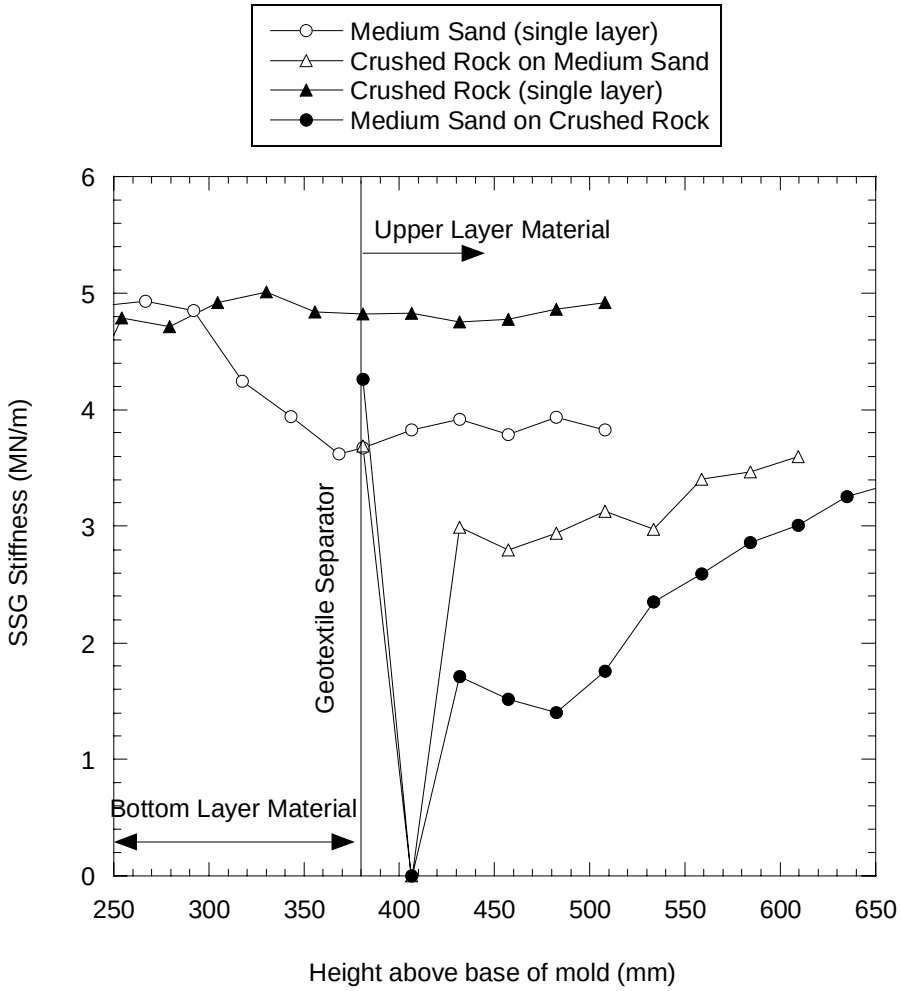

FIGURE 10 Layered sample tests with a geotextile sheet as a separator.

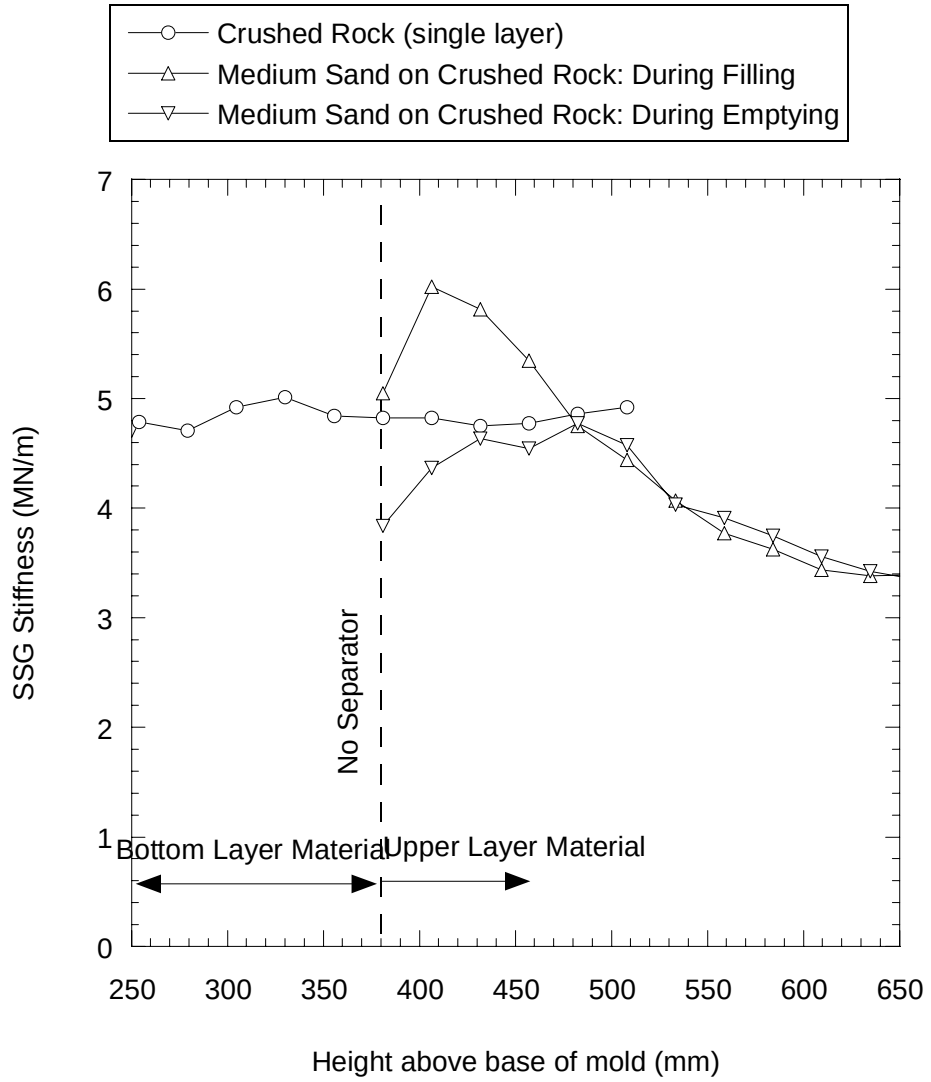

FIGURE 11 Layered sample test with medium sand on crushed rock but without a separator.

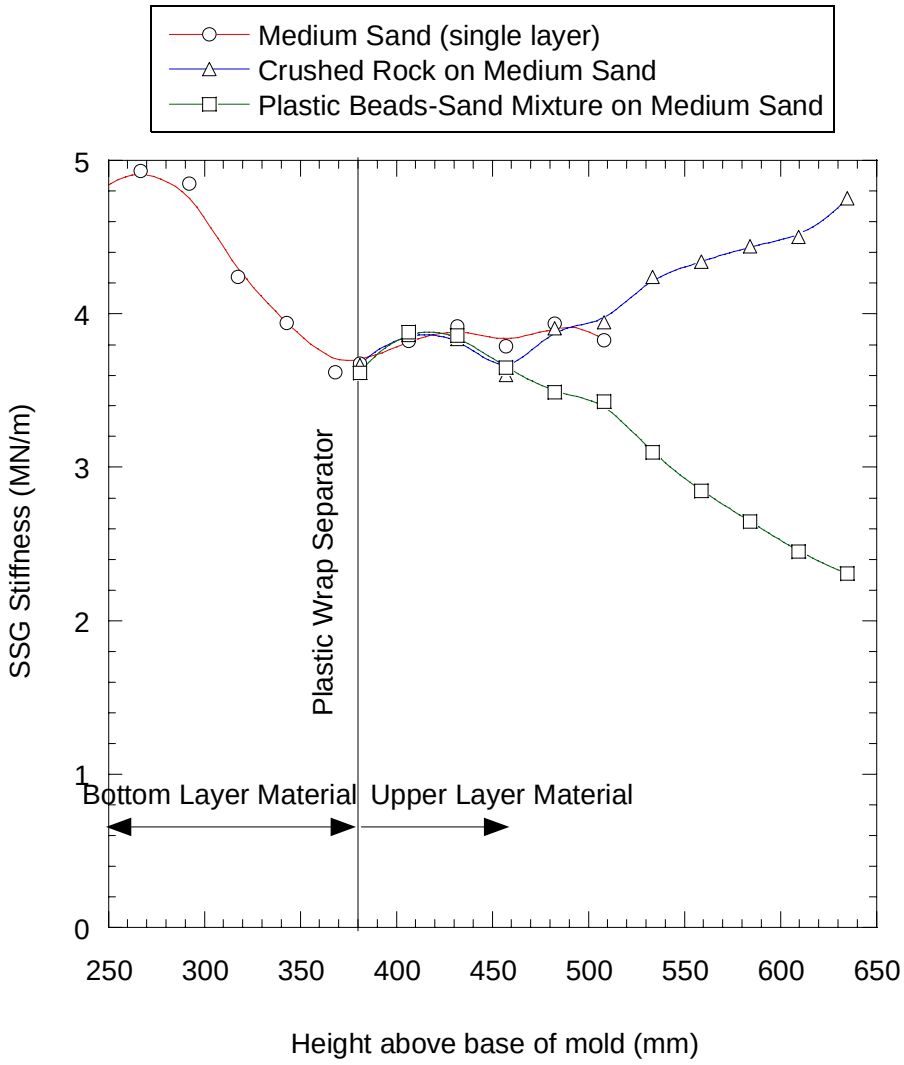

FIGURE 12 SSG stiffness of layered sample tests- over medium sand.

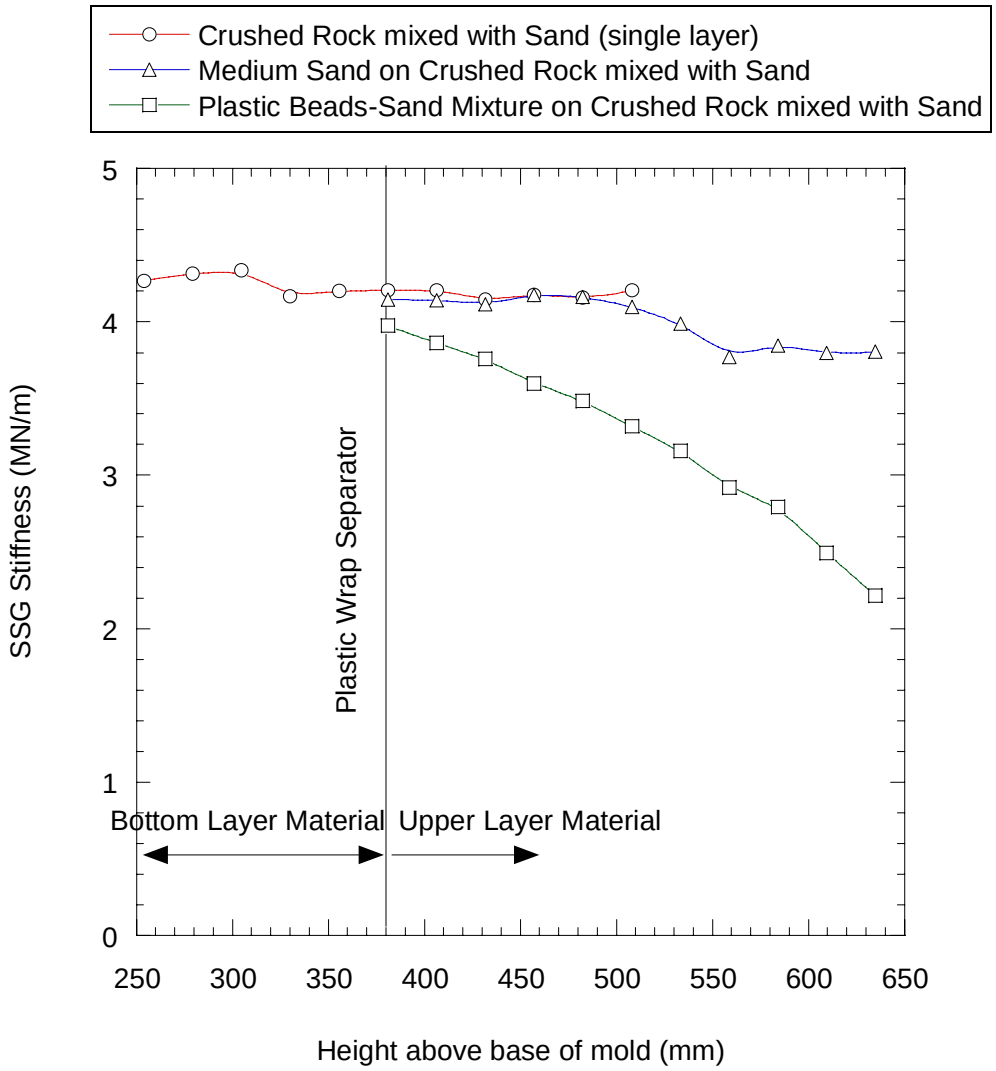

FIGURE 13 SSG stiffness of layered sample tests- over crushed rock mixed with sand.

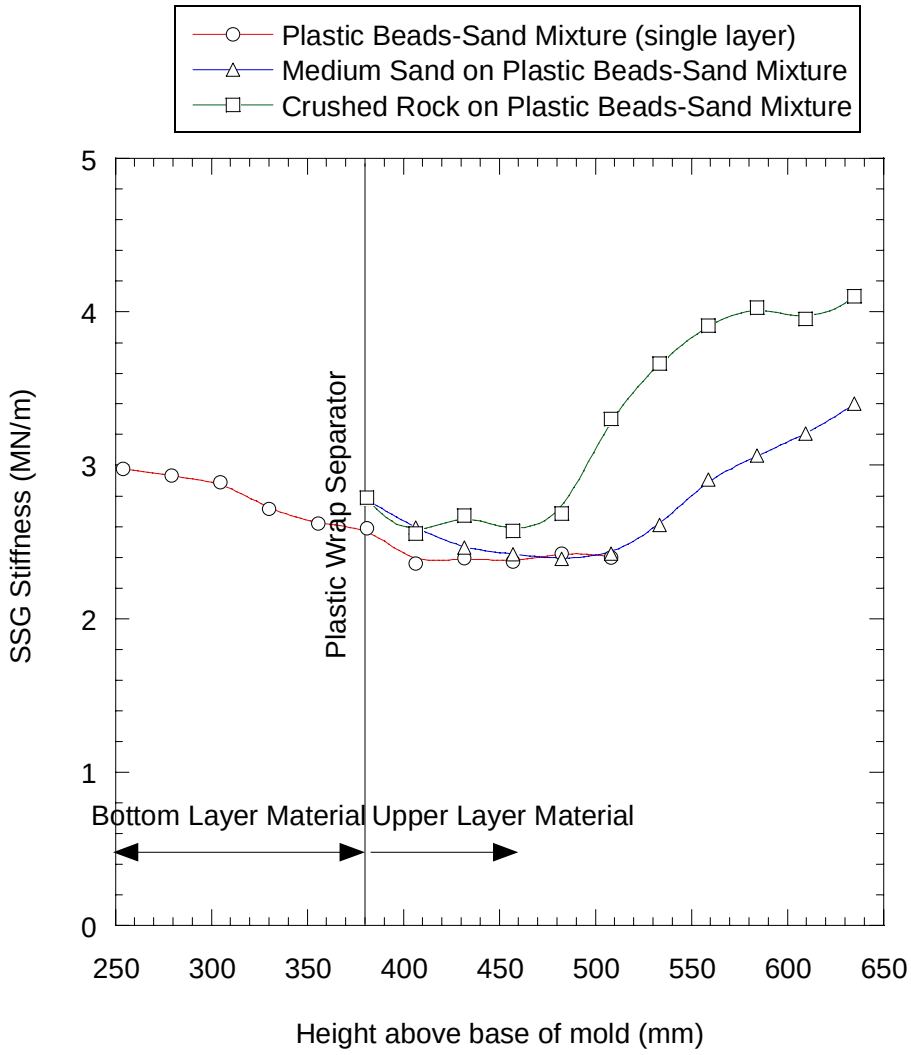

FIGURE 14 SSG stiffness of layered sample tests- over plastic beads-sand mixture.

Paper No. 03-4089

TITLE:

RELATIONSHIP BETWEEN SOIL STIFFNESS GAUGE MODULUS AND OTHER TEST MODULI FOR GRANULAR SOILS

Author(s):

Auckpath Sawangsuriya
Tuncer B. Edil
Peter J. Bosscher

Department of Civil and Environmental Engineering
2226 Engineering Hall, 1415 Engineering Dr.
The University of Wisconsin-Madison, Madison, WI, 53706
sawangsuriya@students.wisc.edu, edil@engr.wisc.edu,
bosscher@engr.wisc.edu

Paper submitted for presentation and publication at the

Transportation Research Board
82nd Annual Meeting
January 12-16, 2003
Washington, D.C.

Abstract: Recently, there has been a concerted effort to develop methods for direct measurement of soil stiffness and/or modulus. A new field test device called the soil stiffness gauge (SSG), which is currently marketed as GeoGauge™, shows potential to assess near-surface stiffness. This study presents a comparison of moduli obtained from the SSG with moduli obtained from other tests on granular soils. The maximum single amplitude dynamic force produced during the SSG measurement is determined to be 10-17.3 N. Based on this, an estimate of the shear strain amplitude produced from the SSG is made using finite element analysis. A plot of shear modulus versus shear strain amplitude on a medium sand obtained from different laboratory tests, including the SSG, is presented. The comparison of the SSG modulus with the moduli from other laboratory tests indicates that the SSG outputs a dynamic modulus corresponding to a strain amplitude approximately 20 times higher than the expected range and with a magnitude lower than it should be on the basis of the induced strain. Nevertheless, the SSG modulus is still higher than that from the resilient modulus test typically used for pavement design.

Key Words: soil stiffness, modulus, shear strain amplitude, soil stiffness gauge, resonant column, resilient modulus, seismic

INTRODUCTION

Developed from land-mine detection technology of the U.S. military, the soil stiffness gauge (SSG) manufactured by the Humboldt Manufacturing Company is a portable field device that provides a simple, safe, and rapid means of directly measuring soil stiffness and modulus. The device is purported to provide construction control of earthwork by using the same physical parameters as the design process (*1*). The SSG also provides an alternative means of measuring dry soil density in conjunction with an independent measurement of moisture content. More details of the device can be found in other references (*1*, *2*, *3*, *4*).

Wu et al. (*2*) reported a comparison of the SSG with other quality control techniques used for assessing pavement construction. The other techniques included the portable seismic pavement analyzer (PSPA), the falling weight deflectometer (FWD), and the spectral analysis of surface waves (SASW). A linear correlation was found between stiffness measured by the SSG and the modulus measured using these techniques. They also concluded that the SSG has great potential for use as an alternative quality control device in pavement construction.

The design of pavement structures requires assessment of material modulus. Use of the SSG to quantify material moduli has potential; however, additional research is warranted before the SSG can be used with confidence for this purpose. Experiments are needed to correlate modulus from the SSG to other laboratory measurements of modulus such as resilient modulus used in the mechanistic design of pavement structures. This paper presents the results of a laboratory investigation of the comparison of moduli from the SSG with those from other modulus tests, i.e., triaxial compression, resilient modulus, resonant column, and seismic tests on granular soils (*3*).

Soil modulus is known to change as a function of strain amplitude and stress state; consequently any modulus must be defined and understood in terms of these factors, and the comparison of moduli from various tests must be done on the basis of comparable levels of stress and strain. Consequently, a plot of shear modulus versus shear strain

amplitude obtained from different laboratory tests on medium sand at the same stress level is presented and the modulus obtained from the SSG is placed in relation to the other moduli.

TEST MATERIALS

The SSG test data were collected on several granular materials in two different test setups. Three types of granular materials characterized as high stiffness, intermediate stiffness, and low stiffness were used in the tests conducted in a specially constructed test box. The high stiffness material is 19-mm crushed lime rock with an angle of internal friction of 40° in the loose state. The intermediate stiffness material is a medium, uniformly-graded quartz sand classified as SP and A-3 (0) according to the Unified Soil Classification System (USCS) and the American Association of State Highway and Transportation Officials (AASHTO) classification system, respectively. It has a uniformity coefficient (C_u) of 1.3 and an effective grain size (D_{10}) of 0.45 mm. This sand has maximum and minimum unit weights of 17.86 and 15.25 kN/m^3, respectively and a solids specific gravity of 2.65. It has an average grain roundness of 0.85 and an internal friction angle of 35° in the loose state. The low stiffness material is a 50:50 mixture (by volume) of nylon plastic beads (produced by Zeier Plastics) and the medium sand. The plastic beads have a prismatic shape and pass sieve No. 4 but are retained on sieve No. 8 with dimensions of approximately 2.5 x 2.5 x 1.5 mm. Its angle of repose is approximately 40°.

The SSG data was also obtained on Wisconsin Grade 2 gravel in a large test pit. Grade 2 gravel has the gradation and Atterberg limits requirements specified in WisDOT Specification Section 302 (*5*). It is classified as GW and A-1-a (0) by the USCS and the AASHTO, respectively. The maximum dry unit weight and optimum water content of this material is 22.6 kN/m^3 and 8.2%, respectively.

SSG TESTS

The SSG measures near-surface stiffness by imparting small vertical forces to the soil through a ring-shaped foot, which causes small deflections. The SSG determines soil stiffness as the ratio of force to deflection. To determine the strain amplitude induced by the SSG, the dynamic force produced is estimated based on an experimental measurement and a finite-element analysis (FEA). To determine the stress level (both bulk stress and confining pressure) in the SSG test, elastic theory is utilized.

Test Box

A 1.2 m x 1.2 m x 1.2 m wooden box was built for this study. A cylindrical mold with a radius of 0.3-m made of a woven geotextile (GT) was used to hold the test materials in the test box and separate them from the energy absorbing boundary material that was placed in the wooden box. The energy absorbing boundary material consisted of expanded-polystyrene beads and foam peanuts filling the horizontal and vertical space between the cylindrical mold and the container. Note that this configuration was shown by preliminary tests to be free of boundary effects (*4*).

Testing Procedure in the Test Box

1) The material to be tested with the SSG was poured slowly from a scoop into the 0.3-m radius woven GT cylindrical mold, which was already placed in the test box. It is understood that other deposition methods would produce different soil fabrics and thus different densities and moduli.
2) The unit weight of the test material deposited was obtained by placing a metal cup of known volume in the GT mold during the deposition process. Then, the cup was excavated and weighed to determine the unit weight of the deposited test material.
3) The stiffness of the test materials was measured by the SSG at the center of the cylindrical mold after every 25-mm increment of deposition from the bottom up. The surface of test materials in the cylindrical mold was leveled prior to each measurement.

Measured Stiffness in the Test Box

The three materials selected, i.e., medium sand, crushed lime rock, and plastic beads-sand mixture, were tested in the 0.3-m radius GT mold in a loosely deposited state. Results of the tests using these three test materials are graphically shown in Figure 1. The average stiffness of each material was determined when the stiffness values became stable, i.e., at a height of 380-mm above the base. Before this height is reached, the zone of influence of the SSG overlaps the mold base, resulting in variable stiffness measurements. Results show that the crushed rock has the highest average stiffness of about 4.83 MN/m. The average stiffness of medium sand is about 3.83 MN/m. The plastic beads-sand mixture has the lowest average stiffness of about 2.39 MN/m.

Test Pit

SSG data were also obtained on Wisconsin Grade 2 gravel that was deposited in a 3 m x 3 m x 3 m test pit used for testing of pavement structures. A layer of Grade 2 gravel was placed in the test pit and compacted to 87% relative compaction and to a thickness of 0.45 m and SSG measurements were made on the surface of this material. The average stiffness of Grade 2 gravel was approximately 8.67 MN/m.

ANALYSIS OF STRESS AND STRAIN IN SSG TEST

Estimation of Strain Amplitude Induced by the SSG

The strain amplitude of the SSG is needed for moduli comparison. The strain is directly related to the vibration displacement amplitude, which in turn, is related to the acceleration. An experimental test was setup for directly measuring the vertical acceleration produced by the SSG during its operation. The test procedures and analysis results are described as follows.

Acceleration Measurement of the SSG

An accelerometer was attached to the rigid ring-shaped foot of the SSG. The signal from the accelerometer was amplified using a charge amplifier and recorded by a digital audio tape recorder. The medium sand was packed in a 0.3-m radius cylindrical cardboard mold with 140-mm thick foam block placed at the bottom. The method of sample

preparation used was the same as that was used in the test box resulting in a unit weight of about 16 kN/m^3. The SSG with the accelerometer attached under its ring-shaped foot was placed on the surface of the sand. The acceleration signal produced by the SSG during its stiffness measurement was recorded. Three replicated tests were conducted.

Since the measured signal of the accelerometer is in voltage (V), a calibration for the accelerometer is required to obtain acceleration in engineering units. The average calibration factor of about 0.122 V/g was obtained in this study. The accelerometer was calibrated with a shaker, with a known calibration factor at various frequencies.

A computer program called PCSCAN II was utilized for analyzing the measured signal. The peak-to-peak amplitudes of measured signal were collected at different frequencies using spectral analysis techniques provided in the program. For the ease of analysis, the acceleration was converted to displacement. The results of acceleration measurement are shown in Figure 2(a) as the single amplitude displacement plotted as a function of frequency. The jump in the displacement at 135 Hz was noted in all measurements, those from the SSG output and also the authors' accelerometers. This jump may be due to control aberrations in the SSG electronics.

Finite-Element Analysis

A commercial finite-element analysis (FEA) program called PLAXIS (*6*) was utilized in this study to estimate the dynamic force and the strain amplitude in the SSG test. In the analysis, the medium sand in the cylindrical mold was modeled as an axi-symmetrical problem. An energy-absorbing element was employed at the boundary for geometrical or radiation damping. PLAXIS utilizes an implicit time-integration method and incorporates Rayleigh internal damping. The soil was modeled with an elastic-perfectly plastic model (Mohr-Coulomb). The only plasticity noted occurred in a small tension zone near the soil surface. A parametric study is required in order to simulate a realistic dynamic behavior for this problem. The parameters studied included the model geometry, Poisson's ratio, modulus, and material (internal) damping. It is also noted that most of the parameters used in this analysis were selected based on property tests, which are described in the previous section. The basic input parameters for the FEA are the unit weight of 16 kN/m^3 and the angle of friction angle of 35°. Dynamic force was input to the model, which yielded a dynamic displacement.

The first parameter selected in the parametric study was the model geometry. The original model geometry used was the same as the actual size of the cylindrical mold used in the experimental test, that is, 0.3-m radius and 0.53-m height. Then, the FEA was performed with the model size changed to be 0.6-m radius and 0.53-m height and 0.9-m radius and 0.9-m height. The study indicated that the size of the model significantly affected the results if no internal damping is assumed, however with internal damping the size is not as critical. The damped model with the same geometry as the actual size provided the closest behavior to the measured results. The other geometries were also close but they had different resonances.

The second parameter studied was Poisson's ratio. Based on the test materials, two values of Poisson's ratio, 0.25 and 0.3, were selected for the analysis. The study indicated that this range of Poisson's ratio had a small influence on the results.

The third and fourth parameters that were investigated were modulus (E) and material damping (ξ), respectively. The moduli used were 30, 35, and 40 MPa, which is

close to those obtained from the modulus tests. The material damping values were selected according to the Rayleigh alpha (a) and beta (b), which ranged from 0.01 to 0.0001. The Rayleigh alpha (a) and beta (b) respectively determine the influence of the mass and the stiffness in the damping of the system. The damping ratio (δ) can then be obtained as (*7*):

$$\delta = 2\pi\xi = 2\pi\left(\frac{a}{2\omega_n} + \frac{b\omega_n}{2}\right) \quad (1)$$

where ω_n is the frequency at a certain mode of vibration. Figure 2(b) shows the FEA results of different moduli and material (internal) damping. Obviously, the modulus has a significant effect on the response of the system. As expected, a low modulus value shows high response and vice versa. The effects of the material damping are also important. The effect of modulus might not be very obvious in this study compared to that of material damping since the modulus value was not varied over a large range of values in contrast to the damping, which was widely varied.

Finally, the FEA results were compared with the measurement results as shown in Figure 2(a). The results of the parametric study indicate that FEA modeled with minimal material damping (i.e., a = 0.0001 and b = 0.0001) and the modulus value of 35 MPa provides a reasonable response. These material-damping parameters resulted in a similar damping ratio to that obtained from the resonant column test, depending on the frequency. Note that an applied dynamic force of 10 N tends to give an accurate response at higher frequencies; however, for frequencies less than 130 Hz, a value of 17.3 N is required.

Strain Amplitude induced by the SSG

After calibrating the FEA model, the level of strain amplitude induced by the SSG could be determined from the FEA. In order to further verify the FEA results, the analytical solution for computing the total static vertical stress presented by Poulos and Davis (*8*) was employed. Figure 3(a) shows an acceptable correlation between the analytical solution and the FEA results for vertical stress distribution (i.e., the geostatic plus the induced static vertical stress due to the weight of SSG). Note that these stresses were computed at the axis of symmetry. The FEA model then was used to calculate the dynamic vertical strain distribution due to 10 and 17.3 N dynamic loading by the SSG as shown in Figure 3(b). It can be seen that the vertical strain amplitude averaged over the depth from 125 to 178 mm, i.e., within the depth of interest during the SSG measurement based on a previous study (*4*), ranges from $2.7\text{x}10^{-4}$ to $4.3\text{x}10^{-4}$ %.

Determination of Bulk Stress and Confining Pressure in SSG Test

For granular materials, the moduli obtained from different laboratory tests are often related to the bulk stress (σ_b) or confining pressure (σ_o). The selected depth of interest ranged from 125 to 178 mm (*4*). This range avoids the blind zone in SSG measurements (less than 125 mm) and emphasizes the higher stress-strain conditions within the measurement zone, i.e., 125 to 300 mm. The vertical stress induced by the self-weight of the SSG through an annular footing is estimated using an analytical solution presented by Poulos and Davis (*8*), as follows:

$$\sigma_z = \frac{3pz^3\ell}{(\ell^2 + z^2)^{5/2}} \quad (2)$$

where ℓ is the distance from the center of the annular footing to the centerline of the ring, z is the depth below the centerline of annular footing, and p is an annular line load acting at a distance ℓ from the centerline of the footing. The SSG has a weight of 11.34 kg (resulting in p = 0.35 kN/m on the annular footing) and has ℓ = 50.8 mm. The total vertical stress at the mid-plane of the SSG effective measurement zone (i.e., at z = 152 mm) under the center of the ring is equal to the sum of the vertical stress due to the annular line load exerted by the SSG (1.8 kPa) and the geostatic stress in the sand (2.4 kPa). Thus the vertical stress is equal to 4.2 kPa. Assuming that the intermediate stress can be taken equal to the minor stress, the confining pressure (σ_o) can be calculated as the average stress at any depth as $\sigma_v(1+2K_o)/3$. For K_o = 0.426 (estimated from Jaky's relationship $K_o = 1-\sin\phi$ (*9*) for $\phi = 35°$ of the sand), σ_o at z = 152 mm is calculated to be 2.6 kPa.

OTHER MODULUS TESTS

Moduli of the test materials were also measured by several other common tests for comparison with the SSG moduli. The triaxial and resonant column tests were not conducted on all of the test materials because they are not appropriate for some of the larger granular materials.

Triaxial Compression Test

The stress-strain relationship of medium sand at the same density state as this material was tested by the SSG in the test box (dry unit weight of 16 kN/m^3) was obtained from a static triaxial compression test. Even though a confining pressure of 2.6 kPa is desired, 6.9 kPa was applied during the test because that is the minimum amount that could be accurately controlled. Two methods were used to estimate the moduli from the triaxial test. In the first method, axial strain (ε_a) divided by deviator stress (σ_1-σ_3) was plotted against axial strain (ε_a) to linearize the stress-strain relationship assuming a hyperbolic model (*10*). The initial tangent modulus (E_i) of 4.55 MPa was obtained, as shown in Figure 4, by determining the inverse of the intercept of the linearized relationship. For an estimated Poisson's ratio (υ) of 0.3, the corresponding shear modulus (G) was determined to be about 1.75 MPa.

The second method comes from Janbu (*11*) who also suggested an empirical equation in which the stress dependency is taken into account and E_i can be estimated as:

$$E_i = \kappa P_a \left(\frac{\sigma_3}{P_a}\right)^n \quad (3)$$

where σ_3 is the confining pressure, P_a is the atmospheric pressure, κ is the modulus number, and n is the modulus exponent. For this medium sand, κ and n are approximately 472 and 0.47, respectively in the loose state (dry unit weight of 15.25 kN/m^3) based on other triaxial tests at higher confining pressures. E_i is estimated to be about 8.58 MPa at a confining pressure of 2.6 kPa based on Eq. (3). This initial modulus is reasonably close to the one directly measured in the triaxial compression test giving support to it.

Resilient Modulus Test

The resilient modulus (M_r) of medium sand, crushed rock, and plastic beads-sand mixture were determined at the same unit weight as they were in the SSG test box following the AASHTO test protocol T294-94 (*12*) with certain exceptions. The unit weight of medium sand, crushed rock, and plastic beads-sand mixture was about 16, 14, and 14.5 kN/m^3, respectively. The resilient modulus of WisDOT Grade 2 gravel with water content of about 5% was compacted at 85% relative compaction (RC) in order to replicate the density conditions in the test pit (87% RC). For medium sand and plastic beads-sand mixture, the deviator stress (σ_d) used in the test was reduced by 50% of that given in the AASHTO test protocol T294-94 (*12*) because the densities of these materials were too weak to withstand the deviator stresses as specified. The confining pressure was kept the same as required in T294-94 (*12*).

Figure 5 shows the resilient moduli of medium sand, crushed rock, plastic beads-sand mixture, and Grade 2 gravel as a function of bulk stress (σ_b). The range of resilient moduli of these materials corresponding to low and high bulk stresses is given in Table 1. It is noted that the resilient modulus of medium sand at low bulk stress is slightly higher than that of crushed rock because of the use of 50% lower deviator stress.

Resonant Column Test

The dynamic shear modulus (G) and damping ratio (D) of medium sand and a plastic beads-sand mixture were obtained using a torsional resonant column test. The apparatus used was developed by Hardin and Music (*13*) and is capable of vibrating cylindrical specimens in a torsional mode. Test specimens, fixed at their base, are driven from the specimen cap by means of an oscillator. The method of resonant column testing and the computation of results are described by Hardin (*14*). Solid specimens, 36 mm in diameter and 76 mm high, were prepared at the same density as these two materials were tested by the SSG in the test box and six resonant column tests were performed at different strain amplitudes. Figure 6 shows dynamic shear modulus (G) as a function of confining pressure (σ_o) for medium sand and the plastic beads-sand mixture at an approximate average strain amplitude of 0.0097 %. The shear modulus of medium sand ranges from 45.1 MPa at low confining pressure (35 kPa) to 166 MPa at high confining pressure (410 kPa), while the plastic beads-sand mixture has a shear modulus ranging from 47.5 MPa at low confining pressure (70 kPa) to 94.4 MPa at high confining pressure (275 kPa). As expected, at any given confining pressure, the shear modulus of medium sand is higher than that of plastic beads-sand mixture. The peak-to-peak shear strain amplitudes obtained ranged from $1.0\text{x}10^{-4}$ to $2.3\text{x}10^{-4}$ mm/mm for medium sand and from $1.7\text{x}10^{-4}$ to $3.1\text{x}10^{-4}$ mm/mm for the plastic beads-sand mixture.

Seismic Test

Seismic tests were conducted on medium sand in the test box. The travel times of P-waves from an impulse source were measured. The Young's modulus of this sand can be determined from the P-wave velocity (v_p) and by knowing the unit weight (γ) of this sand (about 16 kN/m^3), and its Poisson's ratio (υ).

$$E = \frac{\gamma}{g} v_p^2 \frac{(\upsilon + 1) \cdot (2\upsilon - 1)}{\upsilon - 1} \quad (4)$$

where g is the acceleration due to gravity. Shear modulus (G) can be determined from Young's modulus using:

$$G = \frac{E}{2(1+\upsilon)} \quad (5)$$

Based on an estimated Poisson's ratio (υ) of 0.3, Young's modulus (E) and shear modulus (G) of this sand were calculated to be about 53.8 MPa and 20.7 MPa, respectively.

COMPARISON OF MODULI OBTAINED FROM DIFFERENT LABORATORY TESTS

The moduli of granular materials obtained from different laboratory tests are stress and strain-dependent, whereas the SSG moduli are measured under in situ stress conditions. In order to effectively compare these moduli tests, the state of in situ stress must be known.

Stiffness of medium sand, crushed rock, and plastic beads-sand mixture obtained from the SSG testing in the test box and the stiffness of WisDOT Grade 2 gravel obtained from the SSG testing in the test pit were converted to a Young's modulus and compared with the Young's moduli obtained from the various tests for these materials. Young's modulus (E) of the test materials were calculated from the SSG stiffness measurement (K) using (*15*):

$$E = \frac{K(1-\upsilon^2)}{R}\omega \quad (6)$$

where υ is Poisson's ratio, R is the outside radius of the ring-shaped foot of the SSG, and ω is a shape factor related the ratio of inside to outside radius (for the SSG ω is equal to 0.565). The υ values for different test materials were estimated from the internal friction angle (ϕ) and the coefficient of lateral earth pressure at rest (K_o), as follows:

$$\upsilon = \frac{K_o}{1+K_o} \quad \text{where} \quad K_o = 1-\sin\phi \quad (7)$$

The Young's moduli of different test materials obtained from the laboratory tests are compared with that measured from the SSG as shown in Table 1. In the case of the resilient modulus and the resonant column tests, the modulus is an extrapolated estimate at low bulk stress or low confining pressure at which the SSG operates. Figure 7 shows the average Young's moduli of the three test materials used in the test box. It is noted that all of the modulus tests cited were performed only on medium sand; for the remaining materials only some of the tests are available for comparison with the SSG modulus. This is because the grain size of some test materials is too large to perform certain tests. For medium sand, the comparison of the results among the modulus tests show that the seismic test gives the highest modulus which is approximately 56% higher than the SSG modulus. On the other hand, the modulus from the resonant column test is about 6% smaller than that from the SSG. The modulus from the resilient modulus test seems to be significantly lower (about 26%) than that of the SSG. The static triaxial compression test gives the lowest modulus (about 87% lower compared to the SSG modulus).

For the plastic beads-sand mixture, the modulus from the resonant column test is about 7% higher than that of the SSG. The modulus from the resilient modulus test is

25% less than that of the SSG. For crushed rock, the modulus from the resilient modulus test is about 53% lower than that of the SSG. The resilient modulus of Grade 2 gravel at 85% relative compaction (RC) was compared with the modulus from the SSG measurement in the test pit (87% RC). Results showed that the resilient modulus of Grade 2 gravel at 85% RC is about 54% lower than that obtained from the SSG measurement.

Modulus Comparison for Different Tests on Basis of Strain Amplitude

Because of the dependency of modulus on strain amplitude, a plot of the shear modulus versus shear strain amplitude for medium sand at confining pressure of 2.6 kPa (or bulk stress of 7.9 kPa) and unit weight of 16 kN/m^3 was developed for modulus comparison of different tests as shown in Figure 8. In addition, the shear modulus of medium sand at the same confining pressure was obtained from an empirical relationship proposed by Hardin and Drnevich (*16*) and plotted in Figure 8 over a range of shear strain amplitudes (γ). The shear modulus obtained from the seismic test was assumed to be the maximum shear modulus (G_{max}). This value was used to obtain the backbone curve in Figure 8 using the Hardin and Drnevich relationship (*16*) (limited to $\gamma \leq$ 0.2%).

Even though the seismic test cannot provide strain amplitude, it is reasonable to assume that it is very small (*17*). The vertical recoverable strain amplitude of the resilient modulus test was calculated by dividing the deviator stress by the resilient modulus. The computed vertical strain is then converted to shear strain by multiplying vertical strain by $(1+\upsilon)$ (*18*). The range calculated is marked on Figure 8 and is similar to that reported by Lee et al. (*19*). The resilient modulus used was at the same in situ bulk stress level of the SSG. Similarly, the deviator stress used corresponded to the in situ deviator stress of the SSG. As expected, the strain amplitude obtained from the triaxial compression test was very high.

Figure 8 indicates that the moduli measured on medium sand using different test methods follow the general dependency of modulus on shear strain amplitude as reported in the literature (*16*). The SSG modulus appears to correspond to a strain amplitude level lower than the strain amplitude of the resilient modulus used in pavement design but much larger than the strain amplitude of seismic test even though, on the basis of this analysis, the SSG induces a strain amplitude comparable with that of seismic test.

CONCLUSIONS

Acceleration of the SSG was measured on medium sand and the corresponding displacement was compared with that obtained from the finite-element analysis (FEA). In the FEA, a dynamic force of 10-17.3 N provided a reasonable correlation with the measurement results. The calibrated FEA model then provided range of strain amplitudes generated by the SSG.

A comparison of moduli obtained from different laboratory tests indicates that the seismic test gives the highest modulus. The resilient modulus test tends to give a lower modulus compared to the SSG modulus. However, the estimated range of shear strain amplitude for the SSG suggests that the SSG modulus should be higher than that given by the device and closer to that from seismic tests. It is not clear if the modulus reported by the SSG device has been reduced by a factor. The initial tangent modulus obtained from a static triaxial compression test is the lowest modulus of all of the tests. It should be

noted that in the resilient modulus and resonant column tests, the modulus is an extrapolated estimate at low stress under which SSG operates. In addition to stress level, shear strain amplitude of different tests is also an important parameter that should be considered in comparing moduli obtained from different tests. It should be noted that all testing in this study was conducted on dry granular soils. Moist soils typically found in the field may exhibit different moduli relationships between the various tests.

Being aware of the fact that the SSG induces a relatively low strain amplitude under a low confining pressure is important in interpreting its utility for design purposes. If resilient modulus is considered to be the modulus representative of the field traffic loading conditions, the SSG would provide an unconservatively higher modulus (about 25% to 50%) than the resilient modulus for granular soils.

ACKNOWLEDGEMENT

This research was funded in part by the Wisconsin Highway Research Program (WHRP). The senior author was supported on a scholarship from the Royal Thai Government. The content of this paper solely reflects the views of the authors. This paper does not endorse or approve any commercial product, even though trade names may be cited, does not reflect official views or policies of the WHRP (WisDOT) or FHWA (US DOT), and does not constitute a standard specification or regulation of these agencies.

REFERENCES

1. Fiedler, S., Nelson, C., Berkman, E. F., and DiMillio, A. (1998), "Soil Stiffness Gauge for Soil Compaction Control," Public Roads, U.S. Department of Transportation, Federal Highway Administration, Vol. 61, No. 4, March/April.

2. Wu, W., Arellano, M., Chen, D., Bilyeu, J., and He, R. (1998), "Using a Stiffness Gauge as an Alternative Quality Control Device in Pavement Construction," Texas Department of Transportation, Austin, TX.

3. Sawangsuriya, A. (2001), "Evaluation of the Soil Stiffness Gauge," M.S. Thesis, University of Wisconsin-Madison, WI.

4. Sawangsuriya, A., Bosscher, P. J., and Edil, T. B. (2002), "Laboratory Evaluation of the Soil Stiffness Gauge," Transportation Research Record 1808, National Research Council, Washington, D.C., pp. 30-37.

5. Wisconsin (1996), Standard Specification for Highway and Structure Construction, Wisconsin Department of Transportation, Madison, WI.

6. PLAXIS (1998), Finite Element Code for Soil and Rock Analysis, Version 7.2, Plaxis B.V.

7. Clough, R. W. and Penzien, J. (1993), Dynamics of Structures, McGraw-Hill, Inc., NY, pp. 234-235.

8. Poulos, H. G. and Davis, E. H. (1974), Elastic Solutions for Soils and Rock Mechanics, John Wiley & Sons Inc., NY, pp. 167-168.

9. Jaky, J. (1994), "The Coefficient of Earth Pressure at Rest," Journal of the Society of Hungarian Architects and Engineers, Vol. 7, pp. 355-358.

10. Kondner, R. L. (1963), "Hyperbolic Stress-Strain Response: Cohesive Soils," Journal of the Soils Mechanics and Foundation Engineering Division, ASCE, Vol. 89, No. SM1, pp. 115-143.

11. Janbu, N. (1963), "Soil Compressibility as Determined by Oedometer and Triaxial Tests," Proceeding of European Conference of Soil Mechanics and Foundation, Vol. 1, pp. 259-263.

12. AASHTO (1993), Guide for Design of Pavement Structures, American Association of State Highway and Transportation Officials, Washington, D.C.

13. Hardin, B. O. and Music, J. (1965), "Apparatus for Vibration of Soil Specimens During the Triaxial Test," Instruments and Apparatus for Soil and Rock Mechanics, ASTM STP 392, pp. 55-74.

14. Hardin, B. O. (1970), "Suggested Methods of Test for Shear Modulus and Damping of Soils by the Resonant Column," ASTM STP 479, No. 479, pp. 516-529.

15. Egorov, K. E. (1965), "Calculation of Bed for Foundation with Ring Footing," Proceedings 6th International Conference of Soil Mechanics and Foundation Engineering, Vol. 2, pp. 41-45.

16. Hardin, B. O. and Drnevich, V. P. (1972), "Shear Modulus and Damping in Soils: Design Equations and Curves," Journal of the Soil Mechanics and Foundations Division, Proceedings of ASCE, Vol. 98, No. SM7, pp. 667-692.

17. Kramer, S. L. (1996), Geotechnical Earthquake Engineering, Prentice-Hall Inc., Upper Saddle River, NJ.

18. Kim, D. S. and Stokoe II, K. H. (1992), "Characterization of Resilient Modulus of Compacted Subgrade Soils Using Resonant Column and Torsional Shear Tests," Transportation Research Record 1369, National Research Council, Washington, D.C., pp. 83-91.

19. Lee, W., Bohra, N.C., and Altschaeffl, A. G. (1995), "Resilient Characteristics of Dune Sand," Journal of Transportation Engineering, ASCE, pp. 502-506.

LIST OF TABLES

LIST OF FIGURES

TABLE 1 Comparison of Young's Modulus (E) (MPa) from Different Laboratory Tests

Test methods	Medium sand	Plastic beads-sand mixture	Crushed rock	Grade 2 gravel
SSG	34.4 (0.30)[1]	22.0 (0.26)[1]	44.4 (0.26)[1]	78.8 (0.28)[1]
Triaxial compression test	4.6-8.6	NA	NA	NA
Resilient modulus test	91.1-235.6* (70-530)[2] 25.4** (7.9)[2]	57.8-71.1* (70-135)[2] 16.6** (6.9)[2]	91.2-300.1* (80-655)[2] 20.8** (6.8)[2]	154.1-406.3* (80-665)[2] 34.2** (9.6)[2]
Resonant column test	117.2-431.4* (35-410)[3] 32.3** (2.6)[3]	119.9-238.5* (70-275)[3] 23.4** (2.3)[3]	NA	NA
Seismic test	53.8	NA	NA	NA

[1]Estimated Poisson's ratio, [2]Bulk stress (kPa), [3]Confining pressure (kPa)
NA = Not applicable and/or available
*Test range, **Extrapolated estimate

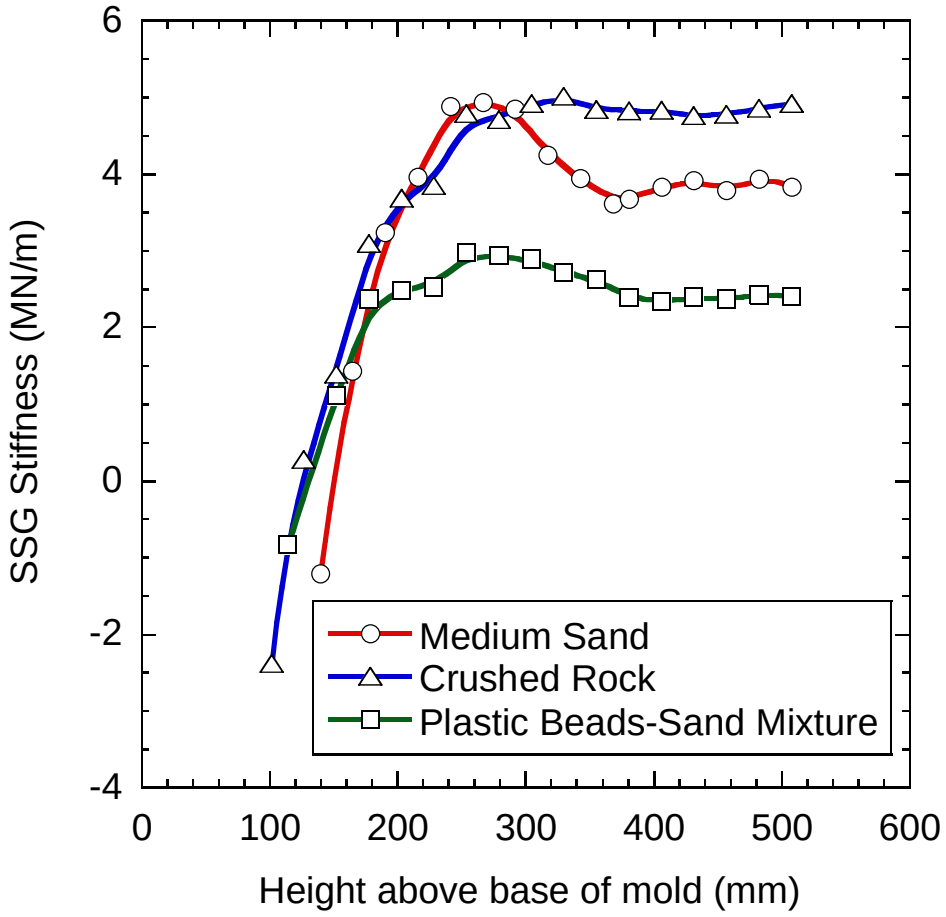

FIGURE 1 SSG Stiffness of medium sand, crushed rock, and plastic beads-sand mixture in 0.3-m radius mold.

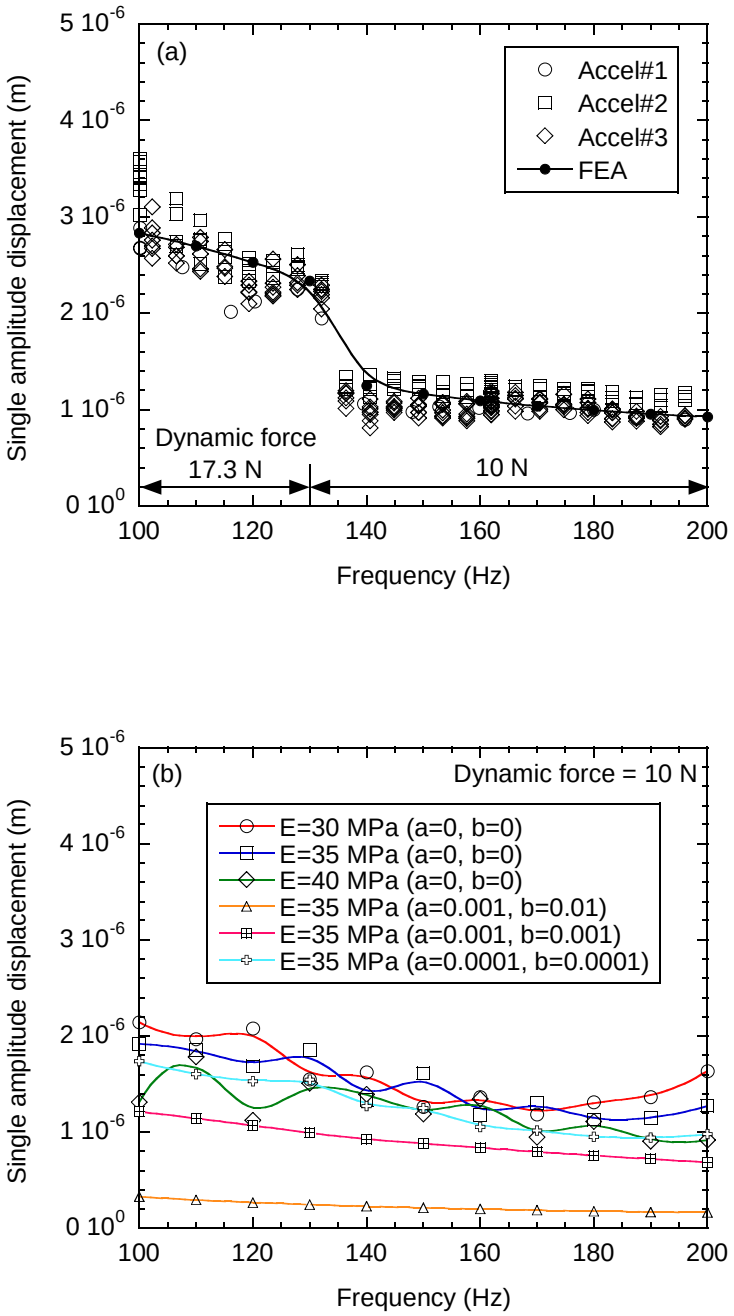

FIGURE 2 Results of acceleration measurement as a function of frequency and their comparison with the FEA (a) and FEA results of different moduli and material (internal) damping (b).

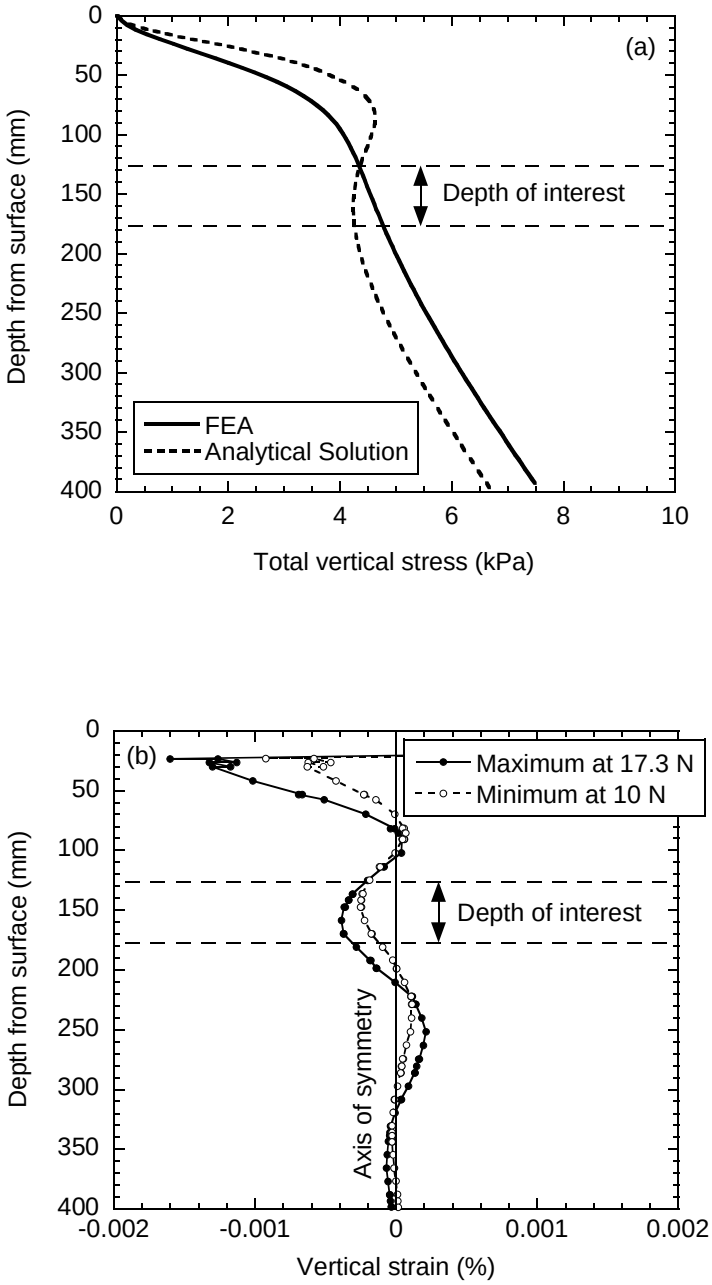

FIGURE 3 Correlation between the analytical solution and the FEA results at various depths for the total vertical stress (a) and SSG-induced vertical strain at various depths as obtained from the FEA (b).

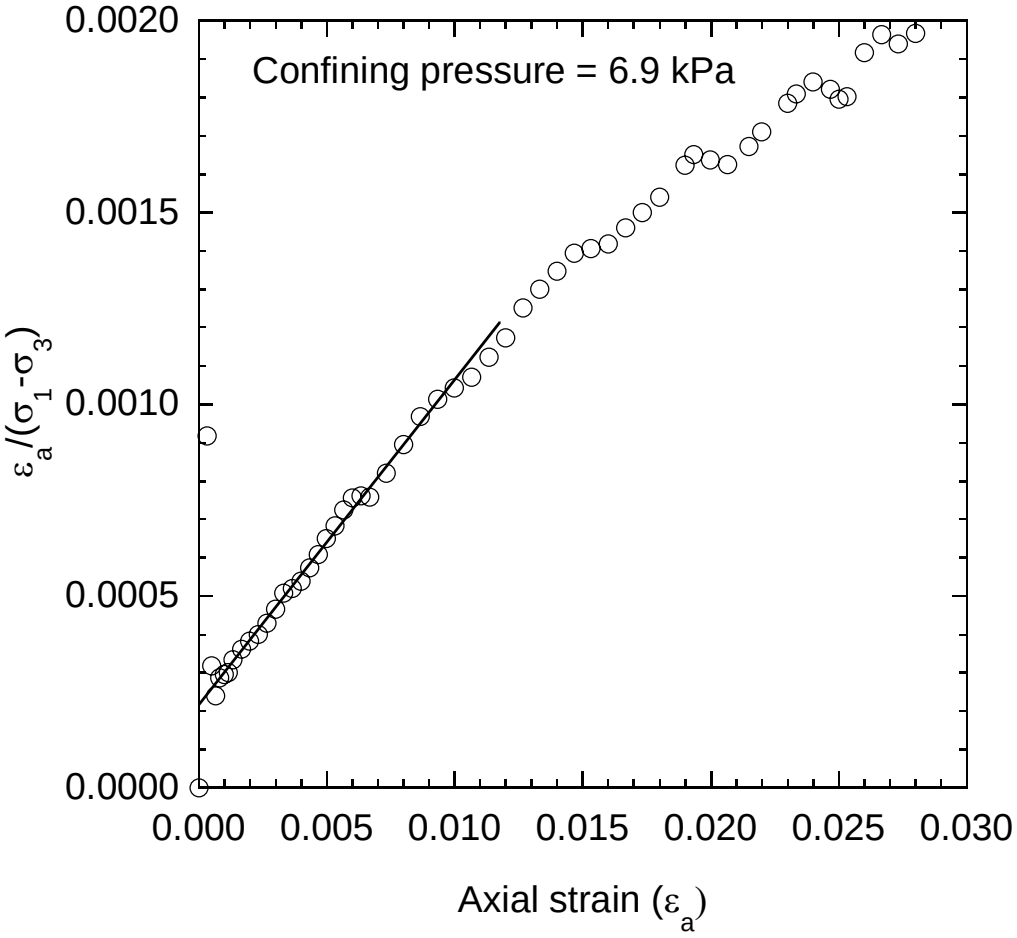

FIGURE 4 Result of triaxial compression test on medium sand in hyperbolic plot.

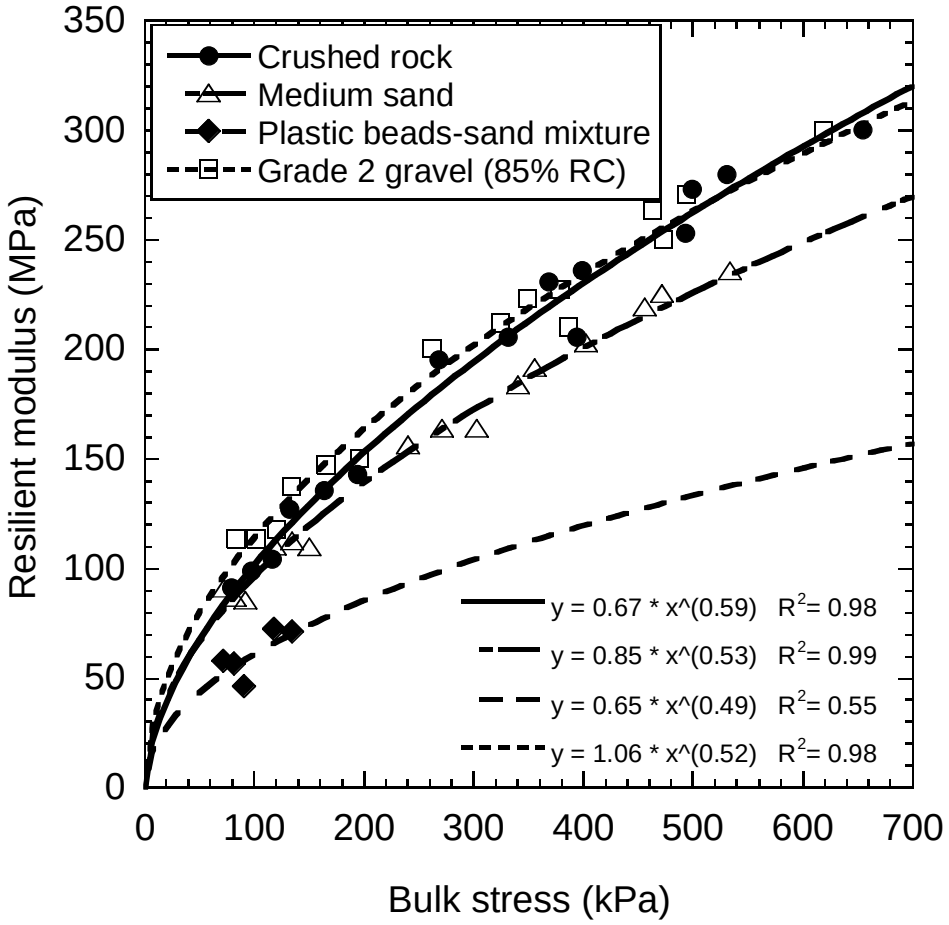

FIGURE 5 Resilient modulus of crushed rock, medium sand, plastic beads-sand mixture, and Grade 2 gravel as a function of bulk stress.

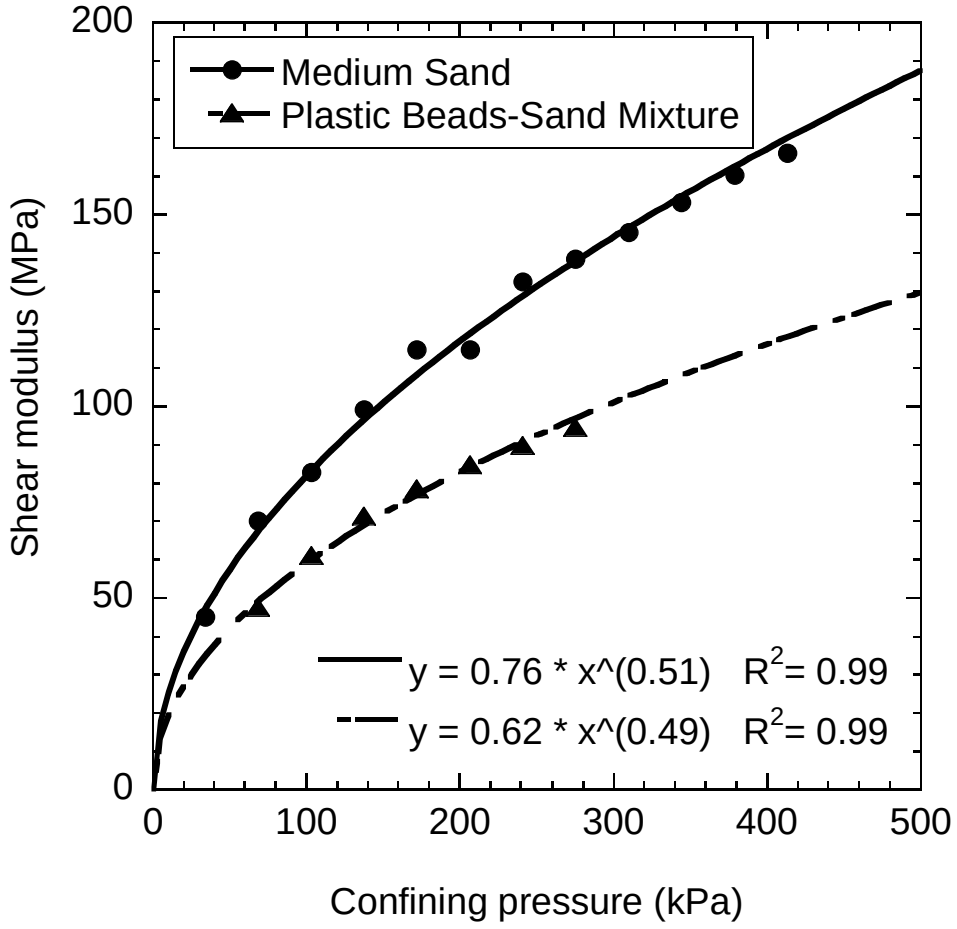

FIGURE 6 Resonant column dynamic shear modulus as a function of confining pressure for medium sand and plastic beads-sand mixture.

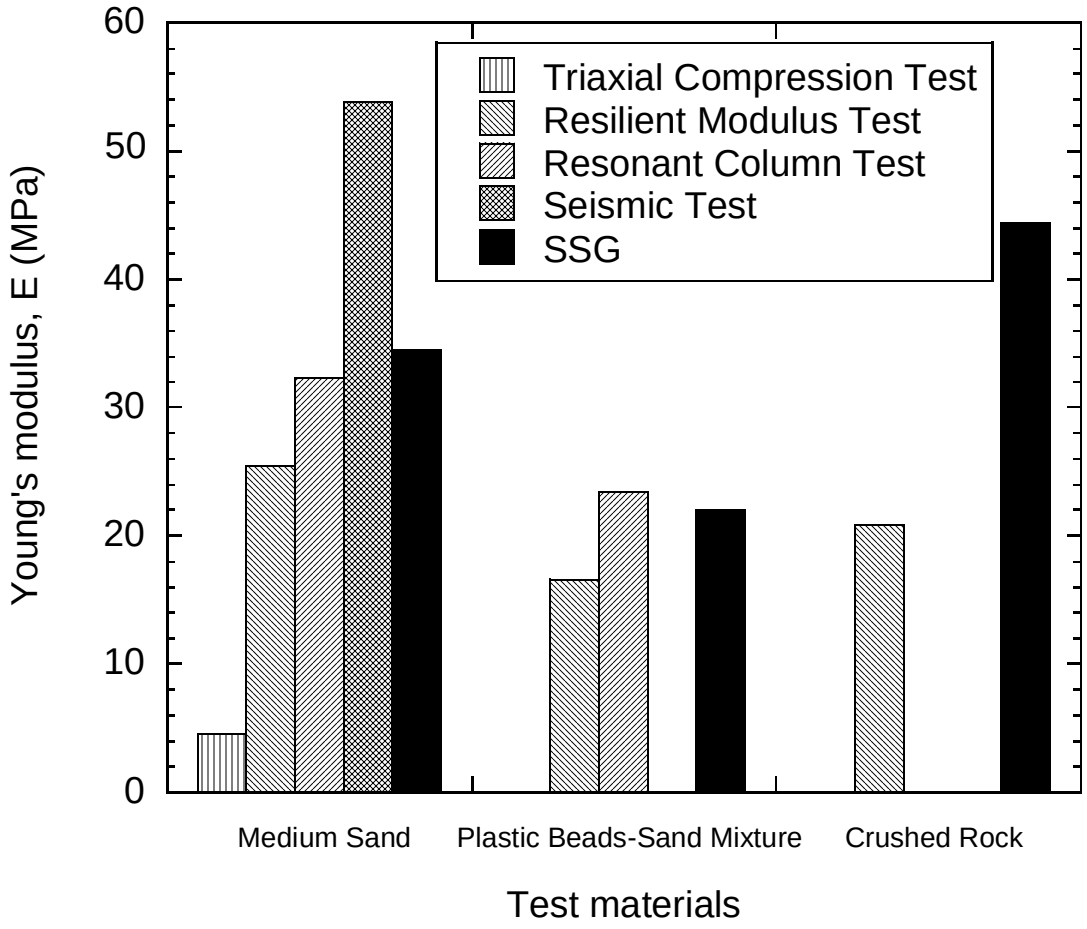

FIGURE 7 Comparison of Young's modulus (E) of three test materials obtained from the modulus tests.

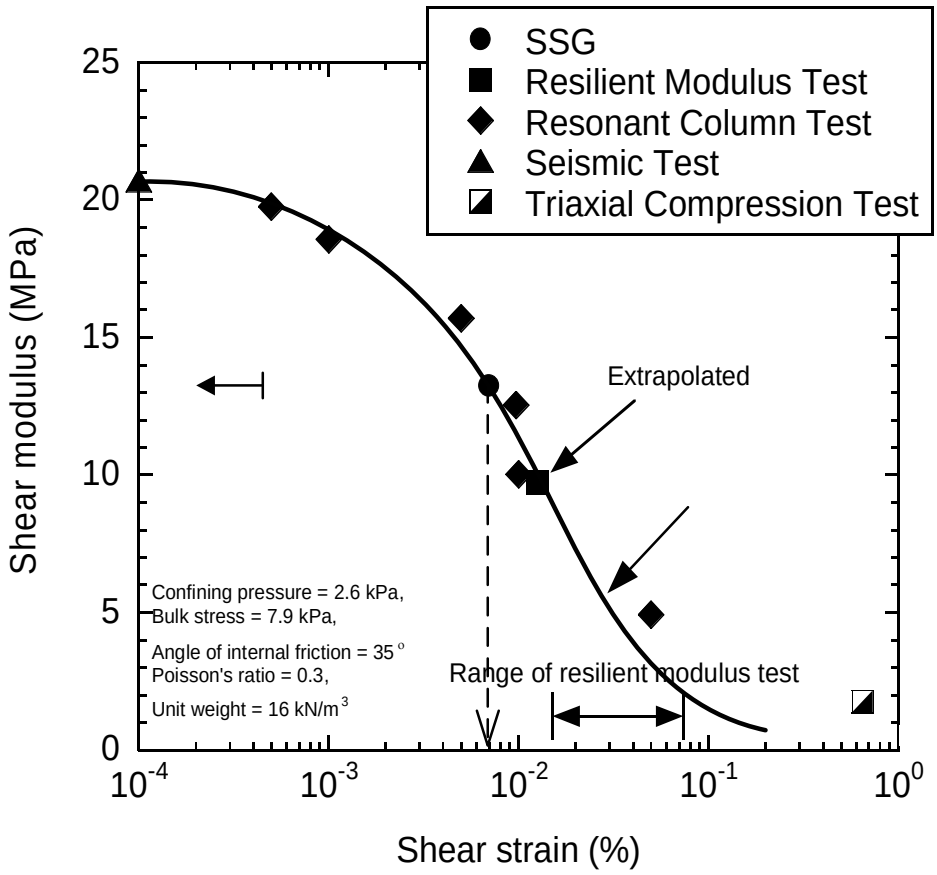

FIGURE 8 Modulus comparison for different tests with shear strain amplitude.

Evaluating Stiffness and Strength of Pavement Materials

Authors:

1. **Auckpath Sawangsuriya**
   Graduate Research Assistant, Dept. of Civil and Environmental Engineering, University of Wisconsin-Madison, Madison, WI 53706, USA.
   Tel: (608)-262-6281 Fax: (608) 263-2453 E-mail: sawangsuriya@wisc.edu

2. **Tuncer B. Edil, PhD, PE (Corresponding Author)**
   Professor, Dept. of Civil and Environmental Engineering, University of Wisconsin-Madison, Madison, WI 53706, USA.
   Tel: (608) 262-3225 Fax: (608) 263-2453 E-mail: edil@engr.wisc.edu

Keywords: pavement design, quality control, strength and testing of materials

Proceedings of the Institution of Civil Engineers-Geotechnical Engineering, 2005

Abstract: Current mechanical empirical-based pavement design requires use of the mechanical properties of pavement materials. For quantitative evaluations of the mechanical properties, i.e., stiffness and strength, field tests are emphasized. In this paper, a recently developed instrument called the soil stiffness gauge (SSG) and dynamic cone penetrometer (DCP) have been used to assess respectively the in situ stiffness and strength of natural earthen materials, industrial by-products, and chemically stabilized soils from ten highway construction sites around the state of Wisconsin, USA. The SSG and DCP survey data were analyzed to develop a relationship between the SSG stiffness and DCP penetration index (DPI) values for individual material types and for all materials combined. A simple linear semi-logarithmic model is obtained between the SSG stiffness and DPI values with the coefficient of determination, R^2, ranging from 0.47 to 0.75 for individual material types and a R^2 value of 0.72 for all materials combined. The SSG stiffness and DPI values can be also correlated with modulus (E) and California bearing ratio (CBR) of the materials, respectively. A good relationship is obtained between E from the SSG and CBR from the DCP and is compared with the well-known equations developed by Powell et al. [1] and AASHTO [2] as well as other available correlations from different in situ tests, i.e., the falling weight deflectometer (FWD), German light drop weight (LDW), and plate load tests. Finally, the proposed power model is validated with a data set from two other test sites. Either or both devices show good potential for future use in the pavement and subgrade materials evaluation. The in situ stiffness and strength properties of various materials can be rapidly and directly monitored in companion with the conventional compaction control tests during pavement construction. Modulus of pavement and subgrade materials is uniquely related to CBR's regardless of soil type and site and their relationship is also applicable to both as-compacted and post-construction states.

INTRODUCTION

Given the importance of the mechanical properties, i.e., stiffness and strength, in pavement materials evaluation, there has been a concerted effort in recent years to develop methods for quantitative evaluations of these properties. Direct monitoring of stiffness and strength is consistent with the transition from empirical to current mechanistic-empirical pavement design procedures for structural design of flexible pavements. To successfully implement mechanistic-empirical pavement design procedure and to move toward performance-based specifications that are required to control the long-term functional and structural performance, additional in situ stiffness and strength measurements should be included along with the conventional compaction control tests (i.e., nuclear density or laboratory moisture content samples), which do not give mechanical properties of pavement materials directly.[3, 4] Direct monitoring of stiffness and strength would facilitate quantitative evaluations of alternative construction practices and materials, such as recycled and reclaimed materials that result in cost savings and environmental benefits.[4] For instance, the use of recycled and reclaimed materials both as working platform over poor subgrade and as a subbase in pavement structure is being explored by the transportation community. Evaluation of these new materials on the basis of index property measurements such as moisture-density or past subjective experience based on natural soil behaviour is also severely limited. Most of the correlations for modulus (E) are based on water content, dry density, and degree of saturation and were developed from tests on laboratory-compacted specimens. Since field compaction curves and the associated lines of optimum are often different from those of laboratory compaction and since the moisture condition of pavement materials changes with time after construction, use of these laboratory-based correlations may cause significant error in estimating the operating pavement and subgrade moduli. Empirical correlations based on California bearing ratio (CBR) [1, 5] or stress causing 1% strain ($S_{u1.0\%}$) in the unconfined compression test [6] have been successfully used in evaluating pavement and subgrade moduli. Moreover, the relationship between E and CBR or E and $S_{u1.0\%}$ is not affected by the changes in subgrade condition after construction and therefore is applicable to both as-compacted and post-construction states.

The soil stiffness gauge (SSG), a recently developed instrument, and the dynamic cone penetrometer (DCP), which is commonly used by pavement community, offer a means of directly monitoring in situ stiffness and index of strength of surficial materials. SSG stiffness

and DCP penetrometer index (DPI) have been also correlated to modulus and CBR, respectively.[7, 8] In this study, these two devices will be implemented in a number of projects over two construction seasons in the state of Wisconsin, USA. The objectives of this study are: (1) to examine the use of the SSG and DCP for pavement materials evaluation, (2) to explore the degree of correlation and appropriate effective depth zone for statistically significant empirical correlations between the two devices, and (3) to develop the modulus and CBR relationship obtained from these devices and compare it with the other well-known relationships as well as different in situ tests.

SOIL STIFFNESS GAUGE (SSG)

Description

Soil stiffness gauge (SSG), which is currently marketed as the Humboldt GeoGauge™ (Fig. 1a), is a recently developed instrument for directly measuring in situ stiffness of soils. The SSG measures near-surface stiffness by imparting small dynamic force to the soil though a ring-shaped foot at 25 steady state frequencies between 100 and 196 Hz. Based upon the force and displacement-time history, stiffness is calculated internally as the average force per unit displacement over the measured frequencies and reported. In a previous investigation, the acceleration and corresponding displacement were measured[7]. Knowing the soil properties, the force induced by the SSG was estimated based on the finite element analysis. The maximum single amplitude dynamic force produced during the SSG measurement is determined to be 10 to 17 N. A measurement takes only about 1.5 minutes. Sawangsuriya et al. [9] studied the zone of measurement influence and the effects of layered materials on the SSG measurement in granular materials. A finite-element analysis and the SSG measurements in a test box indicated that the radius of measurement influence extends to 300 mm. For two-layer materials with different stiffness, the SSG starts to register the stiffness of an upper-layer material of 125 mm or thicker. The effect of the lower layer may continue to be present even at an upper-layer material thickness of 275 mm, depending on the relative stiffness (or contrast) of the layer materials. A comparison of moduli of granular soils obtained from the SSG with moduli obtained from other tests on the basis of comparable stress levels indicates that the SSG measures moduli in the very small strain amplitude range (i.e., 2.7×10^{-4} to 4.3×10^{-4} % which is

less than 10^{-3}%). The SSG induced strain amplitudes are lower than the strain amplitudes induced in the resilient modulus test, however, larger than the strain amplitude of seismic test.[7]

The measured soil stiffness from the SSG can be used to calculate the modulus of the materials at near surface. For a rigid ring-shaped foot resting on a linear-elastic, homogeneous, and isotropic infinite half-space, the stiffness (K_{SSG}) is related to modulus of soil (E_{SSG}):[10]

$$K_{SSG} = \frac{1.77 E_{SSG} R}{(1-\nu^2)} \quad (1)$$

where ν is Poisson's ratio of the materials and R is the outside radius of the ring (57.2 mm). Note that K_{SSG} and E_{SSG} are expressed in MN/m and MPa, respectively. Because of very small strain amplitudes induced by the SSG, elastic response of the soils is assumed and the use of Eq. (1) is justified.

Correlation with Other Moduli

Back-calculated moduli of base and subgrade soils from the falling weight deflectometer (FWD) test have been used extensively in pavement design, construction, and maintenance. Wu et al. [11] found that the relationship between SSG stiffness (K_{SSG}) and back-calculated modulus from the FWD (E_{FWD}) can be presented in the following form:

$$E_{FWD} = 22.96e^{0.12K_{SSG}} \qquad R^2 = 0.66 \quad (2)$$

Note that K_{SSG} and E_{FWD} are expressed in MN/m and MPa, respectively. Wu et al. [11] also noted that the difference between these methods can be from the in situ variability of the material properties. Since E_{FWD} is obtained through inversion based on all seven deflection measurements, which cover a distance of about 2 meters, E_{FWD} of pavement layers is therefore a weighted average value over 2 meters. On the other hand, the SSG only measures the near-surface soil stiffness right underneath its ring foot with the measurement influence of less than 0.3 meters. Chen et al. [12] suggest that a general linear relationship between K_{SSG} and E_{FWD} is discernable as the following:

$$E_{FWD} = 37.65K_{SSG} - 261.96 \qquad R^2 = 0.82 \quad (3)$$

Again, K_{SSG} and E_{FWD} are also expressed in MN/m and MPa, respectively. Wu et al. [11] provided the correlation between SSG stiffness and modulus from seismic tests including Dirt-Seismic Pavement Analyser (D-SPA) and Spectral Analysis of Surface Waves (SASW) for

soft- to medium-stiff subgrades to very stiff bases. They indicate that the modulus obtained from the SSG is about 3 times smaller than that obtained from seismic tests. A linear relationship is obtained between the SSG stiffness (K_{SSG}) and the seismic modulus (E_{SEIS}):

$$E_{SEIS} = 47.53K_{SSG} + 79.05 \qquad R^2 = 0.62 \qquad (4)$$

Note that K_{SSG} and E_{SEIS} are expressed in MN/m and MPa, respectively. The discrepancy between these two tests is explained by the difference in the stress-strain level used in these two tests as well as the uncertainty of the effective depth of the SSG, which varies with stiffness, density, and types of materials being tested.[11] Chen et al. [12] also conducted a similar study and indicate that the relationship between K_{SSG} and E_{SEIS} from D-SPA and SASW for soft- to medium-stiff subgrades to very stiff bases can be expressed as:

$$E_{SEIS} = 55.42K_{SSG} - 162.94 \qquad R^2 = 0.81 \qquad (5)$$

Again, the units of K_{SSG} and E_{SEIS} are in MN/m and MPa, respectively. The relationship between K_{SSG} and E_{SEIS} is found to be obvious and convincing. The operation of the SSG is very simple and feasible for the purpose of quality control; however, it only yields a stiffness value at near surface. The seismic tests can generate a stiffness-depth profile; however, its operation is more complicated.[12]

DYNAMIC CONE PENETROMETER (DCP)

Description

Scala [13] developed the Scala penetrometer for assessing in situ California Bearing Ratio (CBR) of cohesive soils. In the last decade, the Scala penetrometer has evolved into the dynamic cone penetrometer (DCP) test for determining in situ CBR and modulus. The DCP is now being used extensively in South Africa, the United Kingdom, the United States, Australia, and other countries because it is simple, rugged, economical, and able to provide a rapid in situ index of strength and more indirectly modulus of subgrade as well as pavement structure.

The DCP is used for measuring the material resistance to penetration in terms of millimetres per blow while the cone of the device is being driven into the pavement structure or the subgrade. The typical DCP consists of an 8-kg hammer that drops over a height of 575 mm, which yields a theoretical driving energy of 45 J or 14.3 J/cm^2, and drives a 60-degree 20-mm-base diameter cone tip vertically into the pavement structure or the subgrade (Fig. 1b).

The steel rod to which the cone is attached has a smaller diameter than the cone (16 mm) to reduce skin friction. The number of blows during operation is recorded with depth of penetration. The slope of the relationship between number of blows and depth of penetration (in millimeters per blow) at a given linear depth segment is recorded as DCP penetration index (DPI). In addition to soil profiling (i.e., the thickness and nature of each layer in a given pavement), DCP data are correlated with various pavement design parameters, i.e., CBR, shear strength, modulus, back-calculated modulus from the FWD, and others.[12, 14, 15, 16, 17, 18] The DCP has been available longer than the SSG and has been used as a convenient field tool; however, it is not a direct property test but an index test based on dynamic impact loading.

Since DCP testing is basically a measure of penetration resistance, expressed as DCP penetration index (DPI), the analysis of the DCP data must be interpreted to generate a representative value of penetration per blow for the material being tested following a standardized procedure. This representative value can be obtained by averaging the DPI across the entire penetration depth at each test location. Two methods of calculating the representative DPI value for a given penetration depth of interest are considered: (i) arithmetic average and (ii) weighted average.[19] The arithmetic average can be obtained as follows:

$$\mathrm{DPI}_{\mathrm{avg}} = \frac{\sum_{i}^{N} (\mathrm{DPI})_i}{N} \tag{6}$$

where N is the total number of DPI recorded in a given penetration depth of interest. On the other hand, the weighted average technique uses the following formula:

$$\mathrm{DPI}_{\mathrm{wt\,avg}} = \frac{1}{H} \sum_{i}^{N} \left[(\mathrm{DPI})_i \cdot (z)_i \right] \tag{7}$$

where z is the penetration distance per blow set and H is the overall penetration depth of interest. These two methods are graphically presented in Fig. 2 for a lean clay with sand (STH 100 in Table 1). Allbright [20] reported that the weighted average method yielded narrower standard deviation for the representative DPI value and provided better correlations to other field tests than the arithmetic average method based on field data available. In this study, the weighted average method is employed to calculate the representative DPI value.

The influence of layers below and above the cone tip must also be considered in the analysis of the DCP data. Since cone penetration is associated with the development of a

failure surface, the penetration resistance is influenced by the presence of a layer if the cone tip is located within a few cone diameters of the interface of two highly-contrasting layers. Little effect on penetration resistance is noticed as the cone tip approaches the interface if both layers have similar properties. The extent of the zone of influence depends on size of the cone, soil type, soil density, stress state, and the contrast in properties of adjacent layers.[21] The weighted average DPI was calculated over various DCP penetration depths, i.e., from surface to 76, 152, 229, 305, and 381 mm, in the analyses to identify the most representative depth in correlating DPI to SSG stiffness. The only exception was the chemically stabilized soils where the maximum penetration depth was limited by the thickness of the stabilized layer (i.e., 305 mm). Since these selected penetration depths over which the DPI was calculated, were generally well within a layer, the DPI obtained is considered to have negligible influence from an interface. It has been shown that vertical confinement (i.e., due to rigid pavement structure or upper granular/cohesive layers) and rod friction (i.e., due to a collapse of the granular material on the rod surface during penetration) may affect DPI values.[22] These effects were not an issue in this investigation since the current study involved only subgrade and subbase evaluation during construction such that the DCP tests were performed directly on exposed surface of these materials.

Correlation with California Bearing Ratio (CBR)

To assess the structural properties of the pavement materials, the DCP penetration index (DPI) values are usually correlated with the California bearing ratio (CBR) of the pavement materials. Extensive research has been conducted to develop an empirical relationship between DPI and CBR for a wide range of pavement and subgrade materials. These include research by Livneh et al.,[22] Kleyn,[23] Harison,[24] Livneh,[25] McElvaney and Djatnika,[26] Webster et al.,[27] and Livneh and Livneh.[28] Based on their researches, many of the relationships between DPI and CBR can be quantitatively presented in the form of:

$$\log(\mathrm{CBR}) = \alpha + \beta \log(\mathrm{DPI}) \qquad (8)$$

where α and β are coefficients ranging from 2.44 to 2.56 and -1.07 to -1.16, respectively, which are valid for a wide range of pavement and subgrade materials. Note also that CBR is in percent and DPI is in millimetres per blow (mm/blow). For a wide range of granular and cohesive materials, the US Army Corps of Engineers use the coefficients α and β of 2.46 and -

1.12, which have been also adopted by several agencies and researchers [21, 27, 29, 30] and is in general agreement between the various sources of information. Livneh et al. [22] also show that there exists a universal correlation between the DPI and CBR for a wide range of pavement and subgrade materials, testing conditions, and technologies. In addition, the relationship between DPI and CBR is independent of water content and dry unit weight since both water content and dry unit weight equally influence DPI and CBR.

FIELD TESTING PROGRAM

Data Collection

A Humboldt SSG manufactured by Humboldt Mfg Co. was used to measure the in situ stiffness properties of the pavement materials in this study. The SSG stiffness measurements were made in accordance with ASTM D6758. The SSG assesses near-surface stiffness with a maximum measurement depth of approximately 300 to 380 mm. Sawangsuriya et al. [7, 9] reported that the depth of measurement significance ranges from 125 to 178 mm where the higher stress-strain conditions occur within the measurement zone (i.e., 125 to 300 mm) and this is also beyond a blind zone that exists at less than 125 mm in SSG measurements. These findings were based on granular soils but similar conditions can also be expected in the fine-grained (cohesive) soils.

A DCP manufactured by Kessler Soils Engineering Products, Inc. was used to measure the in situ strength index properties of the pavement materials in this study. DCP penetration index (DPI), in millimetres per blow, which can be used to estimate the shear strength characteristics of soils was calculated in accordance with ASTM D6951. The DCP is typically used to assess material properties to a depth of 1 m below the ground surface. The size of the cone tip relative to the average grain size of the material that is penetrated is found to influence the penetration resistance.[21] This is because of the number of grains that come into contact with the face of the cone and the failure surface. Therefore, the DCP cannot be used in very coarse-grained materials containing large percentage of aggregates greater than 50 mm as well as in highly stabilized or cemented materials.

Site Description

SSG and DCP measurements were made at ten highway construction sites around the state of Wisconsin, USA. STH 60 test section is located approximately 40 km north of the city of Madison and consists of a 1.4 km segment of the highway. This project consisted of field demonstration of alternative soft subgrade reinforcement methods. Detailed description of each test section is given in Edil et al. [31] The SSG and DCP tests were conducted in each test section.

Scenic Edge development project is a 0.7 km city street constructed as a residential subdivision in Cross Plains by stabilizing the soft subgrade in place with fly ash. Both the subgrade soil and the fly ash-stabilized subgrade layer were tested using the SSG and DCP.

Gils Way development project using soil-lime mixture is also located in Cross Plains. The construction section was approximately 400 m long. Due to the time constraint, only the SSG was performed before the liming process, i.e., on the untreated subgrade. The SSG and DCP were performed after the liming process, i.e., on the lime-stabilized subgrade layer.

Seven highway construction sites that involved use of only natural earthen materials were from different soil regions of Wisconsin.[19] The SSG and DCP were performed on the exposed subgrade soils that were either compacted (five sites) or had not been re-compacted (two sites).

MATERIAL CLASSIFICATION AND PROPERTIES

Samples were collected either along the centreline or near the shoulder of the roadway from ten highway construction sites to determine index properties, soil classification, and compaction characteristics. A summary of the natural earthen materials encountered and their properties along with their classification are tabulated in Table 1. Compaction curves corresponding to standard compaction effort described in ASTM D698 were developed except for breaker run. Note that breaker run is the excavated and crushed rock including cobbles (75 to 350 mm in diameter) with a soil fraction. It was retrieved from the cuts in parts of the project route. Its soil fraction consisted of approximately 30% gravel, 65% sand, and 5% fines.

Properties of the processed construction materials (i.e., other than the natural earthen materials) along with their classification are summarized in Table 2. These materials are subdivided into two main categories: (a) industrial by-products and (b) chemically stabilized soils. The by-products consisted of bottom ash, foundry slag, and foundry sand. Bottom ash

and foundry slag are well-graded coarse-grained sand-like materials and thus are insensitive to moisture content during compaction. Foundry sand is primarily a mixture of fine sand and sodium bentonite (~10% by weight) that also contains small percentages of other additives. The foundry sand is sensitive to water content when compacted, and exhibits a conventional compaction curve.

Chemical stabilization involved a mixture of natural soil and either fly ash or lime. The fly ash-stabilized soil at STH 60 test section and Scenic Edge development sites was prepared by mixing Class C fly ash with subgrade soil at its natural water content (wetter than the optimum water content). Analysis from a series of mix designs evaluated in the laboratory indicated that the subgrade soil stabilized using a fly ash content of 10% for the STH 60 test section site and 12% for the Scenic Edge development site (on the basis of dry weight) provided sufficient strength and hence was adopted for field construction. The lime-stabilized soil at Gils Way development in Cross Plains was prepared by mixing 5% lime with subgrade soil at its natural water content (wetter than the optimum water content).

SSG STIFFNESS AND DCP PENETRATION INDEX (DPI)

Table 3 summarizes the results of SSG and DCP measurements made. The mean SSG stiffness and DPI of various materials are also illustrated in Fig. 3 graphically. Fly ash-stabilized soils have the highest mean stiffness, which increases with time of curing. For the lime-stabilized soil, the mean stiffness after liming is nearly twice the untreated subgrade. These results clearly indicate that the SSG can be used to monitor increase in stiffness due to stabilization reactions. In general, the granular earthen materials including breaker run are stiffer than fine-grained earthen materials. Among three types of industrial by-products, foundry sand has the highest stiffness with bottom ash and foundry slag having nearly half its stiffness.

Dynamic cone penetration is controlled primarily by the strength of a material and therefore, DPI (amount of penetration per blow) is inversely proportional to shear strength. The patterns exhibited by the DPI, in general, parallel those of the SSG stiffness in Fig. 3 with some exceptions (e.g., compare the relative stiffness and strength of industrial by-products and fine-grained soils). Data in Table 3 indicate that the standard error associated with DPI is considerably larger than that of the SSG stiffness.

CORRELATION BETWEEN SSG STIFFNESS AND DPI VALUES

The correlation of SSG stiffness to DPI is examined based on six material categories: (1) natural earthen materials (both granular and fine-grained soils), (2) granular materials (natural soils, bottom ash, and foundry slag), (3) fine-grained (cohesive) soils, (4) fly ash-stabilized soils, (5) fine-grain materials including fly ash-stabilized soils, and (6) all materials combined including foundry sand. Breaker run is not included because the DCP cannot be performed on this material. Foundry sand exhibits both granular and fine-grained material behaviour so it is only included only in category 6. Table 4 summarizes the results of the linear regression analyses between SSG stiffness and log DPI in these material categories. Only those tests that were conducted at the same location are included in the analysis. For all material categories in Table 4, the best correlations (i.e., highest R^2) were obtained when DPI was averaged over a DCP penetration depth of 152 mm after examining correlations of average DPI calculated over varying DCP penetration depths.[19] It is also noted that for natural subgrade soils, a better correlation was obtained after they were compacted [19] probably due to more uniform conditions that result in reduction of the dispersion of the data. Fig. 4 illustrates the correlation between stiffness and DPI for all materials combined. The SSG stiffness is related to DPI in a simple linear semi-logarithmic relationship. The dispersion of the data is explainable to a degree by the fact that while stiffness and strength are related in a general sense, there is not always a one-to-one relationship as demonstrated in Fig. 3. Nonetheless, the SSG stiffness and DPI correlate well with a R^2 of 0.72.

CORRELATION BETWEEN MODULUS AND CBR (ALSO DPI)

Previous Research

Empirical correlations between modulus (E) and CBR (also DPI) have been proposed by a number of researchers. A well-known U.K. Transportation Research Laboratory (TRL) equation developed between modulus (E) and CBR of the subgrade soil has been given by Powell et al.[1] This equation has been established primarily from the comprehensive data relating modulus measured by wave propagation to in situ CBR tests on both remoulded and undisturbed subgrade soils.[32] After taken into account the effects of the very low strain levels generated in the wave propagation technique and other information obtained from repeated load triaxial test conducted at realistic stress levels and in situ measurements of transient stress and

strain in experimental pavements, the modulus from seismic test was adjusted and the corresponding equation is expressed as follows:[1]

$$E_{SEIS-MOD} = 17.6 \times CBR^{0.64} \quad (9)$$

Note that for the sake of clarity, the modulus used in Eq. (9) is denoted as modulus from seismic test after adjusted to realistic stress and strain levels for the pavement ($E_{SEIS\text{-}MOD}$). $E_{SEIS\text{-}MOD}$ and CBR units are in MPa and percent, respectively. Another well-known relationship, which is widely used in North America, is the one proposed by Heukelom and Foster.[33] It has been adopted by the American Association of State Highway and Transportation Officials (AASHTO) in the Guide for Design of Pavement Structures:[2]

$$E_{RM} = 10 \times CBR \quad (10)$$

where E_{RM} is the modulus from the resilient modulus test in MPa. In addition to these two well-known relationships, Chen et al. [34] suggested the following relationship between back-calculated moduli from the FWD (E_{FWD}) and DPI and is given in the form of:

$$E_{FWD} = 338 \times DPI^{-0.39} \quad (11)$$

where E_{FWD} and DPI units are in MPa and millimetres per blow (mm/blow), respectively. Konrad and Lachance [21] present a relationship between DPI using a 51-mm diameter cone and modulus of unbound aggregates, gravelly, and sandy soils back-calculated from plate load tests (E_{PLT}) by the following equation:

$$\log(E_{PLT}) = -0.884 \log(DPI) + 2.906 \quad (12)$$

where DPI is the DCP penetration index in millimetres per blow (mm/blow) using a 51-mm diameter cone and a 63.5-kg hammer dropping 760 mm and E_{PLT} is expressed in MPa. Livneh and Goldberg [35] carried out comparative German light drop weight (LDW) and DCP tests. The relationship between the modulus measured by the LDW (E_{LDW}) and the in situ CBR values obtained from the DCP are expressed in Eq. (13) and Eq. (14) for clayey and sandy soils, respectively.

$$E_{LDW} = 600 \times \ln \frac{300}{300 - 6.019 \times CBR^{(1/1.41)}} \quad (13)$$

$$E_{LDW} = 600 \times \ln \frac{300}{300 - 4.035 \times CBR^{(1/1.41)}} \quad (14)$$

where E_{LDW} and CBR units are in MPa and percent, respectively.

Development of Empirical Correlations

After a simple linear semi-logarithmic relationship between SSG stiffness (K_{SSG}) and DPI values was determined (i.e., K_{SSG} = 25.6-12·log DPI) based on the direct regression from the actual measured data for all materials combined (Fig. 4), such correlation can be further developed to become a more meaningful and useful equation, which can be used in the design of pavements. To accomplish that, the measured SSG stiffness is converted to SSG modulus (E_{SSG}) of the pavement materials using Eq. (1). Values for Poisson's ratio (ν) of the granular soils including foundry slag and bottom ash were assumed to be 0.40. For fly ash-stabilized soils and fine-grained soils including foundry sand, the ν values of 0.25 and 0.35 were used. These values were selected according to their typical ranges suggested in Huang.[36] Similarly, the weighted average DPI value obtained from the DCP can be converted to California bearing ratio (CBR) of the pavement materials using the well-established correlation as given in Eq. (8) with the coefficients α and β of 2.46 and -1.12, respectively. Fig. 5 illustrates the plot of calculated SSG modulus (E_{SSG}) versus CBR from the DCP. The regression equation obtained is expressed as follows:

$$E_{SSG} = 18.77 \times CBR^{0.63} \qquad R^2 = 0.74 \qquad (15)$$

where E_{SSG} and CBR units are in MPa and percent, respectively. It can be seen that a unique relationship exists between E_{SSG} and CBR, regardless of soil type and site although the coefficient of correlation of Eq. (15) is inherently dependent on the coefficient of correlation of Eq. (8). The results of SSG tests and DCP tests are expected to be affected by the same factors (i.e., relating both test results directly excludes the influence of water content, dry density, and other basic indices). Furthermore, such a relationship is not affected by the change in pavement condition and is also applicable to both as-compacted and post-construction states. This equation yields almost identical values to those obtained from the equation given by Powell et al.,[1] i.e., Eq. (9). Fig. 6 illustrates the comparison between moduli from the SSG (E_{SSG}) and those from the DCP (E_{DCP}) using the regression equations given in Eq. (8) and (9). Remarkably good agreement is obtained with an independent widely used approach.

A regression equation obtained in this study is also compared with that obtained from different in situ tests including the FWD, LWD, and plate load tests as shown in Fig. 7. The

equations obtained for the FWD, LWD, and plate load test are given by Chen et al.,[34] Livneh and Goldberg,[35] and Konrad and Lachance,[21] respectively. Note also that the parameter DPI in Eq. (11) and (12) can be converted to CBR using Eq. (8) with the coefficients α and β of 2.46 and -1.12, respectively. The comparison results suggest that the regression equation obtained in this study is best correlated to the equation given by Powell et al. [1], i.e., Eq. (9), established between modulus and CBR.[1] Within the CBR values ranging from 0 to 20%, the FWD and LWD (on sand) tests, respectively, provide the highest and lowest E for a given CBR. The relationship from the plate load test is in between the curve of Eq. (9) and LDW test (on sand). The suggested equation by AASHTO [2] gives the highest modulus when the CBRs are greater than 10%. Large deviation from the other modulus tests is observed at relatively high CBRs as well. Using Fig. 7, modulus can be estimated for any pavement condition if CBR is obtained for the corresponding condition. It is perhaps not surprising that the modulus given in Eq. (9) by Powell et al. and the SSG modulus given in Eq. (15) as developed in this study as a function of CBR agree well. The reason might be due to the fact that both moduli were adjusted to realistic strain amplitude and stress level from those corresponding to the wave propagation technique. According to Powell et al., their moduli were adjusted to strain amplitude and stress level in pavements from those corresponding to the wave propagation technique. In the case of the SSG, it was shown by Sawangsuriya et al. (2003) that the SSG modulus corresponds to strain amplitudes larger than the strain amplitudes of the wave propagation technique, even though the SSG induces strain amplitudes comparable to that of wave propagation technique. In fact, the stress and strain levels induced by the SSG are 2 kPa and less than 10^{-3} %, respectively. It has also been shown that a somewhat reduced modulus is reported by the internal computation of the SSG device.[7]

Model Validation

To verify the power model given in Eq. (15), field measurement data from another two test sites are plotted onto the developed power model and Powell's equation as shown in Fig. 8. The test sites include: (1) a section of State Trunk Highway (STH) 32 located in Port Washington and (2) a section of STH 12 located between Cambridge and Fort Atkinson, both in Wisconsin, USA. The SSG and DCP data from these sites were obtained recently and were not included in the development of Eq. (15). The predominant subgrade soil of STH 32 is

clayey sand classified as SC and A-4(0) according to the Unified Soil Classification System (USCS) and the AASHTO classification system, respectively. The predominant subgrade soil of STH 12 is comprised of lean clay with sand (CL or A-6(15)) and clayey sand with gravel (SC or A-2-6(0)). Results show that both the developed model (Eq. (15)) and Powell's equation fit reasonably well to the data set from STH 12 and STH 32 and thus Eq. (15) appears to be useful for estimating the subgrade modulus. Additionally, the equation suggested in AASHTO (1993) overestimates the subgrade modulus for soils with relatively high CBRs.

CORRELATION BETWEEN MODULUS TEST AND UNCONFINED COMPRESSION TEST

Beside the correlation with CBR from the DCP, the modulus from the SSG can be correlated with the strength from the conventional unconfined compression test. Lee et al. [6] suggested an empirical correlation between the modulus from resilient modulus test (AASHTO T274-82) (E_{RM}) and the stress causing 1% axial strain ($S_{u1.0\%}$) in conventional unconfined compressive test (ASTM D2166) for the cohesive soils sampled from five in-service subgrades. The relationship is as follows:

$$E_{RM} = 10{,}748.4 + 5{,}744.9 S_{u1.0\%} - 48 S_{u1.0\%}^{2} \qquad (16)$$

where the units of E_{RM} and $S_{u1.0\%}$ are both in kPa. Note that the E_{RM} values used to develop Eq. (16) are at axial deviator stress ($\sigma_1 - \sigma_3$) of 41.4 kPa and confining stress (σ_3) of 20.7 kPa. $S_{u1.0\%}$ was found to have the best correlations with E_{RM}, compared to other variables (i.e., in-service water content and dry density) and was chosen as a predictor variable instead of the unconfined compressive strength because its strain level is comparable with those of the resilient modulus test and the stresses at smaller axial strains may have larger error due to incorrect readings or imperfect contact between the specimen and top cap.[6]

In this study, the moduli from the SSG (E_{SSG}) conducted on subgrade soils at STH 60 (test section) are correlated with the $S_{u1.0\%}$ values from the conventional unconfined compression test. Unconfined compression tests were conducted following ASTM D2166 on undisturbed specimens (50-mm diameter and 100-mm height) trimmed from the tube samples. The test was performed using a strain rate of 2% per min and the stress at about 1% axial strain was reported. A regression analysis was conducted to obtain a relationship between E_{SSG} and

$S_{u1.0\%}$ and the coefficient of determination (R^2) for this relationship is 0.64. A plot of E against $S_{u1.0\%}$ was made as shown in Fig. 9 in order to compare the correlation results obtained with Eq. (16). At a similar $S_{u1.0\%}$, the E_{SSG} value is higher than E_{RM} obtained from Eq. (16) and as $S_{u1.0\%}$ increases, the difference between E_{SSG} and E_{RM} becomes higher. This difference may be contributed to the fact that the E_{RM} values used in Eq. (16) are at higher stress and hence higher corresponding strain levels, whereas the E_{SSG} are measured at much lower stress-strain levels.[7]

SUMMARY AND CONCLUSIONS

SSG and DCP survey data of natural earthen materials, industrial by-products, chemically stabilized soils, and other materials from 10 construction sites around the state of Wisconsin are presented along with their correlation with each other. The data display considerable dispersion, characteristic of the conditions and sampling sizes typical during construction. SSG provides in-place near-surface soil stiffness averaged over a limited zone, whereas DCP provides individual points of an index of in situ shear strength expressed as DCP penetration index (DPI) as a function of depth. Therefore, each fundamentally relates to a different material property and is presented in a spatially different manner. To deal with the latter issue, weighted average of DPI over the depth of measurement is employed to obtain a representative strength index of the material. This approach provided better correlations than the arithmetic average. It is also noted that the standard error associated with DPI is considerably larger than that of the SSG stiffness, reflective of the nature of the two tests.

A simple linear semi-logarithmic relationship is observed between SSG stiffness and DPI. DPI weighted average over a DCP penetration depth of 152 mm yields the highest coefficient of determination and also yields a statistically significant relationship between the SSG stiffness and DPI for most materials. This depth is consistent with the significant depth of measurement for the SSG as shown in previous studies. The relationship is indicative of the fact that although there is not always a one-to-one relationship, stiffness and strength are related in a general sense.

Results of the regression analysis show that there is a significant correlation between the CBR obtained from the DCP and the modulus obtained from the SSG. A power model developed between these two properties is found to be in good agreement with the well-known equation given by Powell et al.[1] An equation suggested by the AASHTO [2] tends to

overestimate the pavement modulus for relatively high CBRs. The modulus from the SSG is also correlated well with the axial stress at 1% strain in the conventional unconfined compression test.

The modulus and CBR are affected in a similar manner by changes of pavement condition and that the relationship between modulus and CBR may be similar for a given soil under any condition if the soil was initially compacted by the same method. Therefore, the modulus for the as-compacted or the post-construction state may be estimated from Fig. 7, if CBR is measured or estimated from DCP on the subbase and subgrade materials being subjected to the same conditions.

The study indicates that either or both devices show good potential for future use in the pavement and subgrade property evaluation during construction phase. The in situ stiffness and strength properties of various materials can be rapidly and directly monitored in companion with the conventional compaction control tests (i.e., nuclear density or laboratory moisture content samples) during earthwork construction. Stiffness and strength are material properties that are needed in different phases of highway design, i.e., for long-term pavement performance as well as during-construction working platform support and stability. For post-construction conditions, modulus can be monitored using DCP and the correlations provided since direct access for SSG is not convenient. The experience with recycled and reclaimed materials as well as chemically stabilized soils is limited compared to natural earthen materials in terms of moisture-density relationships and the related mechanical behaviour. Direct monitoring of stiffness and strength of these new materials using these two devices also appears to be as effective as in natural earthen materials.

ACKNOWLEDGEMENT

This research was funded by the Wisconsin Department of Transportation (WisDOT), USA. The content of this paper are those of the authors and do not reflect the opinions or policies of WisDOT. The senior author gratefully acknowledges the financial support through a scholarship from the Royal Thai Government. The authors acknowledge Robert Allbright, David Staab, Mark Fredrickson, and Bert Trzebiatowski for their assistances with the laboratory and field tests and Drs. Craig Benson and Peter Bosscher for their suggestions. Thanks to Dr. Aykut Senol for providing the unconfined compression test data. Finally, the

authors also express their sincere gratitude to Robert Arndorfer and other WisDOT personnel for their cooperation in arranging access to the sites.

REFERENCES

1. Powell, W. D., Potter, J. F., Mayhew, H. C., and Nunn, M. E. *The Structural Design of Bituminous Roads*. TRRL Laboratory Report 1132, Transportation and Road Research Laboratory, Crowthorne, Berkshire, 1984, 62 pp.
2. AASHTO. *Guide for Design of Pavement Structures*. American Association of State Highway and Transportation Officials, Washington, D.C., 1993.
3. Pinard, M. I. Innovative Compaction Techniques for Improving the Bearing Capacity of Roads and Airfields. *Proceeding of the Fifth International Conference on the Bearing Capacity of Roads and Airfields*, Norway, 1998, 3, pp. 1471-1480.
4. Fleming, P. R. Recycled Bituminous Planings as Unbound Granular Materials for Road Foundations in the UK. *Proceeding of the Fifth International Conference on the Bearing Capacity of Roads and Airfields*, Norway, 1998, 3, pp. 1581-1590.
5. Brown, S. F. The Relationship between California Bearing Ratio and Elastic Stiffness for Compacted Clays. *Ground Engineering*, 1990, 23, No. 8, pp. 27-31.
6. Lee, W., Bohra, N. C., Altschaeffl, A.G., and White, T. D. Resilient Modulus of Cohesive Soils and the Effect of Freeze-Thaw. *Canadian Geotechnical Journal*, 1995, 32, pp. 559-568.
7. Sawangsuriya, A., Edil, T. B., and Bosscher, P. J. Relationship between Soil Stiffness Gauge Modulus and Other Test Moduli for Granular Soils. *Transportation Research Record 1849*, TRB, National Research Council, Washington, D.C., 2003, pp. 3-10.
8. Livneh, M. Validation of Correlations between a Number of Penetration Tests and In Situ California Bearing Ratio Tests. *Transportation Research Record 1219*, TRB, National Research Council, Washington, D.C., 1989, pp. 56-67.
9. Sawangsuriya, A., Bosscher, P. J., and Edil T. B. Laboratory Evaluation of the Soil Stiffness Gauge. *Transportation Research Record 1808*, TRB, National Research Council, Washington, D.C., 2002, pp. 30-37.
10. Egorov, K. E. Calculation of Bed for Foundation with Ring Footing. *Proceedings of the Sixth International Conference of Soil Mechanics and Foundation Engineering*, 1965, 2, pp. 41-45.
11. Wu, W., Arellano, M., Chen, D-H., Bilyeu, J., and He, R. *Using a Stiffness Gauge as an Alternative Quality Control Device in Pavement Construction*. Texas Department of Transportation, Austin, TX, 1998, 17 pp.
12. Chen, D-H., Wu, W., He, R., Bilyeu, J., and Arrelano, M. Evaluation of In Situ Resilient Modulus Testing Techniques. *Recent Advances in the Characterization of Transportation Geo-Materials*, GSP No. 86, ASCE, 1999, pp. 1-11.
13. Scala, A. J. Simple Methods of Flexible Pavement Design Using Cone Penetrometer. *New Zealand Engineering*, 1956, 11, No. 2.
14. Kleyn, E., Maree, J., and Savage, P. The Application of a Portable Pavement Dynamic Cone Penetrometer to Determine In Situ Bearing Properties of Road Pavement Layers and Subgrades in South Africa. *Proceedings of the Second European Symposium of Penetration Testing*, Amsterdam, 1982.

15. Chua, K. M. Determination of CBR and Elastic Modulus of Soils Using a Portable Pavement Dynamic Cone Penetrometer. *Penetration Testing*, 1988, pp. 407-414.
16. Newcomb, D. E., Chadbourn, B. A., VanDeusen, D. A., and Burnham, T. R. *Initial Characterization of Subgrade Soils and Granular Base Materials at the Minnesota Road Research Project*. MN/RC 96-19, 1996, 149 pp.
17. Syed, I. and Scullion, T. In-Place Engineering Properties of Recycled and Stabilized Pavement Layers. *Proceeding of the Fifth International Conference on the Bearing Capacity of Roads and Airfields*, Norway, 1998, 3, pp. 1619-1630.
18. Saarenketo, T., Scullionm, T., and Kolisoja, P. Moisture Susceptibility and Electrical Properties of Base Course Aggregates. *Proceeding of the Fifth International Conference on the Bearing Capacity of Roads and Airfields*, Norway, 1998, 3, pp. 1401-1410.
19. Edil, T. B. and Sawangsuriya, A. *Investigation of the DCP and SSG as Alternative Methods to Determine Subgrade Stability*. Report No. 0092-45-18, Wisconsin Department of Transportation, Madison, WI, 2004.
20. Allbright, R. L. Evaluation of the Dynamic Cone Penetrometer and its Correlations with Other Field Instruments. MS thesis, Dept. of Civ. and Envir. Engrg., University of Wisconsin-Madison, WI, 2002.
21. Konrad, J.-M. and Lachance D. Use of In Situ Penetration Tests in Pavement Evaluation. *Canadian Geotechnical Journal*, 2001, 38, No. 5, pp. 924-935.
22. Livneh, M., Ishao, I., and Livneh, N. A. Effect of Vertical Confinement on Dynamic Cone Penetrometer Strength Values in Pavement and Subgrade Evaluations. *Transportation Research Record 1473*, TRB, National Research Council, Washington, D.C., 1995, pp. 1-8.
23. Kleyn, E. G. *The Use of the Dynamic Cone Penetrometer (DCP)*. Report No. 2/74, Transvaal Roads Department, South Africa, 1975.
24. Harison, J. R. Correlation between California Bearing Ratio and Dynamic Cone Penetrometer Strength Measurement of Soils. *Proceeding of Institute of Civil Engineers*, Part 2, 1987, 83, Technical Note No. 463.
25. Livneh, M. Validation of Correlations between a Number of Penetration Tests and In Situ California Bearing Ratio Tests. *Transportation Research Record 1219*, TRB, National Research Council, Washington, D.C., 1987, pp. 56-67.
26. McElvaney, J. and Djatnika, B. I. Strength Evaluation of Lime-Stabilized Pavement Foundations Using the Dynamic Cone Penetrometer. *Australian Road Research*, 1991, 21, No. 1.
27. Webster, S. L., Grau, R. H., and Williams, T. P. *Description and Application of Dual Mass Dynamic Cone Penetrometer*. Instruction Report GL-92-3, U.S. Army Engineers Waterways Experimental Station, Vicksburg, MS, 1992, 17 pp.
28. Livneh, M. and Livneh, N. A. Subgrade Strength Evaluation with the Extended Dynamic Cone Penetrometer. *Seventh International Association of Engineering Geologists Congress*, ISBN 90 5410 503 8, 1994.
29. Siekmeier, J. A., Young, D., and Beberg, D. Comparison of the Dynamic Cone Penetrometer with Other Tests during Subgrade and Granular Base Characterization in Minnesota. *Nondestructive Testing of Pavements and Back Calculation of Moduli*, ASTM STP 1375, West Conshohocken, PA, 1999.

30. Chen, D-H., Wang, J-N., and Bilyeu, J. Application of the Dynamic Cone Penetrometer in Evaluation of Base and Subgrade Layers. *Transportation Research Record 1764*, TRB, National Research Council, Washington, D.C., 2001, pp. 1-10.
31. Edil, T. B., Benson, C. H., Bin-Shafique, S., Tanyu, B. F., Kim, W-H., and Senol, A. Field Evaluation of Construction Alternatives for Roadway Over Soft Subgrade, *Transportation Research Record 1786*, TRB, National Research Council, Washington, D.C., 2002, pp. 36-48.
32. Jones, R. In Situ Measurements of the Dynamic Properties of Soil by Vibration Methods. *Geotechnique*, 1958, 8, No.1, pp. 1.
33. Heukelom, W. and Foster, C. R. Dynamic Testing of Pavement. *Journal of the Structural Division*, ASCE, 1960, 86, No. SM1.
34. Chen, J., Hossain, M., and LaTorella, T. M. Use of Falling Weight Deflectometer and Dynamic Cone Penetrometer in Pavement Evaluation. *Transportation Research Record 1655*, TRB, National Research Council, Washington, D.C., 1999, pp. 145-151.
35. Livneh, M. and Goldberg, Y. Quality Assessment during Road Formation and Foundation Construction: Use of Falling-Weight Deflectometer and Light Drop Weight. *Transportation Research Record 1755*, TRB, National Research Council, Washington, D.C., 2001, pp. 69-77.
36. Huang, Y. H. *Pavement Analysis and Design*. Prentice-Hall, Englewood Cliffs, NJ, 1993

LIST OF TABLES

LIST OF FIGURES

Table 1. Properties of Natural Earthen Materials and their Classification.

(a) Fine-Grained Soils

Site	Soil Name	Specific Gravity	Liquid Limit	Plasticity Index	Classification		W_N (%)	W_{OPT} (%)	$\gamma_{d\,max}$ (kN/m^3)
					USCS	AASHTO			
STH 60 (Test Section)	Joy Silt Loam	2.70	39	15	CL-ML	A-6(16)	25.0	19.0	16.5
Scenic Edge Development	Plano Silt Loam	2.71	44	20	CL	A-7-6(20)	27.0	20.0	16.2
Gils Way Development	Plano Silt Loam	2.71	46	20	CL	A-7-6(20)	23.4	19.5	16.3
STH 26	Lean Clay with Sand	2.64	32	11	CL	A-6(7)	20.7	13.5	19.2
STH 100	Lean Clay with Sand	2.74	29	14	CL	A-6(9)	14.2	14.4	18.2
STH 44	Silty, Clayey Sand	2.70	23	7	SM-SC	A-4(0)	9.8	11.7	19.8

(b) Predominantly Granular Soils

Site	Soil Name	Specific Gravity	D_{10} (mm)	D_{60} (mm)	C_u	% Fines	Classification		W_{OPT} (%)	$\gamma_{d\,max}$ (kN/m^3)
							USCS	AASHTO		
USH 12	Clayey Sand[1]	2.69	NA	0.2	NA	34.45	SC	A-2-4(0)	10.0	18.9
STH 131	Poorly Graded Sand with Silt	2.62	0.09	0.35	3.9	6.54	SP-SM	A-3(0)	8.0	18.0
STH 58	Clayey Sand[2]	2.62	NA	0.25	NA	25.50	SC	A-2-4(0)	8.5	19.8
STH 154	Poorly Graded Sand with Silt	2.63	0.07	0.4	5.7	11.46	SP-SM	A-3(0)	9.0	18.7
STH 60 (Test Section)	Breaker Run	NM	0.25	29.0	116	3.12	GW	A-1-a(0)	None	NM

Notes: NM = not measured, NA = not applicable, [1]LL=24, PI=7, [2]LL=24, PI=8

Table 2. Properties of Processed Construction Materials (Industrial By-Products and Chemically Stabilized Soils) and their Classification.

(a) Industrial By-Products

Site	Soil Name	Specific Gravity	D_{10} (mm)	D_{60} (mm)	C_u	% Fines	Classification		W_{OPT} (%)	$\gamma_{d\ max}$ (kN/m^3)
							USCS	AASHTO		
STH 60 (Test Section)	Bottom Ash[1]	2.65	0.06	1.9	31.7	13.23	SW	A-1-b(0)	None	15.1
	Foundry Sand[2]	2.55	0.0002	0.23	1150	28.92	SC	A-2-7(2)	16.0	16.1
	Foundry Slag[1]	2.29	0.13	2.0	15.4	5.27	SW	A-1-b(0)	None	10

Notes: [1]Non-plastic, [2]LL=44 and PI=25

(b) Chemically Stabilized Soils

Site	Soil Name	Chemical Stabilized Content (%)	Stabilized Soil (No Delay)		Stabilized Soil (2-hr Delay)		Soil Component	
			W_{OPT} (%)	$\gamma_{d\ max}$ (kN/m^3)	W_{OPT} (%)	$\gamma_{d\ max}$ (kN/m^3)	W_{OPT} (%)	$\gamma_{d\ max}$ (kN/m^3)
STH 60 (Test Section)	Fly Ash-Stabilized Soils	10	20	16.6	21.0	16.1	19.0	16.5
Scenic Edge Development	Fly Ash-Stabilized Soils	12	21.0	16.2	21.0	15.6	20.0	16.2
Gils Way Development	Lime-Stabilized Soils	5	NM	NM	NM	NM	19.5	16.3

Note: NM = not measured

Table 3. Results of SSG and DCP Measurements.

(a) SSG Stiffness (MN/m)

Material Type	No. of Tests[b]	Mean[c]	Standard Deviation	Coefficient of Variation	Standard Error	Maximum	Minimum
Natural Earthen							
Granular	18	7.8	1.88	24%	0.44	12.1	5.4
Fine-grained	90	5.6	1.98	35%	0.21	11.0	1.6
Industrial By-Products							
Bottom ash	4	3.9	0.20	5%	0.10	4.1	3.7
Foundry sand	4	7.7	1.07	14%	0.54	9.0	6.4
Foundry slag	18	3.1	1.03	33%	0.24	4.8	1.5
Fly Ash-Stabilized Soils							
24 hours	22	12.9	2.85	22%	0.67	21.1	7.9
7-8 days	15	15.1	3.75	25%	0.97	21.7	7.1
Lime-Stabilized Soils							
Before liming	15	5.3	1.44	27%	0.37	7.0	2.7
After liming	15	9.5	1.59	17%	0.41	12.9	6.8
Other							
Breaker run	8	6.7	1.19	18%	0.42	8.8	4.5

(b) DCP Penetration Index (DPI) (mm/blow)[a]

Material Type	No. of Tests[b]	Mean[c]	Standard Deviation	Coefficient of Variation	Standard Error	Maximum	Minimum
Natural Earthen							
Granular	18	33.9	20.44	60%	4.82	93.3	12.6
Fine-grained	81	44.7	27.89	62%	3.10	170.0	12.2
Industrial By-Products							
Bottom ash	4	52.7	9.99	19%	4.99	63.1	43.8
Foundry sand	3	59.1	16.59	28%	9.58	69.8	40.0
Foundry slag	5	49.8	15.92	32%	7.12	72.0	32.1
Fly Ash-Stabilized Soils							
24 hours	13	18.36	3.60	20%	1.00	26.5	13.4
7-8 days	15	15.15	8.05	53%	2.08	39.1	7.1
Lime-Stabilized Soils							
After liming	15	13.7	1.94	14%	0.50	17.3	11.6

Notes: DCP tests were not performed on lime-stabilized soils-before liming and breaker run, [a]DPI was calculated by weighted average over a penetration depth of 152 mm, [b]corresponding to total number of test locations in the material category, [c]mean of SSG stiffness and weighted average DPI for total number of test locations in the material category.

Table 4. Parameters of Linear Regression Analysis for SSG Stiffness (MN/m) vs. log DPI (mm/blow) Relationship.

Material Category	No. of Points	Intercept	Slope	R^2	Standard Error	P-Value
Natural Earthen	79	17.9	-7.5	0.60	1.44	0.00
Granular	27	19.3	-8.3	0.55	1.73	0.00
Fine-Grained Soils	52	17.1	-7.1	0.64	1.28	0.00
Fly Ash-Stabilized Soils	37	24.8	-10.0	0.40	2.05	0.00
Fine-Grained + Fly Ash-Stabilized Soils	89	26.7	-12.7	0.75	2.16	0.00
All Combined (include Foundry Sand)	119	25.6	-12.0	0.72	2.15	0.00

Notes: DPI was calculated by weighted average over a penetration depth of 152 mm from the surface.

(a)

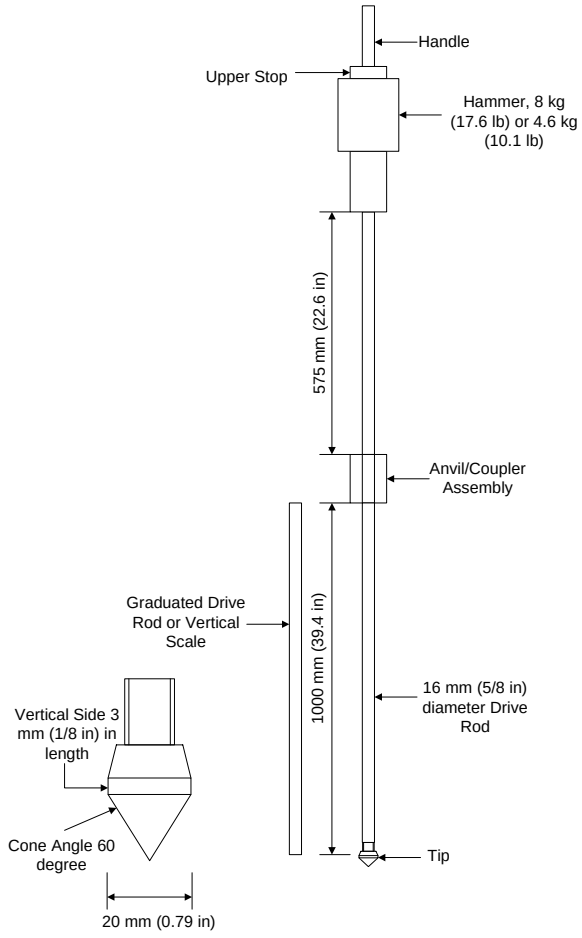

(b)

Fig. 1. Humboldt soil stiffness gauge (SSG) (a) and dynamic cone penetrometer (DCP) (b).

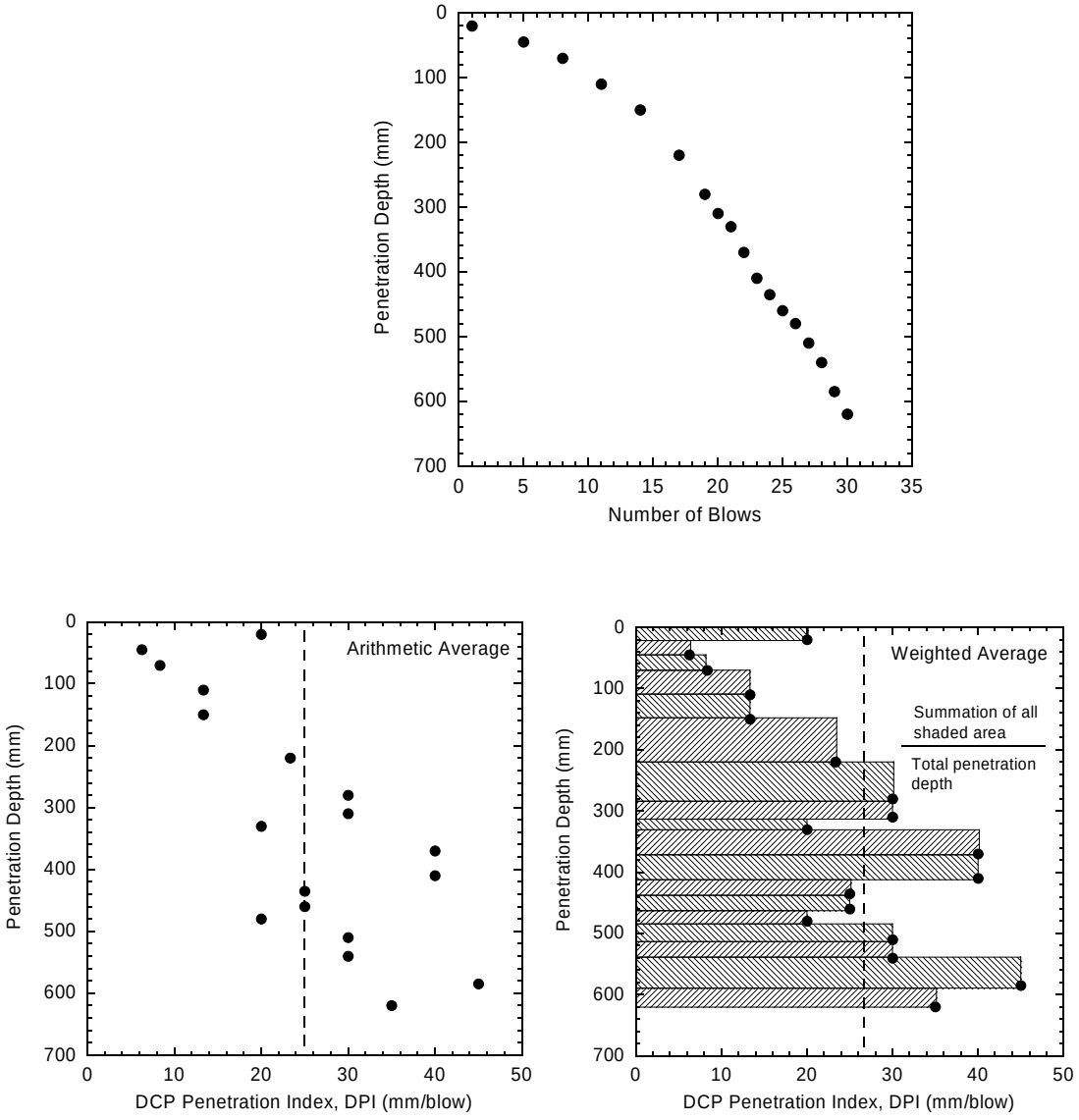

Fig. 2. Two methods for calculating the representative DPI value.

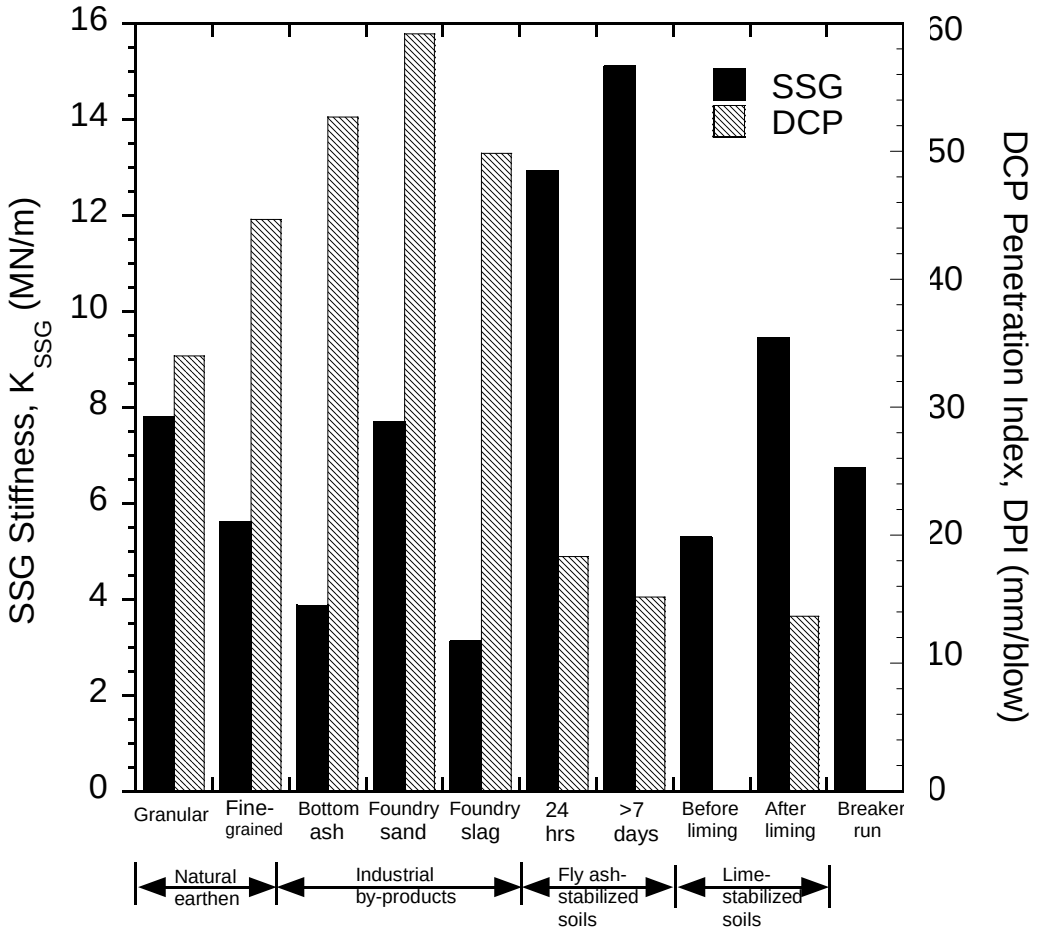

Fig. 3. Mean SSG stiffness and DCP penetration index (DPI) values of various materials.

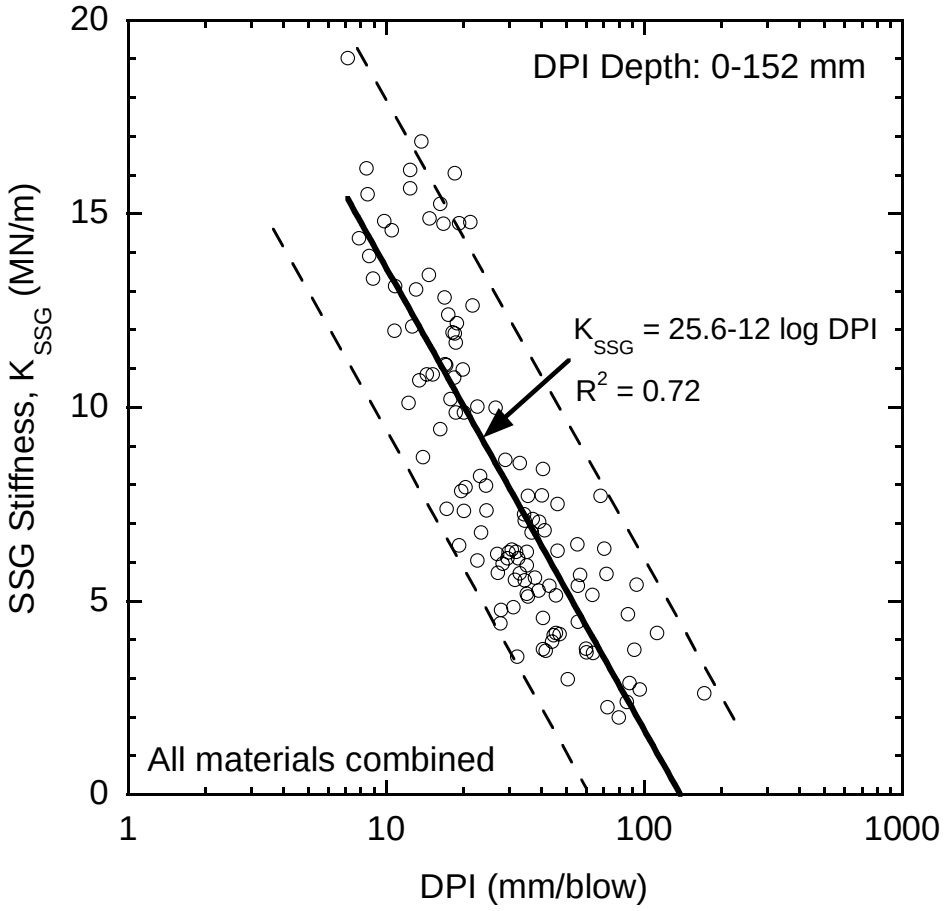

Fig. 4. SSG stiffness-DPI relationship for all materials combined.

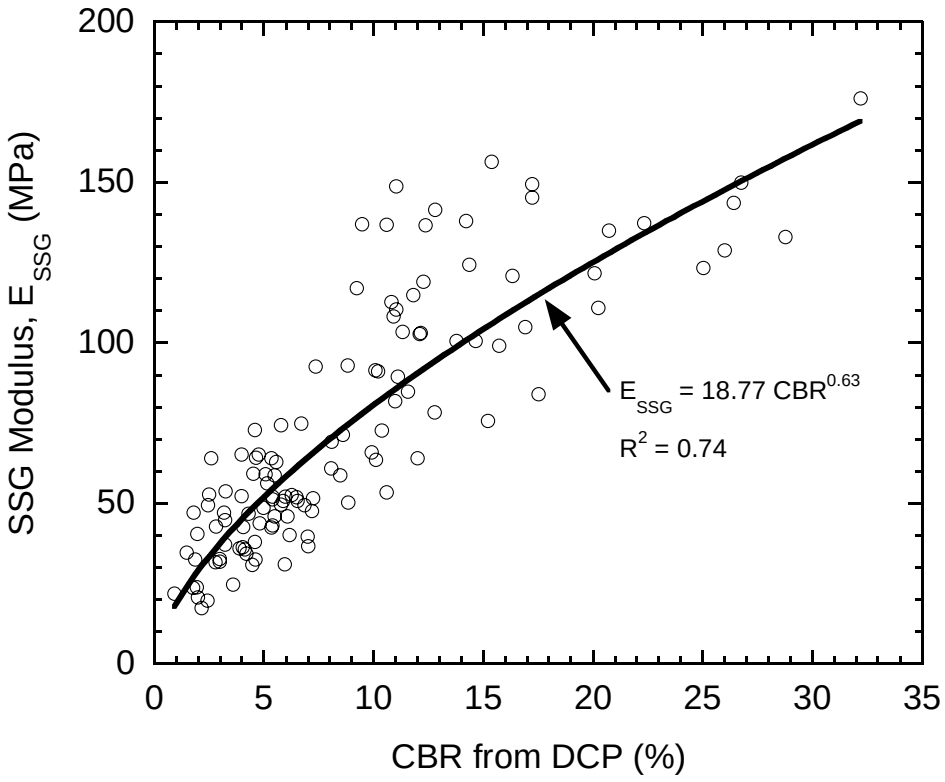

Fig. 5. Correlation between modulus from the SSG and CBR from the DCP.

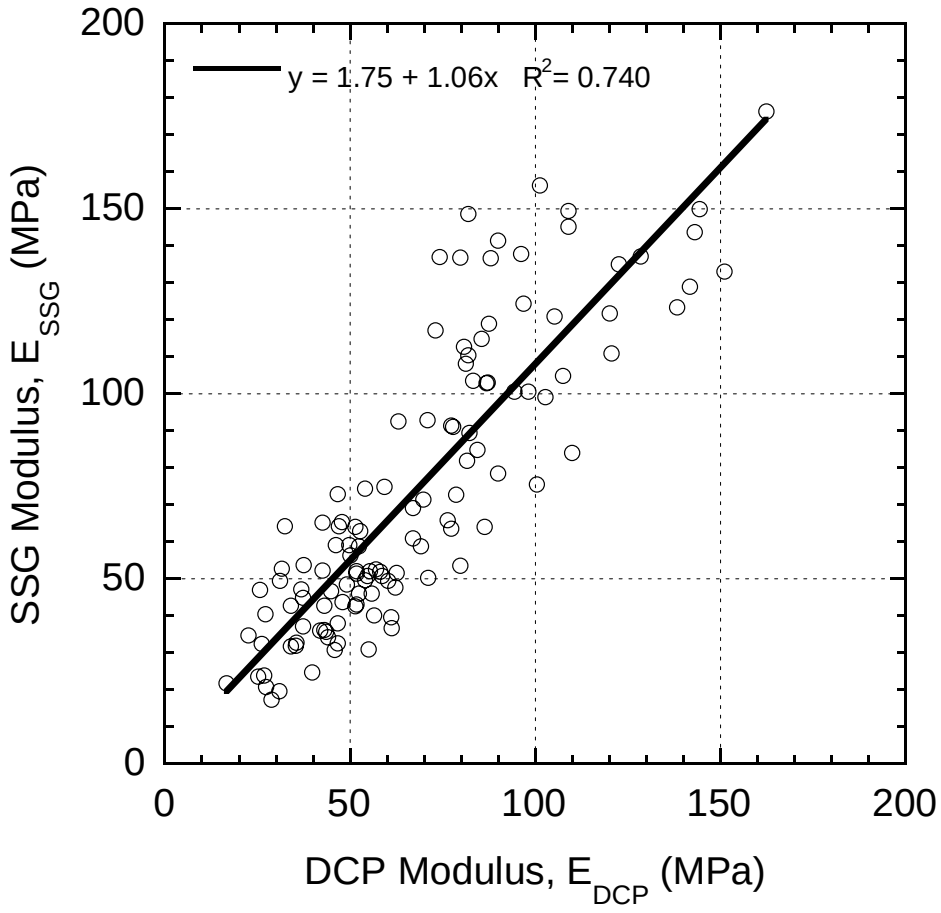

Fig. 6. Comparison between moduli from the SSG and those from the DCP.

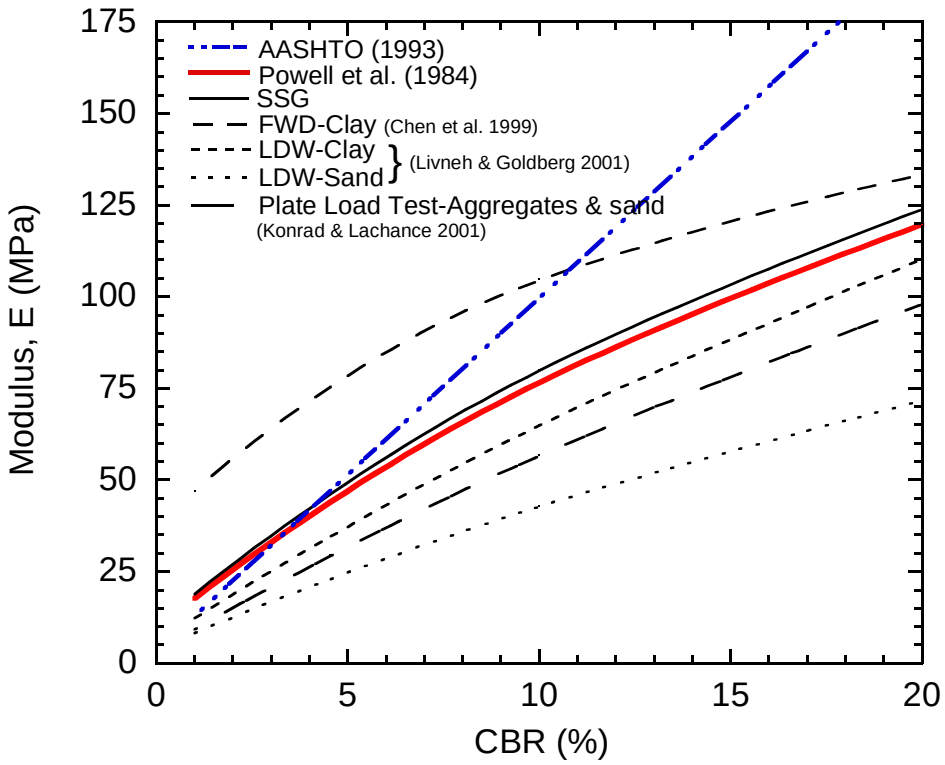

Fig. 7. E-CBR relationship of different methods.

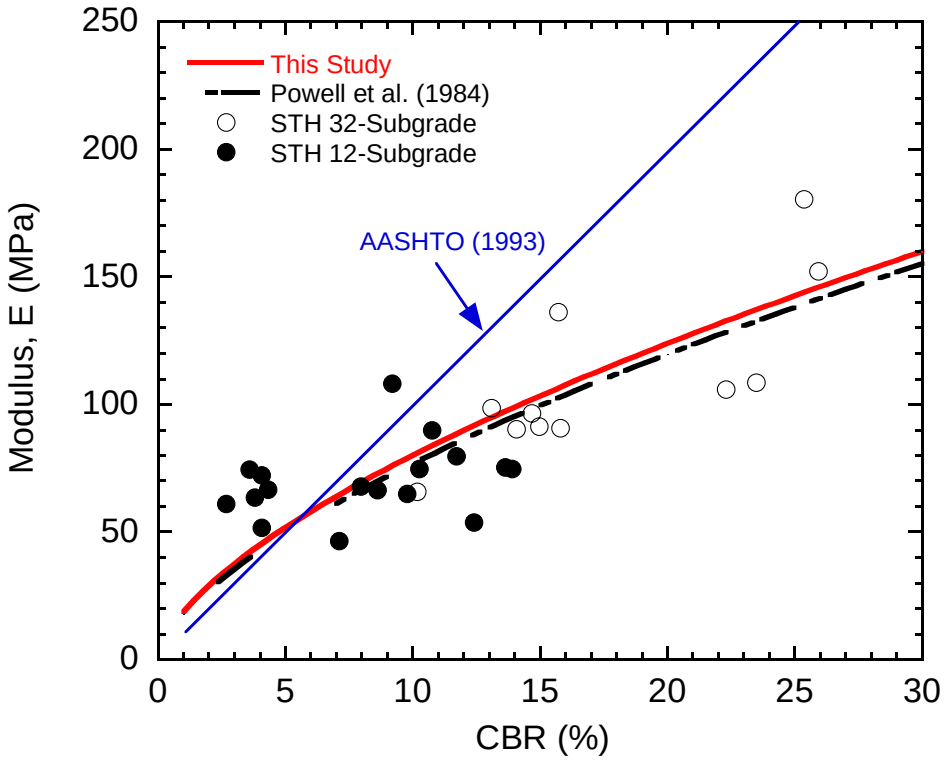

Fig. 8. Comparison of predicted subgrade moduli at STH 32, WI.

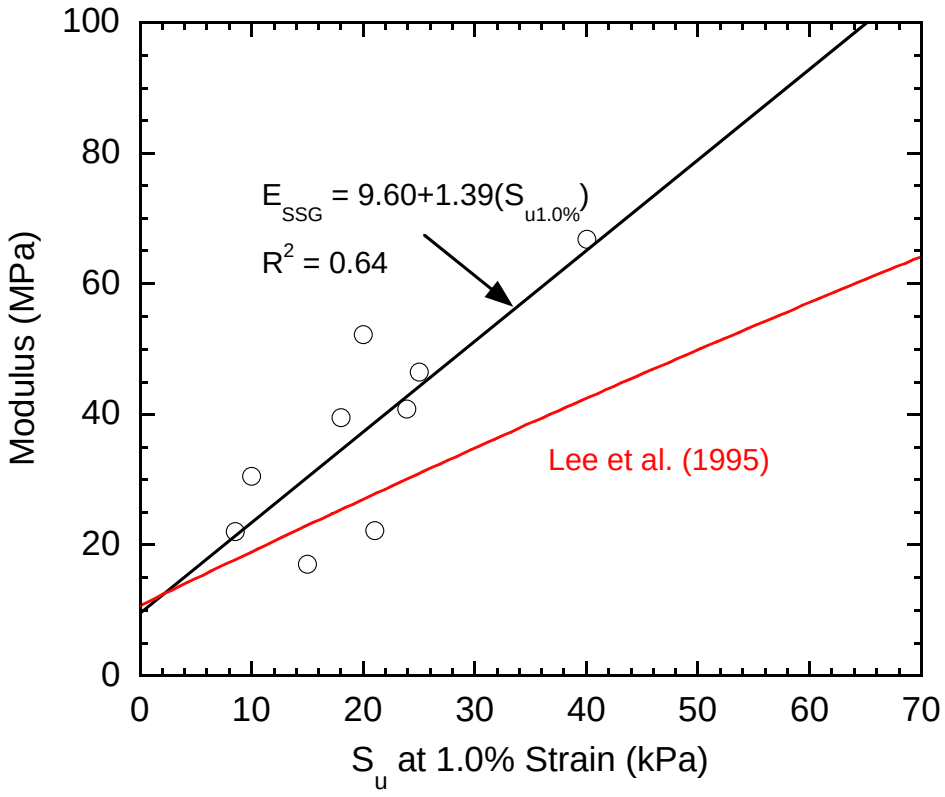

Fig. 9. Relationship between E and $S_{u1.0\%}$ for undisturbed subgrade soils at STH 60 (test section), WI.

Proceedings of the 15th Southeast Asian Geotechnical Conference 2004, Bangkok, Thailand

Assessing Small-Strain Stiffness of Soils Using the Soil Stiffness Gauge

Auckpath Sawangsuriya, Tuncer B. Edil & Peter J. Bosscher
Department of Civil and Environmental Engineering, University of Wisconsin at Madison, 2226 Engineering Hall, 1415 Engineering Drive, Madison, WI 53706, USA
sawangsuriya@wisc.edu, edil@engr.wisc.edu, bosscher@engr.wisc.edu

Abstract: The Soil Stiffness Gauge (SSG), a recently developed technology, provides an alternative means of rapidly and directly assessing in situ near-surface stiffness of soils at small strains. This paper summaries the characteristics and limitations of the SSG stiffness measurement, force and displacement induced by the SSG, and the comparison of SSG modulus with other moduli tests based on extensive experimental studies conducted in previous research. Also presented are additional experimental and numerical studies to verify the boundary and layering effects. The study concludes that the SSG exhibits particular promise for assessing soil stiffness at small strains; however, caution needs to be exercised when the SSG is used in laboratory and field tests because boundary and layering effects might influence the stiffness output from the SSG.

1 INTRODUCTION

The Soil Stiffness Gauge (SSG), which is currently marketed as GeoGauge™ (Fig. 1), is recently developed portable, non-nuclear testing equipment that provides simple and non-destructive means of directly and rapidly measuring near-surface soil stiffness at small strains. The SSG weighs about 11.4 kg, is 28 cm in diameter, 25.4 cm tall, and rests on the soil surface via a ring-shaped foot. The SSG produces small dynamic vertical forces over a range of frequencies from 100 to 200 Hz, which results in small deflections of the foot. By using velocity sensors (i.e. geophones), the SSG measures the deflection of its foot in response to the known applied dynamic force. The force and displacement-time history of the foot are recorded and the average soil stiffness over the range of frequencies is then output from the SSG. Note that the stiffness of soil is expressed as the ratio of applied force to measured displacement. Operation of the SSG is relatively simple and the entire measurement is completed in slightly over 1 minute. The most significant aspect in using the SSG is to ensure a good coupling between the ring-shaped foot and the soil surface. Additional information on the principle of operation, measurement procedure, and calibration of the SSG can be found in ASTM D6758-02, "Standard Test Method for Measuring Stiffness and Apparent Modulus of Soil and Soil-Aggregate In-Place by an Electro-Mechanical Method".

Previous research (Sawangsuriya *et al.*, 2002; Sawangsuriya *et al.*, 2003) focused on comprehensive experimental studies so as to understand the measurement characteristics and limitations of the SSG as well as the comparison of moduli obtained from the SSG and the moduli obtained from other tests. The objective of this paper is to verify the boundary and layering effects observed in the previous research on the basis of numerical analyses and further experimental investigation.

2 PREVIOUS RESEARCH

2.1 *Experimental Setup for SSG Test*

Fig. 1. Soil Stiffness Gauge (GeoGauge™)

Lenke *et al.* (1991) evaluated numerous container shapes and boundary materials using geotechnical centrifuge modeling experiments of a vertically excited circular footing in order to truly model an elastic half-space experiment and to approximate true radiation damping such that reflected wave energy is minimized. Their studies suggested that cubical containers with a compliant energy absorbing boundary material allowed reasonable approximation of an elastic half-space. Sawangsuriya *et al.* (2002) evaluated the SSG in a controlled laboratory environment. A 1.2 m × 1.2 m × 1.2 m wooden test box was selected so as to prevent dynamic reflections from the sides and bottom. Three cylindrical woven geotextile (GT) molds: 0.3 m, 0.6 m, and 0.9 m in diameter were used to hold the test materials in the wooden box and to separate them from the energy absorbing boundary material (Styrofoam beads and foam peanuts) that was placed in the wooden box. This experimental setup established reasonable dimensions of an elastic half-space that would minimize reflected wave energy and also provide a mold size of ≥ 5 times the foot diameter to limit any physical model size effects.

Beside the GT mold, a 0.6-m diameter cylindrical geomembrane (GM) mold has also been used recently.

Preliminary tests have been conducted on materials placed in this GM mold with and without energy absorbing boundary material around the mold, i.e. inside or outside the wooden box. For tests conducted outside the wooden box, the GM mold is placed on the floor either with or without a 140-mm thick styrofoam panel placed at the bottom and without any energy absorbing material on the sides. Comparative studies show no statistically significant difference at a 95% confidence level between the average SSG stiffness obtained from the tests conducted using the GT and GM molds and between the average SSG stiffness obtained from the tests with and without Styrofoam panel placed at the bottom. Therefore, relatively simple experimental setups can be employed in evaluating the SSG performance.

2.2 *Stiffness Characterization Using SSG*

Sawangsuriya *et al.* (2002) used three types of granular materials that are characterized as high stiffness, intermediate stiffness, and low stiffness. The high-stiffness material is 19-mm crushed lime rock classified as GP according to the Unified Soil Classification System (USCS). The intermediate-stiffness material is a medium, uniformly-graded quartz sand classified as SP according to the USCS. The low-stiffness material is a 50:50 mixture by volume of nylon plastic beads and medium sand. The plastic beads have a prismatic shape and pass sieve No. 4 but are retained on sieve No. 8 with dimensions of approximately 2.5 × 2.5 × 1.5 mm. These materials were poured slowly from a scoop into the 0.6-m diameter GT cylindrical mold, which was already placed in the wooden box. The SSG stiffness tests were conducted at the center of the cylindrical mold at each 25-mm increment of deposition of the materials from the bottom up. The surface of test materials in the cylindrical mold was carefully leveled prior to each measurement. Results of SSG stiffness tests on these three materials are shown in Fig. 2. The target value for SSG stiffness of each material was obtained by averaging the stiffness values when they became stable. Ranking from highest to lowest value, the average SSG stiffness of crushed rock, medium sand, and plastic beads-sand mixture are approximately 4.8, 3.8, and 2.4 MN/m, respectively.

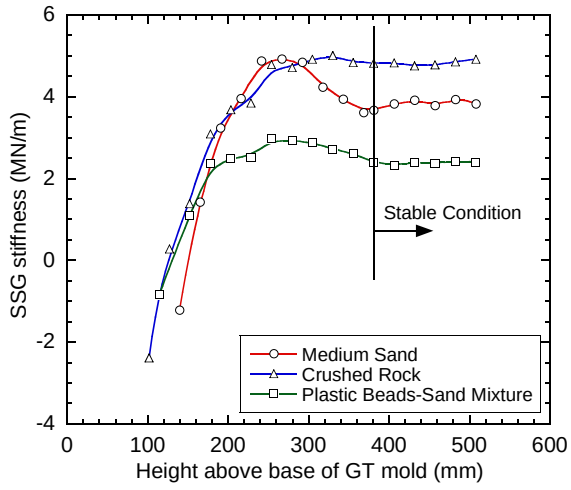

Fig. 2. SSG stiffness of medium sand, crushed rock, and plastic beads-sand mixture in 0.6-m diameter mold (Sawangsuriya *et al.*, 2002).

2.3 *Zone of Measurement Influence*

Sawangsuriya *et al.* (2002) investigated the measurement influence zone of the SSG in a controlled laboratory environment. Their experimental results indicated that the lateral zone of influence of the SSG is less than 0.6 m in diameter; in other words, the radius of SSG measurement influence is less than 0.3 m. The bottom boundary is determined when the reported SSG stiffness ceases to change with increasing depth. The SSG outputs this steady-state stiffness value when the distance to bottom boundaries are on the order of 300 to 380 mm (Fig. 2). Lenke *et al.* (2003) also conducted a similar study but used a cubical test bin lined with 19-mm thick Styrofoam panels as an energy absorbing material. They found that the steady-state value for SSG stiffness is lower for measurements close to the lateral boundary but becomes stabilized at a lateral distance from the boundary higher than approximately 0.2 m. The steady-state value for SSG stiffness is achieved at about 300 to 400 mm deep.

The effect of layering on SSG measurement was studied by developing two-layer systems consisting of the three test materials aforementioned. To separate the two materials and to prevent a stiffness decoupling of the layers (Sawangsuriya *et al.*, 2002), a thin plastic wrap sheet was used at the interface between the two materials. Results of two series of layered sample tests: (i) medium sand at the bottom and crushed rock and plastic beads-sand mixture at the top and (ii) plastic beads-sand mixture at the bottom and medium sand and crushed rock at the top are shown respectively in Figs. 3(a) & 3(b). This study indicated that for two-layer materials with different stiffness, the SSG starts to register the stiffness of an upper-layer material of 125 mm or thicker. The effect of the lower layer, however, may continue to be present even at an upper-layer material thickness of 275 mm, depending on the relative stiffness of the layer materials.

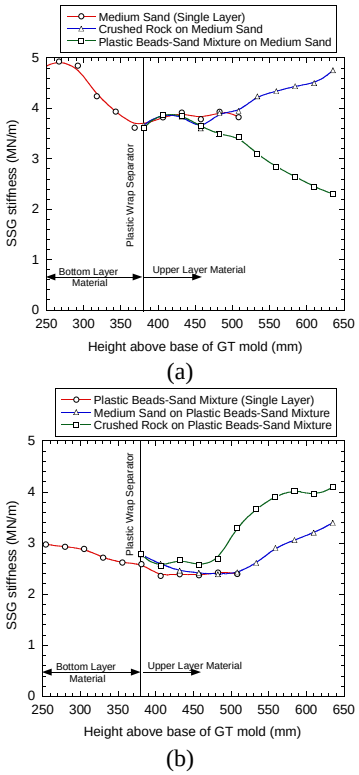

Fig. 3. SSG stiffness of layered sample tests over medium sand (a) and plastic beads-and mixture (b) (Sawangsuriya *et al.*, 2002).

2.4 *Force and Displacement from SSG*

Since modulus is dependent on the levels of stress and strain amplitudes, the force and displacement induced by the SSG must be known. Sawangsuriya *et al.* (2003) established an experimental test setup for directly measuring the vertical acceleration produced by the SSG during its operation. The medium sand was packed in a 0.6-m diameter cylindrical cardboard mold with a 140-mm thick Styrofoam panel placed at the bottom. Note that the size of this test container is proven to be free from boundary effects and the steady-state value for SSG stiffness could be achieved. An accelerometer was attached to the rigid ring-shaped foot of the SSG. The signal from the accelerometer was amplified using a charge amplifier and recorded by a digital audio tape recorder. The SSG with the accelerometer attached under its foot was placed on the surface of the sand. The acceleration signal produced by the SSG during its stiffness measurement was recorded. The measured signal from the accelerometer correlated reasonably well with the SSG's output signal downloaded directly from the embedded software. The measured signal in voltage (V) was converted to acceleration in engineering units (g) by a known calibration factor (i.e. 0.122 V/g). The peak-to-peak amplitudes of measured signal were collected at different frequencies using spectral analysis techniques. The acceleration and corresponding displacement signals are shown in Fig. 4. According to the measurement results, the SSG produces very small displacement of the soil (~ 1.2×10^{-6} m), which is consistent with the manufactured value (Humboldt 1999).

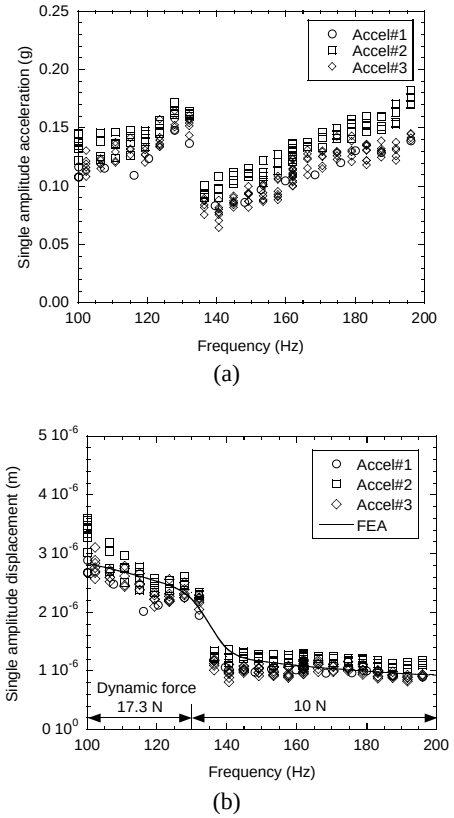

Fig. 4. Acceleration and corresponding displacement signals from accelerometer and the comparison with FEA results (Sawangsuriya *et al.*, 2003).

A PLAXIS finite-element analysis (FEA) program was utilized to estimate the dynamic force (Sawangsuriya *et al.*, 2003). The medium sand in the cylindrical mold was modeled as an axi-symmetrical problem with the same geometry as the actual size of the cylindrical cardboard mold used in the experimental test (i.e. 0.6-m diameter and 0.53-m height). The pertinent material parameters: the unit weight (16 kN/m^3), Poisson's ratio (0.3), Young's modulus (35 MPa), and the material damping value (0.0001 for both the Rayleigh alpha and beta damping parameters) were input in the FEA. These values were selected based on the typical values and preliminary test results of sand. Different applied dynamic forces were applied to the model in such a way that the response obtained from the FEA was close to that obtained from acceleration measurement. Fig. 4(b) illustrates the comparison between the FEA and the measurement results. Results show that an applied dynamic force of 10 N tends to provide an accurate response at higher frequencies; however, for frequencies less than 130 Hz, a value of 17.3 N is required (Sawangsuriya *et al.*, 2003).

2.5 *Comparison with Other Modulus Tests*

To effectively compare the SSG modulus with other modulus tests, the stress and strain levels of these moduli tests must be known. The state of stress within the soil mass is commonly referred to as the confining pressure (σ_o), which is the mean of three principle normal stresses. For the SSG, σ_o can be calculated as $\sigma_v (1 + 2K_o)/3$ by assuming the intermediate stress is equal to the minor stress. The vertical stress (σ_v) is obtained at the mid-plane of the SSG effective measurement zone (i.e. at z = 152 mm) under the center of the ring and is equal to the sum of vertical stress due to the ring load exerted by the SSG and the geostatic stress of the material being tested. The value of K_o is estimated from Jaky's relationship $K_o = 1 - \sin\phi$ (Jaky 1944) with $\phi = 35^o$ for the test sand. In this study, σ_o at z = 152 mm is calculated to be 2.6 kPa.

A level of strain amplitude induced by the SSG is determined from the FEA. The FEA model aforementioned was used to estimate the dynamic vertical strain distribution due to 10 and 17.3 N dynamic forces induced by the SSG. Results from the FEA indicate that the dynamic vertical (major) strain amplitude (ε_v) in the principle plane averaged over the depth from 125 to 178 mm (i.e. within the zone of interest during the SSG measurement) is smaller than 2.7×10^{-4} %. The maximum shear strain amplitude (γ) in principle plane produced during the SSG measurement is therefore computed by multiplying ε_v by $(1 + \nu)$, where ν is Poisson's ratio (taken to be equal to 0.3).

A plot of shear modulus versus shear strain amplitude for test sand at confining pressure of 2.6 kPa and unit weight of 16 kN/m^3 was developed for modulus comparison of different tests including the SSG, resilient modulus, resonant column, seismic, and static triaxial compression tests as shown in Fig. 5. The shear modulus of the test sand at the same confining pressure (i.e. 2.6 kPa) was also obtained from an empirical relationship proposed by Hardin & Drnevich (1972) and plotted in Fig. 5 over a range of shear strain levels. Fig. 5 indicate that the moduli measured on the test sand using different test methods follow the general dependency of modulus on shear strain amplitude. The seismic test gives the maximum shear modulus (G_{max}) since its shear strain amplitude is known to be very small (~10^{-4}%). The values of G and γ obtained from the resonant column test are plotted directly in Fig. 5. More detailed explanations including the procedure to obtain G for each test are reported in

Sawangsuriya *et al.* (2003). A comparison of the results suggests that the SSG modulus corresponding to a strain amplitude larger than the strain amplitude of the seismic test, even though the SSG induces a strain amplitude comparable to that of seismic test. In this study, the modulus ratio between the seismic and the SSG tests on the test sand is approximately 1.6. Chen & Bilyeu (1999) studied the comparison of base and subgrade moduli obtained from the SSG with moduli from the Seismic Pavement Analyzer (SPA) based on seismic wave propagation technique. Their measurement results suggest that the modulus ratio varies from 1.6 to 3.0. Sawangsuriya *et al.* (in prep.) studied the stiffness of sand with different densities and fabrics using the SSG and other modulus tests and found that the modulus ratio varies from 1.2 to 2.0. Therefore, it seems that the modulus reported by the SSG has been reduced internally by a factor. It is presumed that this reduction factor is incorporated by the device so that the modulus reported from the SSG is comparable to the resilient modulus corresponding typically to higher strain levels and commonly used in the design of pavement systems.

Due to the newness of the device and rather limited number of studies conducted on the SSG to date, the need for verifying the experimental results from previous research becomes very important. In particular, the boundary and layering effects must be further investigated before the SSG can be used with confident. These effects are explored in the subsequent sections of this paper.

3 BOUNDARY EFFECT

To verify the radius of SSG measurement influence, six finite-element models: 0.15-, 0.30-, 0.45-, 0.60-, 0.75-, and 0.90-m in diameter with an equal height of 0.53 m were modeled as an axi-symmetric problem using a commercial finite-element analysis (FEA) program called PLAXIS (PLAXIS 1998). An energy-absorbing element was employed at the boundaries for geometrical or radiation damping. These model geometries and their boundary conditions were selected in accordance with the experimental studies described in Sawangsuriya *et al.* (2002). The pertinent input material parameters for the FEA were identical to those given in Sawangsuriya *et al.* (2003), i.e. the unit weight (16 kN/m^3), Poisson's ratio (0.3), Young's modulus (35 MPa), and the material damping value (0.0001 for both Rayleigh alpha and beta). These values were selected based on the typical values and preliminary test results of sand. Dynamic forces of 10 and 17.3 N were input to the model for frequencies ranging from 100 to 200 Hz (i.e. SSG's operated frequency range). These dynamic forces provide a reasonable response as compared with the measured response (Sawangsuriya *et al.*, 2003). In addition to the six model geometries, a Proctor mold (152–mm diameter and 165–mm height) was also modeled with identical input material parameters as described above. Note that this cylindrical Proctor mold has been previously employed in the laboratory SSG test (Lenke *et al.*, 2003; Ooi & Pu, 2003). Fig. 6 shows a plot of dynamic displacement response vs. frequency from the FEA for seven different model geometries. For frequencies less than 130 Hz, the dynamic response of a 0.15-m diameter model indicated a significant effect of boundary. The boundary effect was reduced as the diameter of FEA model increased. No significant effect was observed for the diameter of FEA model equal to or larger than 0.60 m. At higher frequencies (> 130 Hz), the dynamic response, however, shows no significant difference for different FEA model diameters. In the case of the Proctor mold, the boundary effect becomes very significant in both frequ-

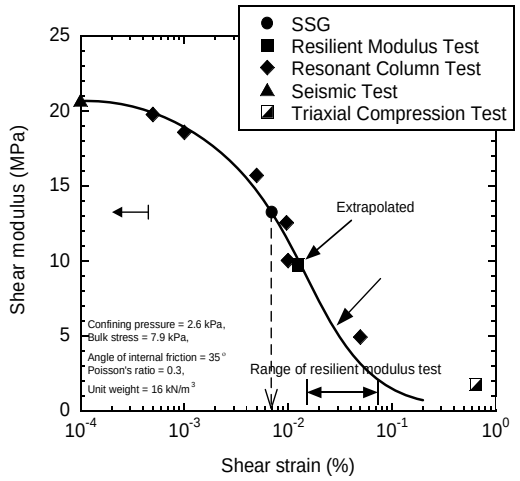

Fig. 5. Modulus comparison of different tests (Sawangsuriya *et al.*, 2003).

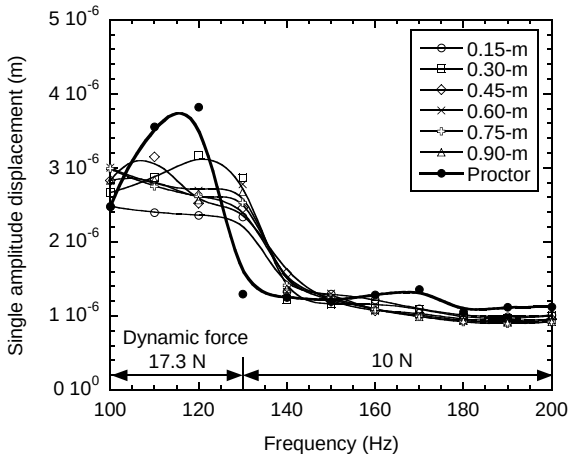

Fig. 6. Effect of boundary geometry on finite-element models.

-ency ranges.

4 LAYERING EFFECT

To further investigate the layering effect, tests were conducted on layered samples of controlled low-strength concrete (flowable fill). Two design mixture proportions resulting in high-stiffness flowable fill (FFH) and low-stiffness flowable fill (FFL) (Dolen & Benavidez 1998) were selected in this study. Table 1 presents the design mixture proportions for the FFH and FFL specimens. Two to three prismatic specimens with dimension of approximately 40 cm × 10 cm × 8 cm (i.e. 4:1 length to width ratio) were prepared and tested with a Geotest Sonometer at different curing times (i.e. 3, 7, and 14 days). The dynamic elastic moduli (E) of these specimens tested at different curing time are shown in Fig. 7. The dynamic elastic modulus ratio between FFH and FFL specimens is approximately 1.3. Similar design mixture proportions were then used to create a total of eight 0.6-m diameter cylindrical specimens for the SSG test. Six of them were formed into two-layer combination material with

varied layer thickness ranging from 76 to 533 mm. Two of them were formed using only single material and are used as reference specimens. SSG stiffnesses of these eight flowable fill specimens tested at 7-day curing time are shown in Fig. 8. At least five SSG measurements were made within a radius of 76 mm from the center. The SSG stiffness ratio between FFH and FFL reference specimens is approximately 1.2. The study showed that the SSG starts to register the stiffness of an upper-layer material (FFL) of 125 mm or thicker. Moreover, the SSG outputs lower stiffness with increase in thickness of FFL layer. For this test, the effect of the lower layer becomes negligible when the thickness of the FFL layer is greater than 457 mm.

Table 1. Design mixture proportions for FFH and FFL specimens.

Mixture ID	Water (kg/m^3)	Cement (kg/m^3)	Bentonite (%)[1]	Sand (kg/m^3)	190-mm Aggregate (kg/m^3)	Total (kg/m^3)
FFH	258	178	0	866	709	2011
FFL	332	142	20[2]	773	633	1916

[1] Bentonite Content - % by dry mass of cement plus bentonite.
[2] (20/80) × 142 = 36 kg/m^3

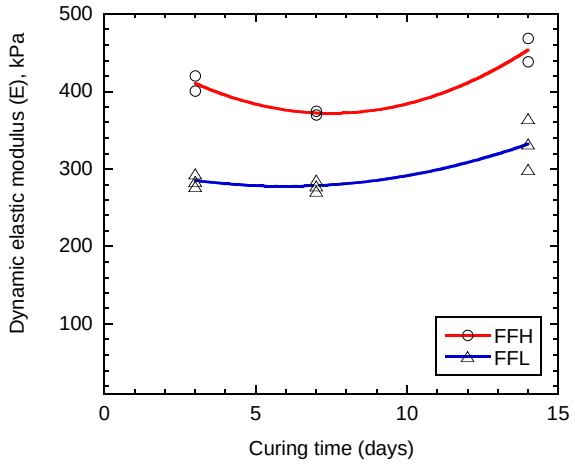

Fig. 7. Dynamic elastic moduli (E) of prismatic specimens tested at different curing time.

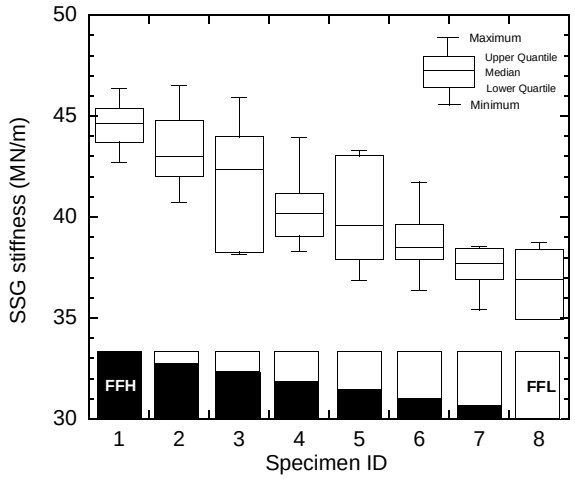

Fig. 8. SSG stiffness of eight flowable fill specimens tested at 7-day curing time.

5 SUMMARY AND CONCLUSIONS

The Soil Stiffness Gauge (SSG) is a recently developed instrument for rapidly and directly assessing in situ near-surface stiffness of soils at small strains. The device measures stiffness by imparting small dynamic forces to the soil though a ring-shaped foot at 25 steady state frequencies between 100 to 200 Hz. Based on the force and displacement-time history, stiffness is calculated as the average force per unit displacement over the operating frequencies.

Previous research on the characteristics and limitations of the SSG stiffness measurement based on extensive experimental studies indicated that the zone of SSG measurement influence to be less than 300 mm laterally and over a maximum depth of approximately 300 to 380 mm. The SSG measurements on layered materials indicated that the SSG starts to register the stiffness of an upper-layer material of 125 mm or thicker and the effect of the lower material may continue to be present even at an upper-layer material thickness of 275 mm, depending on the relative stiffness (or contrast) of the layer materials. A comparison of the moduli of a test sand obtained from the SSG with the moduli obtained from other tests, on the basis of comparable stress and strain amplitudes, indicated that SSG modulus appears to be corresponding to a strain amplitude larger than the strain amplitude of the seismic test, even though the SSG induces a strain amplitude comparable to that of seismic test. Based on the ratio between modulus from the seismic test and modulus from SSG test obtained in this study and others (Chen & Bilyeu, 1999; Sawangsuriya *et al.*, in prep.), it seems that the modulus reported by the SSG has been reduced internally by a factor.

To further verify the boundary effects on the SSG stiffness measurement, the numerical studies using a finite-element analysis (FEA) were employed in this study. To further verify the layering effect, a series of flowable fill specimens were prepared in two layers with different stiffnesses and variable thicknesses. Results obtained from this study were in good agreement with those obtained in the previous research (Sawangsuriya *et al.*, 2002). The FEA shows that the radius of influence extends to about 0.3 m away from the center of SSG measurement. Significant boundary effects are expected based on a numerical analysis of measurements made in a 152-mm diameter Proctor mold. This observation is also in agreement with the results from the experimental investigation reported in Lenke *et al.* (2003). They conclude that a target value of SSG stiffness using Proctor mold is not successful because of the dynamic nature of SSG measurement and associated boundary effects caused by the small volume of soil in relation to the size of the SSG's annular foot. The experimental study on the flowable fill specimens suggests that the SSG starts to output the stiffness of an upper-layer material when its thickness is greater than 125 mm. Due to its operation simplicity and robustness, the SSG is considered as an alternative tool for assessing soil stiffness at small strains; however, caution needs to be exercised when the SSG is to be used in the laboratory and field tests as the boundary and layering effects might influence the stiffness output from the SSG.

ACKNOWLEDGMENTS

This research was funded in part by the Wisconsin Highway Research Program (WHRP). The senior author gratefully acknowledges the financial support through a scholarship from the Royal Thai Government. This paper does not endorse or approve any commercial product, even though trade names may be cited, does not reflect official views or policies of the WHRP (WisDOT), and does not constitute a standard specification or regulation of this agency.

REFERENCES

Chen, D.-H. & Bilyeu, J. 1999. Comparison of Resilient Moduli Between Field and Laboratory Testing: A Case Study. *The 78th Annual Meeting of Transportation Research Board* (in CD-ROM).

Dolen, T.P. & Benavidez, A.A. 1998. Properties of Low-Strength Concrete for Meeks Cabin Dam Modification Project, Wyoming. *The Design and Application of Controlled Low-Strength Materials (Flowable Fill), ASTM STP* 1331: 213-227.

Hardin, B.O. & Drnevich, V.P. 1972. Shear Modulus and Damping in Soils: Design Equations and Curves. *Journal of the Soil Mechanics and Foundations Division* 98(7): 667-692.

Humboldt Soil Stiffness Gauge (GeoGauge) User Guide: Version 3.3. 1999. Humboldt Mfg. Co.

Jaky, J. 1944. The Coefficient of Earth Pressure at Rest. *Journal of the Society of Hungarian Architects and Engineers* 7: 355-358.

Lenke, L.R., Pak, R.Y.S. & Ko, H.-Y. 1991. Boundary Effects in Modeling Foundations Subjected to Vertical Excitation. *Proceedings of the International Conference on Centrifuge*: 473-480.

Lenke, L.R., McKeen, R.G. & Grush, M.P. 2003. Laboratory Evaluation of the GeoGauge for Compaction Control. *Transportation Research Record* 1849: 20-30.

Ooi, P.S.K. & Pu, J. 2003. Use of Stiffness for Evaluating Compactness of Cohesive Pavement Geomaterials. *Transportation Research Record* 1849: 11-19.

PLAXIS Finite Element Code for Soil and Rock Analysis: Version 7.2. 1998. A. A. Balkema, Rotterdam.

Sawangsuriya, A., Bosscher, P.J. & Edil, T.B. 2002. Laboratory Evaluation of the Soil Stiffness Gauge. *Transportation Research Record* 1808: 30-37.

Sawangsuriya, A., Edil, T.B. & Bosscher, P.J. 2003. Relationship Between Soil Stiffness Gauge Modulus and Other Test Moduli for Granular Soils. *Transportation Research Record* 1849: 3-10.

Sawangsuriya, A., Bosscher, P.J. & Edil, T.B. Application of Soil Stiffness Gauge in Assessing Small-Strain Stiffness of Sand with Different Fabrics and Densities. Submitted to Geotechnical Testing Journal, ASTM International (in prep.).

Proceedings of the 16th International Conference on Soil Mechanics and Geotechnical Engineering 2005, Osaka, Japan

Earthwork quality control using soil stiffness

Controle de la qualite des ouvrages en terre par la mesure de la rigidite

T. Edil & A. Sawangsuriya
Department of Civil and Enviromental Engineering, University of Wisconsin-Madison, Wisconsin, U.S.A.

ABSTRACT

The quality of the engineered earthwork depends on the suitability and compaction of the materials used. Earthwork compaction acceptance criteria typically are based on adequate dry density achieved through proper moisture content and compaction energy. This paper presents the implementation of a non-destructive testing device called the soil stiffness gauge (SSG) for construction quality and design parameter control of earthwork

RÉSUMÉ

La bonne tenue des ouvrages en terre dépend considérablement de l'aptitude au compactage des matériaux utilisés. Les critères d'acceptation du compactage sont typiquement basés sur une correcte densité sèche, suffisamment atteinte à la fois par une teneur en eau et une énergie de compactage adéquates. Ce article présente l'implémentation d'un appareil expérimental non destructif appelé «Soil Stiffness Gauge – SSG» utilisé pour contrôler la qualité de la conception et de la mise en œuvre des remblais en terre.

1 INTRODUCTION

The quality of the engineered earthwork depends on the suitability and compaction of the materials used. Earthwork compaction acceptance criteria typically are based on adequate dry density of the placed earthen materials achieved through proper moisture content and compaction energy. According to this approach, by achieving a certain dry density using an acceptable level of compaction energy assures attainment of an optimum available level of structural properties and also minimizes the available pore space and thus future moisture changes. Conventional approach is also based on the premise that monitoring dry density as opposed to a structural property is relatively simple and can be applied to generate data for a statistical evaluation of compaction quality. However, monitoring compaction quality through density measurements, including nuclear moisture-density gauge and sand cone density test, are generally time consuming, labor intensive, and costly. Furthermore, the question of the achieved structural property, which is the ultimate objective of quality control, remains unfulfilled. In important projects, various laboratory and field tests are employed to relate the achieved level of compaction to structural properties. These tests are often limited in number and do not yield a statistical basis of earthwork quality. The difficulty and expense of acquiring quality relevant engineering properties such as stiffness have traditionally caused engineers to rely on discrete density tests. The relative compaction alone is not a reliable indicator of the soil mechanical property (i.e., stiffness and strength). Moreover, the soil density is only a quality index used to judge compaction acceptability and is not the most relevant property for engineering purposes. For compacted highway, railroad, airfield, parking lot, mat foundation, subgrades and support fills, the ultimate engineering parameter of interest is often the soil stiffness and (or) modulus, which is a direct structural property for determining load support capacity and deformation characteristic in engineering design.

Stiffness of compacted soils depends on density and moisture but also on soil texture which varies along the roadway route or in different parts of a burrow pit. The conventional approach of moisture-density control, however, does not reflect the variability of the soil texture and fabric and hence its stiffness. Even if the soil layers satisfy a compaction quality control requirement based on density testing, a large variability in soil stiffness can still be observed (Sargand et al., 2000; Nazarian & Yuan, 2000). Additionally, the comparison between density and stiffness tests suggests that conventional density testing cannot be used to define subtle changes in the modulus of the compacted earth fills (Fiedler et al., 1998). Soil stiffness is a more sensitive measure of the texture and soil fabric uniformity than density. Since the non-uniformity of stiffness is directly related to progressive failures and life-cycle cost, a simple, rapid, and direct stiffness testing which can be conducted independently and in conjunction with conventional moisture-density testing without interference with the construction process is anticipated to increase test coverage, to improve statistical evaluation, and to reduce variability, thus substantially enhance construction quality control of the entire earthwork.

This paper presents the implementation of soil stiffness in practice for construction quality control of earthwork. A non-destructive testing device called the soil stiffness gauge (SSG) exhibits potential for adaptation to earthwork control and is therefore employed to assess the soil stiffness of various materials used in earthwork from different construction sites around the state of Wisconsin, U.S.A. along with the conventional compaction control tests such as nuclear moisture-density gauge and gravimetric moisture content measurement. Use of SSG both for compaction quality control and for design parameter control is presented.

2 IN SITU TEST METHODS FOR SOIL STIFFNESS ASSESSMENT DURING CONSTRUCTION

A number of dynamic non-destructive testing methods to assess in situ soil stiffness have become increasingly available (Lytton, 1989; Siekmeier et al., 1999; Stokoe & Santamarina, 2000; Livneh & Goldberg, 2001; Müller, 2003). A portable device for assessing soil stiffness should not interfere with the construction process but rapidly provide reliable stiffness values. In other words, the measuring device must allow considerably more tests than the conventional moisture-density testing.

The SSG provides direct, simple, and rapid means of stiffness assessment. The SSG is a portable, non-nuclear, and non-destructive testing device that employs an electro-mechanical means. Additional information and operation of the SSG is given in Humboldt (1999a). The test is conducted in accor-

dance with ASTM D 6758, Standard Test Method for Measuring Stiffness and Apparent Modulus of Soil and Soil-Aggregate In-Place by an Electro-Mechanical Method and takes a few minutes to conduct with automatic data acquisition. Sawangsuriya et al. (2002; 2004b) showed that the SSG measures the stiffness of a finite volume of soil below surface. The zone of SSG measurement influence was estimated to be less than 300 mm lateral distance and a maximum depth of approximately 300 to 380 mm. The effect of layered materials on SSG measurements indicated that the SSG starts to register the stiffness of an upper-layer material of 125 mm or thicker and the effect of the lower material may continue to be present even at an upper-layer material thickness of 275 mm, depending on the relative stiffness (or contrast) of the layer materials (Sawangsuriya et al., 2002; 2004b).

3 COMPACTION QUALITY CONTROL

Subgrade soils from seven highway construction sites in Wisconsin, U.S.A. were monitored in terms of their stiffness, dry unit weight, and moisture content (Sawangsuriya & Edil, 2004). The subgrade soils consisted of predominantly granular natural earthen materials with fines content (percent passing No 200 sieve, 0.075 mm size) up to 35% (USCS designations of SC, SC-SM, SP-SM) and also predominantly fine-grained soils with fines content greater than 59% (USCS designations of CL). Tested materials also included industrial by-products such as granular coal combustion bottom ash, foundry slag, and foundry sand (with bentonite mixed). There was also a fly ash stabilized fine-grained soil and a crushed rock of predominantly gravel size (termed "breaker run"). Some of the soils were tested after they were compacted in the field and some were in natural uncompacted state (Sawangsuriya & Edil, 2004).

Fig. 1 shows the relationship of the state of density (i.e., relative compaction, RC defined as the ratio of the field dry unit weight divided by the laboratory maximum standard Proctor dry unit weight) to the deviation of moisture content from the respective optimum moisture content ($w\text{-}w_{opt}$) for the natural subgrade soils tested. Typical compaction specifications call for RC ≥ 95%. Most of the RC of field compacted soils are from 90 to 112.5% with moisture contents dry of the optimum moisture content, whereas uncompacted soils (all CL soils) in their natural state exhibit low dry densities and much wider moisture contents including some wet of the optimum. Furthermore, RC decreases with increasing $w\text{-}w_{opt}$. Fig. 2 shows the variation of SSG stiffness (K_{SSG}) with $w\text{-}w_{opt}$ for the natural subgrade soils. Strong dependency of stiffness on moisture content is evident as stiffness varies from 2 to 12 MN/m for a moisture content deviation of about ±8% of the optimum moisture content. The compacted soils have moisture contents mostly dry of optimum. Of course, there are other factors that may affect stiffness such as dry density, texture, and soil fabric and they cause the spread in K_{SSG} for a given moisture content.

In the case of subgrade soils subjected to the same state of stress (i.e., near-surface), moisture content and dry unit weight of a test soil play significant role on its stiffness and their effects are hard to uncouple. To account for the effect of moisture content, K_{SSG} is divided by ($w\text{-}w_{opt}$). This normalized stiffness is plotted versus RC in Fig. 3. The normalized stiffness varies very little with relative compaction for compacted soils with an average value of -2.4, which can be used to estimate K_{SSG} of a wide variety of properly compacted soils. A larger variation is observed for uncompacted soils perhaps due to their more complex fabric. The implication of this for compacted soils with the typically rather narrow range of RC is that the effect of dry unit weight on stiffness is relatively minor compared to moisture content.

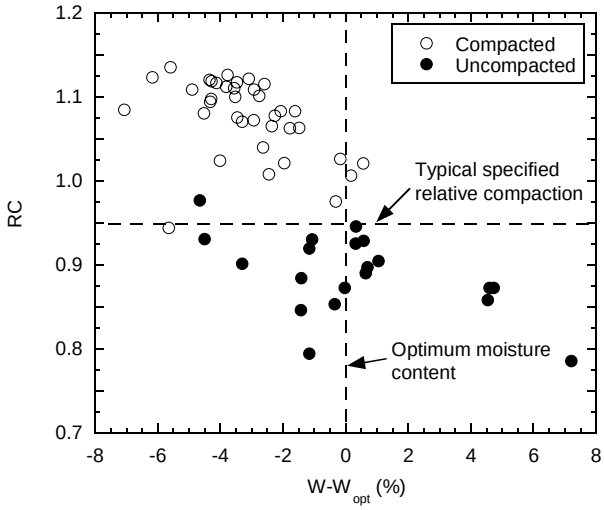

Figure 1. Relative compaction vs. deviation of moisture content from the optimum moisture content for natural earthen materials.

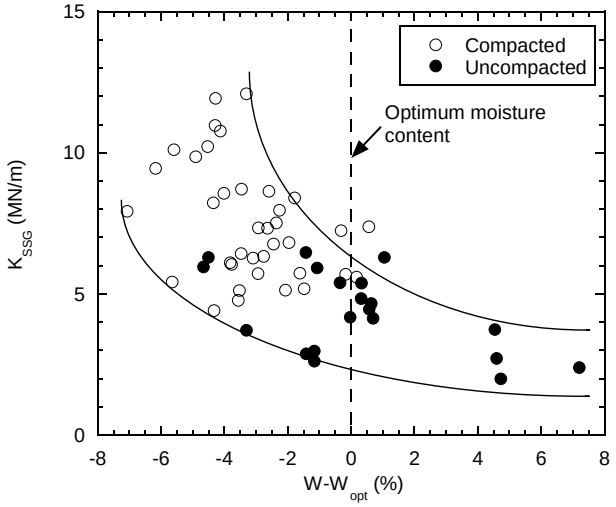

Figure 2. SSG stiffness vs. moisture content variance for natural earthen materials.

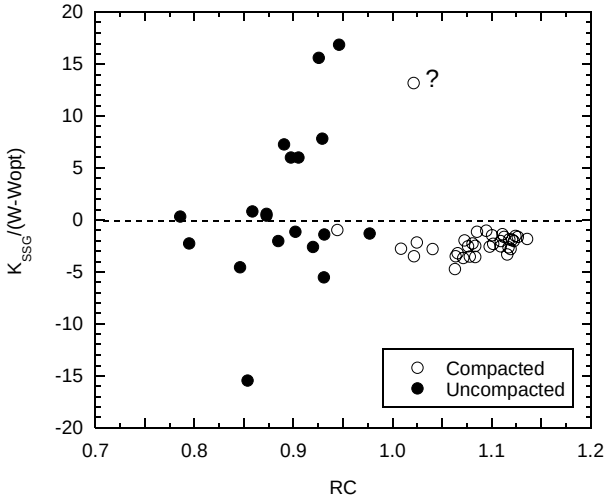

Figure 3. Normalized SSG stiffness vs. relative compaction.

According to the manufacturer, the SSG can be also used to estimate the dry unit weight from soil stiffness and an independently measured moisture content using the following analytical-empirical relationship given in Eq. 1 (Humboldt, 1999b) and thus eliminating the need for a nuclear density gauge. Since stiffness is dependent on both moisture content and dry unit weight, the moisture content must be independently acquired in conjunction with the stiffness measurement for this purpose.

$$\gamma_d = \frac{\gamma_o}{1+1.2\left(\frac{wC}{K_{SSG}}-0.3\right)^{0.5}} \quad (1)$$

where γ_o is the idealized void-free unit weight, C is a stiffness- and moisture-dependent parameter, which is defined based on a linear relationship between C and K_{SSG}/w obtained from companion stiffness, moisture content, and dry unit weight measurements, and the other terms are as defined before. Stiffness, moisture content, and dry unit weight of various materials including industrial by-products, natural earthen materials, and fly ash stabilized soils tested were used to establish such a relationship as shown in Fig. 4. The relationship for C in terms of K_{SSG}/w given in Fig. 4 for the materials tested in this investigation is comparable in slope but slightly different in intercept from the one given by Humboldt (1999b) (i.e., the intercept is 15.41 instead of 21.01). From the measured SSG stiffness, measured gravimetric moisture content, and parameter C from Fig. 4, the dry unit weights were estimated and compared to those measured from the nuclear density gauge in Fig. 5. Compared to the line of equality, all fine-grained soils have lower estimated dry unit weights than those measured using the nuclear gauge. There is a large dispersion of the data. A comparison of gravimetric moisture contents (determined by drying a sample) with those obtained from the nuclear density gauge showed that the latter being consistently lower (Sawangsuriya & Edil, 2004). This also may be contributing to the dispersion of the data. It appears that more evaluations are needed to rely solely on dry density estimated from the stiffness measurement for construction density control. However, if this approach is reliably established, SSG can replace nuclear density device as long as moisture content is also measured. The implementation of Moisture Gauge along with SSG may be considered as a promising means for the moisture content determination in the field.

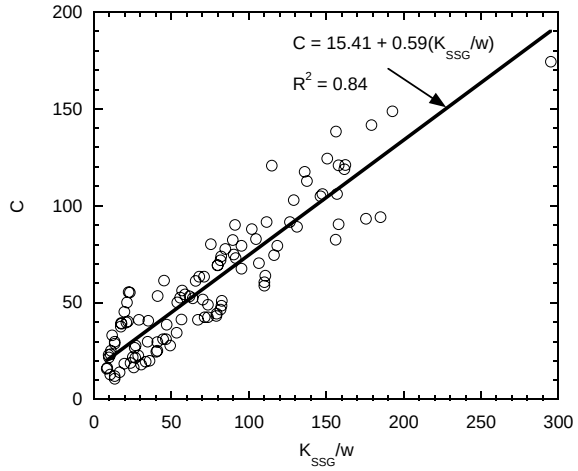

Figure 4. Relationship of C and K_{SSG}/w.

4 DESIGN PARAMETER CONTROL

In general, either the stiffness or strength of compacted earthwork is needed for design. In subgrade and subbase layers for pavement systems, typical structural property used is resilient modulus (elastic modulus under repetitive loading) and/or California Bearing Ratio (CBR). Modulus of soils can be assessed by a variety of methods and it varies with confining stress and strain amplitude. For design, a modulus corresponding to the stress and strain amplitude as well as the moisture state expected under the operating conditions is needed. SSG stiffness can be converted to an elastic modulus obtained near-surface at the moisture conditions prevailing during the measurement with an assumption of Poisson's ratio (Humboldt, 1999a). It is therefore not a modulus necessarily can be used directly in design. However, it can be used to control the structural uniformity of the earthwork and can be also viewed as an index of design modulus. In other words, the SSG stiffness or modulus can be indirectly employed as to control mechanical property for the design.

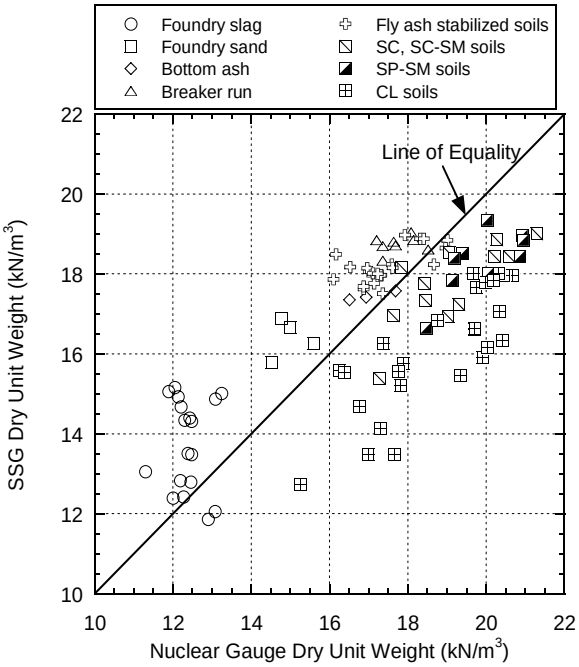

Figure 5. Comparison of dry unit weight from the SSG and the nuclear gauge.

Laboratory tests were performed to establish the general relationship of the SSG modulus with the moduli obtained from other tests on a dry sand and presented on a modulus degradation curve in Fig. 6 (Sawangsuriya et al., 2003). These moduli were determined at the same stress level (confining pressure of 2.6 kPa) over a range of strain amplitudes. The relationship of the SSG modulus to other moduli and particular to the resilient modulus can be seen. Using the modulus degradation curve, the SSG modulus can be adjusted to the modulus at any desired strain level and using the theory stress effects can be taken into account. Alternatively, a modulus ratio can be determined between the SSG modulus and the design modulus on the basis of laboratory tests. Knowing the modulus ratio, the design modulus can be reasonably determined from the measured SSG modulus (Sawangsuriya et al., 2004a). In addition to the modulus variation due to differences in stress and strain levels, one must make the necessary reductions in modulus due to local climatic (i.e., moisture) effects to arrive a design value.

A relationship between the shear strength of soils in term of the CBR and K_{SSG} was given by Sawangsuriya and Edil (2005) as follows.

$$CBR = 0.59K_{SSG}^{1.23};\ R^2 = 0.74 \quad (2)$$

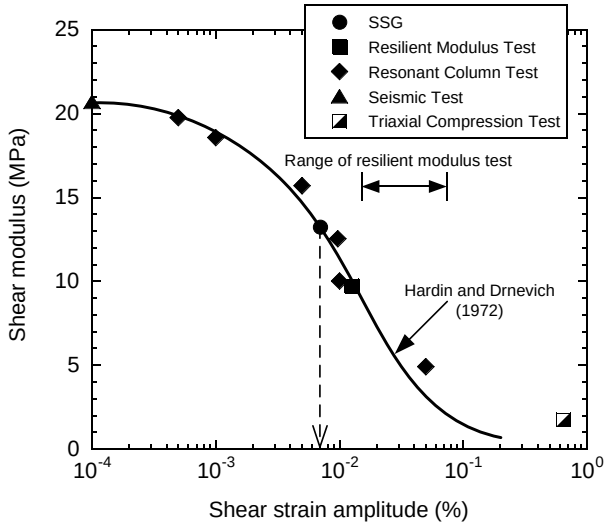

Figure 6. Modulus from different tests (Sawangsuriya et al., 2003).

Using such a relationship, the SSG stiffness can be directly converted to a design CBR and vice versa. Consequently, the CBR value can be used indirectly to control the design soil strength, which is more important during the construction stage. Note that this CBR value can be either obtained in the laboratory or by using the Dynamic Cone Penetrometer (DCP) such that there exists a widely accepted correlation between the DCP penetration index (DPI) and CBR (Webster et al., 1992; Livneh et al., 1995).

5 SUMMARY AND CONCLUSIONS

This paper presents the implementation of a non-destructive testing device called the soil stiffness gauge (SSG) for construction quality as well as design parameter control of earthwork. Use of the convenient SSG in conjunction with conventional moisture-density measurements enhances quality control by achieving more uniform structural property and aids developing a design modulus. SSG stiffness normalized by the deviation of compaction moisture content from the optimum moisture content is remarkably constant around a value equal to -2.4 for compacted natural earthen materials. There is potential for using SSG alone with an independent moisture measurement for both density and stiffness control with further evaluation.

ACKNOWLEDGEMENTS

Financial support for the study describe in this paper was provided by the Wisconsin Department of Transportation (WisDOT). Additionally, Mr. A. Sawangsuriya received financial support through a scholarship from the Royal Thai Government. The conclusions are those of the authors and do not reflect the opinions or policies of WisDOT.

REFERENCES

Fiedler, S. A., Nelson, C. R., Berkman, E. F. and DiMillio, A. F. 1998. Soil stiffness gauge for soil compaction control, *Public Roads*, U.S. Department of Transportation, Federal Highway Administration.

Humboldt Mfg. Co. 1999a. *Humboldt soil stiffness gauge (geogauge) user guide: version 3.3*, Norridge, IL.

Humboldt Mfg. Co. 1999b. *Report estimating dry density from soil stiffness and moisture content*, Norridge, IL.

Livneh, M., Ishao, I., and Livneh, N. A. 1995. Effect of vertical confinement on dynamic cone penetrometer strength values in pavement and subgrade evaluations, *Transportation Research Record 1473*, 1-8.

Livneh, M. and Goldberg, Y. 2001. Quality assessment during road formation and foundation construction: use of falling-weight deflectometer and light drop weight, *Transportation Research Record 1755*, 69-77.

Lytton, R. L. 1989. Backcalculation of layer moduli –state of the art, *Nondestructive Testing of Pavements and Backcalculation of Moduli, ASTM STP 1026*, 7-38.

Müller, C. 2003. *The light falling weight device: a new and innovative compaction testing method –theory and practice*, M.S. Thesis, Institute for Ground Engineering and Soil Mechanics, Vienna University of Technology, Austria.

Nazarian, S. and Yuan, D. 2000. Quality control of compacted layers with field and laboratory seismic testing devices, *Constructing and Controlling Compaction of Earth Fills, ASTM STP 1384*, 311-324.

Sargand, S. M., Masada, T., and Wasniak, D. L. 2000. Variability of initial subgrade modulus at Ohio SHRP test road, *Constructing and Controlling Compaction of Earth Fills, ASTM STP 1384*, 274-289.

Sawangsuriya, A., Bosscher, P. J., and Edil, T. B. 2002. Laboratory evaluation of the soil stiffness gauge, *Transportation Research Record 1808*, 30-37.

Sawangsuriya, A., Bosscher, P. J., and Edil, T. B. 2004a. Application of soil stiffness gauge in assessing small-strain stiffness of sand with different fabrics and densities, *Submitted to Geotechnical Testing Journal*, ASTM.

Sawangsuriya, A. and Edil, T. B. 2004. *Investigation of the DCP and SSG as alternative methods to determine subgrade stability*, Report No. 0092-01-05, Wisconsin Department of Transportation, Madison, WI, 93p.

Sawangsuriya, A. and Edil, T. B. 2005. Use of the soil stiffness gauge and dynamic cone penetrometer for pavement materials evaluation, *Geotechnical Engineering*, Institution of Civil Engineers, U.K. (accepted for publication).

Sawangsuriya, A., Edil, T. B., and Bosscher, P. J. 2003. Relationship between soil stiffness gauge modulus and other test moduli for granular soils, *Transportation Research Record 1849*, 3-10.

Sawangsuriya, A., Edil, T. B., and Bosscher, P. J. 2004b. Assessing small-strain stiffness of soils using the soil stiffness gauge, *Proceedings of the 15th Southeast Asian Geotechnical Society Conference*, 101-106.

Siekmeier, J. A., Young, D., and Beberg, D. 1999. Comparison of the dynamic cone penetrometer with other tests during subgrade and granular base characterization in Minnesota, *Nondestructive Testing of Pavements and Backcalculation of Moduli, ASTM STP 1375*, 175-188.

Stokoe, K. H., II and Santamarina, J. C. 2000. Seismic–wave–based testing in geotechnical engineering –state of the art, *GeoEng 2000*, 1490-1536.

Webster, S. L., Grau, R. H., and Williams, T. P. 1992. *Description and application of dual mass dynamic cone penetrometer*, Instruction Report GL-92-3, U.S. Army Engineers Moistureways Experiments Station, Vicksburg, MS, 17 p.

Apparent shear strain for SSG modulus

Proceedings of the 13th Annual Great Lakes Geotechnical and Geoenvironmental Engineering Conference 2005, Milwaukee, WI

ALTERNATIVE TESTING TECHNIQUES FOR MODULUS OF PAVEMENT BASES AND SUBGRADES

Auckpath Sawangsuriya[1], Peter J. Bosscher[2], P.E., Member, ASCE, Tuncer B. Edil[2], P.E., Member, ASCE

ABSTACT: The importance of stiffness measurements has gained increased recognition in geotechnical applications in pavements. Two alternative testing techniques: bender elements and soil stiffness gauge (SSG) have been recently adopted as they show some potential and promising means of monitoring the stiffness and/or modulus of pavement materials. Since each technique has its own range of stress and strain levels, the relationship between the elastic moduli and nonlinear behavior exhibited by soils at large strains is required so that the measured modulus can be adjusted or corrected to a modulus corresponding to the desired strain levels. This paper presents the implications of these testing techniques in stiffness and/or modulus assessment of pavement bases and subgrades. To adjust the modulus measured in these materials, the desired strain amplitudes must be known. The strains incurred in the pavement base and subgrade layers that are subjected to the typical traffic loadings are summarized from a number of studies including finite-element analyses, large-scale model experiments, and in-situ test sections. The typical range of strain amplitudes imposed by the bender elements and the SSG is compared with those incurred in the pavement base and subgrade layers to evaluate their suitability in the assessment of pavement layer stiffness and/or modulus. Finally, some comments on the practical implications of these techniques to monitor the pavement layer stiffness and/or modulus are provided.

[1] Graduate Research Assistant, Department of Civil and Environmental Engineering, University of Wisconsin-Madison, Madison, WI 53706, sawangsuriya@wisc.edu

[2] Professor, Department of Civil and Environmental Engineering and Geological Engineering Program, University of Wisconsin-Madison, Madison, WI 53706.

INTRODUCTION

For proper design of a pavement, the stress and strain conditions within the pavement structure due to traffic loading must be determined. The states of stress and strain are not only a function of the traffic loading but also of the moduli of the various pavement layers whereas these moduli are in turn a function of the stress state. Stiffness and/or modulus are the engineering properties that are needed for the evaluation of the long-term pavement performance. In pavement engineering, the resilient modulus is a laboratory measure of the elastic modulus of soil under various states of stress common within pavement layers and has been commonly adopted as the important property for characterizing pavement materials especially the design of flexible pavements. The test generally consists of a number of loading steps, where the specimen is subjected to different confining pressures and deviator stresses at each step as well as a number of loading cycles. In addition to the resilient modulus test, the alternative testing techniques such as the soil stiffness gauge and the bender elements can be chosen as the supplementary tests for characterizing pavement materials. The objective of this paper is to describe the implications of these alternate methods for obtaining moduli for pavement bases and subgrades.

ALTERNATIVE TESTING TECHNIQUES FOR SOIL MODULUS

In additional to the resilient modulus test commonly used in pavement design, two currently available modulus tests are considered as alternative testing techniques. The first method is to employ bender elements to measure the travel time of an elastic wave propagating through the soil. This method is robust in that it can be combined with a variety of geotechnical laboratory tests and also shows a great potential for future use in monitoring the stiffness at small-strains by utilizing the characteristic of elastic wave propagation in different media. The second method is to utilize the soil stiffness gauge (SSG), which has been developed to measure the in-place surficial soil stiffness by means of electro-mechanical vibration. A brief description of each method is given below.

Bender Elements

An elastic wave propagation technique that utilizes two-layer piezoceramic bender elements as source and receiver provides a means of measuring the shear wave velocity and the corresponding small-strain shear modulus. The bender element test has become increasingly popular in a variety of geotechnical laboratory applications (Dyvik and Madshus 1985; Thomann and Hryciw 1990; Souto et al. 1994; Fam and Santamarina 1995; Zeng and Ni 1998; Fioravante and Capoferri 2001; Pennington et al. 2001; Mancuso et al. 2002). The transmitting bender element produces a shear wave (S-wave) which propagates through the soil when it is excited by an applied voltage signal. This S-wave impinges on the receiving bender element, causing it to bend, which in turn produces a very small voltage signal. Fig. 1 illustrates typical input and output signals from the transmitting and receiving bender elements.

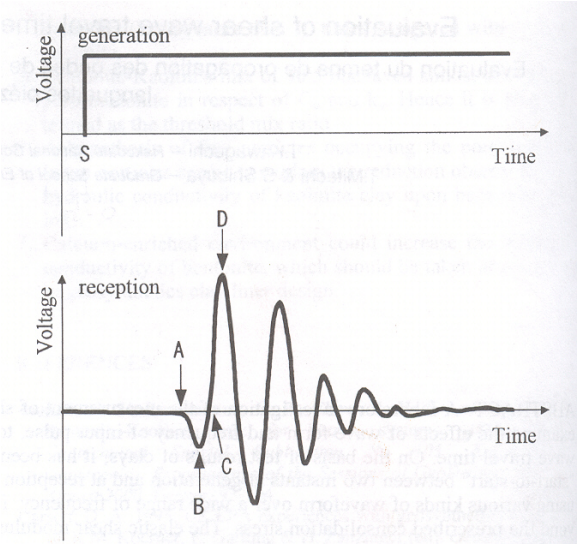

FIG. 1. Typical input and output signals from the transmitting and receiving bender elements

In general, the signals may be different from those in Fig. 1, possibly due to the stiffness of the soil, the boundary conditions, the test apparatus, the degree of fixity of the bender element into the platen or housing, and the size of the bender element and specimen. By measuring the travel time of the S-wave and the tip-to-tip distance between transmitting and receiving bender elements, the S-wave velocity of the soil is obtained. The small-strain shear modulus (G) can be calculated according to elastic theory using the measured S-wave velocity (v_s) and total density of the soil (ρ) with the relationship $G = \rho v_s^2$.

Soil Stiffness Gauge

A recently developed equipment called the soil stiffness gauge (SSG) is a portable, non-nuclear, and non-destructive testing device that provides an alternative means of rapidly and directly assessing in-place surficial stiffness and/or modulus of soils at small strains. Unlike other modulus tests, the operation of the SSG is relatively simple and does not require a skilled operator. Moreover, this device has built-in capability to make computations in order to acquire the stiffness and/or modulus of test materials. Further information and operation of the SSG is provided by Humboldt (1999). The test is conducted in accordance with ASTM D 6758, Standard Test Method for Measuring Stiffness and Apparent Modulus of Soil and Soil-Aggregate In-Place by an Electro-Mechanical Method. Because of its rapid and direct measurement, the SSG appears to have real potential as a supplementary non-nuclear method for earthwork quality control (Edil and Sawangsuriya 2005). The modulus from the SSG appears to correspond to a strain amplitude larger than the strain amplitude of the seismic test, even though the SSG induces a strain amplitude comparable to that of a seismic test (Sawangsuriya et al. 2003). It looks as if the modulus reported by the SSG has been internally reduced by a factor (Sawangsuriya

et al. 2003; 2004) possibly to correspond to the resilient modulus. However, this is not disclosed by the manufacturer.

RESULTS AND ANALYSIS OF MODULUS TESTS

Modulus from Bender Elements

A bender element test was performed on a specimen 36 mm in diameter and 78 mm high subjected to a range of confining pressures. The base and top cap were modified to include the transmitting and receiving bender elements respectively inserted in the soil specimen. In order to verify the bender element test, the test was initially conducted on dry Ottawa 20-30 sand, for which published modulus data are available. Note also that in this study, the travel time of the S-wave is determined on the basis of time-domain analysis in such a way that the first arrival in output signal is determined manually. The first arrivals corresponding to points B and C (Fig. 1) were chosen for the determination of the travel time in order to avoid the near-field effect in a triaxial specimen due to wave reflection from the cap boundaries (Arulnathan et al. 1998). This near-field effect may mask the arrival of the S-wave when the distance between the source and receiver (d) is in the range ¼ to 4 wavelengths (λ), which can be estimated from $\lambda = v_s/f$ where v_s is the S-wave velocity and f is the mean frequency of the received signal (Mancuso and Vinale 1988). In this study, the ratio d/λ ranged from 1.6 to 2.5.

Fig. 2 shows the plot of shear modulus obtained from the bender element (BE) tests as a function of confining pressure. Results from the bender element tests were also compared with those from the resonant column (RC) tests which were conducted at two shear strain levels, $5x10^{-3}$ and $1x10^{-2}$%. Note that the resonant column tests were conducted on an identically prepared specimen in terms of dry density and method of preparation. The shear modulus of this sand was also computed using the empirical equations given by Hardin and Black (1968) and Seed and Idriss (1970). The shear moduli obtained from the bender element test, the resonant column test, and the empirical equations are compared as shown in Fig. 2. Results indicated good agreement with those suggested by Hardin and Black (1968) and Seed and Idriss (1970).

Another series of bender element tests were conducted on dry medium sand specimens (36 mm in diameter and 78 mm high). Five methods of specimen preparation: (1) scooping, (2) tamping, (3) rodding, (4) vibrating, and (5) pluviating were used. Details of these methods are described in Sawangsuriya et al. (2004). Fig. 3 shows the plot of shear modulus of these sands prepared by these five methods as a function of confining pressure. The shear moduli of sands as measured by the bender element (BE) tests follow the general dependency of modulus on confining stress. Results obtained from the resonant column (RC) tests at two shear strain amplitudes (i.e., $5x10^{-3}$ and $1x10^{-2}$%) are also shown in Fig. 3 (results of replicate testing). The modulus-confining stress relationships obtained from the BE tests compare well with those from the RC tests. In general, the moduli from the BE tests are greater than those from the RC test at shear strain amplitude of $1x10^{-2}$%.

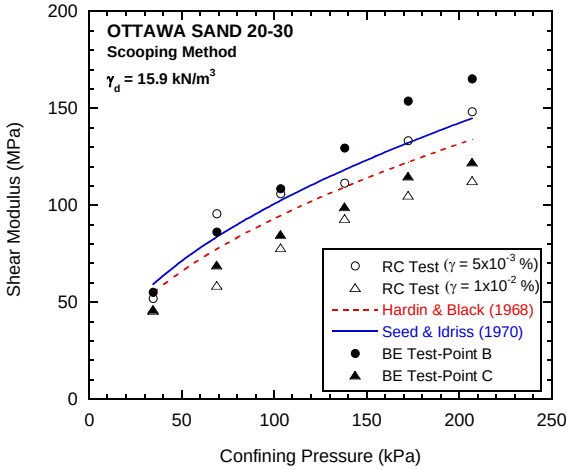

FIG. 2. Shear modulus vs. confining pressure relationship for dry Ottawa 20-30 sand

Modulus from the SSG

Dry medium sand was placed in a 0.3-m radius cylindrical cardboard mold to a height of 530-mm following the five methods described above for the SSG and seismic tests (Sawangsuriya et al. 2004). The SSG test was conducted at the center of the top of the specimens. For the rigid ring-shaped foot of the SSG resting on sand, the measured stiffness of sand (K_{SSG}) from the SSG can be converted to the shear modulus (G) as follows (assuming a linear-elastic, homogeneous, and isotropic infinite half-space which is appropriated for small strains induced by the SSG):

$$G = \frac{K_{SSG}(1-\nu)}{3.54R} \tag{1}$$

where ν is the Poisson's ratio of the soil and R is outside radius of the ring-shaped foot of the SSG.

Comparison of Measured Modulus with Maximum Modulus

The modulus from the bender element and the SSG tests are compared with the maximum modulus (denoted by G_o or G_{max}), which establishes a benchmark value of modulus for deformation problems (Burland 1989). This maximum modulus defines the starting point of a modulus degradation curve (the variation of the modulus with log strain amplitude) and is useful for defining the initial modulus of an empirical stress-strain curve for nonlinear models of soil behavior (Hardin and Drnevich 1972; Jardine et al. 1986; Jardine and Potts 1988; Tatsuoka et al. 1993).

In this study, G_o for the sand specimens prepared by the five methods of specimen preparation was obtained using a pulse echo test. The pulse echo test was performed after the SSG test. A compressional wave (P-wave) was generated by an impulse source at the top of the sand specimens using a hand-held hammer and an aluminum

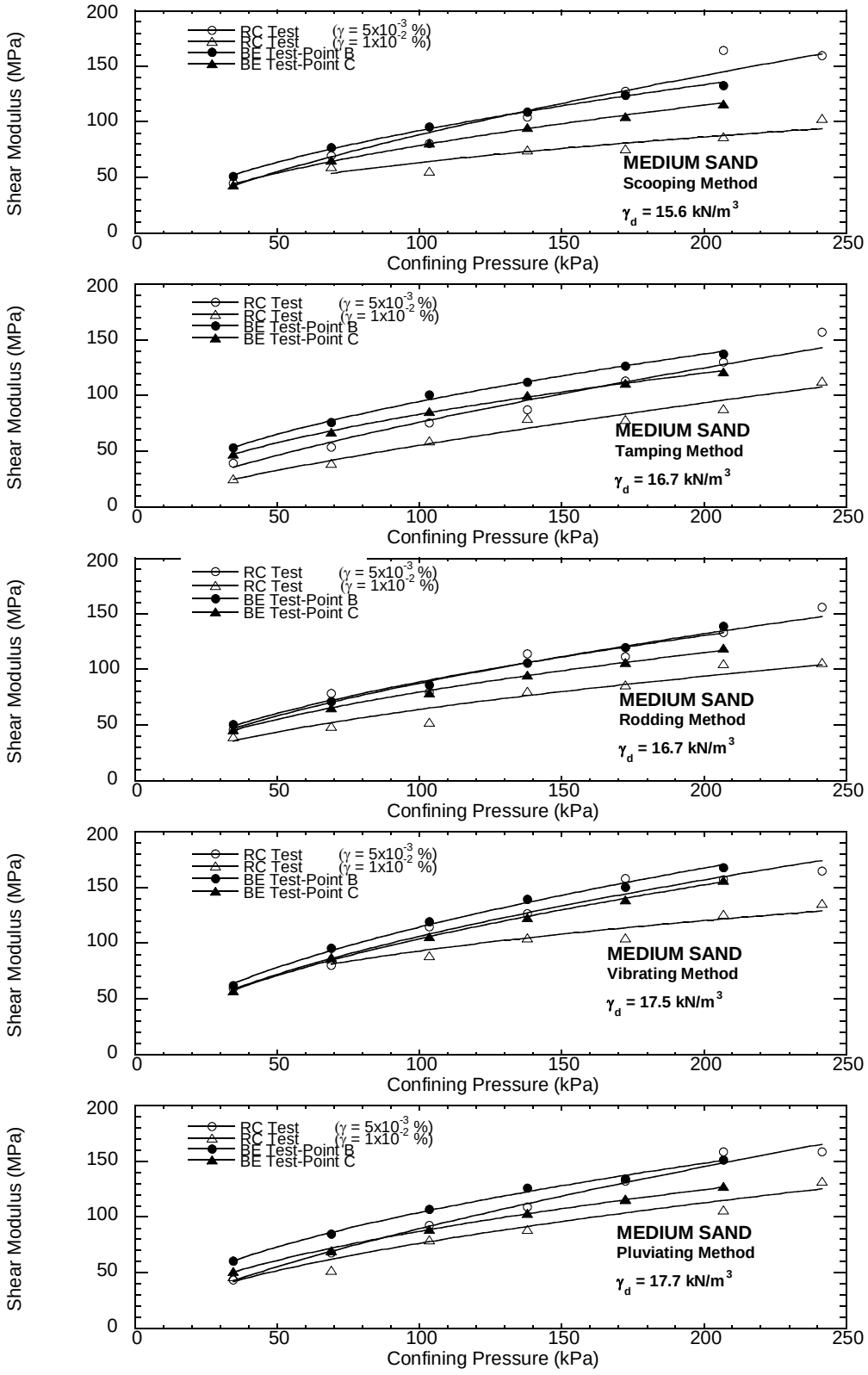

FIG. 3. Shear modulus vs. confining pressure relationship of sands prepared by five methods: scooping, tamping, rodding, vibrating, and pluviating

plate. This P-wave travels along the specimen and is then received by the geophone, which was attached to another aluminum plate located at the bottom of the mold. The travel time of the P-wave from the source to the receiver was recorded by an oscilloscope. Based on the travel time of P-wave and the distance between source and the receiver, the P-wave velocity was calculated. Knowing the density of the specimen and the estimated Poisson's ratio (ν), the Young's modulus and the corresponding shear modulus of the sand specimen for were determined.

Shear moduli of sands obtained from the bender element and the SSG tests are compared with those obtained from the pulse echo tests in Fig. 4. Note that the shear

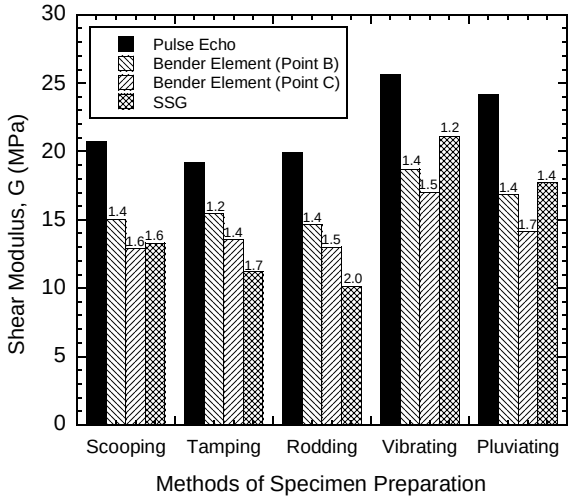

FIG. 4. Comparison of shear modulus of sands prepared by five methods

moduli obtained from the bender elements are extrapolated estimates at the stress level comparable to that induced by the SSG and the pulse echo tests (i.e., 2.6 kPa). The shear moduli obtained from the pulse echo test are consistently higher than those obtained from the bender element tests. However, inconsistency was observed between the shear moduli obtained from the bender elements and the SSG. The ratios of modulus obtained from the pulse echo test to that from the bender elements range 1.2-1.4 for the travel time of S-wave taken at point B and 1.4-1.7 taken at point C, whereas the modulus ratios between the pulse echo and the SSG range 1.2-2.0 (noted above the bars in Fig. 4).

STRAIN LEVELS IN PAVEMENT BASES AND SUBGRADES

The strains induced in the pavement bases and subgrades that are subjected to the typical traffic loadings were compiled from other studies. In general, they can be classified into three main groups: (1) finite-element analysis, (2) large-scale model experiment, and (3) in-situ test section. Table 1 presents the vertical strains in base, subbase, and subgrade layers summarized from various studies. The type of measurement and/or analysis, pavement structure, and loading characteristic employed in each study are also reported herein. Typically, the vertical strains in base, subbase, and subgrade layers are approximately 0.01-0.3%, 0.01-0.7%, and.

TABLE 1. Vertical strains in base, subbase, and subgrade layers

References (1)	Method of Estimating Strain (2)	Type of Measurement and/or Analysis (3)	Pavement Structure (4)	Loading Characteristic (5)	Vertical Strain (%)		
					Base (6)	Subbase (7)	Subgrade (8)
Brown & Pappin (1981)	2-D finite-element analysis	Nonlinear	- 50-mm surface - 170-mm base - Subgrade	- 8-kN wheel load - 530-kPa contact pressure	0.15	NA	0.12-0.18
Chen et al. (1986)	3-D finite-element analysis	Linear elastic	- 38-mm, 50-mm, 76-mm & 100-mm surface - 200-mm base - 4293-mm subgrade	- 20-kN & 24-kN wheel loads - 518-kPa, 621-kPa & 759-kPa contact pressures	NA	NA	0.035-0.074
Hardy & Cebon (1993)	Test section	LVDTs	- 150-mm surface - 300-mm base - 914-mm subgrade	- Four-axle vehicle: 29.1-kN steering axle, 40.4-kN-drive axial, 37.9-kN trailer's tandem axle group - Speed: 50 & 80 km/h	NA	NA	0.04-0.07
Marsh & Jewell (1994)	Test section	Vertical strain transducers	- 30-mm surface - 75-mm base - 250-mm subbase - 400-mm subgrade	- 553-kPa & 725-kPa contact pressures	NA	NA	$7x10^{-3}$-0.012
Chen et al. (1995)	- 2-D &3-D finite-element analysis - Multilayered elastic-based program	Linear & nonlinear	- 76-mm, 152-mm & 229-mm surface - 305-mm base - Subgrade	- 40.5 kN wheel load - 689 kPa contact pressure	NA	NA	0.013-0.13
Pidwerbesky (1995)	Large-scale model experiment	Strain coil sensors	- 25-mm, 35-mm & 85-mm surface - 135-mm, 200-mm & 300-mm base - 200-mm subgrade	- 21-kN, 31-kN, 40-kN & 46-kN wheel load - 550-kPa, 700-kPa & 825-kPa contact pressures	0.09-0.32	NA	0.09-0.35
Dai & Van Deusen (1998)	Test section	LVDTs	- 127-mm & 200-mm surface - 305-mm, 460-mm & 710-mm base - 2690-mm, 2940-mm & 3168-mm subgrade	- Five-axle tractor-trailer: 53.4-kN steering axle, 75.2-kN front axle, 73.9-kN back axle, 69.4-kN front axle & 81.9-kN back axle of tractor tandem - Speed: 16-78 km/h	NA	NA	$1.9x10^{-3}$-0.019

Helwany et al. (1998)	2-D & 3-D finite-element analysis	Linear & nonlinear	- 150-mm surface - 250-mm base - 650-mm subbase - Subgrade	- 90-kN axle load (45-kN wheel load) - 550-kPa contact pressure	NA	0.012-0.058	NA
Saleh et al. (2003)	Large-scale model experiment	Strain coil sensors	- 25-mm surface - 275-mm base - 1200-mm subgrade	- 40-kN, 50-kN & 60-kN wheel loads - 650-kPa, 700-kPa, 750-kPa, 800-kPa & 850-kPa contact pressures - Speed: 6 km/h	0.02-0.13	NA	0.09-0.35
Tanyu et al. (2003)	Multilayered elastic-based program	- Linear & nonlinear	- 125-mm surface - 255-mm base - 220-mm to 900-mm subbase - 450-mm subgrade	- 35-kN wheel load - 700-kPa contact pressure	NA	0.036-0.77	NA
Tutumluer et al. (2003)	- Large-scale model experiment - 2-D finite-element analysis	- Strain coil sensors - Linear & nonlinear - Isotropic & anisotropic	- 89-mm surface - 203-mm base - 1270-mm subgrade	- 28.9-kN wheel load - 689-kPa contact pressure	0.011-0.062	NA	0.175-0.25
de Pont et al. (2004)	Large-scale model experiment	Strain coil sensors	- 85-mm surface - 200-mm base - Subgrade	- 98-kN axle load (49-kN wheel load) - Speed: 45 km/h	0.06-0.21	NA	0.15-0.31
Huang (2004)	Multilayered elastic-based program	Linear elastic	- 25-mm to 203-mm surface - 102-mm to 406-mm base - Subgrade	- 80-kN axle load (40-kN wheel load) - 690-kPa contact pressure	NA	NA	0.025-0.4

0.002-0.4%, respectively. By assuming that the vertical strains in each layer are in the principal plane, the maximum shear strains in the principal plane are computed by multiplying vertical strains by (1+ν) (Kim and Stokoe 1992). Poisson's ratios (ν) of 0.35, 0.35, and 0.45 were respectively assumed for the base, subbase, and subgrade The range of maximum shear strains in principle plane are therefore computed to be 0.014-0.41% for base, 0.014-0.95% for subbase, and 0.003-0.58% for subgrade.

RELATIONSHIP BETWEEN SMALL-STRAIN AND LARGE-STRAIN MODULUS

For pavement bases and subgrades, the stress-strain behavior of soil is highly nonlinear and soil modulus may decay with strain by orders of magnitude. A relationship between the small-strain (linear-elastic) modulus (strains less than 10^{-2} %) and nonlinear behavior exhibited by soils at large strains (above 10^{-2} %) must be established. The shear modulus of soil at various shear strain levels for different pavement layers and modulus tests is shown in Fig. 5. Generally, strains in base and

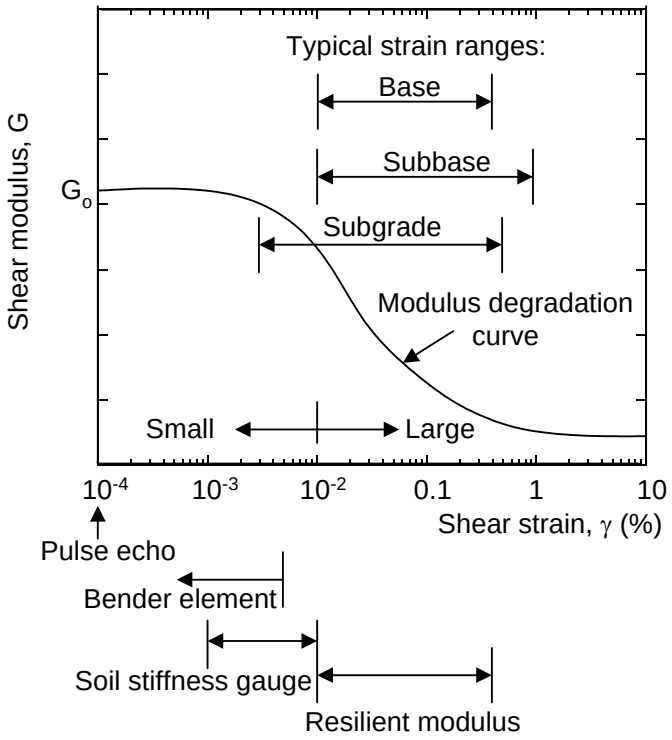

FIG. 5. Typical variation in shear modulus with various shear strain levels

subbase vary from 0.01 to 1%, whereas those in subgrade may vary from 0.003-0.6%. Therefore, the pavement base, subbase, and subgrade layers involve strains at higher levels, i.e., typical strain range of 10^{-2} to 1%, and soil exhibits nonlinear properties. Fig. 5 also shows that the resilient modulus (M_r) test operates within these strain range. However, the measured soil modulus from the bender element and the SSG must be adjusted or corrected to the modulus corresponding to these strain levels.

Since the soil moduli obtained from a variety of tests is likely to be stress- and stain-dependent, the moduli obtained from one test to the others must be effectively compared at the same stress level. A normalized modulus reduction curve (either E/E_o versus log ε_a or G/G_o versus log γ) may be used to assess the variation in moduli with strain amplitude without the effect of state of stress (Seed and Idriss 1970; Hardin and Drnevich 1972; Kokusho et al. 1982; Jardine et al 1986; Sun et al. 1988; Vucetic and Dobry 1991; Tatsuoka and Shibuya 1991; Puzrin and Burland 1996). Once the normalized modulus reduction curve is obtained by using either a database of resonant column test results or a typical modulus degradation scheme (Kim et al. 1997), the elastic modulus of a given soil obtained from either the laboratory or in situ small-strain stiffness measurements can be adjusted to the modulus corresponding to larger strains where the soil exhibits nonlinear behavior. In other words, the strain-dependent modulus of the soil can be predicted using a normalized modulus reduction curve. The modulus at a desired strain level can be determined by combining the measured modulus with the normalized modulus reduction curve as follows:

$$G_r = RF_{\text{data base or deg radation scheme}} \times G_{\text{SSG or BE}} \quad (2)$$

where G_r is design resilient shear modulus, RF is reduction factor that accounts for shear strain amplitude difference between resilient shear modulus and SSG or BE shear modulus which can be obtained from the database or degradation scheme, and $G_{SSG\ or\ BE}$ is the measured SSG or BE shear modulus. RF is computed as the ratio between the shear modulus corresponding to the shear strain amplitude of resilient modulus test and the shear modulus corresponding to the shear strain amplitude of the SSG or BE. It can be estimated approximately using the modulus degradation curve obtained either from a database of various modulus tests e.g., resonant column, resilient modulus, SSG, BE tests or from the typical modulus degradation scheme proposed by different investigators for soils as mentioned above. The shear strain levels induced by the SSG or BE, which is used to determine the reduction factor can be estimated approximately from Fig. 5. Resilient shear modulus can be converted to axial resilient modulus using $M_r = 2G_r(1+\nu)$. A comparison of moduli obtained from alternative methods with resilient modulus of the same material is given in Sawangsuriya et al. (2003; 2004).

SUMMARY

This paper presents the application of alternate methods which have not been widely used for obtaining moduli for pavement bases and subgrades. Mechanistic design methods require knowledge of the moduli for all pavement materials to determine the pavement design life. Resilient modulus is used in the mechanistic design; however, it can also be estimated from alternative tests such as the bender elements test in the laboratory and the SSG test in the field. A suggested method for adjusting the small-strain modulus to obtain the large-strain resilient modulus is also described in the paper. Although a medium sand was used in this investigation, the general concepts and procedures are applicable to other base and subgrade materials.

REFERENCES

Arulnathan, R., Boulanger, R. W., and Riemer, M. F. (1998). "Analysis of bender element tests." *Geotech. Testing J.*, 21(2), 120-131.

Brown, S. F., and Pappin, J. W. (1981). "Analysis of pavements with granular bases." *Transp. Res. Rec.*, 810, 17-23.

Burland, J. B. (1989). "The ninth Lauritis Bjerrum memorial lecture: 'small is beautiful'-the stiffness of soils at small strains." *Canadian Geotech. J.*, 26, 499-516.

Chen, D.-H., Zaman, M., Laguros, J., and Soltani, A. (1995). "Assessment of computer programs for analysis of flexible pavement structure." *Transp. Res. Rec.*, 1482, 123-133.

Chen, H. H., Marshek, K. M., and Saraf, C. L. (1986). "Effects of truck tire contact pressure distribution on the design of flexible pavements: a three-dimensional finite element approach." *Transp. Res. Rec.*, 1095, 72-78.

Dai, S., and Van Deusen, D. (1998). "Field study of in situ subgrade soil response under flexible pavement." *Transp. Res. Rec.*, 1639, 23-35.

de Pont, J., Thakur, K., Pidwerbesky, B., and Steven, B. (2004). "Validating a whole life pavement performance model." *Transit New Zealand, CAPTIF Research Facility*, 15

Dyvik, R., and Madshus, C. (1985). "Lab measurements of G_{max} using bender elements." *Proc. Advances in the Art of Testing Soil Under Cyclic Conditions*, ASCE, Detroit, MI, 186-196.

Edil, T. B., and Sawangsuriya, A. (2005). "Earthwork quality control using soil stiffness." *Proc. 16th Int. Conference on Soil Mech. and Geotech. Engrg.*, Osaka, Japan (accepted for publication).

Fam, M., and Santamarina, J. C. (1995). "Study of geoprocesses with complementary wave measurements in an oedometer." *Geotech. Testing J.*, 18(3), 307-314.

Fioravante, V., and Capoferri, R. (2001). "On the use of multi-directional piezoelectric transducers in triaxial testings." *Geotech. Testing J.*, 24(3), 243-255.

Hardin, B. O., and Black, W. L. (1968). "Vibration modulus of normally consolidated clay." *J. Soil Mech. and Found. Div.*, ASCE, 94(SM2), 353-369.

Hardin, B. O., and Drnevich, V. P. (1972). "Shear modulus and damping in soils: design equations and curves." *J. Soil Mech. and Found. Div.*, ASCE, 98(SM7), 667-692.

Hardy, M. S. A., and Cebon, D. (1993). "Response of continuous pavements to moving dynamic loads." *J. Engrg. Mech.*, ASCE, 119(9), 1762-1780.

Helwany, S., Dyer, J., and Leidy, J. (1998). "Finite-element analyses of flexible pavements." *J. Transp. Engrg.*, ASCE, 124(5), 491-499.

Huang, Y. H. (2004). Pavement analysis and design. Pearson Prentice Hall, Upper Saddle River, NJ.

Humboldt Mfg. Co. (1999). *Humboldt soil stiffness gauge (geogauge) user guide: version 3.3*, Norridge, IL.

Jardine, R. J., Potts, D. M., Fourie, A. B., and Burland, J. B. (1986). "Studies of the influence of non-linear stress-strain characteristics in soil-structure interaction." *Geotechnique*, 36(3), 377-396.

Jardine, R. J., and Potts, D. M. (1988). "Hutton tension platform foundation: an approach to the prediction of pile behavior." *Geotechnique*, 38(2), 231-252.

Kim, D.-S., and Stokoe, K. H., II (1992). "Characterization of resilient modulus of compacted subgrade soils using resonant column and torsional shear tests," *Transp. Res. Rec.*, 1369, 83-91.

Kim, D.-S., Kweon, G.-C., and Lee, K.-H. (1997). "Alternative method of determining resilient modulus of compacted subgrade soils using free-free resonant column test." *Transp. Res. Rec.*, 1577, 62-69.

Kokusho, T., Yoshida, Y., and Esashi, Y. (1982). "Dynamic properties of soft clays for wide strain range." *Soils and Found.*, 22(4), 1-18.

Mancuso, C., Vassallo, R., and d'Onofrio, A. (2002). "Small strain behavior of a silty sand in controlled-suction resonant column-torsional shear tests." *Canadian Geotech. J.*, 39(1), 22-31.

Mancuso, C., and Vinale, F. (1988). "Propagazione delle onde Sismiche: Teoria e Misura In Sito." *Atti del Convegno del Gruppo Nazionale di Coordinamento per gli Studi di Ingegneria Geotecnica*, Monselice, Rome, 115-138.

Marsh, J. G., and Jewell, R. J. (1994). "Vertical pavement strain as means of weighing vehicles." *J. Transp. Engrg.*, ASCE, 120(4), 617-632.

Pennington, D. S., Nash, D. F. T., and Lings, M. L. (2001). "Horizontally mounted bender elements for measuring anisotropic shear moduli in triaxial clay specimens." *Geotech. Testing J.*, 24(2), 133-144.

Pidwerbesky, B. D. (1995). "Strain response and performance of subgrades and flexible pavements under various loading conditions." *Transp. Res. Rec.*, 1482, 87-93.

Puzrin, A. M., and Burland, J. B. (1996). "A logarithmic stress-strain function for rocks and soils." *Geotechnique*, 46(1), 157-164.

Saleh, M. F., Steven, B., and Alabaster, D. (2003). "Three-dimensional nonlinear finite element model for simulating pavement response: study at Canterbury accelerated pavement testing indoor facility, New Zealand." *Transp. Res. Rec.*, 1823, 153-162.

Sawangsuriya, A., Bosscher, P. J., and Edil, T. B. (2004). "Application of the soil stiffness gauge in assessing small-strain stiffness of sand with different fabrics and densities." *Submitted to Geotech. Testing J.*, ASTM. (contact authors)

Sawangsuriya, A., Edil, T. B., and Bosscher, P. J. (2003). "Relationship between soil stiffness gauge modulus and other test moduli for granular soils." *Transp. Res. Rec.*, 1849, 3-10.

Seed, H. B., and Idriss, I. M. (1970). "Soil moduli and damping factors for dynamic response analyses." *Report EERC 70-10*, Earthquake Engineering Research Center, University of California, Berkeley, CA.

Souto, A., Hartikainen, J., and Özüdoğru, K. (1994). "Measurement of dynamic parameters of road pavement materials by the bender element and resonant column tests." *Geotechnique*, 44(3), 519-526.

Sun, J. I., Golesorkhi, R., and Seed, H. B. (1988). "Dynamic moduli and damping ratios for cohesive soils." *Report EERC-88/15*, Earthquake Engineering Research Center, University of California, Berkeley, CA.

Tanyu, B. F., Kim, W. H., Edil, T. B., and Benson, C. H. (2003). "Comparison of laboratory resilient modulus with back-calculated elastic moduli from large-scale model experiments and FWD tests on granular materials." *Resilient Modulus Testing for Pavement Components, ASTM STP 1437*, West Conshohocken, PA, 191-208.

Tatsuoka, F., and Shibuya, S. (1991). "Deformation characteristics of soils and rocks from field and laboratory tests." *Proc. 9th Asian Regional Conference on Soil Mech. and Found. Engrg.*, Bangkok, Thailand, 2, 101-170.

Tatsuoka, F., Siddiquee, M. S., Park, C. S., Sakamoto, M., and Abe, F. (1993). "Modeling stress-strain relations of sand." *Soils and Found.*, 33(2), 60-81.

Thomann, T. G., and Hryciw, R. D. (1990). "Laboratory measurement of small strain shear modulus under K_o conditions." *Geotech. Testing J.*, 13(2), 97-105.

Tutumluer, E., Little, D. N., and Kim, S.-H. (2003). "Validated model for predicting field performance of aggregate base courses." *Transp. Res. Rec.*, 1837, 41-49.

Vucetic, M., and Dobry, R. (1991). "Effect of soil plasticity on cyclic response." *J. Geotech. Engrg.*, ASCE, 117(1), 89-107.

Zeng, X., and Ni, B. (1998). "Application of bender elements in measuring G_{max} of sand under K_o condition." *Geotech. Testing J.*, 21(3), 251-263.

Wisconsin Highway Research Program
University of Wisconsin-Madison
1415 Engineering Drive
Madison, WI 53706
608/262-2013
www.whrp.org